Tipping the balance

Cell death deregulation in colorectal cancer

Ramesh, P.

Publication date
2022

Document Version
Final published version

Tipping The Balance

Cell Death Deregulation in Colorectal Cancer

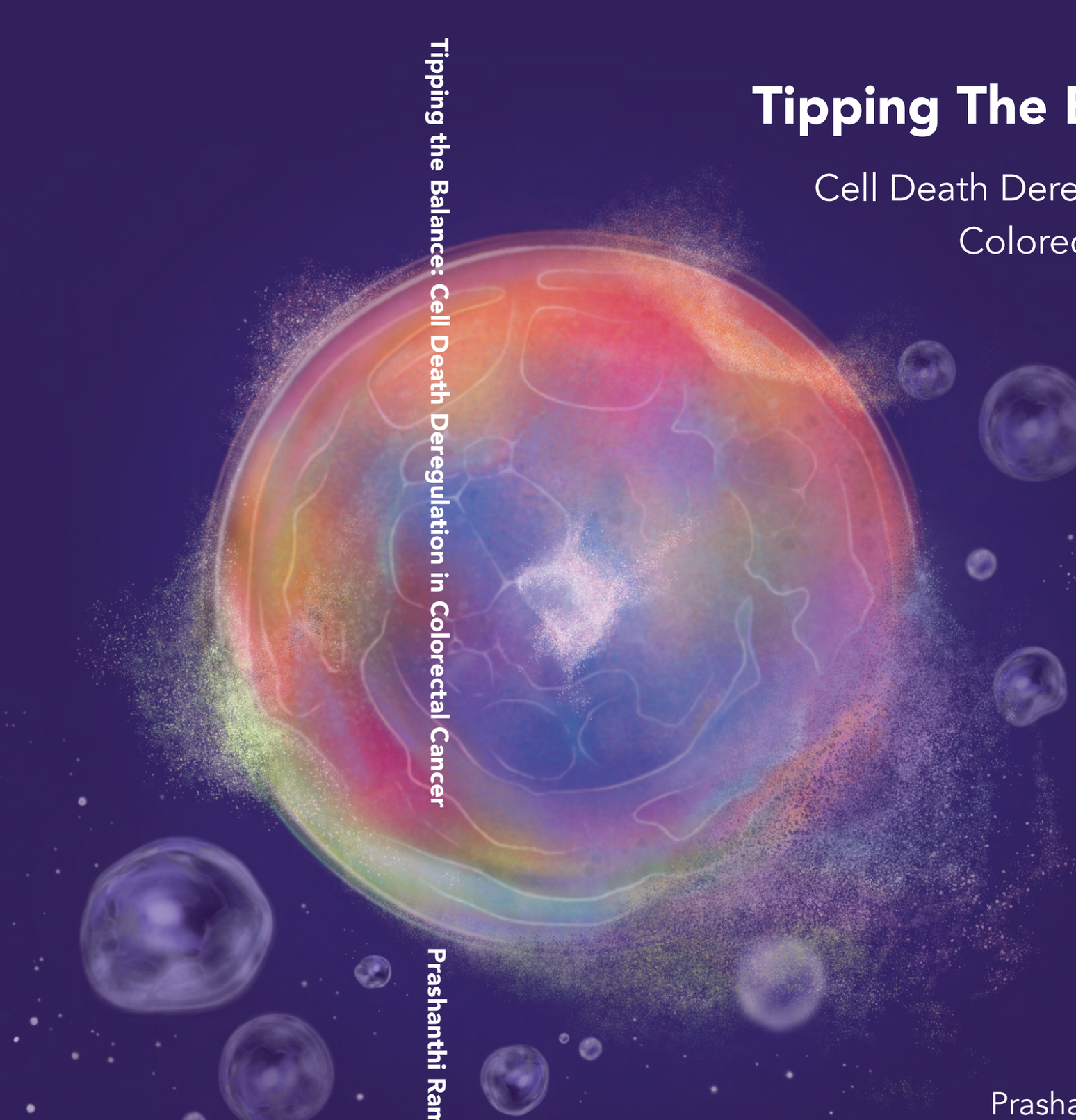

Prashanthi Ramesh

Tipping the Balance: Cell Death Deregulation in Colorectal Cancer

Prashanthi Ramesh

Tipping the Balance:
Cell Death Deregulation in Colorectal Cancer

Prashanthi Ramesh

The research described in this thesis was performed at the Center for Experimental Molecular Medicine (CEMM), and Laboratory for Experimental Oncology and Radiobiology (LEXOR) at the Amsterdam University Medical Centers (AUMC), University of Amsterdam (UvA), The Netherlands.

Financial support for printing of this thesis was kindly provided and supported by Cancer Center Amsterdam.

Cover design: Janani Ramesh
Layout: Janani and Prashanthi Ramesh

Tipping the Balance:
Cell Death Deregulation in Colorectal Cancer

ACADEMISCH PROEFSCHRIFT

ter verkrijging van de graad van doctor
aan de Universiteit van Amsterdam
op gezag van de Rector Magnificus
prof. dr. ir. K.I.J. Maex
ten overstaan van een door het College
voor Promoties ingestelde commissie,
in het openbaar te verdedigen
in de Agnietenkapel
op vrijdag 25 maart 2022, te 10.00 uur

door Prashanthi Ramesh
geboren te Kumbakonam

Promotiecommissie

Promotor:

prof. dr. J.P. Medema	AMC-UvA

Co promotor:

prof. dr. L. Vermeulen	AMC-UvA

Overige leden:

prof. dr. E.F.Eldering	AMC-UvA
dr. M. Spaargaren	AMC-UvA
prof. dr. E. Dekker	AMC-UvA
prof. dr. G.Stassi	University of Palermo
dr. L. Koens	AMC-UvA

Faculteit der Geneeskunde

Table of contents

Chapter 1

Introduction

Adapted from 'BCL-2 family deregulation in colorectal cancer: potential for BH3 mimetics in therapy'.

Prashanthi Ramesh and Jan Paul Medema.

Published in *Apoptosis, 2020.*

Abstract

Apoptosis is a form of programmed cell death that is essential for tissue homeostasis. De-regulation of the balance between proliferation and apoptosis contributes to tumor initiation. Particularly in the colon where apoptosis is a crucial process in intestinal turnover, inhibition of apoptosis facilitates transformation and tumor progression. The BCL-2 family of proteins are key regulators of apoptosis and have been implicated in colorectal cancer (CRC) initiation, progression and resistance to therapy. In this review we outline the current knowledge on the BCL-2 family regulated intrinsic apoptosis pathway and mechanisms by which it is de-regulated in CRC. We further review BH3 mimetics as a therapeutic opportunity to target this pathway and evaluate their potential for CRC treatment.

Introduction

Programmed cell death is an essential process regulating tissue homeostasis and stress response in many organisms. One of the most widely studied and well-characterized forms of programmed cell death is apoptosis, first described in the landmark study of Kerr et all in 1972 [1]. In their study they describe a unique morphology of dying cells which form membrane bound fragments that get phagocytosed by nearby cells. Further understanding of the pathway came from developmental studies conducted in the nematode *Caenorhabditis elegans* [2]. It is now well accepted that this process is tightly regulated by a set of proteins with specific interaction domains, most of which are conserved in mammals [2, 3]. In response to various signals, these proteins orchestrate a cascade of reactions that ultimately dictate the choice between life and death.

While apoptosis occurs in normal tissue development and regeneration, it can also be activated in response to stress signals such as nutrient deprivation, reactive oxygen species and excessive mitogenic signaling usually associated with cancer initiation [4]. Such signals lead to the activation of one of the two main apoptotic pathways – the extrinsic and intrinsic pathways. The extrinsic pathway is regulated by so-called death receptors such as TNFR, FAS, DR3/WSL. Upon ligand binding these receptors activate signaling cascades that result in caspase activation, which is instrumental in the execution of apoptotic cell death. In this review we focus on the role of the BCL-2 family of proteins in cancer and hence on the intrinsic or mitochondrial pathway of apoptosis, which is regulated by this family [5].

Apoptosis is a key cell death mechanism that can counteract tumor formation and growth and for this reason, is often de-regulated in various cancers [6]. Increased proliferation resulting from oncogenic mutations is facilitated by genetic and epigenetic alterations in apoptotic pathways that ultimately allow uncontrolled tumor growth. Homeostasis in the colon is tightly regulated by a balance between proliferation and apoptosis. Disruption

of this balance is an integral step in CRC development and progression. In addition, an increased apoptotic threshold is often observed in CRC tumors which contributes to therapy resistance [7]. In this review we describe how the members of the BCL-2 family regulate apoptosis and how they often get de-regulated to enable CRC progression and chemo-resistance. We further assess the potential of BH3 mimetics – small molecule antagonists of anti-apoptotic BCL-2 family members – as a therapeutic strategy for targeting this pathway and inducing apoptosis in CRC tumors.

The intrinsic apoptosis pathway

In the intrinsic apoptosis pathway, the BCL-2 family of proteins play a key role in determining the decision to undergo apoptosis. The first member of the BCL-2 family to be identified was the pro-survival B-cell lymphoma-2 (*Bcl-2*) gene, which was found to be frequently amplified in lymphomas by an oncogenic translocation [8, 9]. It was soon discovered that this protein was able to promote cancer cell survival by preventing apoptosis [10-12]. More than 15 members of this family have since been identified that can be segregated based on their apoptotic regulation as either pro- or anti-apoptotic [13-17]. Here we describe how these members interact to regulate mitochondrial permeabilization.

The pro- and anti- apoptotic BCL-2 proteins

All members of the BCL-2 family of proteins show homology in one or more of the four BCL-2 homology (BH) domains and are categorized based on the number of homology domains they possess [18]. The anti-apoptotic members all have four BH-domains and include BCL-2, BCL-XL, MCL-1, BCL-W and A1/BFL-1. Of these, the BH1, BH2 and BH3 domains contribute to the formation of a hydrophobic pocket in their tertiary protein structure. The pro-apoptotic proteins can be divided into two sub-groups: the BH3-only proteins and the effector proteins. The BH3-only proteins, thus named as they only show homology to the BH3 domain of BCL-2 include BIM, BAD, BID, PUMA, NOXA, BMF, HRK, BIK and others. The effector proteins

such as BAX and BAK possess three to four BH domains and are able to form macropores in the mitochondrial outer membrane. BOK is another multi-BH3 domain effector protein that has pro-apoptotic functions, which some studies suggest to be independent of BAX and BAK [19-21]. The physical interaction between anti- and pro-apoptotic proteins is a result of the binding of the BH3 domain of the pro-apoptotic proteins to the hydrophobic clefts of the anti-apoptotic proteins [18, 22, 23].

Regulation of mitochondrial permeabilization

The vast majority of BAX and BAK molecules exist as inactive monomers (BAX) or homodimers (BAK) in an equilibrium between the cytosol and mitochondrial membrane [24-26]. BAX/BAK activation leads to the formation of pores that initiates the morphological changes associated with apoptosis [27]. Recent findings have shed light into detailed interaction models between these proteins that help provide new insights for targeting this pathway (Fig.1) [5].

The mechanism by which BH3-only protein promote apoptosis is still a matter of intense debate. There is strong evidence for a "direct" model, which suggests that some BH3-only proteins can directly interact with BAX/BAK to induce conformational changes that leads to their activation [28-30]. These so called "activators" include BIM and BID and more recently PUMA and NOXA have shown to act as activators, although with lesser efficacy [31-34]. The other BH3 proteins such as BAD function as "sensitizers" in this model as they mainly interact with anti-apoptotic BCL-2 proteins to release the "activator" BH3-only proteins [31]. The anti-apoptotic BCL-2 proteins can inhibit apoptosis by two modes: either by directly engaging with and inhibiting activation of BAX/BAK or by sequestering activator BH3-only proteins, both of which prevent oligomerization of BAX and BAK (Fig.1) [35]. Another "indirect" model proposes that the BH3-only proteins do not directly interact with BAX/BAK but instead act by binding to and neutralizing the anti-apoptotic proteins to release BAX/BAK and allow pore formation [36, 37]. A recent study employed genome editing to delete all BH3-only proteins to generate an apoptosis resistant cell line. Interestingly, when

MCL-1 and BCL-XL were inhibited in these cells the kinetics of apoptosis was similar to the cells that did express all BH3-only proteins. The authors therefore suggest that BH3-only proteins are not required for the direct activation of BAX and BAK and that they mainly function to repress BCL-XL and MCL-1 [37]. Even if they are not essential for BAX/BAK activation, this does not exclude that BH3 activators can indeed facilitate pore formation through such direct interactions. Regardless of the prevailing model, when the balance is tipped in favor of pro-apoptotic molecules, BAX and BAK will multimerize to form pores in the outer mitochondrial membrane. Although less well studied, BOK was initially identified by its interactions with MCL-1 and is also suggested to have pore forming abilities [38, 39]. However, studies now propose its activation to be regulated by the endoplasmic reticulum-associated degradation pathway, independent of other BCL-2 protein interactions [20, 39, 40].

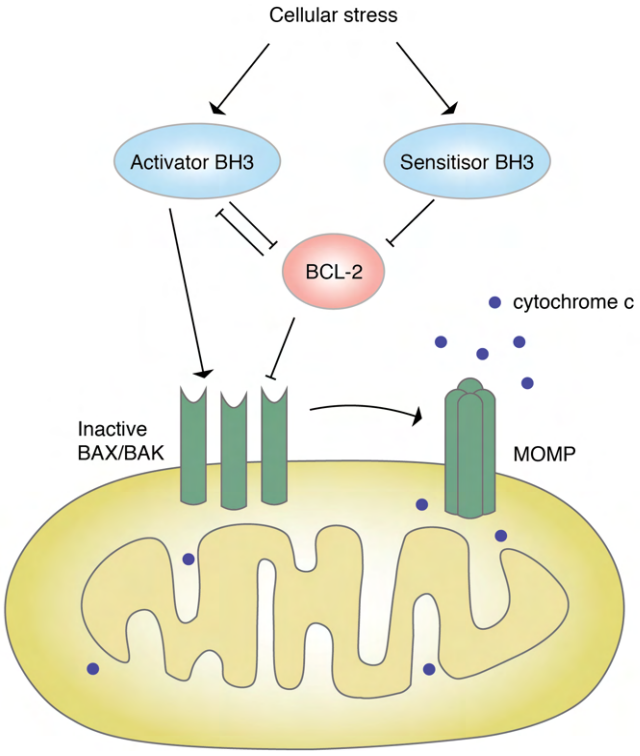

Figure 1. BCL-2 family protein interactions regulate mitochondrial outer membrane permeabilization (MOMP).

Additional layers of complexity are added to these interaction models as the different members of the BCL-2 family show preferential binding patterns among each other. For instance, BH3-only proteins bind to pro-survival members with different affinities (Fig.2). BH3-only proteins such as BIM, PUMA and tBID ("activators") can engage with all anti-apoptotic proteins whereas others are more limited in their interactions [41, 42]. BAD interacts with BCL-2, BCL-XL and BCL-W, while HRK binds specifically to BCL-XL and NOXA shows preferential binding to MCL-1 and A1. Studies also show preferential interactions between activator BH3-only proteins and BAX and BAK. So while BID prefers to interact with BAK, BIM shows either no preference or preference for activation of BAX [30, 43]. An additional layer of complexity is introduced by specific interactions between anti-apoptotic proteins and effector proteins. For example, BAK is not inhibited by BCL-2 while MCL-1 and BCL-XL do restrain its activation [44]. Retrotranslocation of BAX and BAK away from the mitochondria into the cytosol is also regulated by the different pro-survival proteins. While BAX is retrotranslocated by BCL-2, BCL-XL and MCL-1, BAK retrotranslocation is only regulated by BCL-XL and MCL-1 [26]. This retrotranslocation process prevents the activation of BAX/BAK at the mitochondrial outer membrane and thereby also prevents pore formation and mitochondrial outer membrane permeabilization (MOMP).

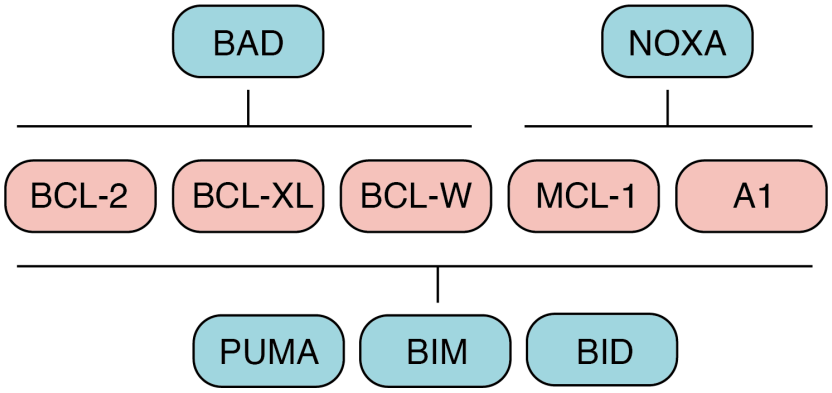

Figure 2. BH3-only proteins have specific affinities for anti-apoptotic proteins.

Outcomes of MOMP

MOMP is often considered to be the point of no return for apoptosis to occur [45]. Once the outer membrane is permeabilized by BAX/BAK pore formation, soluble proteins such as cytochrome c are released from the mitochondrial intermembrane space into the cytosol [46-48]. Here cytochrome c binds to APAF-1 to form the apoptosome, which activates caspase-9 and ultimately leads to cleavage and activation of effector caspases such as caspase-3 or 7. MOMP also leads to the release of other proteins such as second mitochondria derived activator of caspase (SMAC) which releases caspase-3 from inhibitory proteins such as X-linked inhibitor of apoptosis (XIAP) [49]. The effector caspases are responsible for the cleavage of various proteins and eventual dismantling of the cell into apoptotic bodies. Despite being the executors of apoptosis, prevention of caspase activation does not always circumvent apoptosis. Permeabilized mitochondria can still lead to a cell's death in the absence of caspases due to mitochondrial distress, a form of death termed caspase-independent cell death [50-52]. Interestingly, several studies report cell survival despite caspase activation [53-55]. When only a minority of mitochondria commit to MOMP, cells may prevent cell death and maintain their clonogenic potential [56]. In fact, the limited caspase activation resulting from this so called "minority MOMP" can induce caspase associated DNAse activity and thereby DNA damage. Cells that survive despite activation of the apoptotic pathway by such mechanisms may thus become genetically unstable and potentially tumorigenic [56-58].

Mechanisms of apoptotic de-regulation

De-regulated apoptosis is observed in most tumor types and is considered one of the hallmarks of cancer. Evasion of apoptosis allows tumor cells to bypass oncogene-induced cell death and can also promote sustained tumor growth, survival during metastatic spread and therapy resistance. De-regulation of the BCL-2 family not only occurs during tumorigenesis and outgrowth but is also observed as part of the tumor evolution that takes

place in response to therapy [59-61]. The intrinsic pathway of apoptosis is often modified to tip the balance towards reduced apoptosis by altering one or both of the two main components of the pathway.

Not surprisingly, an increased expression of pro-survival BCL-2 proteins is found in several cancer types. This increase can be achieved by several mechanisms including chromosomal translocations [8], gene amplifications [62], increased transcription [63-65] and post-transcriptional and post-translational modifications (PTM) [66, 67]. Chromosomal gain mediated amplification of *Mcl-1* and *Bcl-xL* were found to be the most frequent alterations across 26 tumor types, particularly in solid tumors [62]. Anti-apoptotic adaptation can also occur through PTMs that enhance the activity of pro-survival proteins [68, 69]. Most tumors generally rely on the up-regulation of one or two anti-apoptotic proteins for resistance, which varies from tumor-to-tumor and even within the same tumor type [70-73]. Thus, most cancers present heterogeneous expression and dependence on anti-apoptotic proteins.

Another mechanism of altering the apoptotic threshold is to decrease the expression or modulate the activity of pro-apoptotic BH3-only proteins. Loss of BH3-only proteins is only mildly oncogenic on its own but can be tumorigenic in certain contexts such as co-occurrence with MYC activation [74]. Loss of P53 occurs in many cancers and leads to the downregulation of its transcriptional targets PUMA and NOXA [75, 76]. Several studies document other tumor-associated changes in BH3-only proteins by various mechanisms including mutation, loss of heterozygosity or epigenetic silencing [77]. Reduced expression or activity of the BCL-2 family effector proteins is also a potent mechanism for apoptosis evasion in tumor cells. BAX somatic frameshift mutations are selected for in microsatellite instable gastric, colon and endometrial tumors [78]. Localization changes can also affect their apoptotic activity as observed in AML [79]. Studies have noted changes in their activity induced by phosphorylation and anti-cancer therapy that affect their pore forming abilities [59, 80]. BOK deletions are quite frequently detected in a range of tumors [62]. However, BOK

deficient mice show no overt phenotypic changes and cells derived from these mice are not hampered in apoptosis [81]. Several studies suggest that BOK exerts its anti-tumorigenic effects through non-apoptotic functions [82, 83]. On the other hand, a pro-tumorigenic role for BOK is reported in hepatocellular carcinoma where deletion of BOK is infrequent [84].

De-regulation of the BCL-2 family in CRC

Anti-apoptotic adaptation is a crucial step in CRC initiation and advancement. An accumulation of alterations that enable apoptosis evasion is observed as CRC progresses from adenoma-to-carcinoma stages. The increased apoptotic threshold hampers the efficacy of various chemotherapeutics and thus presents itself as a valuable target for CRC therapy. Several studies highlight modifications in the intrinsic apoptosis pathway at various stages of the disease. Here we review the role of the BCL-2 family in transformation of a healthy colon into adenomas and examine the pathway's de-regulation as the disease progresses towards the carcinoma stage.

Apoptosis in the normal colon

Homeostasis in the colon is maintained by a balance between proliferation and apoptosis. The colonic epithelium consists of a single layer of epithelial cells that is organized to form invaginations called crypts [85]. Lgr5+ stem cells reside at the bottom of these crypts, which proliferate to give rise to intermediate transit amplifying cells [86]. Transit amplifying cells differentiate into various lineages as they move along the crypt towards the luminal face of the colon where they eventually get shed and die by apoptosis [87]. The entire colon gets renewed within 4-5 days thus making apoptosis an active pathway in intestinal regeneration and maintenance. Two forms of apoptosis occur in the intestine – spontaneous apoptosis and damage-induced apoptosis. Spontaneous apoptosis occurs in general intestinal turnover whereas damage-induced apoptosis is elicited in response to stresses such as irradiation, chemotherapy and pathogens.

Several anti-apoptotic proteins and pro-apoptotic effectors are expressed in the colon and have important functions in both forms of apoptosis (Table 1). Studies on BCL-2 expression in the colon all conclude that it is mainly localized in the bottom of the crypt, where the stem cells reside [88]. On the other hand, BCL-XL and MCL-1 show more general expression in the normal intestine, not localized to a particular crypt compartment but specifically showing an apical staining pattern in cells [89, 90]. BCL-W was hardly detectable in human normal tissue however a study in mice did show expression in the intestine [91, 92]. BAX and BAK expression in the crypts is more pronounced in the upper 2/3rd part than the bottom, in contrast to pro-survival BCL-2 [90, 93]. These expression studies support the observed pattern of proliferation in the bottom of the crypt and apoptosis at the top.

Knockout (KO) mouse models of pro- and anti-apoptotic proteins provide insight into their role in spontaneous and damage-induced apoptosis in the colon. Homozygous BCL-2 null mice show increased spontaneous apoptosis compared to wild-type mice in the crypt bottom of the colon [88]. This however was not observed in the small intestine of BCL-2 KO mice, which show no overt phenotypic changes [88, 94]. An increase in damage-induced apoptosis upon irradiation and 5-FU treatment is also observed in the colonic stem cells of BCL-2 KO mice [95]. Intestinal specific BCL-XL KO mice do not present with any changes to spontaneous apoptosis, thus maintaining colon integrity [96]. Similarly, knocking out BCL-W does not affect spontaneous intestinal apoptosis. However, these KO mice do display an important role for BCL-W in damage-induced apoptosis, particularly in the small intestine [92]. Both spontaneous and damage-induced apoptosis are unaffected by BAX KO, while the colon in BAK-null mice is significantly affected with crypt hyperplasia and reduced damage-induced apoptosis [95, 97]. The colon of BAK KO mice present with an increase in goblet cell numbers and a decrease in endocrine populations resulting from reduced basal apoptosis levels [97]. This suggests a unique role for BAK in regulating intestinal homeostasis that is not interchangeable with BAX.

BCL-2 family protein	Normal	Adenoma	Adeno-carcinoma	Reference
BCL-2	Expressed	Increase	Decrease	[100-105]
			Increase	[106,107]
		Decrease	Decrease	[99]
		No change	Increase	[96,98]
BCL-XL	Expressed	Increase	Increase	[90,96,99,114]
BCL-W	Not expressed	Not expressed	Increase	[91]
MCL-1	Expressed	Increase	Decrease	[99]
		Decrease		[96]
BAX	Expressed	No change	No change	[90,99]
BAK	Expressed	Decrease	Decrease	[90,99]
PUMA	Expressed	-	Increase	[128]
NOXA	Expressed	-	No change	[129]
BID	Expressed	-	Increase	[132,133]

Table 1. Expression alterations of BCL-2 family members in CRC progression from adenoma-to-carcinoma compared to healthy epithelium.

The BCL-2 family in intestinal transformation

A progressive inhibition of apoptosis occurs during CRC progression [98]. This is particularly crucial during initiation where the tumor cell needs to overcome the apoptotic check in response to oncogenic signaling. Immunohistochemical (IHC) analysis of BCL-2 family protein expression in normal and adenoma tissues suggest that various members are de-regulated upon transformation (Table 1). IHC data indicate that colon adenomas have increased levels of anti-apoptotic protein BCL-XL while BCL-W is hardly detectable [91, 96, 99]. BCL-2 and MCL-1 stainings show inconsistent results in different studies. While several studies find an increase in BCL-2 protein levels in adenomas [100-107], there are also reports of either a decrease or no change in expression compared to normal tissue

[96, 98, 99] (Table 1). However, the expression of BCL-2 specifically in the stem cells of the healthy colon has an important role in tumorigenesis [94]. Deletion of APC leads to adenoma formation in the mouse small intestine due to hyperactivation of the Wnt pathway. In stem cell-specific BCL-2 null mice, loss of APC gives rise to significantly fewer adenomas, thus indicating that BCL-2 is crucial for tumor initiation and survival [94]. Another study suggests an important role for BCL-XL in CRC development where intestinal epithelial cell-specific BCL-XL KO mice develop fewer tumors in an inflammation-driven tumor model [96]. Similarly, PUMA loss facilitates CRC progression as PUMA KO mice develop more adenomas in both the APC Min/+ and inflammation-driven tumor models [108]. As PUMA is driven largely by a p53 response, this suggests that oncogenic stress elicited by APC deletion drives a p53-dependent apoptotic response. IHC expression data of the effector proteins suggest that levels of pro-apoptotic protein BAX remain unchanged, while BAK is clearly decreased in adenomas (Table 1) [90, 99]. The observed downregulation of BAK could in part be due to oncogenic KRAS signaling. Ectopic re-expression of BAK in KRAS-transformed intestinal cells reduces their tumorigenicity [109]. More recently, a lesser known member of the BCL-2 family, namely BCL-G, was found to play a crucial role in colon tumorigenesis [110]. BCL-Gs (splice variant) only has the BH3 domain and has pro-apoptotic activity as it can bind to and inhibit BCL-XL [111]. Loss of BCL-G resulted in accelerated tumor formation in an inflammation-driven tumor model but not in the APC Min/+ mouse model [110]. Importantly, it is unclear whether this relates to its apoptotic functions as deletion affects the Mucin structure of the mucosal layer, indicating a non-apoptotic role for BCL-G in this context.

The BCL-2 family in CRC carcinogenesis

CRC develops in a step-wise manner with sequential accumulation of specific genetic mutations that dictate the progression from adenoma-to-carcinoma stages [112]. This progression is accompanied by several changes in the apoptotic threshold of the cancer cells with an overall inhibition of apoptosis [98]. Most members of the BCL-2 family show altered expression patterns in CRC tumors, which plays a role in cancer

progression and therapy resistance.

Of the anti-apoptotic proteins, BCL-2 and MCL-1 expression is found to be decreased in CRC while BCL-XL and BCL-W show increased expression (Table 1). While BCL-2 plays a key role in adenoma formation, a progressive decrease in its expression during tumor progression indicates less of a role in CRC survival and resistance [90, 94, 100-105, 113]. The mechanism behind this decrease in expression has not been explored but studies suggest reciprocal regulation of BCL-2 and BCL-XL due to their inverse expression patterns [99]. Of all cancer types, *Bcl-xL* is amplified most often in cancers of the colon and a vast majority of CRCs present with BCL-XL overexpression [90, 96, 99, 114, 115]. This increased expression has been shown to be crucial for CRC survival and progression [90, 96, 115]. Colon cancer stem cells (CSCs) in particular are considered to be the chemo-refractory sub-population in primary CRC cultures and this resistance is mainly BCL-XL dependent [116]. Indeed, overexpression of BCL-XL in these cultures renders the differentiated population chemo-resistant [116]. De-regulation of anti-apoptotic MCL-1 also plays a crucial role in CRC chemo-resistance. While MCL-1 expression studies suggest decreased levels in CRC, it is important to note that its protein turnover rates are quite high with a half-life of approximately 30 minutes [117, 118]. Phosphorylation of MCL-1 by GSK3ß facilitates binding of FBW7, an E3 ubiquitin ligase which ubiquitylates and causes proteasomal degradation of MCL-1 [118, 119]. This degradation of MCL-1 is necessary for the efficacy of various targeted therapeutics against CRC cell lines [120]. Alterations in proteins regulating this degradation process often occur in CRC. Inactivating FBW7 mutations are found in CRC cell lines which promote MCL-1 stability and therefore, resistance to chemotherapy [119]. USP9X, a deubiquitinase enzyme that is reported to deubiquitinate and thus stabilizes MCL-1 protein levels, is also higher expressed in CRC cell lines [121].

In addition to the de-regulation of anti-apoptotic BCL-2 family members, several studies indicate altered expression and activity of the apoptosis effector proteins in CRC. BAK expression levels are decreased in colorectal

tumors, but in most cases BAX levels appear to be unchanged [90, 99]. However, mutation analyses reveal the incidence of *Bak* mutations to be relatively low in CRC, but on the other hand, *Bax* frameshift mutations are quite frequently selected for in microsatellite instable tumors and this results in reduced apoptosis in BAX negative tumors [122-124]. The pro-apoptotic protein BAX interacting factor-1 (BIF-1) is found to be decreased in CRC tissues which might also result in reduced efficacy of BAX in CRC [125]. A recent study indicates a role for BOK in chemo-resistance in CRC as primary patient-derived organoids that are 5-FU resistant show decreased BOK expression compared to 5-FU sensitive organoids. This role is independent of its pro-apoptotic activity as the study shows BOK regulates uridine metabolism and thereby 5-FU chemo-conversion, thus a decrease in its expression promotes 5-FU resistance [126].

Of the pro-apoptotic BH3-only proteins, occasional mutations have been reported for Bad, but no mutations were detected in *Noxa, Puma* and *Bik* in CRC tumors [127-130]. 293T cells transfected with tumor-associated mutant BAD show decreased apoptosis induction and mutant BAD binds inefficiently to BCL-2 and BCL-XL [127]. Although mutations are infrequent, altered expression of BH3-only proteins is frequently observed in CRC. The promoter region of *Hrk* is found to be methylated in some CRC cases and treatment of cell lines with de-methylating agents re-introduces *Hrk* expression and sensitivity to chemotherapy [131]. An increased expression of PUMA and BID is detected in CRC, while NOXA levels remain unchanged (Table 1) [128, 129, 132, 133]. This increase in pro-apoptotic proteins might be counter-intuitive for apoptosis evasion but most likely, such mechanisms are employed by a cell as a protective measure against transformation. Therefore, this increased expression could indicate the presence of compensatory mechanisms that enable tumor cells to override such selection pressures. PTMs that de-regulate BH3-only proteins are also reported in CRC such as an increase in BAD phosphorylation, which attenuates BAD pro-apoptotic activity and facilitates tumorigenesis [128, 134, 135].

Considering the frequent alterations in the BCL-2 family that occur in CRC, various studies have assessed the potential of different members of the family as prognostic biomarkers for the disease [136]. However, due to the complex interactions of the various regulators of this pathway, none of the proteins on their own could reliably predict clinical response to therapy [136]. For this reason, a recent study employed a computational model that reflects the dynamic regulation of MOMP by the BCL-2 proteins to successfully identify high-risk CRC patients [137]. This highlights the importance of the various interactions among the BCL-2 family members that play a major role in determining tumor progression and therapy response.

Targeting the BCL-2 family

Cancer cells adapt to the various pressures of oncogenic transformation such as checkpoint evasion, metabolic stress and replicative damage by de-regulating the BCL-2 family and becoming more refractory to apoptosis. In order to handle these stress signals, the cancer cell is in a precarious position where it requires this apoptotic block to hold. This dependence on the BCL-2 family presents a therapeutic window of opportunity where pushing this block can specifically target cancer cells for apoptosis. Highly specific small molecule inhibitors called BH3 mimetics have therefore been developed to target anti-apoptotic BCL-2 proteins by mimicking the action of BH3-only proteins (Fig.3). Here we review the reported efficacy of these inhibitors and examine their potential for CRC therapy.

BH3 mimetics: pushing the apoptotic block

Early efforts to overcome the anti-apoptotic defense mechanism in cancer were mainly driven by screening libraries of natural products, which yielded several classes of compounds that can inhibit anti-apoptotic BCL-2 proteins [138]. Two of these, AT-101 and Obatoclax (GX15-070), have been tested in clinical trials for solid and hematological malignancies (see clinicaltrials.gov). Although these compounds can inhibit multiple anti-apoptotic BCL-

2 members, they do not show sufficient clinical efficacy to warrant their approval [138, 139]. Using structure-based design to selectively target anti-apoptotic proteins proved successful with the generation of ABT-737, the first BH3-mimetic to be developed [140]. Designed using NMR-based screening, this compound mimics the binding pattern of BAD to inhibit the hydrophobic groove of BCL-2, BCL-XL and BCL-W. For clinical use, an orally bioavailable analog of ABT-737 was developed named ABT-263 or Navitoclax [141]. Notwithstanding the remarkable efficacy shown by this drug in pre-clinical studies [141-144], its use in the clinic is hampered by severe platelet toxicity [145]. Inhibition of BCL-XL in particular is found to be the cause of the observed thrombocytopenia, revealing its role in regulating platelet lifespan [146].

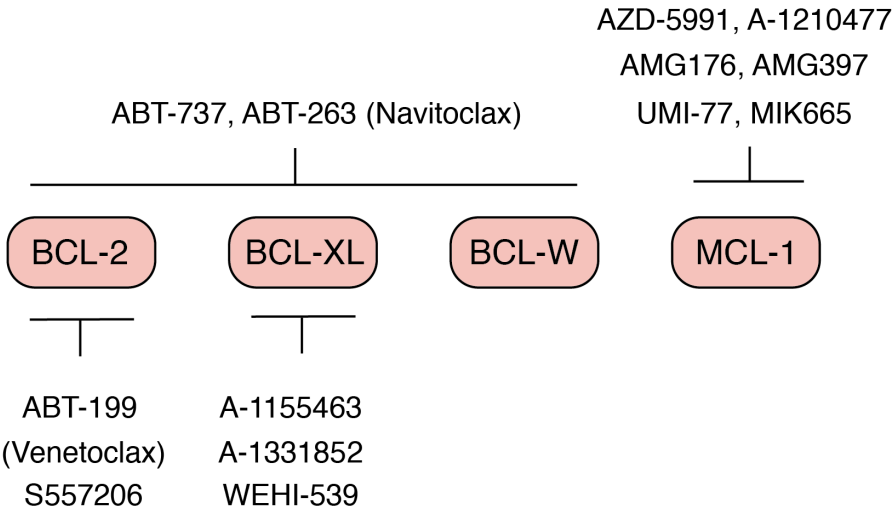

Figure 3. An overview of selective BH3 mimetics designed to inhibit anti-apoptotic proteins.

However, appropriate dosing strategies can help control the thrombocytopenia and indeed, several clinical trials testing the safety and efficacy of ABT-263 in a range of tumor types are ongoing (see clinicaltrials.gov) [139]. Another dual BCL-2 and BCL-XL inhibitor, AZD4320 shows potent tumor regression *in vivo* in hematological and solid malignancies [139]. This drug, re-formulated as a novel nanomedicine (AZD0466), is currently in a phase I clinical trial for both blood and solid tumors (NCT04214093). APG-

1252 is another newly developed inhibitor of BCL-2 and BCL-XL that shows potent activity *in vivo* in small cell lung cancer models and triggers less platelet toxicity compared to Navitoclax [147]. The authors claim that this is because the drug on its own is poorly permeable but is converted to an active metabolite particularly in the tumor cells. This metabolite effectively reduces tumor growth while hardly being detected in the plasma, thereby avoiding toxicity [147]. Further study is needed and will come from phase I clinical trials, which are currently ongoing for lung cancer and other solid tumors in several countries (NCT03387332, NCT03080311, NCT04001777) [148].

To circumvent the observed platelet toxicity of inhibiting BCL-XL, it was hypothesized that specifically targeting BCL-2 could provide a wider therapeutic window with fewer toxicities. This led to the development of ABT-199 or Venetoclax, the first BH3 mimetic to receive FDA approval for relapsed/refractory chronic lymphocytic leukemia (R/R CLL) [149]. This landmark drug registration was followed by two more FDA approvals for Venetoclax in combination therapy for patients with R/R CLL and treatment naïve acute myeloid leukemia (AML) [139]. More than 200 clinical trials, particularly for hematological malignancies, have since been conducted or are ongoing (see clinicaltrials.gov) [150]. S55746 is another BCL-2 specific inhibitor which demonstrates significant efficacy against BCL-2 dependent tumors *in vitro* and *in vivo* and has been tested in two clinical trials (NCT02920697, NCT02603445) [139]. The results of the dose-escalation study have been recently released which show that the trial had to be terminated as the target active exposure of the drug in patients was not reached.

Studies of Venetoclax in solid tumors are limited with so far a trial in combination with tamoxifen for estrogen receptor positive breast cancers (ISRCTN98335443) and three others in a range of solid tumors (NCT03000257, NCT04029688, NCT03082209). These trials will test Venetoclax efficacy in combination with diverse compounds, which include the trail receptor agonist ABBV-621, MDM2 inhibitor Idasanutlin and

anti-PD1 monoclonal antibody ABBV-181. Although there are promising indications for BCL-2 inhibition in solid tumors, anti-apoptotic adaptation is more closely associated with the overexpression of BCL-XL [151]. Several BCL-XL inhibitors have been designed and the first specific inhibitor, WEHI-539, binds to BCL-XL with high selectivity and affinity [152]. Since then, further efforts led to the design of A-1155463 and A-1331852, two far more potent inhibitors of which the latter is also orally bio-available [153, 154]. Studies show promise for these inhibitors alone and in combination for treatment of solid tumors [153, 155]. A-1331852 enhances the efficacy of docetaxel in a range of solid tumors including breast cancer, NSCLC, and ovarian cancer both *in vitro* and *in vivo* [155]. In addition to this efficacy, BCL-XL inhibition does not result in neutropenia, which is a common toxicity of Venetoclax, shown to result from BCL-2 inhibition specifically [155]. While both these inhibitors induce platelet toxicity *in vivo*, this toxicity is reversible and therefore could be overcome by proper dosing strategies [153, 155]. These promising inhibitors are yet to enter clinical trials.

In the wake of inhibitors targeting BCL-2 and BCL-XL, MCL-1 is emerging as an increasingly promising target given its role in malignant cell survival and resistance to various anti-cancer therapies. Several tumor types show heterogeneous dependence on MCL-1 including breast, lung, multiple myeloma (MM) and MYC-driven lymphomas [139]. Interestingly, there is evidence of MCL-1 expression levels increasing upon treatment with ABT-737 and this is implicated in resistance to other BH3 mimetics such as Navitoclax and Venetoclax, which do not inhibit MCL-1 [156, 157]. MCL-1 is also involved in resistance to various chemotherapeutics, making it a promising target for combination and second-line treatment in resistant tumors [158, 159]. MCL-1 has proven far more difficult to target and only recently, successful specific inhibition has been achieved by BH3 mimetics such as A-1210477, UMI-77, S63845, AZD-5991 and AMG176 [160]. A-1210477 shows *in vitro* efficacy against a range of cancer cell lines while UMI-77 is effective *in vitro* and *in vivo* against pancreatic and breast cancers [161, 162]. AMG176 is the first MCL-1 inhibitor to enter a clinical trial for MM and AML (NCT02675452) [163]. It is also being tested

in combination with Venetoclax for AML and non-Hodgkin's lymphoma (NHL) (NCT03797261). A similar Amgen MCL-1 inhibitor, AMG-397, is also being tested in the clinic for MM, AML and NHL (NCT03465540) [160]. However, trials for both these inhibitors have been recently suspended due to potential cardiac toxicity. Another MCL-1 specific inhibitor AZD-5991 shows significant anti-tumor activity *in vivo* with complete regression in mouse models of MM and AML, based on which a phase I clinical trial has been set up for patients with hematological malignancies (NCT03218683) [164]. A highly potent derivative of S63845 called S64315/MIK655 shows substantial *in vivo* activity against MM, AML and MYC-driven lymphomas and is also being tested in clinical trials for these malignancies as a monotherapy (NCT02992483, NCT02979366) and in combination with Venetoclax (NCT03672695) [165].

The approval of Venetoclax has heralded a new era of significant progress in therapeutic targeting of anti-apoptotic BCL-2 proteins (Fig.3). A major challenge in the clinical application of these inhibitors is to predict the appropriate anti-apoptotic molecules to inhibit in a context-dependent and perhaps even a personalized manner. Dynamic BH3 profiling is one such technique that not only predicts the anti-apoptotic dependencies of a tumor, but also predicts response to various chemotherapeutics [18]. In this technique, control vs. drug-treated tumor cells are incubated with BH3 peptides that have specific anti-apoptotic binding partners (Fig.2). Subsequent retention of cytochrome c is measured to assess the overall efficacy of the compound and the possible anti-apoptotic proteins that the tumor depends on. Such insight can not only predict treatment response in patients, but also greatly benefit the rationalized use of BH3-mimetics for treatment. Overall, these inhibitors not only show great promise for cancer therapy but also serve as invaluable tools for understanding the ever-changing anti-apoptotic landscape of this disease.

BH3 mimetics for CRC therapy

While there are no CRC specific clinical trials testing the efficacy of BH3 mimetics, there is compelling evidence for the use of these inhibitors in

CRC treatment. De-regulated expression of anti-apoptotic proteins is observed in all stages of CRC development and these changes can guide the use of BH3 mimetics for treatment. A recent study conducted in a panel of diverse cell lines finds that BCL-2 dependence directly correlates with BCL-2 expression levels, such that high expressers are more sensitive to ABT-199 treatment [166]. BCL-2 is expressed in crypt stem cells and plays a critical role in facilitating intestinal stem cell transformation and adenoma survival [94]. Treatment with ABT-199 while intestinal stem cells are undergoing APC deletion and hence transformation strongly impairs adenoma outgrowth, which suggests that BCL-2 is a potential target for CRC chemoprevention in patients with high risk conditions such as familial adenomatous polyposis [94]. However, BCL-2 expression is gradually lost as the disease progresses and most CRC cell lines are insensitive to ABT-199 [166]. Colon CSCs, which are particularly chemo-resistant, no longer express any BCL-2 and do not respond to ABT-199 treatment [116].

Considering the high levels of BCL-XL found in most CRC tissues, it has been a target of prime interest for CRC treatment [90, 96, 115]. Indeed the same colon CSCs that do not respond to BCL-2 inhibition are very sensitive to BCL-XL specific inhibitor WEHI-539, which impairs CSC clonogenicity and enhances the efficacy of chemotherapy [116]. The dual inhibitor ABT-737 also potently induces cell death in these CSCs while also showing efficacy on CRC ex vivo tissue and cell lines in combination with diverse chemotherapies [96, 116, 167, 168]. Several studies indicate that the efficacy of ABT-737, or its orally bioavailable counterpart ABT-263, in solid tumors is primarily due to the inhibition of BCL-XL [96, 116, 155]. The efficacy of BCL-XL inhibition is closely associated with MCL-1 activity, in particular predicted by NOXA expression which specifically inhibits MCL-1 [166]. Cells that express high level of NOXA either basally or induced by other therapies show increased sensitivity to BCL-XL inhibition by A-1155463 and ABT-737 [115, 169]. This suggests that concurrent treatment with MCL-1 inhibitors might potentiate the effect of BCL-XL inhibition in tumors that either present with high MCL-1 or low NOXA levels [170, 171]. In a CRC cell line HCT116, treatment with A-1155463 alone was sufficient

to induce apoptosis, while MCL-1 inhibitor S63845 alone did not induce any apoptosis. However, combining the two compounds resulted in more pronounced apoptosis even in the absence of all BH3-only proteins, in a BAX dependent manner [170].

Taken together, these pre-clinical data suggest that BH3 mimetics hold great promise for CRC treatment. Early stage high risk adenomas that express BCL-2 might benefit from BCL-2 inhibition with ABT-199, thus preventing tumor progression. On the other hand treatment of more advanced carcinomas with BCL-XL specific inhibitors, perhaps in combination with MCL-1 inhibition might prove more effective. The main hindrance for the use BCL-XL inhibitors in clinical practice is the observed thrombocytopenia, as BCL-XL regulates platelet lifespan [146]. This can be managed by appropriate dosing strategies, particularly by using lower doses of the inhibitors in synergistic combinations with other chemotherapeutics [139]. Pre-clinical studies that test such possibilities would greatly aid the advancement of the use of BH3 mimetics in CRC therapy.

Conclusions and scope of this thesis

Recent findings have provided novel insights into the interactions of the BCL-2 family members that regulate the intrinsic pathway of apoptosis. Although the intricacies of this regulation are complex and still a matter of intense debate, it is clear that this family of proteins has an important role to play in homeostasis and tumorigenesis in the colon. De-regulation of the BCL-2 family occurs through various mechanisms and many CRC tumors show dependence on different anti-apoptotic proteins through different stages of the disease, making them a promising target for therapy. BH3 mimetics show potent induction of apoptosis *in vitro* and *in vivo* in various models. While BCL-2 inhibition can inhibit early adenoma outgrowth, CRC tumors respond well to BCL-XL specific inhibition, more so in combination with Mcl-1 inhibition. Implementing strategies to reduce the toxicities associated with these inhibitors and determining the appropriate BH3

mimetic to administer in a context-dependent and personalized manner (for example with dynamic BH3 profiling) could help untap the full potential of these novel inhibitors in CRC treatment.

This thesis explores the role of BCL-2 family regulated cell death in CRC. In **Chapter 2**, we establish and characterize models to assess anti-apoptotic dependencies in intestinal stem cells. In **Chapter 3**, we employ these methods to elucidate BCL-2 family protein reliance in organoid models that reflect the progression pathway of CRC. Thereby, we establish BCL-XL to be crucial for CRC progression, which presents a key vulnerability of the disease and therefore also a valuable therapeutic target. Based on these findings, in **Chapter 4**, we performed a high throughput drug screen, which identified kinase targets that synergize with BCL-XL inhibition to target colon cancer stem cells. More importantly, we elucidate a novel resistance mechanism that is rapidly activated upon BH3 mimetic treatment and is mediated by FGFR4 signaling induced MCL-1 expression. In **Chapter 5**, we evaluate BCL-2 family dependencies in a panel of CRC cell lines, thereby assessing molecular features that could predict sensitivity to specific BH3 mimetics. Lastly, in **Chapter 6**, we integrate the findings outlined in this thesis and discuss their implications for our understanding of cell death regulation in CRC development, progression and therapy response.

References

1. Kerr, J.F., A.H. Wyllie, and A.R. Currie, Apoptosis: a basic biological phenomenon with wide-ranging implications in tissue kinetics. Br J Cancer, 1972. 26(4): p. 239-57.
2. Horvitz, H.R., Genetic control of programmed cell death in the nematode Caenorhabditis elegans. Cancer Res, 1999. 59(7 Suppl): p. 1701s-1706s.
3. Opferman, J.T., Attacking cancer's Achilles heel: antagonism of anti-apoptotic BCL-2 family members. Febs j, 2016. 283(14): p. 2661-75.
4. Elmore, S., Apoptosis: a review of programmed cell death. Toxicol Pathol, 2007. 35(4): p. 495-516.
5. Singh, R., A. Letai, and K. Sarosiek, Regulation of apoptosis in health and disease: the balancing act of BCL-2 family proteins. Nat Rev Mol Cell Biol, 2019. 20(3): p. 175-193.
6. Zhang, L. and J. Yu, Role of apoptosis in colon cancer biology, therapy, and prevention. Curr Colorectal Cancer Rep, 2013. 9(4).
7. Ramachandran, A., M. Madesh, and K.A. Balasubramanian, Apoptosis in the intestinal epithelium: its relevance in normal and pathophysiological conditions. J Gastroenterol Hepatol, 2000. 15(2): p. 109-20.
8. McDonnell, T.J. and S.J. Korsmeyer, Progression from lymphoid hyperplasia to high-grade malignant lymphoma in mice transgenic for the t(14; 18). Nature, 1991. 349(6306): p. 254-6.
9. Vaux, D.L., S. Cory, and J.M. Adams, Bcl-2 gene promotes haemopoietic cell survival and cooperates with c-myc to immortalize pre-B cells. Nature, 1988. 335(6189): p. 440-2.
10. Hockenbery, D., et al., Bcl-2 is an inner mitochondrial membrane protein that blocks programmed cell death. Nature, 1990. 348(6299): p. 334-6.
11. Strasser, A., et al., Novel primitive lymphoid tumours induced in transgenic mice by cooperation between myc and bcl-2. Nature, 1990. 348(6299): p. 331-3.
12. Oltvai, Z.N., C.L. Milliman, and S.J. Korsmeyer, Bcl-2 heterodimerizes in vivo with a conserved homolog, Bax, that accelerates programmed cell death. Cell, 1993. 74(4): p. 609-19.
13. Boise, L.H., et al., bcl-x, a bcl-2-related gene that functions as a dominant regulator of apoptotic cell death. Cell, 1993. 74(4): p. 597-608.
14. Kozopas, K.M., et al., MCL1, a gene expressed in programmed myeloid cell differentiation, has sequence similarity to BCL2. Proc Natl Acad Sci U S A, 1993. 90(8): p. 3516-20.
15. Lin, E.Y., et al., A1, a Bcl-2 family member, prolongs cell survival and permits myeloid differentiation. Blood, 1996. 87(3): p. 983-92.
16. O'Connor, L., et al., Bim: a novel member of the Bcl-2 family that promotes apoptosis. Embo j, 1998. 17(2): p. 384-95.
17. Campbell, K.J. and S.W.G. Tait, Targeting BCL-2 regulated apoptosis in cancer. Open Biol, 2018. 8(5).
18. Montero, J. and A. Letai, Why do BCL-2 inhibitors work and where should we use them in the clinic? Cell Death Differ, 2018. 25(1): p. 56-64.
19. Einsele-Scholz, S., et al., Bok is a genuine multi-BH-domain protein that triggers apoptosis in the absence of Bax and Bak. J Cell Sci, 2016. 129(11): p. 2213-23.

20. Llambi, F., et al., BOK Is a Non-canonical BCL-2 Family Effector of Apoptosis Regulated by ER-Associated Degradation. Cell, 2016. 165(2): p. 421-33.
21. Brem, E.A. and A. Letai, BOK: Oddball of the BCL-2 Family. Trends Cell Biol, 2016. 26(6): p. 389-390.
22. Sattler, M., et al., Structure of Bcl-xL-Bak peptide complex: recognition between regulators of apoptosis. Science, 1997. 275(5302): p. 983-6.
23. Liu, X., et al., The structure of a Bcl-xL/Bim fragment complex: implications for Bim function. Immunity, 2003. 19(3): p. 341-52.
24. Edlich, F., et al., Bcl-x(L) retrotranslocates Bax from the mitochondria into the cytosol. Cell, 2011. 145(1): p. 104-16.
25. Schellenberg, B., et al., Bax exists in a dynamic equilibrium between the cytosol and mitochondria to control apoptotic priming. Mol Cell, 2013. 49(5): p. 959-71.
26. Todt, F., et al., Differential retrotranslocation of mitochondrial Bax and Bak. Embo j, 2015. 34(1): p. 67-80.
27. Westphal, D., R.M. Kluck, and G. Dewson, Building blocks of the apoptotic pore: how Bax and Bak are activated and oligomerize during apoptosis. Cell Death Differ, 2014. 21(2): p. 196-205.
28. Letai, A., et al., Distinct BH3 domains either sensitize or activate mitochondrial apoptosis, serving as prototype cancer therapeutics. Cancer Cell, 2002. 2(3): p. 183-92.
29. Merino, D., et al., The role of BH3-only protein Bim extends beyond inhibiting Bcl-2-like prosurvival proteins. J Cell Biol, 2009. 186(3): p. 355-62.
30. Sarosiek, K.A., et al., BID preferentially activates BAK while BIM preferentially activates BAX, affecting chemotherapy response. Mol Cell, 2013. 51(6): p. 751-65.
31. Chen, H.C., et al., An interconnected hierarchical model of cell death regulation by the BCL-2 family. Nat Cell Biol, 2015. 17(10): p. 1270-81.
32. Dai, H., et al., Transient binding of an activator BH3 domain to the Bak BH3-binding groove initiates Bak oligomerization. J Cell Biol, 2011. 194(1): p. 39-48.
33. Kim, H., et al., Hierarchical regulation of mitochondrion-dependent apoptosis by BCL-2 subfamilies. Nat Cell Biol, 2006. 8(12): p. 1348-58.
34. Du, H., et al., BH3 domains other than Bim and Bid can directly activate Bax/Bak. J Biol Chem, 2011. 286(1): p. 491-501.
35. Llambi, F., et al., A unified model of mammalian BCL-2 protein family interactions at the mitochondria. Mol Cell, 2011. 44(4): p. 517-31.
36. Andreu-Fernandez, V., et al., Bax transmembrane domain interacts with prosurvival Bcl-2 proteins in biological membranes. Proc Natl Acad Sci U S A, 2017. 114(2): p. 310-315.
37. O'Neill, K.L., et al., Inactivation of prosurvival Bcl-2 proteins activates Bax/Bak through the outer mitochondrial membrane. Genes Dev, 2016. 30(8): p. 973-88.
38. Hsu, S.Y., et al., Bok is a pro-apoptotic Bcl-2 protein with restricted expression in reproductive tissues and heterodimerizes with selective anti-apoptotic Bcl-2 family members. Proc Natl Acad Sci U S A, 1997. 94(23): p. 12401-6.
39. Zheng, J.H., et al., Intrinsic Instability of BOK Enables Membrane Permeabilization in Apoptosis. Cell Rep, 2018. 23(7): p. 2083-2094.e6.
40. Carpio, M.A., et al., BCL-2 family member BOK promotes apoptosis in response to endoplasmic reticulum stress. Proc Natl Acad Sci U S A, 2015. 112(23): p. 7201-6.
41. Kuwana, T., et al., BH3 domains of BH3-only proteins differentially regulate Bax-mediated mitochondrial membrane permeabilization both directly and indirectly. Mol

Cell, 2005. 17(4): p. 525-35.
42. Chen, L., et al., Differential targeting of prosurvival Bcl-2 proteins by their BH3-only ligands allows complementary apoptotic function. Mol Cell, 2005. 17(3): p. 393-403.
43. Lopez, J., et al., Mito-priming as a method to engineer Bcl-2 addiction. Nat Commun, 2016. 7: p. 10538.
44. Willis, S.N., et al., Proapoptotic Bak is sequestered by Mcl-1 and Bcl-xL, but not Bcl-2, until displaced by BH3-only proteins. Genes Dev, 2005. 19(11): p. 1294-305.
45. Tait, S.W. and D.R. Green, Mitochondrial regulation of cell death. Cold Spring Harb Perspect Biol, 2013. 5(9).
46. Kluck, R.M., et al., The release of cytochrome c from mitochondria: a primary site for Bcl-2 regulation of apoptosis. Science, 1997. 275(5303): p. 1132-6.
47. Liu, X., et al., Induction of apoptotic program in cell-free extracts: requirement for dATP and cytochrome c. Cell, 1996. 86(1): p. 147-57.
48. Bossy-Wetzel, E., D.D. Newmeyer, and D.R. Green, Mitochondrial cytochrome c release in apoptosis occurs upstream of DEVD-specific caspase activation and independently of mitochondrial transmembrane depolarization. Embo j, 1998. 17(1): p. 37-49.
49. Maas, C., et al., Smac/DIABLO release from mitochondria and XIAP inhibition are essential to limit clonogenicity of Type I tumor cells after TRAIL receptor stimulation. Cell Death Differ, 2010. 17(10): p. 1613-23.
50. Brunet, C.L., et al., Commitment to cell death measured by loss of clonogenicity is separable from the appearance of apoptotic markers. Cell Death Differ, 1998. 5(1): p. 107-15.
51. Lartigue, L., et al., Caspase-independent mitochondrial cell death results from loss of respiration, not cytotoxic protein release. Mol Biol Cell, 2009. 20(23): p. 4871-84.
52. Tait, S.W., et al., Resistance to caspase-independent cell death requires persistence of intact mitochondria. Dev Cell, 2010. 18(5): p. 802-13.
53. Green, D.R., The Coming Decade of Cell Death Research: Five Riddles. Cell, 2019. 177(5): p. 1094-1107.
54. Sun, G., et al., A molecular signature for anastasis, recovery from the brink of apoptotic cell death. J Cell Biol, 2017. 216(10): p. 3355-3368.
55. Ding, A.X., et al., CasExpress reveals widespread and diverse patterns of cell survival of caspase-3 activation during development in vivo. Elife, 2016. 5.
56. Ichim, G., et al., Limited mitochondrial permeabilization causes DNA damage and genomic instability in the absence of cell death. Mol Cell, 2015. 57(5): p. 860-872.
57. Liu, X., et al., Caspase-3 promotes genetic instability and carcinogenesis. Mol Cell, 2015. 58(2): p. 284-96.
58. Giampazolias, E., et al., Mitochondrial permeabilization engages NF-kappaB-dependent anti-tumour activity under caspase deficiency. Nat Cell Biol, 2017. 19(9): p. 1116-1129.
59. Goldsmith, K.C., et al., Mitochondrial Bcl-2 family dynamics define therapy response and resistance in neuroblastoma. Cancer Res, 2012. 72(10): p. 2565-77.
60. Winter, P.S., et al., RAS signaling promotes resistance to JAK inhibitors by suppressing BAD-mediated apoptosis. Sci Signal, 2014. 7(357): p. ra122.
61. Maji, S., et al., Bcl-2 Antiapoptotic Family Proteins and Chemoresistance in Cancer. Adv Cancer Res, 2018. 137: p. 37-75.
62. Beroukhim, R., et al., The landscape of somatic copy-number alteration across human

cancers. Nature, 2010. 463(7283): p. 899-905.
63. Allen, J.C., et al., c-Abl regulates Mcl-1 gene expression in chronic lymphocytic leukemia cells. Blood, 2011. 117(8): p. 2414-22.
64. Catz, S.D. and J.L. Johnson, Transcriptional regulation of bcl-2 by nuclear factor kappa B and its significance in prostate cancer. Oncogene, 2001. 20(50): p. 7342-51.
65. Sevilla, L., et al., Transcriptional regulation of the bcl-x gene encoding the anti-apoptotic Bcl-xL protein by Ets, Rel/NFkappaB, STAT and AP1 transcription factor families. Histol Histopathol, 2001. 16(2): p. 595-601.
66. Cui, J. and W.J. Placzek, Post-Transcriptional Regulation of Anti-Apoptotic BCL2 Family Members. Int J Mol Sci, 2018. 19(1).
67. Kampen, K.R., et al., The ribosomal RPL10 R98S mutation drives IRES-dependent BCL-2 translation in T-ALL. Leukemia, 2019. 33(2): p. 319-332.
68. Dai, H., et al., Contribution of Bcl-2 phosphorylation to Bak binding and drug resistance. Cancer Res, 2013. 73(23): p. 6998-7008.
69. Kutuk, O. and A. Letai, Regulation of Bcl-2 family proteins by posttranslational modifications. Curr Mol Med, 2008. 8(2): p. 102-18.
70. Chonghaile, T.N., et al., Maturation stage of T-cell acute lymphoblastic leukemia determines BCL-2 versus BCL-XL dependence and sensitivity to ABT-199. Cancer Discov, 2014. 4(9): p. 1074-87.
71. Vogler, M., Targeting BCL2-Proteins for the Treatment of Solid Tumours. Adv Med, 2014. 2014: p. 943648.
72. de Jong, M.R.W., et al., Heterogeneous Pattern of Dependence on Anti-Apoptotic BCL-2 Family Proteins upon CHOP Treatment in Diffuse Large B-Cell Lymphoma. Int J Mol Sci, 2019. 20(23).
73. Leverson, J.D., et al., Found in Translation: How Preclinical Research Is Guiding the Clinical Development of the BCL2-Selective Inhibitor Venetoclax. Cancer Discov, 2017. 7(12): p. 1376-1393.
74. Egle, A., et al., Bim is a suppressor of Myc-induced mouse B cell leukemia. Proc Natl Acad Sci U S A, 2004. 101(16): p. 6164-9.
75. Oda, E., et al., Noxa, a BH3-only member of the Bcl-2 family and candidate mediator of p53-induced apoptosis. Science, 2000. 288(5468): p. 1053-8.
76. Nakano, K. and K.H. Vousden, PUMA, a novel proapoptotic gene, is induced by p53. Mol Cell, 2001. 7(3): p. 683-94.
77. Labi, V., et al., BH3-only proteins in cell death initiation, malignant disease and anticancer therapy. Cell Death Differ, 2006. 13(8): p. 1325-38.
78. Ouyang, H., et al., The BAX gene, the promoter of apoptosis, is mutated in genetically unstable cancers of the colorectum, stomach, and endometrium. Clin Cancer Res, 1998. 4(4): p. 1071-4.
79. Reichenbach, F., et al., Mitochondrial BAX Determines the Predisposition to Apoptosis in Human AML. Clin Cancer Res, 2017. 23(16): p. 4805-4816.
80. Kale, J., et al., Phosphorylation switches Bax from promoting to inhibiting apoptosis thereby increasing drug resistance. EMBO Rep, 2018. 19(9).
81. Ke, F., et al., BCL-2 family member BOK is widely expressed but its loss has only minimal impact in mice. Cell Death Differ, 2012. 19(6): p. 915-25.
82. Chu, J., et al., B-cell lymphoma 2 ovarian killer suppresses testicular cancer cell malignant behavior, but plays a role in platinum resistance. Anticancer Drugs, 2018.

29(9): p. 839-846.
83. Moravcikova, E., et al., BOK displays cell death-independent tumor suppressor activity in non-small-cell lung carcinoma. Int J Cancer, 2017. 141(10): p. 2050-2061.
84. Rabachini, T., et al., BOK promotes chemical-induced hepatocarcinogenesis in mice. Cell Death Differ, 2018. 25(4): p. 708-720.
85. Blander, J.M., On cell death in the intestinal epithelium and its impact on gut homeostasis. Curr Opin Gastroenterol, 2018. 34(6): p. 413-419.
86. Barker, N., et al., Identification of stem cells in small intestine and colon by marker gene Lgr5. Nature, 2007. 449(7165): p. 1003-7.
87. Blander, J.M., Death in the intestinal epithelium-basic biology and implications for inflammatory bowel disease. Febs j, 2016. 283(14): p. 2720-30.
88. Merritt, A.J., et al., Differential expression of bcl-2 in intestinal epithelia. Correlation with attenuation of apoptosis in colonic crypts and the incidence of colonic neoplasia. J Cell Sci, 1995. 108 (Pt 6): p. 2261-71.
89. Backus, H.H., et al., Differential expression of cell cycle and apoptosis related proteins in colorectal mucosa, primary colon tumours, and liver metastases. J Clin Pathol, 2002. 55(3): p. 206-11.
90. Maurer, C.A., et al., Apoptosis inhibiting factor Bcl-xL might be the crucial member of the Bcl-2 gene family in colorectal cancer. Dig Dis Sci, 1998. 43(12): p. 2641-8.
91. Wilson, J.W., et al., Bcl-w expression in colorectal adenocarcinoma. Br J Cancer, 2000. 82(1): p. 178-85.
92. Pritchard, D.M., et al., Bcl-w is an important determinant of damage-induced apoptosis in epithelia of small and large intestine. Oncogene, 2000. 19(34): p. 3955-9.
93. Liu, L.U., et al., Human right and left colon differ in epithelial cell apoptosis and in expression of Bak, a pro-apoptotic Bcl-2 homologue. Gut, 1999. 45(1): p. 45-50.
94. van der Heijden, M., et al., Bcl-2 is a critical mediator of intestinal transformation. Nat Commun, 2016. 7: p. 10916.
95. Pritchard, D.M., et al., Damage-induced apoptosis in intestinal epithelia from bcl-2-null and bax-null mice: investigations of the mechanistic determinants of epithelial apoptosis in vivo. Oncogene, 1999. 18(51): p. 7287-93.
96. Scherr, A.L., et al., Bcl-xL is an oncogenic driver in colorectal cancer. Cell Death Dis, 2016. 7(8): p. e2342.
97. Duckworth, C.A. and D.M. Pritchard, Suppression of apoptosis, crypt hyperplasia, and altered differentiation in the colonic epithelia of bak-null mice. Gastroenterology, 2009. 136(3): p. 943-52.
98. Bedi, A., et al., Inhibition of apoptosis during development of colorectal cancer. Cancer Res, 1995. 55(9): p. 1811-6.
99. Krajewska, M., et al., Elevated expression of Bcl-X and reduced Bak in primary colorectal adenocarcinomas. Cancer Res, 1996. 56(10): p. 2422-7.
100. Hawkins, N., et al., Pathological and genetic correlates of apoptosis in the progression of colorectal neoplasia. Tumour Biol, 1997. 18(3): p. 146-56.
101. Kaklamanis, L., et al., Early expression of bcl-2 protein in the adenoma-carcinoma sequence of colorectal neoplasia. J Pathol, 1996. 179(1): p. 10-4.
102. Watson, A.J., et al., Evidence of reciprocity of bcl-2 and p53 expression in human colorectal adenomas and carcinomas. Br J Cancer, 1996. 73(8): p. 889-95.
103. Kikuchi, Y., W.N. Dinjens, and F.T. Bosman, Proliferation and apoptosis in proliferative

lesions of the colon and rectum. Virchows Arch, 1997. 431(2): p. 111-7.
104. Nakamura, T., T. Sakai, and S. Nariya, Cell death in colorectal polyps as evaluated by in situ 3'-tailing reaction and its relationship to BCL-2 expression. Pathol Int, 1995. 45(10): p. 721-8.
105. Flohil, C.C., P.A. Janssen, and F.T. Bosman, Expression of Bcl-2 protein in hyperplastic polyps, adenomas, and carcinomas of the colon. J Pathol, 1996. 178(4): p. 393-7.
106. Sinicrope, F.A., et al., bcl-2 and p53 oncoprotein expression during colorectal tumorigenesis. Cancer Res, 1995. 55(2): p. 237-41.
107. Bronner, M.P., et al., The bcl-2 proto-oncogene and the gastrointestinal epithelial tumor progression model. Am J Pathol, 1995. 146(1): p. 20-6.
108. Qiu, W., et al., PUMA suppresses intestinal tumorigenesis in mice. Cancer Res, 2009. 69(12): p. 4999-5006.
109. Rosen, K., et al., Downregulation of the pro-apoptotic protein Bak is required for the ras-induced transformation of intestinal epithelial cells. Curr Biol, 1998. 8(24): p. 1331-4.
110. Nguyen, P.M., et al., Loss of Bcl-G, a Bcl-2 family member, augments the development of inflammation-associated colorectal cancer. Cell Death Differ, 2020. 27(2): p. 742-757.
111. Guo, B., A. Godzik, and J.C. Reed, Bcl-G, a novel pro-apoptotic member of the Bcl-2 family. J Biol Chem, 2001. 276(4): p. 2780-5.
112. Fearon, E.R. and B. Vogelstein, A genetic model for colorectal tumorigenesis. Cell, 1990. 61(5): p. 759-67.
113. Ofner, D., et al., Immunohistochemically detectable bcl-2 expression in colorectal carcinoma: correlation with tumour stage and patient survival. Br J Cancer, 1995. 72(4): p. 981-5.
114. Zhang, Y.L., et al., Significance of Bcl-xL in human colon carcinoma. World J Gastroenterol, 2008. 14(19): p. 3069-73.
115. Zhang, H., et al., Genomic analysis and selective small molecule inhibition identifies BCL-X(L) as a critical survival factor in a subset of colorectal cancer. Mol Cancer, 2015. 14: p. 126.
116. Colak, S., et al., Decreased mitochondrial priming determines chemoresistance of colon cancer stem cells. Cell Death Differ, 2014. 21(7): p. 1170-7.
117. Adams, K.W. and G.M. Cooper, Rapid turnover of mcl-1 couples translation to cell survival and apoptosis. J Biol Chem, 2007. 282(9): p. 6192-200.
118. Maurer, U., et al., Glycogen synthase kinase-3 regulates mitochondrial outer membrane permeabilization and apoptosis by destabilization of MCL-1. Mol Cell, 2006. 21(6): p. 749-60.
119. Tong, J., et al., FBW7 mutations mediate resistance of colorectal cancer to targeted therapies by blocking Mcl-1 degradation. Oncogene, 2017. 36(6): p. 787-796.
120. Tong, J., et al., Mcl-1 Degradation Is Required for Targeted Therapeutics to Eradicate Colon Cancer Cells. Cancer Res, 2017. 77(9): p. 2512-2521.
121. Schwickart, M., et al., Deubiquitinase USP9X stabilizes MCL1 and promotes tumour cell survival. Nature, 2010. 463(7277): p. 103-7.
122. Sakamoto, I., et al., Mutational analysis of the BAK gene in 192 advanced gastric and colorectal cancers. Int J Mol Med, 2004. 13(1): p. 53-5.
123. Miquel, C., et al., Role of bax mutations in apoptosis in colorectal cancers with

microsatellite instability. Am J Clin Pathol, 2005. 123(4): p. 562-70.
124. Rampino, N., et al., Somatic frameshift mutations in the BAX gene in colon cancers of the microsatellite mutator phenotype. Science, 1997. 275(5302): p. 967-9.
125. Coppola, D., et al., Down-regulation of Bax-interacting factor-1 in colorectal adenocarcinoma. Cancer, 2008. 113(10): p. 2665-70.
126. Srivastava, R., et al., BCL-2 family protein BOK is a positive regulator of uridine metabolism in mammals. Proc Natl Acad Sci U S A, 2019. 116(31): p. 15469-15474.
127. Lee, J.W., et al., Inactivating mutations of proapoptotic Bad gene in human colon cancers. Carcinogenesis, 2004. 25(8): p. 1371-6.
128. Kim, M.R., et al., Pro-apoptotic PUMA and anti-apoptotic phospho-BAD are highly expressed in colorectal carcinomas. Dig Dis Sci, 2007. 52(10): p. 2751-6.
129. Jansson, A.K., et al., Noxa in colorectal cancer: a study on DNA, mRNA and protein expression. Oncogene, 2003. 22(30): p. 4675-8.
130. Abdel-Rahman, W., et al., Death pathway genes Fas (Apo-1/CD95) and Bik (Nbk) show no mutations in colorectal carcinomas. Cell Death Differ, 1999. 6(5): p. 387-8.
131. Obata, T., et al., Identification of HRK as a target of epigenetic inactivation in colorectal and gastric cancer. Clin Cancer Res, 2003. 9(17): p. 6410-8.
132. Sinicrope, F.A., et al., Proapoptotic Bad and Bid protein expression predict survival in stages II and III colon cancers. Clin Cancer Res, 2008. 14(13): p. 4128-33.
133. Krajewska, M., et al., Expression of Bcl-2 family member Bid in normal and malignant tissues. Neoplasia, 2002. 4(2): p. 129-40.
134. Stickles, X.B., et al., BAD-mediated apoptotic pathway is associated with human cancer development. Int J Mol Med, 2015. 35(4): p. 1081-7.
135. Khor, T.O., et al., Positive correlation between overexpression of phospho-BAD with phosphorylated Akt at serine 473 but not threonine 308 in colorectal carcinoma. Cancer Lett, 2004. 210(2): p. 139-50.
136. Hector, S. and J.H. Prehn, Apoptosis signaling proteins as prognostic biomarkers in colorectal cancer: a review. Biochim Biophys Acta, 2009. 1795(2): p. 117-29.
137. Lindner, A.U., et al., BCL-2 system analysis identifies high-risk colorectal cancer patients. Gut, 2017. 66(12): p. 2141-2148.
138. Lessene, G., P.E. Czabotar, and P.M. Colman, BCL-2 family antagonists for cancer therapy. Nat Rev Drug Discov, 2008. 7(12): p. 989-1000.
139. Ashkenazi, A., et al., From basic apoptosis discoveries to advanced selective BCL-2 family inhibitors. Nat Rev Drug Discov, 2017. 16(4): p. 273-284.
140. Oltersdorf, T., et al., An inhibitor of Bcl-2 family proteins induces regression of solid tumours. Nature, 2005. 435(7042): p. 677-81.
141. Tse, C., et al., ABT-263: a potent and orally bioavailable Bcl-2 family inhibitor. Cancer Res, 2008. 68(9): p. 3421-8.
142. Shoemaker, A.R., et al., Activity of the Bcl-2 family inhibitor ABT-263 in a panel of small cell lung cancer xenograft models. Clin Cancer Res, 2008. 14(11): p. 3268-77.
143. Ackler, S., et al., The Bcl-2 inhibitor ABT-263 enhances the response of multiple chemotherapeutic regimens in hematologic tumors in vivo. Cancer Chemother Pharmacol, 2010. 66(5): p. 869-80.
144. Chen, J., et al., The Bcl-2/Bcl-X(L)/Bcl-w inhibitor, navitoclax, enhances the activity of chemotherapeutic agents in vitro and in vivo. Mol Cancer Ther, 2011. 10(12): p. 2340-9.
145. Schoenwaelder, S.M., et al., Bcl-xL-inhibitory BH3 mimetics can induce a transient

thrombocytopathy that undermines the hemostatic function of platelets. Blood, 2011. 118(6): p. 1663-74.
146. Mason, K.D., et al., Programmed anuclear cell death delimits platelet life span. Cell, 2007. 128(6): p. 1173-86.
147. Bai, L., et al., 338 BM-1252 (APG-1252): a potent dual specific Bcl-2/Bcl-xL inhibitor that achieves complete tumor regression with minimal platelet toxicity. European Journal of Cancer, 2014. 50: p. 109-110.
148. Lakhani, N.J., et al., A phase I study of novel dual Bcl-2/Bcl-xL inhibitor APG-1252 in patients with advanced small cell lung cancer (SCLC) or other solid tumor. Journal of Clinical Oncology, 2018. 36(15_suppl): p. 2594-2594.
149. Souers, A.J., et al., ABT-199, a potent and selective BCL-2 inhibitor, achieves antitumor activity while sparing platelets. Nat Med, 2013. 19(2): p. 202-8.
150. Valentin, R., S. Grabow, and M.S. Davids, The rise of apoptosis: targeting apoptosis in hematologic malignancies. Blood, 2018. 132(12): p. 1248-1264.
151. Amundson, S.A., et al., An informatics approach identifying markers of chemosensitivity in human cancer cell lines. Cancer Res, 2000. 60(21): p. 6101-10.
152. Lessene, G., et al., Structure-guided design of a selective BCL-X(L) inhibitor. Nat Chem Biol, 2013. 9(6): p. 390-7.
153. Tao, Z.F., et al., Discovery of a Potent and Selective BCL-XL Inhibitor with in Vivo Activity. ACS Med Chem Lett, 2014. 5(10): p. 1088-93.
154. Koehler, M.F., et al., Structure-Guided Rescaffolding of Selective Antagonists of BCL-XL. ACS Med Chem Lett, 2014. 5(6): p. 662-7.
155. Leverson, J.D., et al., Exploiting selective BCL-2 family inhibitors to dissect cell survival dependencies and define improved strategies for cancer therapy. Sci Transl Med, 2015. 7(279): p. 279ra40.
156. Williams, M.M., et al., Key Survival Factor, Mcl-1, Correlates with Sensitivity to Combined Bcl-2/Bcl-xL Blockade. Mol Cancer Res, 2017. 15(3): p. 259-268.
157. van Delft, M.F., et al., The BH3 mimetic ABT-737 targets selective Bcl-2 proteins and efficiently induces apoptosis via Bak/Bax if Mcl-1 is neutralized. Cancer Cell, 2006. 10(5): p. 389-99.
158. Wertz, I.E., et al., Sensitivity to antitubulin chemotherapeutics is regulated by MCL1 and FBW7. Nature, 2011. 471(7336): p. 110-4.
159. Akagi, H., et al., Suppression of myeloid cell leukemia-1 (Mcl-1) enhances chemotherapy-associated apoptosis in gastric cancer cells. Gastric Cancer, 2013. 16(1): p. 100-10.
160. Hird, A.W. and A.E. Tron, Recent advances in the development of Mcl-1 inhibitors for cancer therapy. Pharmacol Ther, 2019. 198: p. 59-67.
161. Leverson, J.D., et al., Potent and selective small-molecule MCL-1 inhibitors demonstrate on-target cancer cell killing activity as single agents and in combination with ABT-263 (navitoclax). Cell Death Dis, 2015. 6: p. e1590.
162. Abulwerdi, F., et al., A novel small-molecule inhibitor of mcl-1 blocks pancreatic cancer growth in vitro and in vivo. Mol Cancer Ther, 2014. 13(3): p. 565-75.
163. Caenepeel, S., et al., AMG 176, a Selective MCL1 Inhibitor, Is Effective in Hematologic Cancer Models Alone and in Combination with Established Therapies. Cancer Discov, 2018. 8(12): p. 1582-1597.
164. Tron, A.E., et al., Discovery of Mcl-1-specific inhibitor AZD5991 and preclinical activity in multiple myeloma and acute myeloid leukemia. Nat Commun, 2018. 9(1): p. 5341.

165. Kotschy, A., et al., The MCL1 inhibitor S63845 is tolerable and effective in diverse cancer models. Nature, 2016. 538(7626): p. 477-482.
166. Soderquist, R.S., et al., Systematic mapping of BCL-2 gene dependencies in cancer reveals molecular determinants of BH3 mimetic sensitivity. Nat Commun, 2018. 9(1): p. 3513.
167. Huang, S. and F.A. Sinicrope, Celecoxib-induced apoptosis is enhanced by ABT-737 and by inhibition of autophagy in human colorectal cancer cells. Autophagy, 2010. 6(2): p. 256-69.
168. Raats, D.A., et al., Synergistic killing of colorectal cancer cells by oxaliplatin and ABT-737. Cell Oncol (Dordr), 2011. 34(4): p. 307-13.
169. Okumura, K., S. Huang, and F.A. Sinicrope, Induction of Noxa sensitizes human colorectal cancer cells expressing Mcl-1 to the small-molecule Bcl-2/Bcl-xL inhibitor, ABT-737. Clin Cancer Res, 2008. 14(24): p. 8132-42.
170. Greaves, G., et al., BH3-only proteins are dispensable for apoptosis induced by pharmacological inhibition of both MCL-1 and BCL-XL. Cell Death Differ, 2019. 26(6): p. 1037-1047.
171. Berger, S., et al., Computationally designed high specificity inhibitors delineate the roles of BCL2 family proteins in cancer. Elife, 2016. 5.

Chapter 2

Isolation, propagation and clonogenicity of intestinal stem cells

Prashanthi Ramesh, Aleksandar B Kirov, David J Huels and Jan Paul Medema

Published in *Methods in Molecular Biology, 2019.*

Abstract

Intestinal stem cell research has greatly aided our understanding of the biology of intestinal self-renewal, but has also shed light on the role of cancer stem cells (CSCs) in carcinogenesis, cancer growth and dissemination. With new possibilities for CSC targeting, there is a need to have established techniques for quantifying (cancer) stem cell clonogenicity, particularly in organoid cultures. Here we describe a detailed methodology for the isolation and expansion of mouse intestinal crypts from three different locations – the colon, proximal and distal small intestine. In addition, we describe techniques that allow measurement of stem cell clonogenicity and its manipulation using two approaches – organoid counting and immunohistochemistry.

Introduction

Multi-region sequencing of tumors reveals the presence of different sub-populations that constitute the heterogeneity observed in some cancers [1]. One of the major contributors to this intra-tumor heterogeneity is the presence of cancer stem cells (CSCs) at the apex of the hierarchical organization within tumors [1]. In colon cancer, CSCs have been identified and extensively studied with the help of specific markers (Lgr5, CD133, CD44 etc.) and are suggested to be responsible for tumor maintenance and propagation upon xeno-transplantation [2,3]. However, the nature, plasticity and microenvironmental regulation of CSCs still remains a topic of much debate.

Several studies have suggested CSCs to be therapy resistant, thereby contributing to disease relapse and metastasis [1,4,5].This understanding has fueled attempts to identify treatment opportunities to specifically target CSCs. This creates a need for established culture techniques where stem cells and their differentiated progeny can be faithfully represented in vitro. Crypts isolated from mouse and human intestines can be cultured in a 3D Matrigel matrix allowing stem cells to self-organize into mini-gut structures with crypt-villus physiology [6]. These so-called 'organoids' consist of Lgr5+ stem cells and differentiated enterocytes and secretory cells such as Goblet and Paneth cells [6]. Culturing these stem cells in the presence of Wnt-amplifier R-spondin, BMP inhibitor Noggin and EGF allows indefinite maintenance of organoids in vitro and transplantation in vivo [6,7].

In this chapter, we provide concise methods to study stem cells in crypts derived from genetically modified mouse models. In addition to the extraction of small intestine organoids, we also describe a method for the extraction and culture of mouse colon organoids. 3D culture in Matrigel requires adjustment of usual 2D culture protocols and assays for assessing stem cell sensitivities. In this regard, we outline protocols that allow measurement of treatment-induced changes in clonogenicity and stem

cell specific cell death. Unlike cell lines, seeding organoids is a challenge as the growing structures are often unequally divided between wells, which is further complicated by the fact that only a subset of the cells has the capacity to form new organoids. This experimental variation makes quantification of treatment effects unreliable, which can be overcome by seeding organoids as single cells. However, outgrowth of organoids from single cells is not always successful and requires more time. Here we describe a technique that allows measurement of organoid clonogenicity without having to grow them out from single cells.

Next to the direct measurement of clonogenicity, immunohistochemical analysis of organoids following treatment can provide insights into population specific treatment efficacy and changes in cellular states or compositions. Herein we provide a simple method that allows embedding of whole organoids into paraffin for sectioning and staining. These techniques described can be easily translated to human intestinal and other stem cell derived organoid cultures.

1. Materials

1.1 General equipment and material list

1. Laminar flow cabinet certified for handling biosafety level 2 (ESL-2) specimens.
2. Humidified tissue culture incubator capable for maintaining 37°C and 5% CO_2 atmosphere.
3. Low-speed centrifuge (e.g., Hettich Rotanta 460).
4. Inverted and phase contrast light microscopes equipped with 10x, 20x, and 40x magnification.
5. 4°C cold room.
6. Pipet-aid.
7. Tally counter.
8. Vortex.
9. Sterile disposables plastics: 100 µl filter tips, 1000 µl long reach pipette

tips (VWR), pipettes 1-, 2-, 5-, 10-, and 25 ml volume, 15 and 50 ml polypropylene sterile tubes (Falcon), 10 cm petri dish.

10. Cell culture vessels: 96-,48-, 24-, 12- wells adherent plate (Corning).

1.2 Reagents for mouse crypt isolation, culture and clonogenic assay

1. Sterile surgical tools for dissection (scissors, tweezers).
2. Fresh intestine derived from mice.
3. Sterile disposable plastics: 10 ml syringe, 15 and 50 ml poly-propylene sterile tubes (Falcon), 10 cm tissue culture dishes, 96-,48-, 24-, 12- wells adherent plate, 70 µm nylon mesh filter, glass coverslips.
4. Phosphate-Buffered Saline (PBS) without Ca^{2+} and Mg^{2+}
5. Penicillin-Streptomycin (ThermoFischer Scientific catalog # 15140122)
6. 0.5M EDTA (ThermoFischer Scientific catalog # 15575-020)
7. Advanced DMEM/ F12 (ADF) medium (ThermoFischer Scientific catalog #12634-010) (see Note 1).
8. Growth Factor Reduced Matrigel (Corning) (see Note 2).
9. See Table 1 for crypt culture medium.

1.3 Reagents for paraffin- embedding of organoids

1. Phosphate-Buffered Saline (PBS)
2. 4% Paraformaldehyde (PFA)
3. 100% and 70% Ethanol
4. Hematoxylin
5. Xylene
6. Tissue mold (stainless steel)
7. Tissue cassette
8. Paraffin and paraffin dispenser
9. Hot plate (for melting paraffin at 60°C)
10. Cold plate (for cooling paraffin at 4°C)
11. Disposable plastics: 12-, 24- well plates, transfer pipettes.

Table 1: Crypt culture medium

Component	Supplier	Stock solution	Working dilution	Storage
Mouse crypt culture medium				
Advanced DMEM/F12 (ADF medium)	ThermoFischer Scientific			4°C
B27 supplement	ThermoFischer Scientific	50x	1in 50	-20°C
N2 supplement	ThermoFischer Scientific	100x	1in 100	-20°C
GlutaMAX-I	ThermoFischer Scientific	100x (200mM)	1in 100	RT [a]
Hepes	ThermoFischer Scientific	1M	1 in 100	4°C
N-acetyl cysteine	Sigma-Aldrich	500mM	1 in 500	4°C
Antimycotic/Antibiotic	ThermoFischer Scientific	100x	1 in 100	-20°C
Mouse EGF	Tebu-BIO	500µg/ml	1in 10,000	-20°C
Noggin conditioned medium [b]			10%	-20°C
R-spondin conditioned medium [b]			20%	-20°C
Rock inhibitor [c]		10mM in H_20	1 in 1000	-20°C
CHIR-99021 [d]	Tebu-BIO	10mM in DMSO	1 in 3333.3	-20°C

a RT: room temperature b see Note 3 c see Note 4 d see Note 5

2. Methods

2.1 Isolation of crypts from mouse proximal and distal small intestine and colon

Unless otherwise stated all steps are carried out at room temperature in sterile conditions and the PBS is always supplemented with 50 U/ml

Penicillin and 50 µg/ml Streptomycin.

1. Carefully remove the small intestine from the mouse (see Note 6) and place it on a clean flat surface (see Note 7).
2. Using scissors cut the small intestine into 2 pieces: small intestinal proximal (SIP) and small intestinal distal (SID) (see Note 8; see Fig. 1). Place the two pieces into a new 10cm dish.
3. In a separate 10cm dish, cut and place the colon (see Note 9).
4. Flush all three pieces with 4°C PBS to remove any remaining feces (see Note 10).
5. Carefully cut the intestinal pieces longitudinally open with a sterile scissors (see Note 11) and open up the intestine so that the villi face upwards.
6. Gently scrape the villi off using a glass cover slip (see Note 12).
7. Cut the proximal and distal intestine into small pieces of approximately 0.5cm and transfer to two separate 50ml tubes containing approximately 10ml 4°C PBS. From this step onwards the intestinal pieces should be kept on ice.
8. Cut the colon longitudinally and then into small pieces of approximately 0.5cm. Then place in a new 50ml tube with 10ml 4°C PBS.
9. Perform the following steps separately for the SIP, SID and colon pieces.

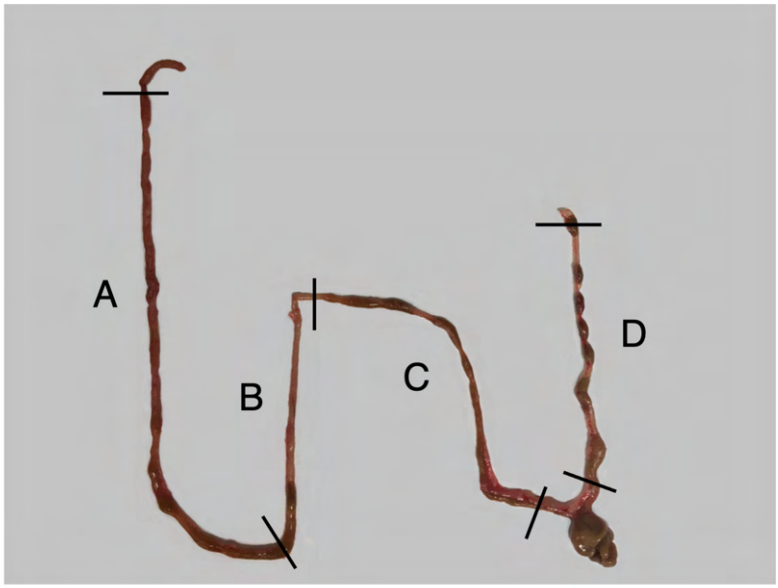

Figure 1. Dissection of the mouse intestine. Region A from the stomach border to the beginning of the Jejunum is the proximal small intestine (SIP). Region B denotes the medial small intestine and Region C from the Ileum to the Colon is the distal small intestine (SID). Region D from the caecum to the anus is the colon. The lines indicate points of division.

10. Wash the intestinal and colon pieces about 5- 10 times with 4°C PBS or until the supernatant is clear (see Note 13).
11. Resuspend the SIP, SID and colon in 25ml of respectively 2mM, 4mM and 25mM EDTA (see Note 14).
12. Place in cold room (4˚C) on a roller for 30 min.
13. Shake vigorously and collect the supernatant in a new 50 ml tube. Keep the supernatant aside on ice for the remaining steps (see Note 15).
14. Repeat washing steps of the pieces two to four times using 10ml 4°C PBS. After each wash collect the supernatant into the same 50 ml Falcon tube (see Note 16).
15. Strain the contents of the 50ml tube through a 70µm mesh filter into a new labelled 50ml tube.
16. Centrifuge the filtered supernatant at 600x g for 5 min.
17. Remove supernatant and wash the cell pellets one to two times with 15 ml 4°C ADF medium (see Note 17).
18. Count the number of crypts per isolation and in each well of a pre-heated 24 well plate (see Note 18) plate approximately 500 cells resuspended in 50µl Matrigel (see Note 19). Subsequently, add medium supplemented with all the growth factors.
19. After 2-3 days the crypts start to bud (see Fig. 2). Refresh the medium every 2-3 days and passage them on a weekly basis (see Note 20).

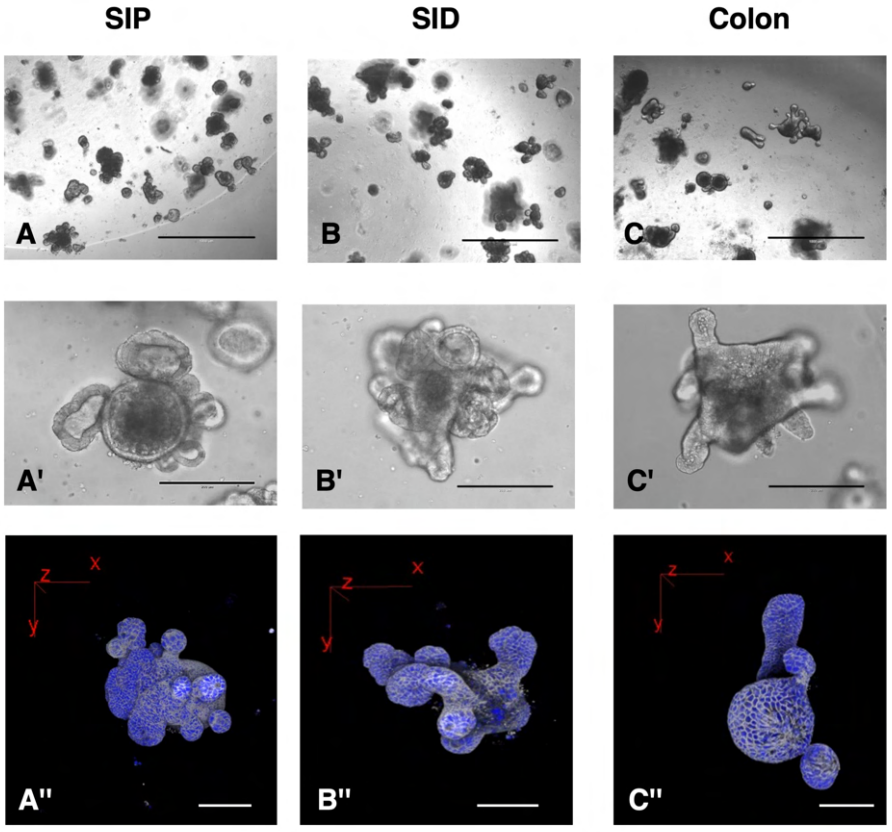

Figure 2. Phase contrast images of mouse organoids isolated from (A and A') Small intestine proximal, (B and B') Small intestine distal and (C and C') Colon. Top row images taken at 4X (Scale bars indicate 1000 µm) and middle row at 20X (Scale bars indicate 200 µm). 3D images assembled from z-stacks taken with confocal microscope of (A'') Small intestine proximal, (B'') Small intestine distal and (C'') Colon organoids stained for Actin with Actin-488 (white) and nuclei with Hoechst (blue) (Scale bar indicates 100 µm).

2.2 Passaging of mouse crypts from mouse colon, proximal and distal small intestine

All steps are performed in sterile conditions.

1. Remove medium from the well.
2. Using a long-reach pipette tip (p1000), pipette 1ml 4°C ADF into the well and collect the crypts by disrupting the Matrigel.

3. Pipette the crypts into a labelled 15ml tube and disrupt vigorously by pipetting up and down (see Note 21).
4. Add 2ml 4°C PBS to the tube and centrifuge at 600g for 3 min (see Note 22).
5. Remove as much supernatant as possible and resuspend the cells in Matrigel (see Note 19). The split ratio for the crypts cells is normally 1:3 (passage one well to three).
6. Allow Matrigel to solidify and then add medium with all the required growth factors (see Fig 3).

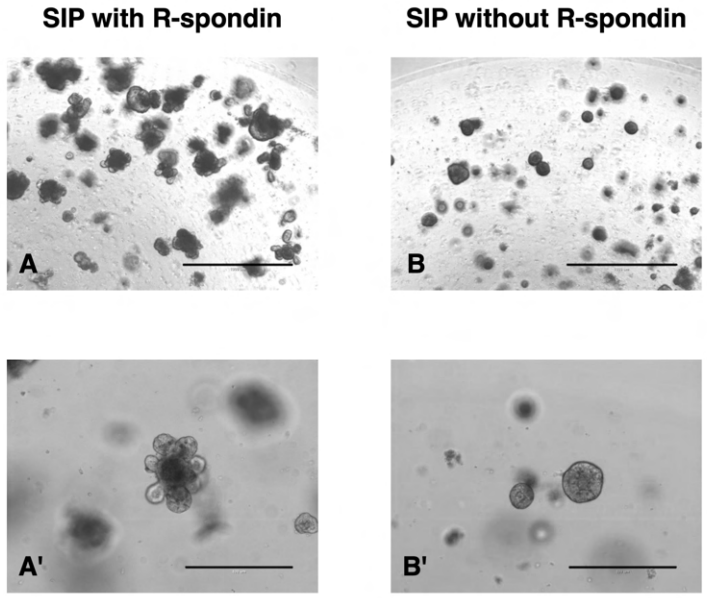

Figure 3. Growth factors are essential for organoid growth. When cultured with all required growth factors, SIP organoids maintain their budding morphology (A and A') and can be expanded over passages. Cultured in the absence of R-spondin (B and B'), this morphology is lost and they eventually die. Top row images taken at 4X magnification (Scale bars indicate 1000 μm), bottom row at 10X magnification (Scale bars indicate 400 μm).

2.3 Clonogenic assay

1. Collect and disrupt organoids in a 15ml tube as done while passaging.
2. Seed the disrupted organoids into the required number of wells of a 48 well plate (see Note 23).

3. After giving the organoid structures time to grow out (usually 3-4 days), count the number of crypts in each well (see Note 24) and treat them in triplicate.
4. After the desired treatment time, collect each well of organoids into labelled 15ml tubes and centrifuge at 600g for 3 min.
5. Remove the supernatant and seed each treatment condition of organoids to a new well of a pre-heated 24-well plate in 50 µl Matrigel (see Note 25).
6. After 3 to 4 days, count the number of organoids that grow out for each condition and replicate. By dividing the number of organoids growing out by the number of organoids originally present in the matched 48 well, we can estimate the clonogenic capacity of the organoids and also assess if a treatment positively or negatively affects the clonogenic population (see Fig 4).

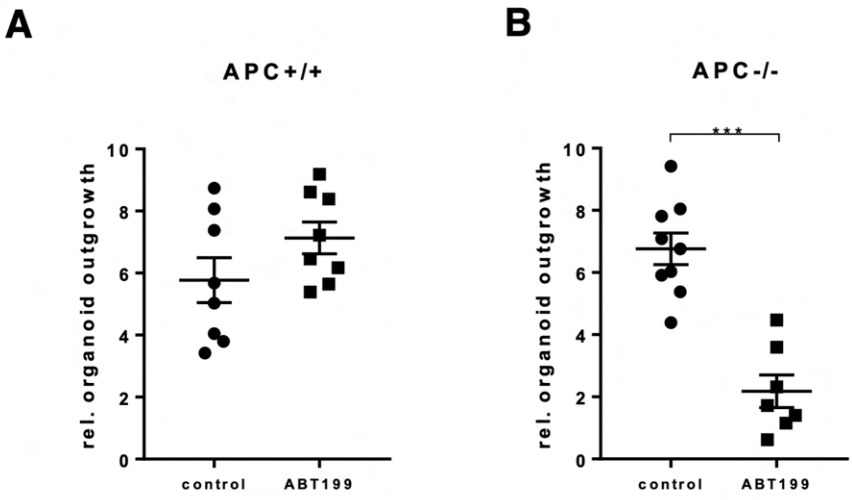

Figure 4. The clonogenic assay as a reliable read-out of stem cell dependencies. SIP organoids obtained from (A) Lgr5.Apc+/+ and (B) Lgr5. Apc-/- mice were treated for 72hr with BH3 mimetic ABT-199 (1µM). Graphs depict the relative outgrowth of organoids counted 3 days after passaging. APC mutant organoids are sensitive to ABT-199 as shown previously [8].

2.4 Paraffin embedding of organoids for IHC

1. Seed organoids in a 12 well plate (see Note 26).
2. After organoids have grown out, take off the medium and wash the wells twice with PBS without disrupting the Matrigel (see Note 27).
3. Add 4% paraformaldehyde and fix at 4°C overnight.
4. Bring the plate to room temperature (RT) for 30 minutes and remove the paraformaldehyde. Add 70% ethanol and incubate at RT for 30 minutes (see Note 28).
5. Remove the 70% Ethanol and add 100% ethanol containing hematoxylin (1:25 dilution). Incubate at RT for 10 to 20 minutes.
6. When the structures starts to become colored, take off the hematoxylin-ethanol and gently scrape off the Matrigel and transfer the pieces to a new labelled 24 well plate (see Note 29).
7. Incubate in hematoxylin-ethanol for another 10 minutes at RT.
8. Remove the hematoxylin-ethanol, add 500µl 100% ethanol and incubate at RT for 20 to 30 minutes. Repeat this step and incubate in 100% ethanol for another 20 to 30 minutes.
9. Transfer the Matrigel pieces to a metal tissue mold with a labelled tissue cassette.
10. Then remove the 100% ethanol and add 500µl xylene in the fume hood, incubate at RT for 20 to 30 minutes. Repeat this step and incubate in Xylene for another 20 to 30 minutes.
11. Remove the Xylene, add liquid paraffin to the metal tissue mold and incubate at 60°C for 20 to 30 minutes.
12. Remove the paraffin using transfer pipettes (see Note 30) and add fresh paraffin, incubate at 60°C for another 20 to 30 minutes.
13. Remove the paraffin using transfer pipettes and add fresh paraffin. Move the mold to the cold plate (see Note 31), place the tissue cassette on top and add some more paraffin to seal the mold. Let cool until the surface has solidified and store the block in -20°C.
14. Slides can be prepared from this block at 4µm thickness and stained as required (see Fig 5).

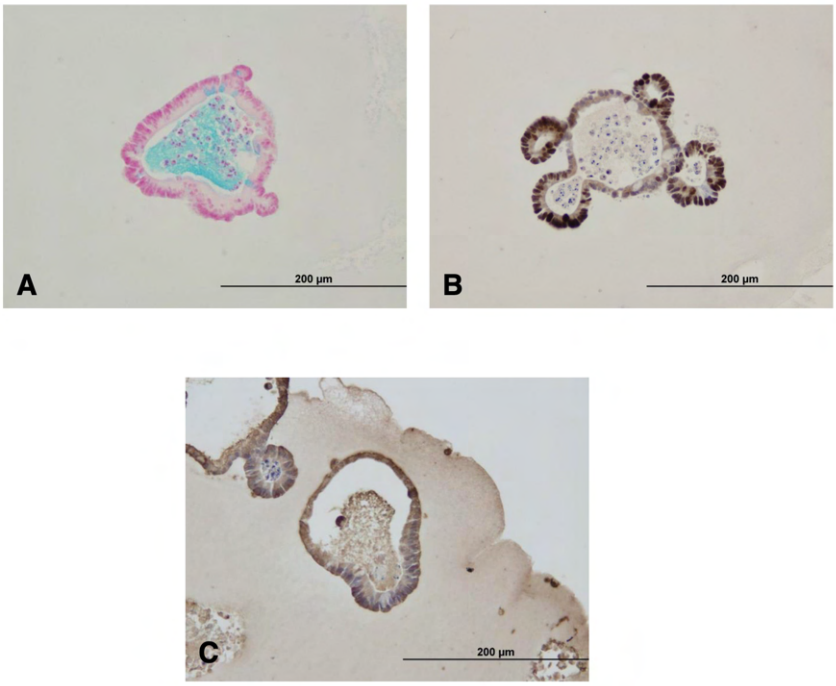

Figure 5. Immunohistochemical staining of organoids. Paraffin embedded organoids can be cut and stained for various markers. Depicted here are SIP organoids stained for Alcian blue and Nuclear Red (A), Ki67 (B) and EPCAM (C). Images taken at 20X (Scale bars indicate 200µm).

Notes

1. For the washing steps in the adenoma isolation procedure, ADF medium is used without any additional factors.
2. To shorten thawing time, we aliquot the Matrigel in 1 ml. Matrigel is thawed on ice at 4°C overnight or it can be placed on ice approximately 1 h before use.
3. We prepare our own R-spondin and Noggin conditioned medium.
4. Rock inhibitor is used to prevent anoikis and is only used when seeding freshly extracted crypts or when organoids are seeded single cell. After the first passage, there is no need to use this anymore.
5. CHIR-99021 is used only for the culture of colon-derived organoids.

Importantly, it is only necessary to use it immediately after passaging of the organoids and should be taken off after 2- 3 days in culture when refreshing the medium.

6. The easiest way to remove the intestine is to cut the junction between the stomach and the esophagus. Grab the stomach with forceps, gently lift and pull, as the stomach rises cut away the tissue attached to the intestine, without damaging the intestine. In this manner both the intestine and colon should untangle, making them easy to remove.
7. We find it easiest to use round 15 cm tissue culture dishes, as they are large enough to easily accommodate the mouse intestine and colon.
8. The proximal small intestine (SIP) refers to the distance from the stomach border with the duodenum to the beginning of the jejunum. The distal small intestine (SID) refers to the distance from the beginning of the ileum to the cecum. Roughly speaking the SIP is the first 6cm of intestine and SID is the last 5cm.
9. The colon refers to the region from the caecum to the anus.
10. For the flushing, the intestine / colon needs to be rinsed inside and out with 4°C PBS. We use a 0.5 x 16mm needle attached to a 10 ml syringe to flush the intestine. The stomach and caecum first need to be removed, by cutting at the attachment sites with the duodenum and colon respectively. The opening of the intestine or colon is then placed over the entry point of the needle and slowly the intestine is filled with PBS. It is important not to fill the intestine too quickly but rather allow the PBS to pass at a passive rate. By lifting the small intestine with the needle, gravity can help the PBS to pass at a passive rate.
11. By segmenting the intestine into three sections, the intestine is easier to cut open longitudinally.
12. The best way to do this is to place the glass cover slip close to where you are holding the beginning of the pieces. Gently press with the glass cover slip and slide towards the opposite end. A white residue should form at the edge of the cover slip, which contains the scraped off villi. This step is not necessary for the colon as it does not contain villi.
13. The washing is performed in order to remove remaining debris.

Antibiotics are included in the PBS in order to avoid bacterial contamination. When washing, shake the 50 ml tube vigorously for 5 seconds, allow adenoma pieces to settle and discard supernatant. Repeat this procedure by adding 10 ml 4˚C PBS.

14. The higher concentrations of EDTA improve crypt yields from the SID and Colon.
15. You may want to discard this supernatant as it usually does not contain most of the crypts.
16. At this point you should see the crypts floating around in the PBS after shaking. If you do not see this, incubate in EDTA for a longer time.
17. Pellet volumes generally range from 100 to 500 µl. If the pellet is small (<100 µl) wash once to avoid excessive cell loss. Extractions from SID often results in smaller pellets than SIP and Colon.
18. The 24-well plate is pre-heated for at least 1hr at 37°C. This helps the solidification of the Matrigel upon plating.
19. For suspension in Matrigel the cells need to be spun down (3 min, 600g) and the supernatant removed. Using 50 µl of Matrigel per well, resuspend the cells and drop the Matrigel in the center of the well. The plate is then placed at 37 °C for 10 to 20 min after which 500 µl of medium per well is added. Avoid making bubbles when resuspending the cells, as this can affect the visualization of structures in the Matrigel.
20. The frequency of passaging is dependent on the rate of crypt growth. Optimally, they should be passaged just before they become overly large, dense or filled with debris.
21. It is important to mechanically disrupt the structures as much as possible by pipetting up and down at least ten times. This can be done by placing the tip onto the plastic while pipetting in order to increase the pressure on the organoids, thereby dissociating them into smaller fragments. This helps to release them from the Matrigel and make them smaller, allowing further expansion.
22. After centrifugation the organoid fragments can be seen at the bottom of the tube. A separate transparent layer of Matrigel can be seen above the cells. The Matrigel can easily be aspired and removed.
23. It is best to seed the disrupted organoids at a density that is easy to

count. We usually seed around 20 – 40 organoids per wells. This can be achieved by either counting the number of fragments in the tube after isolation, or optimization and standardization of the dilution you need depending on the amount of organoids you start with.

24. It is important to keep track of the number of organoids in each well prior to treatment as this will allow normalization of the number of organoids growing out upon re-seeding.
25. The split ratio here is 1:2 to ensure the organoids have enough space to grow out and that counting does not become too difficult.
26. Organoids are seeded in 100µL Matrigel into a 12 well plate in order to have bigger pieces with more organoid structures per paraffin block.
27. Washing and fixing can also be done after any desired treatment conditions.
28. At this point, the plate can be stored in 70% ethanol at 4˚C for another week before embedding.
29. Using a p1000 tip scrape off the Matrigel droplet gently from the sides, trying as much as possible to maintain it in one or two pieces. Bigger pieces are easier to embed and also avoid loss of organoids during washes.
30. Cut the transfer pipettes at the bottom to make it easier to remove the paraffin.
31. It helps to hold the pieces down with a tweezer when placing the mold onto the cold spot as this ensures that the organoids are in approximately the same plane of the block.

Acknowledgements

This work was supported by Oncode Institute, Transcan-2 grant Tactic and Dutch Cancer Society (KWF) Grants UvA2015-7587 and 10150. D.J. Huels was supported by an EMBO long term fellowship ALTF 1102-2017.

References

1. Nassar D, Blanpain C (2016) Cancer stem cells: basic concepts and therapeutic implications. Annu Rev Pathol 11: 47-76
2. Medema JP (2013) Cancer stem cells: the challenges ahead. Nat Cell Biol 15: 338-44
3. Vermeulen L, Todaro M, de Sousa MF, Sprick MR, Kemper K et al (2008) Single-cell cloning of colon cancer stem cells reveals a multi-lineage differentiation capacity. Proc Natl Acad Sci USA 105:13427—13432
4. Oskarsson T, Batlle E, Massagué J (2014) Metastatic stem cells: sources, niches, and vital pathways. Cell Stem Cell 14(3):306-21
5. Colak S, Zimberlin CD, Fessler E, Hogdal L, Prasetyanti PR, et al (2014) Decreased mitochondrial priming determines chemoresistance of colon cancer stem cells. Cell Death Differentiation 21(7):1170-7
6. Sato T, Vries RG, Snippert HJ, van de Wetering M, Barker N, et al (2009) Single Lgr5 stem cells build crypt-villus structures in vitro without a mesenchymal niche. Nature 459:262–265
7. Yui S, Nakamura T, Sato T, Nemoto Y, Mizutani T et al (2012) Functional engraftment of colon epithelium expanded in vitro from a single adult Lgr5+ stem cell. Nat Med 18:618–623
8. Van Der Heijden, M., Zimberlin, C. D., Nicholson, A. M., Colak, S., Kemp, R et al (2016) Bcl-2 is a critical mediator of intestinal transformation. Nature communications 7, 10916

Chapter 3

BCL-XL is crucial for progression through the adenoma to carcinoma sequence of colorectal cancer

Prashanthi Ramesh, Tamsin R. M. Lannagan, Rene Jackstadt, Lidia Atencia Taboada, Nico Lansu, Pratyaksha Wirapati, Sander R. van Hooff, Danielle Dekker, Jessica Pritchard, Aleksandar B. Kirov, Sanne M. van Neerven, Sabine Tejpar, Geert J. P. L. Kops, Owen J. Sansom & Jan Paul Medema.

Published in *Cell Death and Differentiation, 2021.*

Abstract

Evasion of apoptosis is a hallmark of cancer, which is frequently mediated by upregulation of the anti-apoptotic BCL-2 family proteins. In colorectal cancer (CRC), previous work has highlighted differential anti-apoptotic protein dependencies determined by the stage of the disease. While intestinal stem cells (ISCs) require BCL-2 for adenoma outgrowth and survival during transformation, ISC-specific MCL1 deletion results in disturbed intestinal homeostasis, eventually contributing to tumorigenesis. Colon cancer stem cells (CSCs), however, no longer require BCL-2 and depend mainly on BCL-XL for their survival. We therefore hypothesized that a shift in anti-apoptotic protein reliance occurs in ISCs as the disease progresses from normal to adenoma to carcinoma. By targeting anti-apoptotic proteins with specific BH3 mimetics in organoid models of CRC progression, we found that BCL-2 is essential only during ISC transformation while MCL1 inhibition did not affect adenoma outgrowth. BCL-XL, on the other hand, was crucial for stem cell survival throughout the adenoma-to-carcinoma sequence. Furthermore, we identified that the limited window of BCL-2 reliance is a result of its downregulation by miR-17-5p, a microRNA that is upregulated upon APC-mutation driven transformation. Here we show that BCL-XL inhibition effectively impairs adenoma outgrowth *in vivo* and enhances the efficacy of chemotherapy. In line with this dependency, expression of *BCL-XL*, but not *BCL-2* or *MCL-1*, directly correlated to the outcome of chemotherapy-treated CRC patients. Our results provide insights to enable the rational use of BH3 mimetics in CRC management, particularly underlining the therapeutic potential of BCL-XL targeting mimetics in both early and late-stage disease.

Introduction

Intestinal homeostasis is tightly regulated by a balance between proliferation and apoptosis, with intestinal stem cells (ISCs) at the bottom of the crypt driving regeneration [1]. Disruption of this balance is an integral step in colorectal cancer (CRC) initiation and progression. The various pressures associated with oncogenic transformation can activate the apoptosis cascade as an anti-cancer defense mechanism. Deregulation of the apoptosis machinery to allow uncontrolled proliferation is therefore frequently observed in several tumor types, including CRC [2, 3].

Increasing the apoptotic threshold by modulating the expression or activity of the B-cell lymphoma-2 (BCL-2) family proteins is one such mechanism of evading cell death. The BCL-2 family consists of pro- and anti-apoptotic proteins whose interactions dictate whether a cell will undergo mitochondrial outer membrane permeabilization to ultimately activate caspases, the executors of apoptosis [4]. Not surprisingly, tumor cells frequently deregulate BCL-2 family proteins as a mechanism of survival and resistance [5-7]. While BCL-2 is required for apoptosis resistance in several hematological malignancies, amplification of MCL-1 and BCL-XL by chromosomal gain is a frequent alteration especially in solid tumors, making them promising targets for therapy [7]. Inhibiting anti-apoptotic proteins with so-called BH3 mimetics holds great promise for anti-cancer therapy, heralded by the remarkable results obtained with FDA-approved BCL-2 inhibitor Venetoclax (ABT-199), particularly in blood cancers [8].

Although there are promising indications for BCL-2 inhibition in solid tumors [9, 10], BCL-XL is more often found to be upregulated in these tumors and of all tumor types, amplification is most often detected in CRC [7, 11]. Several studies observe an increased expression of BCL-XL in CRC tumors in comparison to normal tissue, where it is crucial for tumor cell survival and resistance [11-15]. In this regard, we have previously shown that colon cancer stem cells (CSCs) present with an increased apoptotic threshold that renders them chemo-refractory, where CSC resistance stems

specifically from BCL-XL expression [16]. Interestingly, when analyzing factors that facilitate intestinal transformation, we identified BCL-2 as a critical mediator of this process [17]. ISC-specific knockdown of BCL-2 severely impaired adenoma outgrowth in mice, as did treatment with the specific inhibitor ABT-199 [17]. In the colon, loss of BCL-2 or BCL-XL does not impair intestinal homeostasis while recent data suggests that MCL1 deletion causes aberrant cell death, thereby prompting Wnt-dependent proliferation that eventually leads to tumor formation, indicating potential detrimental side-effects of targeting this protein [14, 17, 18].

To better assess the role of anti-apoptotic proteins in CRC progression, we made use of a panel of genetically-engineered colon organoids that reflect the classical progression pathway of CRC [19-21]. Clonogenic assays with specific BH3 mimetics revealed that ISCs require BCL-2 activity solely during transformation and that this dependence is lost quickly after, while MCL1 inhibition does not affect ISC clonogenicity and BCL-XL is essential for ISC survival throughout CRC progression. Here we show that loss of sensitivity to BCL-2 inhibition is apparent after acquisition of an APC mutation, which is mediated by the upregulation of microRNA-17-5p that targets and downregulates BCL-2. Furthermore, we find that BCL-XL inhibition impairs adenoma outgrowth in vivo and augments chemotherapy-induced cell death in tumor-derived organoids. Our results provide the mechanism behind transformation-driven changes in anti-apoptotic protein dependence and highlight the therapeutic potential of BCL-XL inhibition in CRC.

Results

BCL-2 and BCL-XL are essential for ISC survival during transformation

Previously we have shown BCL-2 to be critical for stem cell survival following loss of *Apc* [17]. We confirmed the importance of BCL-2 for ISC transformation by performing a clonogenic assay with small intestinal organoids from *Lgr5*Cre^{ER}*Apc*$^{fl/fl}$ mice. This assay measures survival of the stem cell compartment, which is crucial for the clonogenic potential

of the cultures (Fig. 1a). Treatment with BCL-2 specific inhibitor ABT-199 simultaneously with tamoxifen-induced *Apc* loss reduced outgrowth of *Apc*$^{-/-}$ cells, while non-induced organoids remained unaffected by BCL-2 inhibition (Fig. 1b). In the same study, BCL-XL inhibitor WEHI-539 did not affect outgrowth of *Apc*$^{-/-}$ spheroids, thus indicating that BCL-XL is non-essential for adenoma survival [17]. However, BH3 profiling has recently shown that WEHI-539 is only weakly efficient in inducing apoptosis in BCL-XL dependent cells while another higher affinity inhibitor, A-1155463, is far more potent [22, 23]. Analyzing both BCL-XL inhibitors confirmed that WEHI-539 did not impair adenoma outgrowth while A-1155463 clearly reduced *Apc*$^{-/-}$ organoid survival during transformation (Fig. 1c). The observed decrease in organoid clonogenicity was not a result of toxicity as wildtype organoids were insensitive to the combination of tamoxifen and BH3 mimetics (Supplementary Fig. 1a). MCL1 deletion has been shown to drastically affect several cell types including the colonic epithelium, however specific MCL1 inhibitors seem to be well tolerated in several pre-clinical cancer models [18, 24, 25]. To assess the role of MCL1 in ISC transformation, we tested a specific inhibitor, AZD5991, and found that MCL1 targeting did not impair *Apc*$^{-/-}$ organoid outgrowth (Fig. 1d). Taken together, our results provide evidence that BCL-2 and BCL-XL, but not MCL1, are crucial for *Apc*-mutant stem cell survival during transformation.

In contrast to the dependency observed during transformation, we have shown that tumor-derived CSCs are solely BCL-XL-dependent, pointing to a loss of the initial BCL-2 dependence [16]. We confirmed this finding with ABT-199, AZD5991 and A-1155463, where only BCL-XL inhibition induced significant cell death in Wnt-high CSCs, measured by the percentage of cells with active caspase-3 (Supplementary Fig. 1b) [26]. To ensure that the difference in ABT-199 sensitivity between early and late stage disease was not due to a difference between small intestine and colon-derived cultures, we also tested the sensitivity of *Lgr5*Cre^{ER}*Apc*$^{fl/fl}$ colon-derived organoids to BCL-2 and BCL-XL inhibition during transformation and observed strong dependency on both (Fig. 1e), while MCL1 inhibition again had no impact on adenoma outgrowth (Fig. 1f). Our results therefore indicate that while

BCL-2 is essential for *Apc*-mutant stem cell survival during transformation, this dependence is reduced at a certain stage during CRC progression.

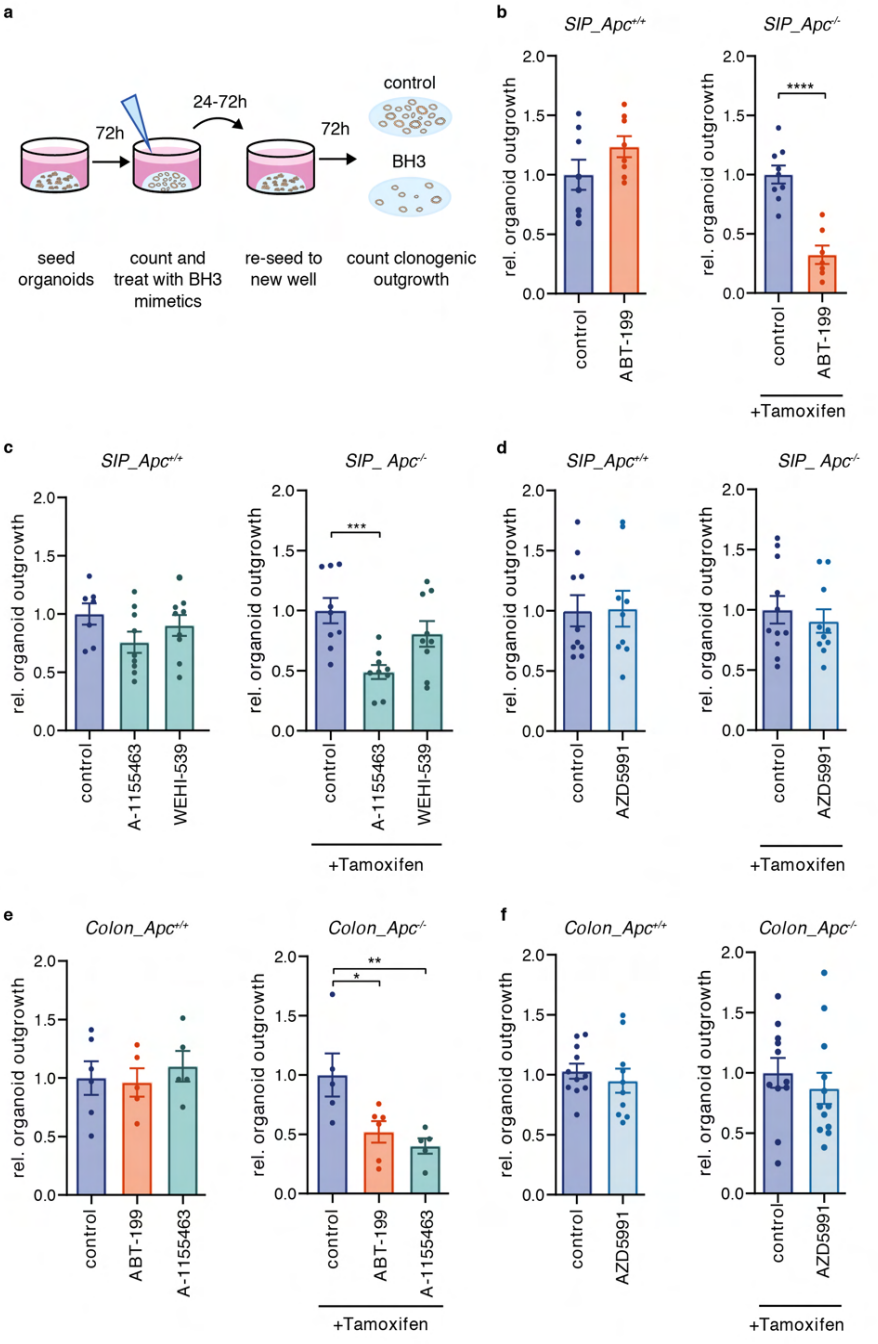

Figure 1. BCL-2 and BCL-XL are essential for ISC survival during transformation.
a. Overview of the organoid clonogenic assay.
b, c, d. Graphs depict relative outgrowth (number of organoid structures relative to the number prior to treatment and reseeding) of proximal small intestine (SIP)-derived organoid structures quantified 3 days after passaging for the indicated genotype, either without treatment or upon treatment with 1μM (b) ABT-199, (c) A-1155463 and WEHI-539 or (d) AZD5991, at the time of induction. Each dot represents a replicate (minimal n=7 per condition, n=3 independent experiments), error bars indicate s.e.m. *** $p < 0.001$, **** $p<0.0001$, student's t-test.
e, f. Graphs depict relative outgrowth of colon-derived organoid structures quantified 3 days after passaging for the indicated genotype, upon treatment with 1μM (e) ABT-199 and A-1155463 or (f) AZD5991, at the time of induction. Each dot represents a replicate (minimal n=5 per condition, n=2 independent experiments), error bars indicate s.e.m. * $p<0.05$, ** $p<0.01$, ordinary one-way ANOVA.

BCL-2 dependence is lost immediately after transformation

The most frequently mutated genes in the classical CRC progression pathway, namely *APC, KRAS, P53* and *SMAD4*, were previously altered in human colon-derived organoids using CRISPR-Cas9-mediated genome editing [20]. We employed this panel of organoids to assess changes in anti-apoptotic protein dependence of ISCs. Clonogenic outgrowth of normal colon organoids was unaffected by treatment with either ABT-199 or A-1155463 (Fig. 2a,b) while in *APC* knock-out (APC^{KO}) organoids, ABT-199 treatment had no effect (Fig. 2c) and A-1155463 treatment strongly impaired organoid clonogenicity (Fig. 2d). To corroborate this finding, we analyzed activation of apoptosis by cleavage of caspase-3 and found clear induction only in APC^{KO} organoids treated with A-1155463, indicating that apoptosis is induced in these organoids upon BCL-XL, but not BCL-2, inhibition (Fig. 2e). Similarly, mouse $Apc^{-/-}$ adenomas were also insensitive to ABT-199 treatment while A-1155463 clearly impaired adenoma outgrowth, indicating that this is not a difference between mouse and human-derived cultures (Supplementary Fig. 2a,b). To exclude that A-1155463 induced apoptosis could arise from off-target effects, shRNA knockdown of BCL-XL was performed. Strikingly, BCL-XL knockdown severely impaired survival

of *APC*^{KO} organoids, while knockdown with a control shRNA had no effect (Fig. 2f, Supplementary Fig. 2c). Reciprocally, BCL-XL overexpression induced significant resistance to A-1155463 in *APC*^{KO} organoids (Fig. 2g, Supplementary Fig. 2d), thus confirming that impaired clonogenicity upon A-1155463 treatment was a direct result of BCL-XL inhibition. In addition, we tested MCL1 dependency with AZD5991, which had no effect on the clonogenicity of both wildtype and *APC*^{KO} organoids (Supplementary Fig. 2e,f). This pattern of sensitivity to BCL-XL inhibition and absence of BCL-2 and MCL1 dependency in transformed ISCs was maintained throughout the progression panel of organoids with increasing mutation loads (Fig. 2h and Supplementary Fig. 2g). Altogether these results indicate that BCL-2 exerts its pro-survival functions during transformation alone while BCL-XL is required for apoptosis evasion throughout the adenoma-to-carcinoma sequence. Intriguingly, triple (*APC*^{KO}*KRAS*^{G12D}*P53*^{KO}) and quadruple (*APC*^{KO}*KRAS*^{G12D}*P53*^{KO}*SMAD4*^{KO}) mutant organoids did show slightly increased resistance to A-1155463, which is consistent with the role of P53 in apoptosis induction [27]. In agreement, shRNA-mediated knockdown of *Smad4* in mouse *Apc*$^{-/-}$*Kras*$^{+/G12D}$ organoids did not induce increased resistance to A-1155463, while quadruple mutant organoids were again more resistant (Supplementary Fig. 2h). This *P53* mutation induced resistance to A-1155463 is likely due to the observed downregulation of its known pro-apoptotic targets such as PUMA and BAX [27, 28] (Supplementary Fig. 7e,f).

BCL-XL is crucial for stem cell survival in patient-derived adenoma and tumor organoids

To ascertain the clinical relevance of the above findings, we tested the response of organoids derived from familial adenomatous polyposis (FAP) and CRC patients to anti-apoptotic protein inhibition. Tubular adenomas (TA) derived from FAP patients represent precursor lesions that have an increased likelihood of developing into carcinomas and are normally the result of loss or mutation of the wild type *APC* allele [19]. All four tested TA cultures were insensitive to increasing doses of BCL-2 inhibition with ABT-199 and treatment did not induce cleavage of caspase-3, similar to the

APC^{KO} human organoids (Fig. 3a,c, Supplementary Fig. 3a,c).

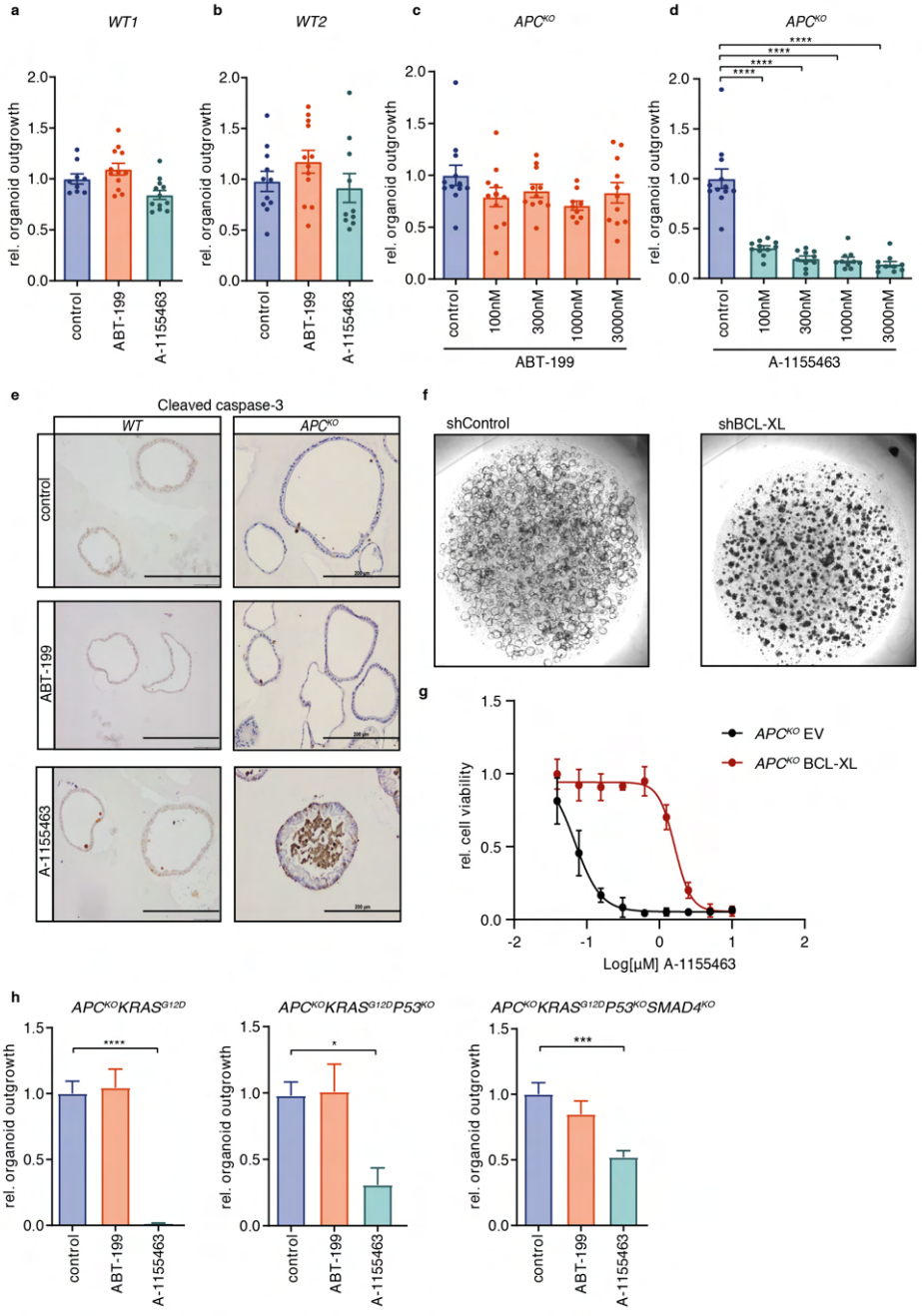

Figure 2. BCL-2 dependence is lost immediately after transformation.
a, b. Graphs depict relative outgrowth of human normal colon organoids (a) WT1 and (b) WT2 quantified 3 days after passaging, upon treatment with 1μM ABT-199 or A-1155463. Each dot represents a replicate (minimal n=9 per condition, n=3 independent experiments), error bars indicate s.e.m.
c, d. Graphs depict relative outgrowth of human *APC*^{KO} organoids quantified 3 days after passaging, upon treatment with indicated doses of (c) ABT-199 or (d) A-1155463. Each dot represents a replicate (minimal n=9 per condition, n=3 independent experiments), error bars indicate s.e.m. **** $p<0.0001$, ordinary one-way ANOVA.
e. Cleaved caspase-3 stained human normal (WT) and *APC*^{KO} organoids after 24 h treatment with 300 nM ABT-199 or A-1155463. Scale bars, 200 μm.
f. Images represent the outgrowth of *APC*^{KO} organoids after transduction with either control or BCL-XL targeting shRNA.
g. Dose-response curve of control vector (black) or BCL-XL overexpressing (red) *APC*^{KO} organoids treated with a titration of A-1155463. Viability data measured by cell titer blue was blank corrected and normalized to untreated control. Data is represented as mean ± SD (n=2 independent experiments).
h. Relative outgrowth of human mutant organoids of indicated genotypes quantified 3 days after passaging, upon treatment with 3 μM of ABT-199 or A-1155463 (n=3 independent experiments). Error bars indicate s.e.m. * $p<0.05$, *** $p<0.001$, **** $p<0.0001$, ordinary one-way ANOVA.

Conversely, BCL-XL inhibition strongly impaired adenoma outgrowth and A-1155463 treated TAs showed elevated expression of cleaved caspase-3 (Fig. 3b,c, Supplementary Fig. 3b,c). Also in this setting, MCL1 inhibition did not impair adenoma clonogenicity, in agreement with the minimal impact of AZD5991 on *APC*^{KO} organoids (Fig. 3d).

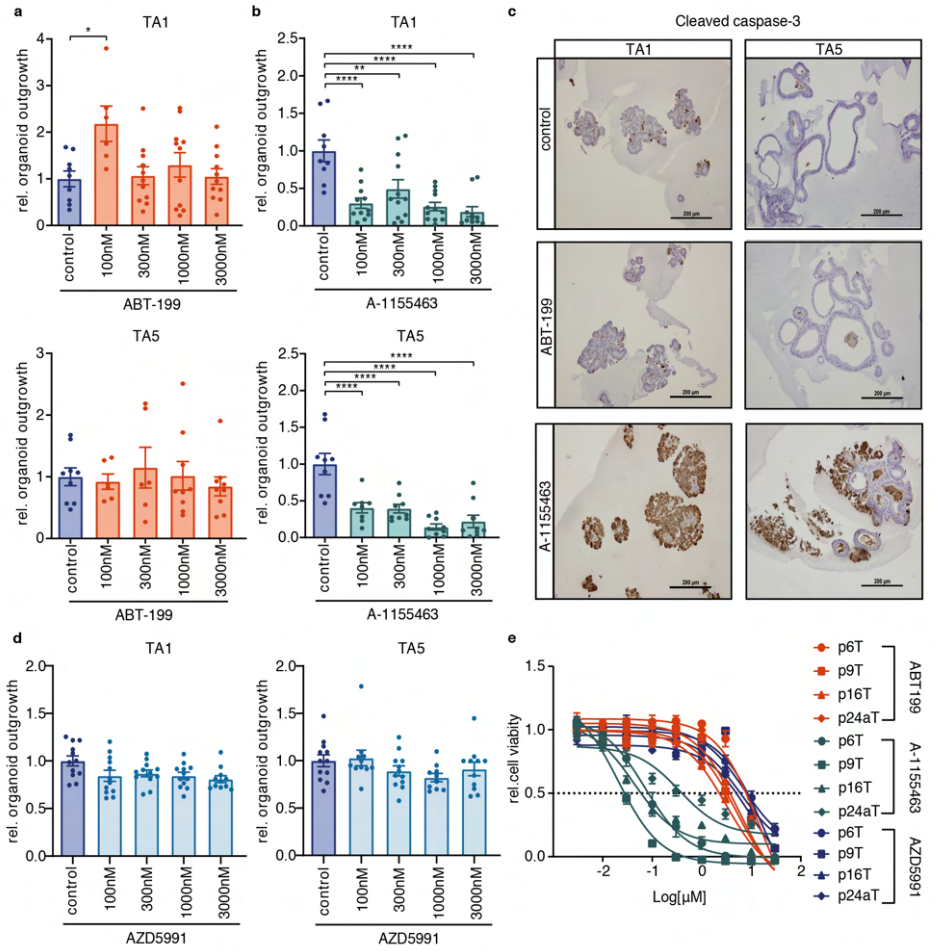

Figure 3. BCL-XL is crucial for stem cell survival in patient-derived adenoma and tumor organoids.

a, b. Graphs depict relative outgrowth of human tubular adenomas TA1 and TA5 quantified 3 days after passaging, upon treatment with indicated doses of (a) ABT-199 or (b) A-1155463. Each dot represents a replicate (minimal n=6 per condition, n=3 independent experiments), error bars indicate s.e.m. * $p<0.05$, ** $p<0.01$, **** $p<0.0001$, ordinary one-way ANOVA.

c. Cleaved caspase-3 stained human TAs after 24 h treatment with 300 nM ABT-199 or A-1155463. Scale bars, 250 μm.

d. Graphs depict relative outgrowth of human tubular adenomas TA1 and TA5 quantified 3 days after passaging, upon treatment with indicated doses

of AZD5991. Each dot represents a replicate (minimal n=6 per condition, n=3 independent experiments), error bars indicate s.e.m.
e. Relative viability of patient-derived CRC organoids upon treatment with a titration of ABT-199 (orange), A-1155463 (green) or AZD5991 (blue) (n=3 independent experiments). Error bars indicate s.e.m.

Tumor organoids established from patient-derived CRC biopsies have been shown to closely reflect several characteristics of the original tumor [21]. We tested four of these tumor organoids (p6T, p9T, p16T and p24aT), all of which were previously confirmed to have alterations in *APC*, *KRAS* and *P53*, with p16T also carrying a *SMAD4* mutation [21]. As expected, all four tumor organoids were more sensitive to BCL-XL inhibition as the IC50s for A-1155463 were much lower than for ABT-199 and AZD5991 (Fig. 3e), confirming that classical CRC precursor and carcinoma lesions depend on BCL-XL for survival while BCL-2 and MCL1 remain non-essential in this context.

BCL-XL inhibition impairs adenoma outgrowth in vivo

Our results suggest that the window for BCL-2 inhibition as a therapeutic strategy for CRC is limited and that MCL1 inhibition on its own is unlikely to be effective. However, BCL-XL inhibition could prevent tumor outgrowth at early stages. To test this in vivo, we injected 4 hydroxy-tamoxifen into the colonic submucosa of *Villin*Cre^{ER}*Apc*$^{fl/fl}$ mice to induce local recombination and orally administered either ABT-199 or A-1155463, once every two days for the duration of the experiment. Small tumors were visible upon colonoscopy in vehicle and ABT-199 treated groups after one and two weeks, while none were detected in the A-1155463 treated mice (Supplementary Fig. 4a,b). After three weeks, all of the ABT-199 treated mice had discernable adenomas while only one of five A-1155463 treated mice presented with a small adenoma (Fig. 4a, b), thus confirming that BCL-XL inhibition effectively attenuates adenoma outgrowth *in vivo*. Intriguingly, BCL-XL inhibition was not effective on pre-existing adenomas in this model (Supplementary Fig. 4c,d), which is likely due to the higher dose of A-1155463 needed to achieve the same level of apoptosis in

fully transformed organoids (Supplementary Fig. 2b) in comparison to transforming organoids (Supplementary Fig. 4e).

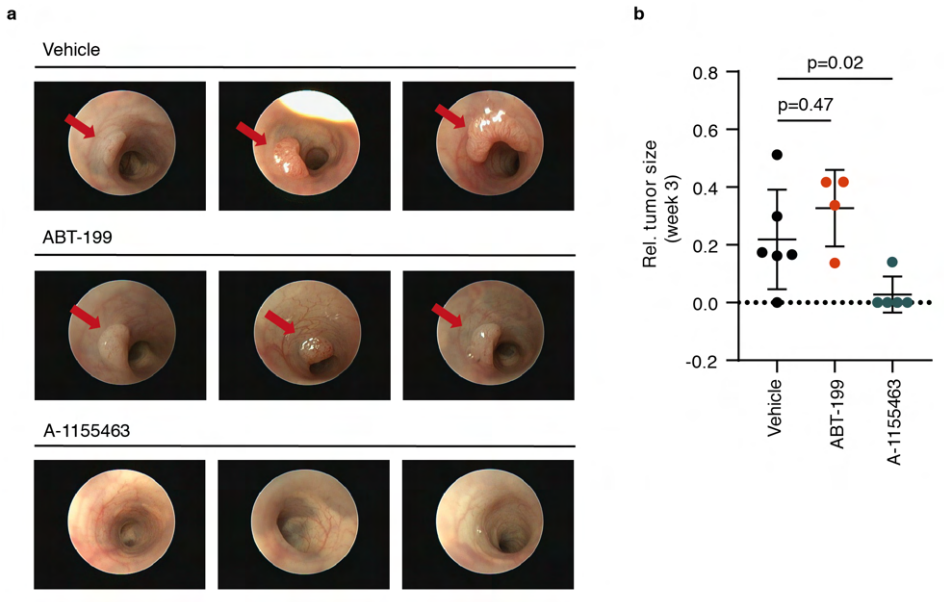

Figure 4. BCL-XL inhibition impairs adenoma outgrowth in vivo.

a. Representative images from a colonoscopy of *Villin*Cre^{ER}*Apc*$^{fl/fl}$ mice, three weeks after being induced with a single injection of 4-hydroxytamoxifen into the colonic sub-mucosa. ABT-199 and A-1155463 treated mice received 100 mg/kg of drug for two days prior to induction followed by treatment every other day until day 28. Red arrows indicate tumors.

b. Quantification of colonic tumor size (normalized to the size of the lumen) of mice described in (a), n = 6 for vehicle, n=5 for A-1155463 and n = 4 for ABT-199, one-way Mann–Whitney U test, p = 0.47 (vehicle vs ABT-199) and P = 0.02 (vehicle vs A-1155463). Data represents mean ± SD.

BCL-2 expression is decreased upon transformation

In a study that assessed determinants of BH3 mimetic efficacy, sensitivity to BCL-2 inhibition could be predicted by expression levels of the protein, where BCL-2 expressing cells respond better to ABT-199 than non-expressers [29]. Having established BCL-2 inhibition to be ineffective after

ISC transformation, we therefore determined whether this relates to its expression pattern during CRC progression by analyzing four publicly-available expression datasets. This revealed a significant decrease in *BCL-2* expression in adenomas compared to healthy tissue and a further decrease in CRC tumors, which was also confirmed in the TCGA COREAD cohort (Fig. 5a, Supplementary Fig. 5a). Conversely, *BCL-XL* expression increased upon progression from normal to adenoma and furthermore in the carcinoma stage (Fig. 5b, Supplementary Fig. 5b). At the protein level, BCL-2 was detected in normal crypts, however its expression was nearly absent in adjacent tumor tissue, while BCL-XL showed strong positive staining in both normal and tumor tissue (Fig. 5c,d). Independent confirmation with a single-cell RNA sequencing dataset of normal and CRC tumor samples [30] revealed a significant decrease in *BCL-2* and concomitant increase in *BCL-XL*, specifically in the epithelial tumor compartment (Fig. 5e,f). Based on these observations, we next ascertained whether the observed decrease in BCL-2 expression occurs already upon acquisition of an *APC* mutation, specifically in the stem cell compartment where BCL-2 is specifically expressed [17]. To do so, we made use of a validated colon stem cell marker, PTK7, and confirmed its function as a stem cell marker for APC^{KO} human organoids as well [31] (Supplementary Fig. 5c,d). Analysis of BCL-2 expression in PTK7-high cells of normal and APC^{KO} human organoids confirmed a decrease in stem cell BCL-2 expression upon loss of *APC* (Fig. 5g, Supplementary Fig. 5e,g). A similar analysis of BCL-XL expression showed no change in expression between normal and APC^{KO} stem cells (Fig. 5h, Supplementary Fig. 5f,g). Our data thus indicates that transformation results in a decrease in BCL-2 expression, which explains the observed lack of impact of BCL-2 inhibition in APC^{KO} and TA cultures.

MiR-17-5p regulates BCL-2 expression in APC-mutant organoids

Next, we assessed the mechanism by which BCL-2 expression levels decrease upon transformation. We first evaluated *BCL-2* mutation status by analyzing the TCGA COAD dataset on cBioPortal, where most tumors did not present with any alterations in the gene (Fig. 6a). Evaluation of promoter methylation in the same dataset showed an absence of methylation in the

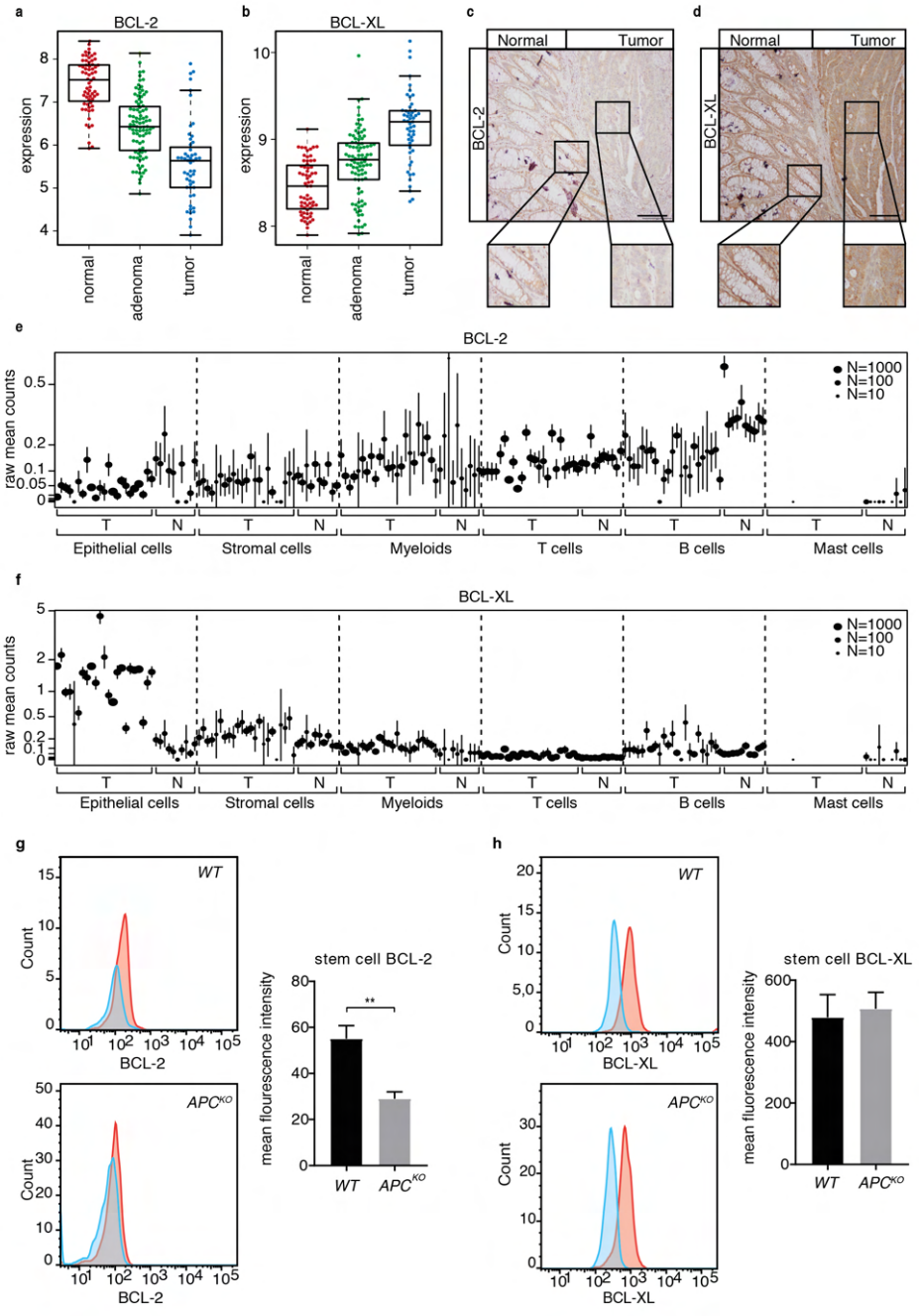
a
BCL-2
expression
normal
adenoma
tumor
b
BCL-XL
expression
normal
adenoma
tumor
c
Normal
Tumor
BCL-2
d
Normal
Tumor
BCL-XL
e
BCL-2
raw mean counts
N=1000
N=100
N=10
T
N
Epithelial cells
Stromal cells
Myeloids
T cells
B cells
Mast cells
f
BCL-XL
raw mean counts
N=1000
N=100
N=10
Epithelial cells
Stromal cells
Myeloids
T cells
B cells
Mast cells
g
WT
Count
BCL-2
APC^KO
stem cell BCL-2
mean flourescence intensity
**
WT
APC^KO
h
WT
Count
BCL-XL
APC^KO
stem cell BCL-XL
mean fluorescence intensity
WT
APC^KO

Figure 5. BCL-2 expression is decreased upon transformation.
a, b. mRNA expression of (a) *BCL-2* and (b) *BCL-XL* in a compiled dataset of colon normal, adenoma and tumor samples.
c, d. Immunohistochemical analysis of (c) BCL-2 and (d) BCL-XL expression in normal and adjacent tumor tissue. Scale bars, 200 μm.
e, f. Gene expression (raw mean counts) of (e) *BCL-2* and (f) *BCL-XL* in a single cell RNA-Seq dataset of normal and tumor samples, separated by cell type. Data is represented as mean ± SE and node size indicates the number of cells per sample. Samples in different cell types are shown in the same order. $p < 0.005$ for the fold change in *BCL-2* and *BCL-XL* expression in normal vs tumor epithelial cells.
g, h. Intracellular FACs staining of (g) BCL-2 and (h) BCL-XL in the PTK7 high fraction of normal and APC^{KO} human organoids. (n=3 independent experiments). Error bars indicate s.e.m. ** $p< 0.01$, student's t-test.

BCL-2 promoter region (Fig. 6a), further confirmed by treatment of APC^{KO} organoids with the de-methylating agent decitabine, which did not affect BCL-2 mRNA levels (Fig. 6b). The BCL-2 gene is located on 18q and could therefore be lost as a consequence of loss of heterozygosity (LOH) of this chromosomal region, which frequently occurs in CRC, albeit at a later stage of the disease [32-34]. However, karyograms of APC^{KO} human organoids did not show loss of 18q [20]. Similarly, single-cell karyotype sequencing to quantify copy number alterations revealed no 18q LOH in any of the TA cultures, thereby excluding LOH as the underlying mechanism of decreased *BCL-2* expression in adenomas (Fig. 6c, Supplementary Fig. 6a).

Several microRNAs show aberrant expression in colon adenoma and carcinoma samples in comparison to normal tissue [35]. We examined the most commonly upregulated microRNAs in early adenomas and found several of them to have binding sites on the *BCL-2* 3'UTR, as predicted by miRmap (Supplementary table 1) [35, 36]. Of these, the miR-17-92 family was of particular interest as it is a direct target of ß-catenin, upregulated upon mutation in the *APC* gene [37]. Several members of this microRNA family have high miRmap scores for binding in the 3'UTR of BCL-2 (Supplementary table 1) [36].

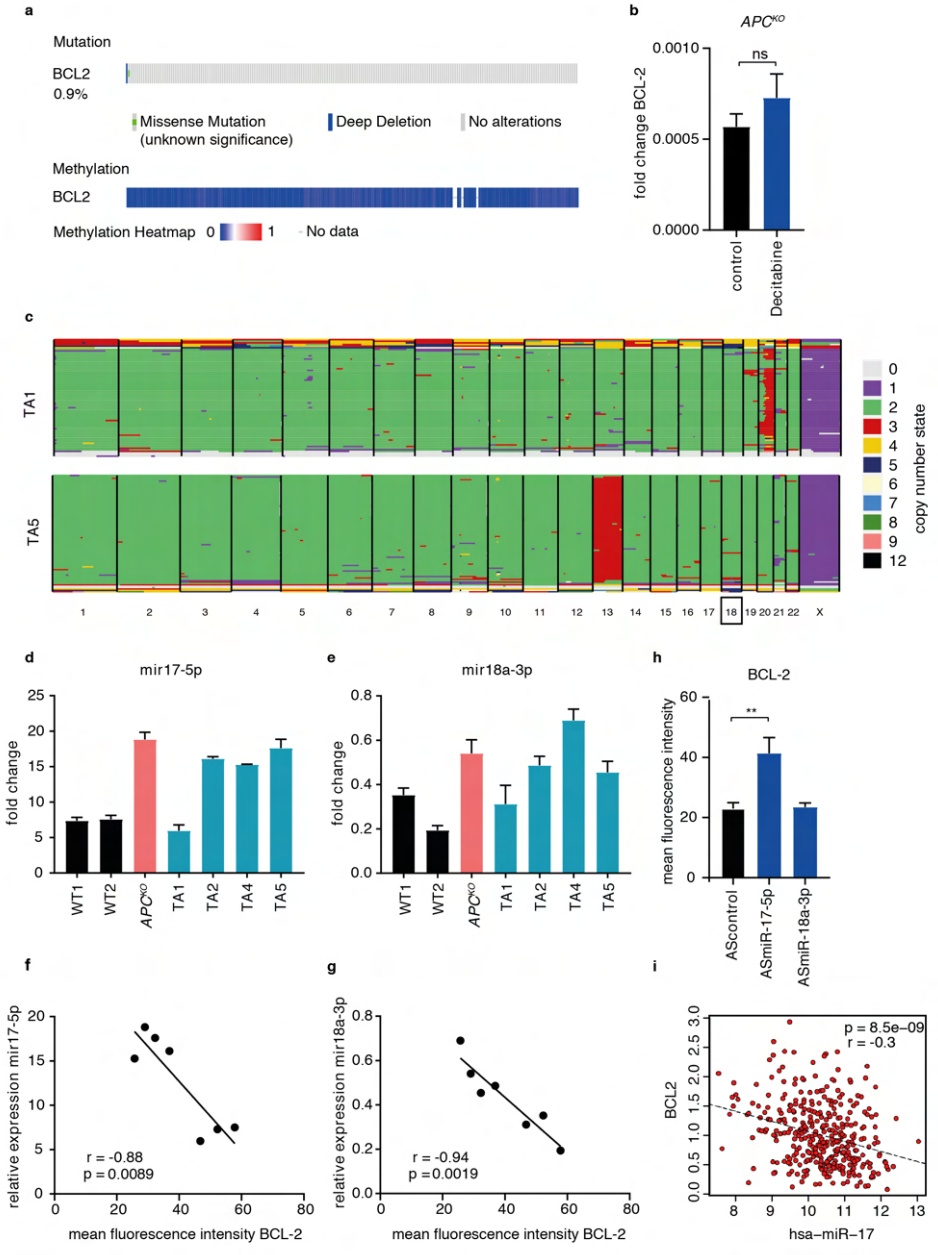
a
Mutation
BCL2
0.9%
Missense Mutation (unknown significance)
Deep Deletion
No alterations
Methylation
BCL2
Methylation Heatmap 0 1 No data
b
APCKO
ns
fold change BCL-2
0.0010
0.0005
0.0000
control
Decitabine
c
TA1
TA5
copy number state
0 1 2 3 4 5 6 7 8 9 12
1 2 3 4 5 6 7 8 9 10 11 12 13 14 15 16 17 18 19 20 21 22 X
d
mir17-5p
fold change
WT1 WT2 APCKO TA1 TA2 TA4 TA5
e
mir18a-3p
fold change
WT1 WT2 APCKO TA1 TA2 TA4 TA5
h
BCL-2
**
mean fluorescence intensity
AScontrol ASmiR-17-5p ASmiR-18a-3p
f
relative expression mir17-5p
r = -0.88
p = 0.0089
mean fluorescence intensity BCL-2
g
relative expression mir18a-3p
r = -0.94
p = 0.0019
mean fluorescence intensity BCL-2
i
p = 8.5e−09
r = -0.3
BCL2
hsa−miR−17

Figure 6. MiR-17-5p regulates BCL-2 expression in APC-mutant organoids.
a. *BCL-2* mutation and methylation status in CRC tumors of the TCGA COAD dataset, analyzed on cBioPortal.
b. mRNA expression of *BCL-2* in decitabine treated APC^{KO} organoids (n=2 independent experiments). Error bars indicate s.e.m.
c. single cell karyotype-seq showing the ploidy in individual cells of TA1 and TA5. Graphs show individual cells (horizontal lines) and colors indicate copy number state for a given chromosome (columns).
d, e. qRT-PCR analysis of (d) miR-17-5p and (e) miR-18a-3p expression in human normal, APC^{KO} and TA cultures, normalized to U6 snRNA expression. Data represents mean ± s.e.m.
f, g. Correlation of (f) miR-17-5p and (g) mir-18a-3p expression data from (d) and (e) respectively to BCL-2 protein levels measured by intracellular FACS. P values are determined by two-tailed Pearson's correlation.
h. Intracellular FACS staining of BCL-2 protein levels in human APC^{KO} organoids transduced with control, miR-17-5p or miR-18a-3p anti-sense (AS) microRNA inhibitors (n=3 independent experiments). Error bars indicate s.e.m. ** $p<0.01$, student's t-test.
i. Correlation of miR-17 and *BCL-2* expression in the TCGA COAD dataset.

Of note, miR-17 and miR-18a have previously been shown to target BCL-2 in a luciferase reporter assay and one or more binding sites for miR-17-5p and miR-18a-3p are present on the *BCL-2* 3'UTR [38] (Supplementary Fig. 6b,c). We therefore examined the expression of these microRNAs in our human normal, APC^{KO} and TA organoids and found that both miR-17-5p and miR-18a-3p were increased in APC^{KO} organoids and in the majority of TA cultures (Fig. 6d,e). A significant negative correlation between the protein levels of BCL-2 and the expression of both miR-17-5p and miR-18a-3p was also observed in these organoids (Fig. 6f,g). To assess if these microRNAs mediate the downregulation of BCL-2, we transduced APC^{KO} organoids with lentiviral microRNA inhibitors that target either mir-17-5p or mir-18a-3p. Protein expression of BCL-2 was found to be significantly upregulated upon mir-17-5p inhibition, but not upon mir-18a-3p inhibition (Fig. 6h, Supplementary Fig. 7a). We confirmed the efficacy of mir-17-

5p inhibition with the observed upregulation of BIM, a known target of mir-17 (Supplementary Fig. 7b) [39]. MYC, another mir-17 target [40], was not altered at the mRNA level and lowly expressed in these cells (Supplementary Fig. 7c,d). Importantly, BCL-XL, which is not a miR-17 target, remained unaffected (Supplementary Fig. 7b). Furthermore, we observed a significant negative correlation between miR-17 and BCL-2 levels in the TCGA dataset of micro-satellite stable (MSS) CRC tumors (Fig. 6i). Our results thus confirm that *APC*-driven transformation results in upregulation of mir-17-5p, which mediates repression of BCL-2.

Altogether, our data explain why ISC transformation results in a rapid decrease in BCL-2 expression and as a consequence, a decrease in BCL-2 dependency. However, to elucidate why transformation results in an increased sensitivity to A-1155463 while normal ISCs are resistant, we profiled the expression of key members of the BCL-2 family and assessed if transformation-driven changes to the apoptotic threshold could explain this shift in BCL-XL dependency [41, 42]. Surprisingly, mRNA and protein levels of several pro-apoptotic proteins were decreased upon transformation. Nevertheless, we also observed a dramatic decrease in MCL1 levels, which, together with the above described repression of BCL-2, results in evident reliance on BCL-XL for survival, thereby making it a key vulnerability in transformed ISCs (Supplementary Fig. 7e,f).

BCL-XL expression is predictive for chemotherapy response

Our data shows that BCL-XL plays a critical role in CRC survival, yet the *in vivo* use of A-1155463 was ineffective in impairing pre-existing adenoma growth (Supplementary Fig. 4c,d). We therefore determined if BCL-XL inhibition could enhance the efficacy of chemotherapy on patient-derived tumor organoids. Matrix titration of A-1155463 and Oxaliplatin revealed that the efficacy of the two compounds is strongly synergistic (Fig. 7a-c, Supplementary Fig. 8a-c). Intriguingly, studies have shown that the proximity of tumor cell mitochondria to the apoptotic threshold is also predictive of chemotherapy response in patients [43]. We therefore analyzed if the changes we detected in anti-apoptotic protein reliance

have clinical relevance in terms of outcome in chemotherapy-treated non-metastatic CRC patients. To exclude variation in chemotherapy response due to CRC subtype differences, we made use of the Marisa dataset and selected the microsatellite stable epithelial subtypes CMS2 and CMS3 (n = 119), which almost invariably carry an *APC* mutation and are therefore representative of the observed *APC*-driven decrease in BCL-2 expression.

Kaplan-Meier analysis for relapse-free survival was performed with a cut-off based on median expression of *BCL-2, MCL-1* or *BCL-XL*. While *BCL-2* and *MCL-1* expression did not differentiate survival probability (Fig. 7d,e), patients with low *BCL-XL* expression and therefore a lower apoptotic threshold displayed a more favorable response to adjuvant chemotherapy in comparison to the high *BCL-XL* expressors (Fig. 7f), thus suggesting that the extent of BCL-XL-driven protection from mitochondrial apoptosis is predictive for response to chemotherapy.

Discussion

The development of BH3 mimetics has greatly facilitated our understanding of the role of anti-apoptotic proteins in normal and disease settings. In particular, their specificity for individual BCL-2 family members allows for dissecting the anti-apoptotic vulnerabilities of cancer cells and thereby define enhanced therapeutic strategies. By employing these powerful tools, we show that while BCL-2 is only essential during ISC transformation, BCL-XL is critical for ISC survival throughout CRC progression. Previous work has shown that transforming B lymphoid cells present with an increased sensitivity to MCL1 loss [44]. However, we find that AZD5991 treatment does not impair ISC transformation in our models, even though MCL1 deletion was shown to severely disrupt intestinal homeostasis [18].

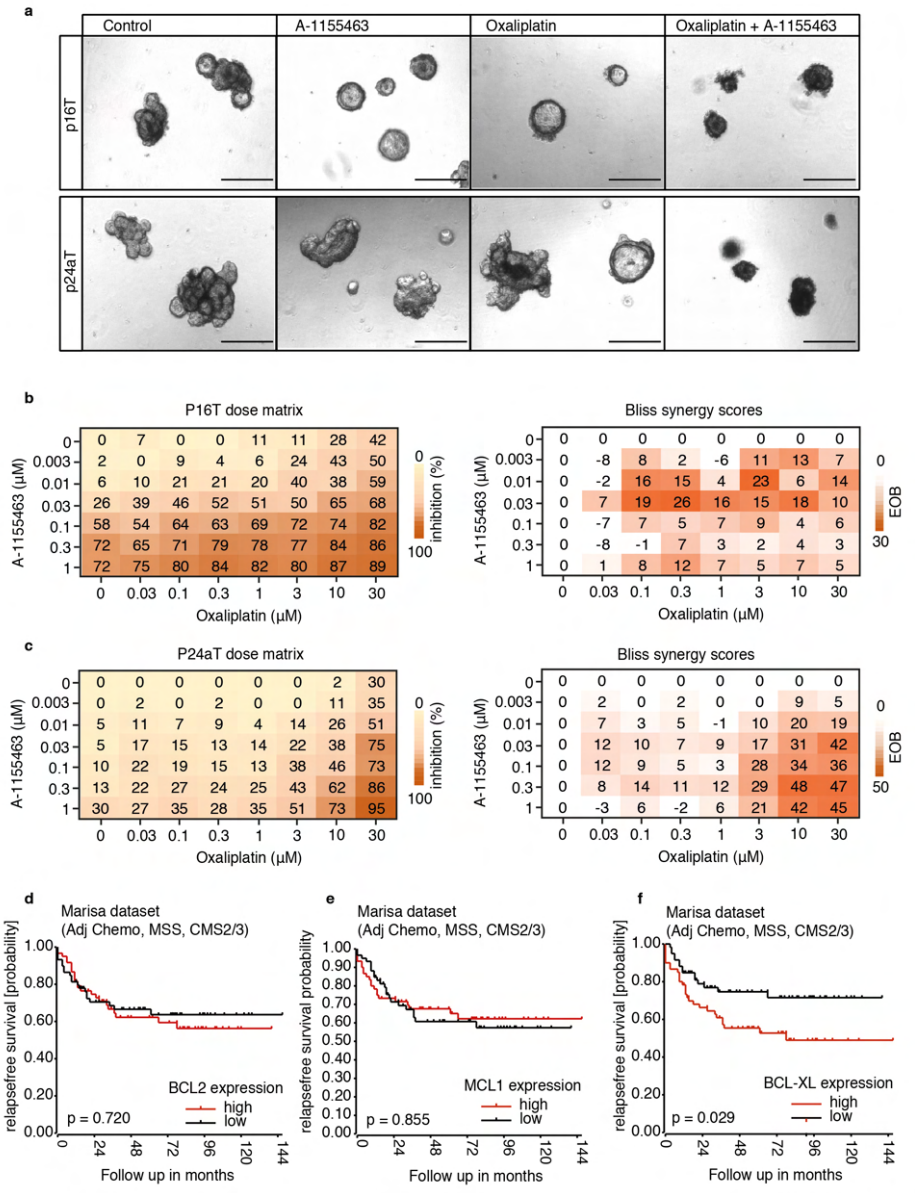

Figure 7. BCL-XL expression is predictive for chemotherapy response.

a. Phase-contrast images of p16T and p24aT human CRC organoids treated for 72h with 10µM oxaliplatin alone and in combination with 30nM A-1155463. Scale bars, 250µm.

b, c. 6 x 7 dose matrices of (b) p16T and (c) p24aT human CRC organoids treated with oxaliplatin in combination with A-1155463 for 5 days. % inhibition was calculated from viability data measured by cell titer blue, after normalizing to control. Data represent the average of two independent experiments. Bliss synergy scores were calculated for each dose combination and positive scores indicate synergistic effects.
d, e, f. Kaplan Meier analysis of the relapse free survival of micro-satellite stable CM2 and CM3 patients in the Marisa dataset who received adjuvant chemotherapy (n=119), based on a cut-off of median expression of (d) *BCL-2*, (e) *MCL-1* or (f) *BCL-XL*. P values are based on the log-rank test. Adj Chemo: patients who received adjuvant chemotherapy. MSS: microsatellite stable. CMS2/3: Consensus Molecular Subtype 2/3.

Earlier observations indicate that MCL1 deletion is not directly comparable to its pharmacological inhibition, which is often well tolerated at therapeutically effective doses [18, 24]. We and others have shown that while most solid tumors including CRC do not respond to MCL1 inhibition, combined inhibition of MCL1 and BCL-XL is very potent, suggesting that high levels of BCL-XL deter the efficacy of MCL1 inhibition alone [24, 25, 29, 45]. Overall, our data indicates that BCL-2 and MCL1 expression is rapidly lost upon transformation and that this results in a shift towards increased BCL-XL dependency. Our data further solidifies BCL-XL as a key factor for apoptosis resistance in CRC and moreover, emphasizes its importance in early stages of the disease. Patient-derived organoids have been used as a model to predict patient response to chemotherapy [46] and our results highlight the therapeutic potential for BCL-XL inhibition in CRC as A-1155463 treatment effectively impairs viability of organoids derived from FAP and CRC patients.

The use of BCL-XL inhibitors in the clinic is hampered by their toxicity to platelets, whose lifespan is determined by BCL-XL expression [47]. However, this could be circumvented with altered dosing strategies, particularly by administering lower doses in combination with other chemotherapeutics. Another possibility for circumventing platelet toxicity

and still achieving CRC tumor killing would be to use BCL-XL inhibitors with reduced oral bioavailability, which could particularly work in the context of intestinal tumors. We therefore used A-1155463 instead of its more orally bioavailable counterpart A-1331852 in our *in vivo* experiments, which showed considerable efficacy in reducing adenoma outgrowth with no observed toxicity, indicating potential for less orally bioavailable BCL-XL inhibitors in CRC therapy. However, oral A-1155463 treatment on its own did not affect the growth of established adenomas in mice, which could be due to inadequate dosing of A-1155463 as transformed cells are not as sensitive to its inhibition as transforming cells. In this case, using higher doses of less orally bioavailable BCL-XL inhibitors would offer potential to improve treatment efficacy but more so, identifying kinase targets whose inhibition could synergize with BCL-XL targeting could provide novel strategies to target CRC tumors. Here we show that BCL-XL inhibition enhances oxaliplatin-induced apoptosis, while earlier studies also observed synergy with inhibitors of kinases such as MEK [48, 49].

Previously, we have shown BCL-2 inhibition with ABT-199 to effectively reduce adenoma burden *in vivo* [17] while in our study this effect is no longer apparent. However, in our *in vivo* experiment tumor formation was localized to the colon rather than the small intestine as was the case in the previous study and so we reason that the orally bioavailable ABT-199 is likely absorbed through the small intestine and fails to reach the tumor in the colon. The limited window of ABT-199 efficacy that we observe in our organoid progression panel is supported by the decrease in BCL-2 expression detected upon transformation. In the context of tumorigenesis, such a decrease in anti-apoptotic protein expression is counter-intuitive. With the aim to resolve this, we identified miR-17-5p as a BCL-2 repressor that is significantly upregulated upon acquisition of an *APC* mutation. In CRC, miR-17-5p expression increases as the disease progresses and is suggested to be regulated by transcription factors such as MYC and ß-catenin [37, 50, 51]. MiR-17-5p has therefore been implicated to have an oncogenic role in the disease and higher expression is associated with a lower overall survival [52-54]. We propose that the observed decrease of

BCL-2 is an inadvertent consequence of transformation-driven miR-17-5p upregulation, whose oncogenic potential might simply outweigh the anti-apoptotic contribution of BCL-2.

Dynamic regulation of apoptosis has been observed during development as tissues progress from a young, proliferative state to a more aged and differentiated state, where MYC acts as a link between cell growth and death [55]. MYC high cells found in younger tissues pay the price for their proliferation with increased apoptotic priming, making them more sensitive to death-inducing stimuli. Such an effect is also observed in tumor cells, particularly driven by oncogenic mutations and regulated by MYC levels [56, 57]. Cancer cells are therefore in a precarious position where they require their anti-apoptotic block to hold in order to ensure their survival. This provides a potential therapeutic strategy and better identification of these transformation-induced vulnerabilities could provide valuable targets for therapy. Here we report transformation-driven changes in anti-apoptotic protein expression and dependence during colorectal cancer initiation and progression. Our findings could guide the rational use of BH3 mimetics as anti-cancer agents, whose clinical application can be aided by evaluating anti-apoptotic dependencies in varying tumor landscapes.

Materials and methods

Mouse organoid isolation and culture

Intestinal crypts were derived from the small intestine (SI) and colon of a wild-type and *Lgr5*Cre^{ER}*Apc*$^{fl/fl}$ mouse. Crypts were isolated and cultured as described previously [58]. Briefly, the intestine was isolated and separated into SI and colon pieces. After flushing with PBS, the intestines were opened longitudinally and villi were scraped off the SI. Both sections were then cut into small pieces of approximately 0.5cm and washed thoroughly with cold PBS supplemented with antibiotics (hereon referred to as PBS + antibiotics). These pieces were then incubated with 2mM (SI) and 25mM (colon) EDTA (Thermo Fischer Scientific, Landsmeer, The Netherlands) in PBS at 4°C on a roller for 30min. Crypts were

isolated by washing the pieces with PBS + antibiotics and vigorously shaking to release crypts into the supernatant, which was collected and filtered through a 70µm strainer (BD Biosciences, Breda, The Netherlands). Crypts were then spun down and plated in growth factor-reduced Matrigel (Corning, Amsterdam, The Netherlands) in advanced DMEM/F12 medium supplemented with N2 and B27 supplement (Thermo Fischer Scientific), 2mM GlutaMAX-I (Thermo Fischer Scientific), 10mM Hepes (Thermo Fischer Scientific), 1mM N-acety-L-cysteine (Sigma-Aldrich, Zwijndrecht, The Netherlands), 1X antimycotic /antibiotic (Thermo Fischer Scientific), mouse EGF 50ng/ml (Tebu-BIO, Heerhugowaard, The Netherlands), 20% R-spondin (conditioned medium) and 10% Noggin (conditioned medium). Mouse *Apc*$^{-/-}$*Kras*$^{+/G12D}$ organoids with shRNA knockdown of *Smad4* and *p53* were generated and selected as previously described [28]. All organoid cultures were confirmed to be mycoplasma negative on a monthly basis.

Human organoid isolation and culture

Normal colon samples (WT1 and WT2; WT1 is the normal organoid source of the CRISPR-Cas9 generated mutant organoids) were obtained from a piece of normal mucosa in the resection specimens of two CRC patients, at a distance of at least 10cm from the cancerous tissue. Normal organoids were isolated as previously described [59]. In short, the submucosal layer was removed and the mucosal piece was washed with PBS + antibiotics. The tissue was then cut into small pieces using a scalpel and washed thoroughly with PBS + antibiotics. The cut pieces were incubated in 8mM EDTA in PBS at 4°C on a roller for 1hr. The EDTA solution was replaced with PBS + antibiotics and crypts were released by vigorous shaking. The supernatant containing crypts was transferred to a new tube and this step was repeated 3 times. The crypts were then spun down, pooled and seeded in Matrigel. Normal colon organoids were maintained in Advanced DMEM/F12 supplemented with N2 and B27 supplement, antimycotic/antibiotic, gentamicin (Thermo Fischer Scientific), 2mM GlutaMAX-1, 10mM HEPES, 1mM N-acety-L-cysteine, 10nM [Leu15]-gastrin I (Sigma-Aldrich), 10mM nicotinamide (Sigma-Aldrich), 500nM A83-01 (Tocris, Abingdon, UK), 3µM SB202190 (Sigma-Aldrich), 50% WNT3A conditioned medium, 50ng/ml human EGF (Peprotech, London, UK), 20% RSPO1 conditioned medium, 10% Noggin conditioned medium, 10nM PGE2 (Santa Cruz Biotechnology, Heidelberg, Germany) and 10µM ROCK inhibitor

(Sigma-Aldrich). Normal organoids were dissociated every 7-10 days and medium was refreshed every 2/3 days.

The CRIPSR-Cas9 derived mutant panel of organoids were generated as previously described [20]. Normal human colon organoids were transfected with plasmids expressing Cas9 endonuclease and sgRNAs targeting *APC, KRAS, P53* or *SMAD4*. In the case of *KRAS*, homologous recombination to introduce the G12D mutation was achieved by co-transfection with a targeted oligonucleotide containing the oncogenic mutation. Following appropriate selection, individual organoids were picked and expanded to obtain clonal populations. The sgRNA sequences have been previously described [20] and genotyping was performed to confirm mutations. Mutant organoids were cultured in normal colon organoid medium as described above, excluding the WNT3A conditioned medium.

Human tubular adenoma cultures TA1, TA2, TA4 and TA5 were isolated and cultured as previously described [19]. Tissues were obtained from resections of familial adenomatous polyposis (FAP) patients and polyps were cut into small pieces, washed and plated in Matrigel. Following mechanical dissociation, viable organoids were propagated in Advanced DMEM/F12 containing N2 and B27 supplement, gentamycin, 2 mM L-glutamine (Lonza, Breda, The Netherlands), 0.15% D-glucose (Sigma-Aldrich), 100 µM ß-mercaptoethanol (Sigma-Aldrich), trace elements B and C (Thermo Fischer Scientific), 5 mM HEPES, 2 µg/ml heparin (Sigma-Aldrich), 10 µg/ml insulin(Sigma-Aldrich), 20 ng/ml human EGF, and 10µM SB202190.

Patient-derived tumor organoids were obtained from the Clevers organoid biobank and established as previously described [21]. P6T was cultured in adenoma medium and P9T, P16T and P24aT were cultured in normal colon organoid medium, excluding the WNT3A conditioned medium. All organoid cultures were tested for mycoplasma on a monthly basis and were confirmed to be mycoplasma negative.

Organoid transduction

For the shRNA knockdown experiment, an equal number of APCKO organoids were transduced with lentiviral shRNA constructs against either control (SHC002,

MISSION shRNA, Merck) or BCL-XL (TRCN0000033500, Mission shRNA, Merck) by spin transduction. Briefly, organoids were collected and trypsinized using TrypLE Express (Thermo Fischer Scientific) for 3 mins at 37°C. Following dissociation, cells were washed, counted and seeded into 48 well plates in organoid medium (see above) containing 10μM ROCK inhibitor (Sigma-Aldrich), 8 μg/ml polybrene (Sigma-Aldrich) and 50μL concentrated virus (AMICON Ultra-15 100k filters, Merck, Schiphol-Rijk, The Netherlands). Plates were spun down at 32°C for 1h at 1800 rpm. After ON incubation, cells were collected by washing with PBS and spun down and either processed for RNA extraction or seeded into Matrigel (Corning) for measuring outgrowth. *APC*^{KO} organoids were transduced with lentiviral pHEFTIR-EV (empty vector) or pHEFTIR-BCL-XL (overexpressor) constructs [16] and selected by sorting for the RFP positive population. *APC*^{KO} organoids were transduced with lentiviral microRNA inhibitors (Merck) targeting hsa-miR-17-5p (HLTUD0264), hsa-miR18a-3p (HLTUD0292) and a negative control cel-mir-243-3p (HLTUD002C). Transduced cells were selected with 4μg/ml puromycin (InvivoGen, Toulouse, France) for 7 days.

Colon cancer spheroid culture

The colon cancer spheroid culture Co01 expressing the TCF/LEF reporter TOP-GFP was generated as previously described [26]. The spheroid culture was maintained in ultra-low adherent flasks (Corning) and cultured in advanced DMEM/F12 supplemented with N2 supplement, 2 mM L-glutamine, 0.15% D-glucose, 100 μM ß-mercaptoethanol, trace elements B and C, 5 mM HEPES, 2 μg/ml heparin, 10 μg/ml insulin, 50ng/ml Epidermal Growth Factor and 10ng/ml basic Fibroblast Growth Factor (Tebu-BIO). Cultures were confirmed to be mycoplasma negative on a monthly basis.

Inhibitors

ABT-199 and WEHI-539 were purchased from Selleck Chemicals (Breda, The Netherlands), A-1155463 and AZD5991 from Chemietek (Indianapolis, USA). 5-Aza-2'-deoxycytidine (Decitabine) and Oxaliplatin were purchased from Sigma Aldrich. All compounds were dissolved in DMSO to a stock of 20mM, except Oxaliplatin, which was dissolved in water to a stock of 12.5mM.

Clonogenic assay

The clonogenic assay on *Lgr5*Cre^{ER}*Apc*$^{fl/fl}$ derived SI and colon organoid cultures was performed as previously described [58]. Briefly, organoids were plated in 48 well plates at a density of 25-50 crypt structures per well. After 3 days, the organoids were counted and treated with 1 μM (Z)-4-hydroxytamoxifen (24h) to induce *Apc* loss and simultaneously treated with 1 μM BH3 mimetics for 72h. To assess the clonogenic potential of the organoids, each well was passaged and the resulting organoid outgrowth was quantified after 3 days and normalized to the pre-treatment count per well and compared to untreated controls.

The clonogenic assay on the human organoids was performed by seeding dissociated organoids in 48 well plates, following which they were treated after 3 days with the indicated dose of BH3 mimetics for 24h. Each well was then passaged to a new well and the clonogenic capacity of organoids was assessed by microscope after 3 days and compared to untreated controls. All clonogenic assays were performed as two or three independent experiments and include at least three technical replicates per run.

Flow cytometry

Co01 expressing TOP-GFP was dissociated with Trypsin and stained for activated caspase-3 after 24h of treatment with 1μM ABT-199 or A-1155463. Staining was performed using RED-DEVD-FMK (CaspaTag caspase 3,7 in situ assay kit, sulforhodamine, Merck) as per the manufacturer's instructions (n=2 independent experiments). Organoids were isolated for FACS staining using cell recovery solution (BD Biosciences) at 4°C for 30 mins to dissolve Matrigel. Organoid structures were then spun down and trypsinized using TrypLE Express (Thermo Fischer Scientific) for 3 mins at 37°C. Following dissociation, cells were washed and stained with PTK7 (188B APC conjugated,1:100, Miltenyi, Paris, France) in 1% BSA in PBS for 30 mins on ice. For intracellular staining of organoids, PTK7 stained cells were washed and permeabilized using the BD cytofix/cytoperm kit (BD Biosciences) as per the manufacturer's instructions. Cells were stained for BCL-2 (sc-7382 FITC conjugated, 1:20, Santa Cruz Biotechnology) and BCL-XL (2764, 1:100, Cell Signaling Technology, Leiden, The Netherlands) for 30 mins on ice. BCL-XL staining was analyzed with Alexa Fluor-594 conjugated anti-rabbit secondary

antibody (Thermo Fischer Scientific). Both BCL-2 and BCL-XL antibodies were validated on Co01 cells overexpressing the respective proteins (Supplementary Fig.5e-g). All flow cytometry analyses were performed on the FACSCanto (BD biosciences) and PTK7 sorting of *APC*^{KO} organoids was performed on the SH800S Cell Sorter (Sony, Hoofdorp, The Netherlands). All stainings were performed as three independent experiments.

RNA and microRNA isolation and quantitative real-time PCR

Organoids cultures were collected for RNA extraction using cell recovery solution to dissolve the Matrigel, following which the cells were pelleted and RNA was extracted using the NucleoSpin RNA II kit (Macherey-Nagel, Leiden, The Netherlands). For isolation of microRNA, Matrigel was dissolved in cell recovery solution and organoids were pelleted and resuspended in TRIzol (Thermo Fischer Scientific). Chloroform was added and the mixture was centrifuged as per the manufacturer's instructions. The aqueous phase was carefully collected in a new tube, mixed with 100% ethanol (1.5x volume of aqueous phase) and RNA was isolated using the NucleoSpin RNA II kit (Macherey-Nagel) following manufacturer's instructions.

For gene expression analysis using quantitative real-time PCR (qRT-PCR), RNA was reverse transcribed to cDNA using Superscript III as per the manufacturer's instructions (Thermo Fischer Scientific). SYBR green (Roche, Woerden, The Netherlands) was used to perform qRT-PCR following manufacturer's instructions on a Roche Light Cycler 480 II. All obtained values were normalized to the expression of *RPLP0* and all primer sequences are provided in supplementary table 2. For analysis of microRNA expression levels using qRT-PCR, RNA was reverse transcribed to cDNA using the reverse transcription enzyme of the miRCURY LNA RT kit (Qiagen, Hilden, Germany) according to the manufacturer's instructions. The miRCURY SYBR Green PCR kit (Qiagen) was used to perform qRT-PCR with the following miRCURY LNA miRNA PCR assays: hsa-mir-17-5p and hsa-mir-18a-3p, as per the manufacturer's instructions (Qiagen). Data shown has been normalized to the expression of U6 snRNA.

Immunohistochemistry

Matrigel cultures were embedded in paraffin as previously described [58]. Briefly, organoids in Matrigel were fixed with 4% paraformaldehyde (PFA, Klinipath, Duiven, The Netherlands) over night at 4°C . PFA was then replaced with 70% ethanol for 30 mins following which dehydration was carried out with 100% ethanol and then xylene, both twice for 30 mins at RT. After dehydration, the Matrigel pieces were incubated in paraffin at 60°C twice for 30 mins and finally embedded in paraffin. 4µm sections were cut from paraffin embedded blocks using the microtome. Slides were stained for cleaved caspase-3 (1:200, 9661, Cell Signaling Technology), BCL-2 (15071S, 1:100, Cell Signaling Technology) and BCL-XL (2764, 1:500, Cell Signaling Technology) using standard procedures according to the manufacturer's protocols.

Immunobloting

For analysis of protein expression, organoids were collected in cell recovery solution (BD Biosciences) at 4°C for 30 mins to dissolve Matrigel and then lysed using 1x RIPA Lysis and Extraction buffer (Thermo Fischer Scientific) containing Halt protease and phosphatase inhibitor cocktail (1:100, Thermo Fischer Scientific). Protein samples were quantified using the Pierce BCA protein assay kit (Thermo Fischer Scientific) as per manufacturer's instructions. 15 µg protein was loaded per well into 4-15% precast gels (Bio-Rad, Lunteren, The Netherlands) and then transferred to PVDF membranes using the Trans-Blot Turbo transfer system (Bio-Rad) according to manufacturer's instructions using the mixed molecular weight transfer settings. Membranes were blocked for 1h in 5% bovine serum albumin (BSA) in Tris-buffered saline and Tween-20 (TBS-T,1x) and stained with primary antibody overnight at 4°C. The following primary antibodies were tested: MCL1 (1:1000, #4572, Cell Signaling), BCL-XL (1:1000, #2764, Cell Signaling), BIM (1:500, ADI-AAP-330-E, Enzo life sciences), c-Myc (1:1000, #9402, Cell Signaling), BAX (1:1000, #2774, Cell Signaling), BAK (1:1000, #3814, Cell Signaling) and BID (1:1000, #2002, Cell Signaling), all diluted in 5% BSA in TBS-T. After washing the blots 4 times for 20 mins each with TBS-T, the secondary antibody anti-rabbit-horseradish peroxidase (1:5000, #4050-05, Southern Biotech, Uden, The Netherlands) or anti-mouse-horseradish peroxidase (1:5000, #1031-05, Southern Biotech) was added for 2h at room temperature. Following another round of 4x

20 min washes, the membranes were developed using the LumiLight western blotting substrate (Sigma-Aldrich) and imaged on the ImageQuanti LAS4000 (GE Healthcare Life Sciences, Rijswijk, The Netherlands). GAPDH was used as a loading control (1:5000, MAB374, Sigma-Aldrich).

Cell viability assay

Tumor organoids were isolated using cell recovery solution (BD Biosciences) at 4 °C for 30 mins to dissolve Matrigel. Organoid structures were then spun down and trypsinized using TrypLE Express (Thermo Fischer Scientific) for 3 mins at 37 °C. Following dissociation, cells were washed, counted and seeded in 96 well plates at a density of 4000 cells per well in 6µL Matrigel drops. After overnight incubation, cells were treated in a titration with BH3 mimetics and/or Oxaliplatin using the HP D300 digital dispenser (Hewlett-Packard, Amstelveen, The Netherlands) for 5 days. Organoids were imaged using the EVOS cell imaging system (Thermo Fischer Scientific) and cell viability was assessed using CellTiter-Blue (Promega, Leiden, The Netherlands) according to the manufacturer's instructions. All viability assays were performed as two or three independent experiments. Synergy was calculated using the Synergy Finder web tool [60] and the Bliss independence model was employed to calculate the Bliss score for the most synergistic 3-by-3 dose window in the dose-response matrices, positive bliss scores are considered indicative of synergistic interactions.

Animal experiments

All experiments were performed according to UK Home Office regulations (Project Licenses 70/8646 and 70/9112), adhered to ARRIVE guidelines and were reviewed by local animal welfare and the ethical review committee at the University of Glasgow. Intracolonic inductions in 12-20 week old male and female *Villin*Cre^{ER}*Apc*$^{fl/fl}$ C57BL/6 mice were performed under general anesthesia wherein a single 70 µl 100 µM dose of 4-hydroxy tamoxifen (H7904-5MG from Sigma) was injected into the colonic sub-mucosa via a colonoscope (Karl Storz TELE PACK VET X LED endoscopic video unit). Mice were treated with ABT-199 (n=4), A-1155463 (n=5) or vehicle-only (n=6) at a dose of 100mg/kg by oral gavage. Drugs were dissolved in 60% Phosal 50PG (Lipoid, Ludwigshafen, Germany), 30% polyethylene glycol 400 and 10% ethanol. For the transformation experiment, treatment was

started two days prior to tamoxifen induction and continued afterwards on every other day for 28 days. To assess efficacy in pre-existing tumors, colonic adenomas were allowed to grow out for two weeks after which mice were treated with either vehicle (n=4) or A-1155463 (n=4), five times a week for 28 days. Tumor growth in the colon was monitored weekly, for three weeks by colonoscopy. Tumor size was measured relative to lumen size with ImageJ. For the transformation study, mice were randomly assigned to treatment groups and scoring of tumor burden was blinded. For the post-transformation study, mice were scoped to determine tumor presence and as we detect a spread of tumor sizes at this point, they were equally distributed across treatment groups, tumor burden scoring was blinded. Only mice which were lost due to non-tumor growth related factors were excluded, such as puncture during tamoxifen bolus injection or endoscopic examination related death. This led to the exclusion of one mouse in the ABT-199 treatment group of the transformation study. For mouse sample size calculation we aimed to identify a difference in adenoma growth of 50% or more at a 95% confidence interval. Based on the relatively high variation in adenoma growth from mouse to mouse that was estimated to be around 30%, the power calculation indicated that n=4 per group was sufficient to achieve a power of 80%. In addition, due to potential drop outs due to colon puncture during injection, the final group size of 5 was chosen for the transformation setting. In the case of the therapeutic setting n=4 was used as the groups were assigned after tumor initiation and therefore dropouts due to faulty injections were no longer relevant.

Data analysis and visualization

BCL-2 and BCL-XL expression graphs were generated from a collection of three public Affymetrix datasets (GSE20916, GSE8671 & GSE4183), which were rma normalized and merged using quantile normalization in R. P values were calculated using the Mann-Whitney test. RNA-sequencing (RNA-Seq) data from the TCGA cohort was normalised from raw counts to FPKM (log2 transformed).

The single-cell RNA-Seq data and cell type annotations were previously published [30] and available from NCBI GEO with accession GSE132465 and GSE144735. The raw counts per sample (separate tumor vs normal per patient) and major cell types are summarized into the mean and standard error, visualized as forest plots

and statistically tested using the R package acdx (https://github.com/pwirapati/acdx). Fold-change and bootstrap p-value calculation (200 replicates) is based on random-effects gamma GLM model.

Single-cell karyotype sequencing was performed on TA cultures, which were isolated using cell recovery solution at 4 °C for 30 mins to dissolve Matrigel. Organoid structures were then spun down and trypsinized using TrypLE Express (Thermo Fischer Scientific) for 3 mins at 37 °C. The single cell suspensions were lysed in a nuclei suspension buffer containing 10µg/ml Hoechst 34580 (Sigma-Aldrich). Nuclei were then sorted into a 384-well plate using the BD FACS Fusion, and stored at −20 °C until further processing for library preparation and sequencing. For library preparation, cells were first lysed with proteinase K (Thermo Fischer Scientific) and the genome was subsequently NlaIII digested, individual cell DNA was labeled with an adapter for library preparation consisting of a cell-specific 8 bp barcode, a 3 bp random molecular barcode (UMI), the 5' Illumina TruSeq small RNA kit adapter and a T7 promoter. Cell samples were pooled, in vitro transcribed and then fragmented and reverse transcribed to cDNA. Illumina sequencing libraries were prepared using the TruSeq small RNA primers (Illumina, Eindhoven, The Netherlands) and sequenced for 1x 75bp single-end sequencing on the Nextseq500 system. After sequencing the data was trimmed (unique identifiers and adaptor flanks) and aligned to genome build 'GRCh38.p10'. PCR-duplicate reads were removed and single cell calls were determined using Aneufinder (v1.14) using the Hidden-Markov-Method and DNAcopy described previously [61].

The Marisa dataset is publically available (GSE39582) and was analyzed using Genomics Analysis and Visualization Platform R2 [62].

Data availability

The authors declare that all data supporting the findings of this study are available within the article and its Supplementary Information files. Data used to generate figures 5a,b,e,f are publically available (GSE20916, GSE8671, GSE4183, GSE132465 and GSE144735), as is the Marisa dataset (GSE39582). The publically available TCGA COAD dataset was used to generate Figure 6i and supplementary figure 5a and b.

Acknowledgements

This work was supported by Oncode, KWF project 2015-7587 and 10150 funding to JPM lab, Cancer Research UK core funding to the CRUK Beatson Institute, A17196, and Cancer Research UK core funding to OJS lab, A21139. RJ was also funded by a Marie Sklodowska Curie Actions Individual Fellowship, 659666. The authors would like to thank Wouter L Smit and Jarom Heijmans for kindly providing the mouse AK, AKS and AKSP organoids.

References

1. Barker, N., et al., Identification of stem cells in small intestine and colon by marker gene Lgr5. Nature, 2007. 449(7165): p. 1003-7.
2. Ramesh, P. and J.P. Medema, BCL-2 family deregulation in colorectal cancer: potential for BH3 mimetics in therapy. Apoptosis, 2020. 25(5-6): p. 305-320.
3. Hanahan, D. and R.A. Weinberg, The hallmarks of cancer. Cell, 2000. 100(1): p. 57-70.
4. Bock, F.J. and S.W.G. Tait, Mitochondria as multifaceted regulators of cell death. Nat Rev Mol Cell Biol, 2020. 21(2): p. 85-100.
5. Rampino, N., et al., Somatic frameshift mutations in the BAX gene in colon cancers of the microsatellite mutator phenotype. Science, 1997. 275(5302): p. 967-9.
6. Campbell, K.J. and S.W.G. Tait, Targeting BCL-2 regulated apoptosis in cancer. Open Biol, 2018. 8(5).
7. Beroukhim, R., et al., The landscape of somatic copy-number alteration across human cancers. Nature, 2010. 463(7283): p. 899-905.
8. Souers, A.J., et al., ABT-199, a potent and selective BCL-2 inhibitor, achieves antitumor activity while sparing platelets. Nat Med, 2013. 19(2): p. 202-8.
9. Merino, D., et al., BH3-Mimetic Drugs: Blazing the Trail for New Cancer Medicines. Cancer Cell, 2018. 34(6): p. 879-891.
10. Vaillant, F., et al., Targeting BCL-2 with the BH3 mimetic ABT-199 in estrogen receptor-positive breast cancer. Cancer Cell, 2013. 24(1): p. 120-9.
11. Zhang, H., et al., Genomic analysis and selective small molecule inhibition identifies BCL-X(L) as a critical survival factor in a subset of colorectal cancer. Mol Cancer, 2015. 14: p. 126.
12. Maurer, C.A., et al., Apoptosis inhibiting factor Bcl-xL might be the crucial member of the Bcl-2 gene family in colorectal cancer. Dig Dis Sci, 1998. 43(12): p. 2641-8.
13. Krajewska, M., et al., Elevated expression of Bcl-X and reduced Bak in primary colorectal adenocarcinomas. Cancer Res, 1996. 56(10): p. 2422-7.
14. Scherr, A.L., et al., Bcl-xL is an oncogenic driver in colorectal cancer. Cell Death Dis, 2016. 7(8): p. e2342.
15. Zhang, Y.L., et al., Significance of Bcl-xL in human colon carcinoma. World J Gastroenterol, 2008. 14(19): p. 3069-73.
16. Colak, S., et al., Decreased mitochondrial priming determines chemoresistance of

colon cancer stem cells. Cell Death Differ, 2014. 21(7): p. 1170-7.
17. van der Heijden, M., et al., Bcl-2 is a critical mediator of intestinal transformation. Nat Commun, 2016. 7: p. 10916.
18. Healy, M.E., et al., MCL1 Is Required for Maintenance of Intestinal Homeostasis and Prevention of Carcinogenesis in Mice. Gastroenterology, 2020. 159(1): p. 183-199.
19. Fessler, E., et al., TGFß signaling directs serrated adenomas to the mesenchymal colorectal cancer subtype. EMBO Mol Med, 2016. 8(7): p. 745-60.
20. Drost, J., et al., Sequential cancer mutations in cultured human intestinal stem cells. Nature, 2015. 521(7550): p. 43-7.
21. van de Wetering, M., et al., Prospective derivation of a living organoid biobank of colorectal cancer patients. Cell, 2015. 161(4): p. 933-45.
22. Villalobos-Ortiz, M., et al., BH3 profiling discriminates on-target small molecule BH3 mimetics from putative mimetics. Cell Death Differ, 2020. 27(3): p. 999-1007.
23. Tao, Z.F., et al., Discovery of a Potent and Selective BCL-XL Inhibitor with in Vivo Activity. ACS Med Chem Lett, 2014. 5(10): p. 1088-93.
24. Kotschy, A., et al., The MCL1 inhibitor S63845 is tolerable and effective in diverse cancer models. Nature, 2016. 538(7626): p. 477-482.
25. Tron, A.E., et al., Discovery of Mcl-1-specific inhibitor AZD5991 and preclinical activity in multiple myeloma and acute myeloid leukemia. Nat Commun, 2018. 9(1): p. 5341.
26. Vermeulen, L., et al., Wnt activity defines colon cancer stem cells and is regulated by the microenvironment. Nat Cell Biol, 2010. 12(5): p. 468-76.
27. Aubrey, B.J., et al., How does p53 induce apoptosis and how does this relate to p53-mediated tumour suppression? Cell Death Differ, 2018. 25(1): p. 104-113.
28. Smit, W.L., et al., Driver mutations of the adenoma-carcinoma sequence govern the intestinal epithelial global translational capacity. Proc Natl Acad Sci U S A, 2020. 117(41): p. 25560-25570.
29. Soderquist, R.S., et al., Systematic mapping of BCL-2 gene dependencies in cancer reveals molecular determinants of BH3 mimetic sensitivity. Nat Commun, 2018. 9(1): p. 3513.
30. Lee, H.O., et al., Lineage-dependent gene expression programs influence the immune landscape of colorectal cancer. Nat Genet, 2020. 52(6): p. 594-603.
31. Jung, P., et al., Isolation of Human Colon Stem Cells Using Surface Expression of PTK7. Stem Cell Reports, 2015. 5(6): p. 979-987.
32. Miyaki, M., et al., Genetic changes and histopathological types in colorectal tumors from patients with familial adenomatous polyposis. Cancer Res, 1990. 50(22): p. 7166-73.
33. Kikuchi-Yanoshita, R., et al., Loss of expression of the DCC gene during progression of colorectal carcinomas in familial adenomatous polyposis and non-familial adenomatous polyposis patients. Cancer Res, 1992. 52(13): p. 3801-3.
34. Meijer, G.A., et al., Progression from colorectal adenoma to carcinoma is associated with non-random chromosomal gains as detected by comparative genomic hybridisation. J Clin Pathol, 1998. 51(12): p. 901-9.
35. Slattery, M.L., et al., MicroRNA profiles in colorectal carcinomas, adenomas and normal colonic mucosa: variations in miRNA expression and disease progression. Carcinogenesis, 2016. 37(3): p. 245-261.
36. Vejnar, C.E. and E.M. Zdobnov, MiRmap: comprehensive prediction of microRNA

target repression strength. Nucleic Acids Res, 2012. 40(22): p. 11673-83.
37. Li, Y., et al., Adenomatous polyposis coli (APC) regulates miR17-92 cluster through ß-catenin pathway in colorectal cancer. Oncogene, 2016. 35(35): p. 4558-4568.
38. Scherr, M., et al., Differential expression of miR-17~92 identifies BCL2 as a therapeutic target in BCR-ABL-positive B-lineage acute lymphoblastic leukemia. Leukemia, 2014. 28(3): p. 554-65.
39. Li, Y., et al., MYC through miR-17-92 suppresses specific target genes to maintain survival, autonomous proliferation, and a neoplastic state. Cancer Cell, 2014. 26(2): p. 262-72.
40. Swier, L., et al., Intricate crosstalk between MYC and non-coding RNAs regulates hallmarks of cancer. Mol Oncol, 2019. 13(1): p. 26-45.
41. Muthalagu, N., et al., BIM is the primary mediator of MYC-induced apoptosis in multiple solid tissues. Cell Rep, 2014. 8(5): p. 1347-53.
42. Sarosiek, K.A. and A. Letai, Directly targeting the mitochondrial pathway of apoptosis for cancer therapy using BH3 mimetics - recent successes, current challenges and future promise. Febs j, 2016. 283(19): p. 3523-3533.
43. Ni Chonghaile, T., et al., Pretreatment mitochondrial priming correlates with clinical response to cytotoxic chemotherapy. Science, 2011. 334(6059): p. 1129-33.
44. Kelly, G.L., et al., Targeting of MCL-1 kills MYC-driven mouse and human lymphomas even when they bear mutations in p53. Genes Dev, 2014. 28(1): p. 58-70.
45. Zhang, L., et al., BH3 Mimetic Sensitivity of Colorectal Cancer Cell Lines in Correlation with Molecular Features Identifies Predictors of Response. International Journal of Molecular Sciences, 2021. 22(8): p. 3811.
46. Ooft, S.N., et al., Patient-derived organoids can predict response to chemotherapy in metastatic colorectal cancer patients. Sci Transl Med, 2019. 11(513).
47. Mason, K.D., et al., Programmed anuclear cell death delimits platelet life span. Cell, 2007. 128(6): p. 1173-86.
48. Cragg, M.S., et al., Treatment of B-RAF mutant human tumor cells with a MEK inhibitor requires Bim and is enhanced by a BH3 mimetic. J Clin Invest, 2008. 118(11): p. 3651-9.
49. Verissimo, C.S., et al., Targeting mutant RAS in patient-derived colorectal cancer organoids by combinatorial drug screening. Elife, 2016. 5.
50. Dews, M., et al., Augmentation of tumor angiogenesis by a Myc-activated microRNA cluster. Nat Genet, 2006. 38(9): p. 1060-5.
51. O'Donnell, K.A., et al., c-Myc-regulated microRNAs modulate E2F1 expression. Nature, 2005. 435(7043): p. 839-43.
52. Yu, G., et al., Prognostic values of the miR-17-92 cluster and its paralogs in colon cancer. J Surg Oncol, 2012. 106(3): p. 232-7.
53. Ma, Y., et al., Elevated oncofoetal miR-17-5p expression regulates colorectal cancer progression by repressing its target gene P130. Nat Commun, 2012. 3: p. 1291.
54. Xu, J., et al., Long Noncoding RNA MIR17HG Promotes Colorectal Cancer Progression via miR-17-5p. Cancer Res, 2019. 79(19): p. 4882-4895.
55. Sarosiek, K.A., et al., Developmental Regulation of Mitochondrial Apoptosis by c-Myc Governs Age- and Tissue-Specific Sensitivity to Cancer Therapeutics. Cancer Cell, 2017. 31(1): p. 142-156.
56. Montero, J. and A. Letai, Why do BCL-2 inhibitors work and where should we use them in the clinic? Cell Death Differ, 2018. 25(1): p. 56-64.

57. Murphy, D.J., et al., Distinct thresholds govern Myc's biological output in vivo. Cancer Cell, 2008. 14(6): p. 447-57.
58. Ramesh, P., et al., Isolation, Propagation, and Clonogenicity of Intestinal Stem Cells. Methods Mol Biol, 2019. 2002: p. 61-73.
59. Sato, T., et al., Long-term expansion of epithelial organoids from human colon, adenoma, adenocarcinoma, and Barrett's epithelium. Gastroenterology, 2011. 141(5): p. 1762-72.
60. Ianevski, A., et al., SynergyFinder: a web application for analyzing drug combination dose-response matrix data. Bioinformatics, 2017. 33(15): p. 2413-2415.
61. Bolhaqueiro, A.C.F., et al., Ongoing chromosomal instability and karyotype evolution in human colorectal cancer organoids. Nat Genet, 2019. 51(5): p. 824-834.
62. The Department of Human Genetics in the Amsterdam Medical Centre (AMC): R2 database. Genomic analysis and visualization platform. 2020.

Supplemental information

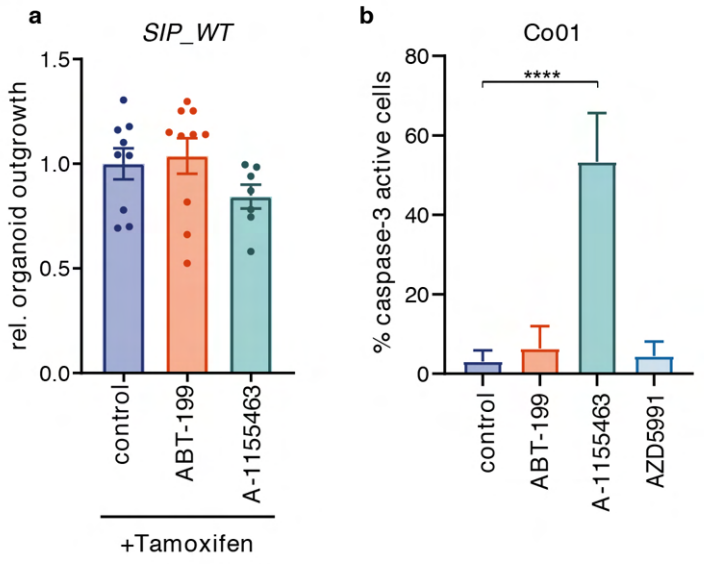

Supplementary Figure 1. BCL-2 and BCL-XL are essential for ISC survival during transformation.

a. Graphs depict relative outgrowth of wild type (WT) proximal small intestine (SIP)-derived organoid structures quantified 3 days after passaging, upon treatment with 1μM ABT-199 or A-1155463 in combination with 1 μM Tamoxifen. Each dot represents a replicate (minimal n=7 per condition, n=3 independent experiments), error bars indicate s.e.m.

b. Percentage of activated caspase-3 in the 10% TOP-GFP high Co01 cells after 24 h treatment with 1 μM ABT-199, AZD5991 or A-1155463. Data represents mean ± SD. (n=2 independent experiments). ****$p < 0.0001$, student's t-test.

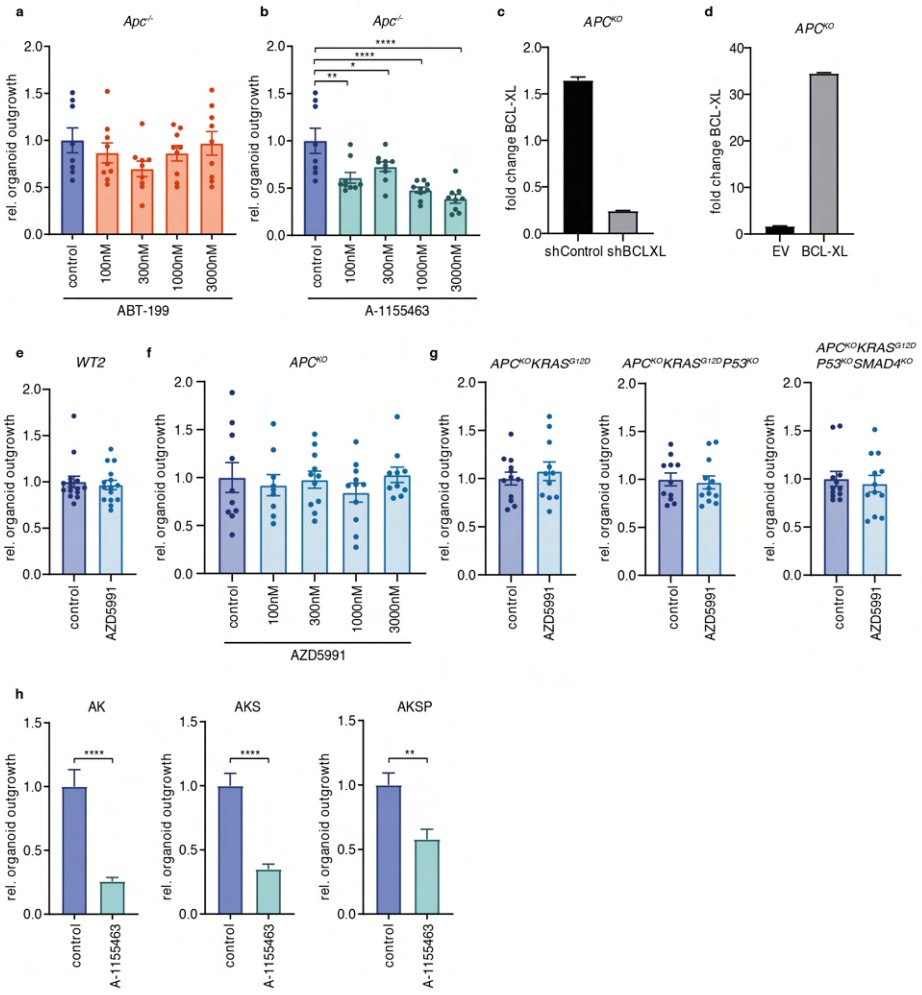

Supplementary Figure 2. BCL-2 dependence is lost immediately after transformation.

a, b. Graphs depict relative outgrowth of mouse *Apc*$^{-/-}$ organoids quantified 3 days after passaging, upon treatment with indicated doses of (a) ABT-199 or (b) A-1155463. Each dot represents a replicate (minimal n=8 per condition, n=3 independent experiments), error bars indicate s.e.m. * $p<0.05$, ** $p<0.01$, **** $p<0.0001$, ordinary one-way ANOVA.

c. qRT-PCR analysis of *BCL-XL* expression in *APC*^{KO} organoids transduced with control or BCL-XL targeting shRNA, normalized to *RPLP0* expression. Data represents mean ± SD.

d. qRT-PCR analysis of *BCL-XL* expression in *APC*^{KO} organoids transduced with control or BCL-XL overexpression constructs, normalized to *RPLP0* expression. Data represents mean ± SD.
e. Graphs depict relative outgrowth of human normal colon organoids (*WT2*) quantified 3 days after passaging, upon treatment with 1 μM AZD5991. Each dot represents a replicate (minimal n=15 per condition, n=3 independent experiments), error bars indicate s.e.m.
f. Graphs depict relative outgrowth of human *APC*^{KO} organoids quantified 3 days after passaging, upon treatment with indicated doses of AZD5991. Each dot represents a replicate (minimal n=9 per condition, n=3 independent experiments), error bars indicate s.e.m.
g. Relative outgrowth of human mutant organoids of indicated genotypes quantified 3 days after passaging, upon treatment with 3 μM of AZD5991 (n=3 independent experiments). Error bars indicate s.e.m.
h. Relative outgrowth of mouse organoids of indicated genotypes quantified 3 days after passaging, upon treatment with 3 μM of A-1155463 (n=3 independent experiments). Error bars indicate s.e.m. **p<0.01, **** p<0.0001, student's t-test. AK: *ApcKras*, AKS: *ApcKrasSmad4*, AKSP: *ApcKrasSmad4p53*.

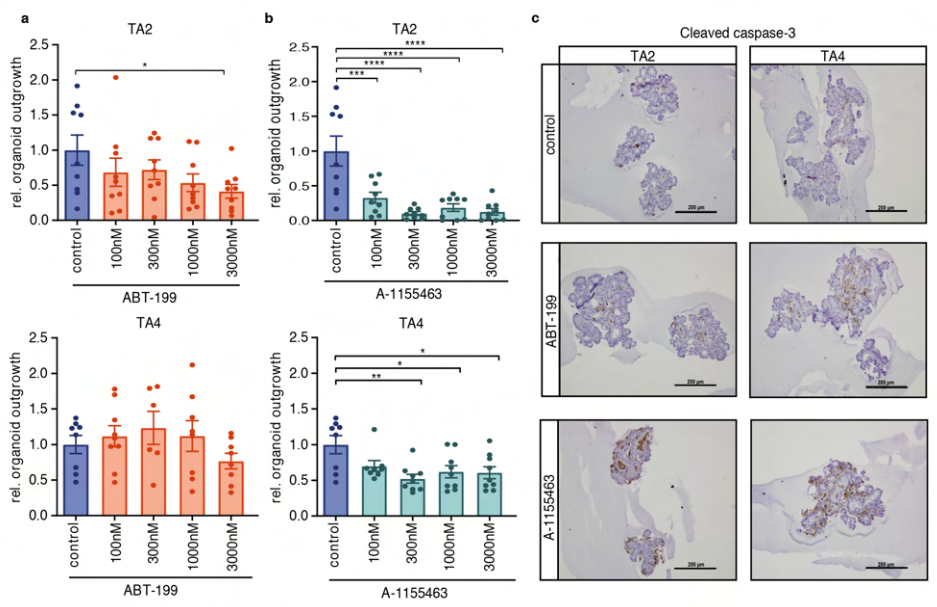

Supplementary Figure 3. BCL-XL is crucial for stem cell survival in patient-derived tubular adenoma organoids.

a, b. Graphs depict relative outgrowth of human tubular adenomas (a) TA2 and (b) TA4 quantified 3 days after passaging, upon treatment with indicated doses of ABT-199 or A-1155463. Each dot represents a replicate (minimal n=6 per condition, n=3 independent experiments), error bars indicate s.e.m. * $p<0.05$, ** $p<0.01$,***$p<0.001$, **** $p<0.0001$, ordinary one-way ANOVA.

c. Cleaved caspase-3 stained human TAs after 24h treatment with 300 nM ABT-199 or A-1155463. Scale bars, 200 µm.

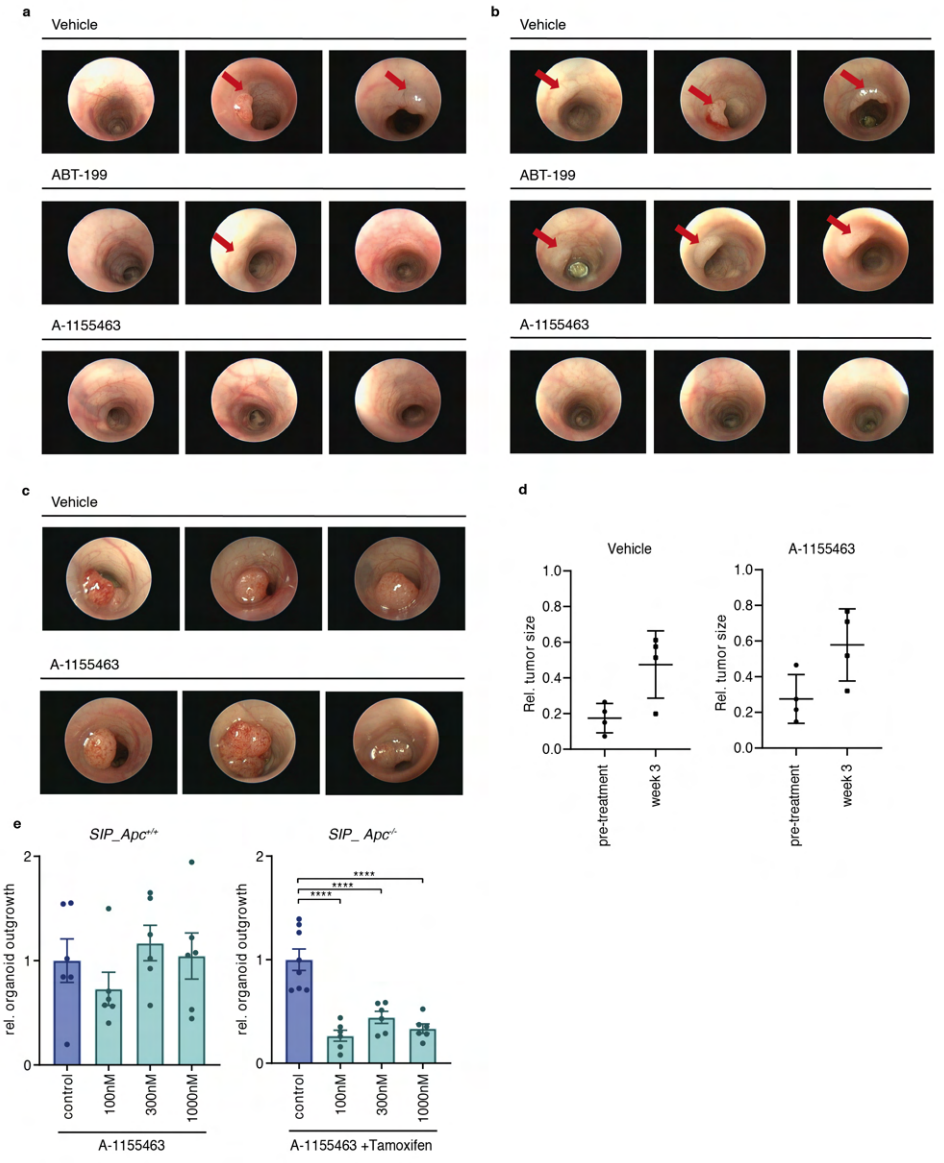

Supplementary Figure 4. BCL-XL inhibition impairs adenoma outgrowth in vivo. a, b. Representative images from a colonoscopy of *Villin*Cre^{ER}*Apc*$^{fl/fl}$ mice, one (a) and two (b) weeks after being induced with a single injection of 4-hydroxytamoxifen into the colonic sub-mucosa. ABT-199 and A-1155463 treated mice received 100 mg/kg of drug for two days prior to induction followed by treatment every other day until day 28. Red arrows indicate tumors.

c. Representative images from a colonoscopy of *Villin*Cre^{ER}*Apc*$^{fl/fl}$ mice three weeks after treatment with either vehicle or A-1155463. Mice were induced with a single injection of 4-hydroxytamoxifen into the colonic sub-mucosa and treatment began two weeks after induction and continued for 28 days.

d. Quantification of colonic tumor size (normalized to the size of the lumen) of mice described in (c), at pre-treatment and after three weeks of treatment. n = 4 for vehicle and n=4 for A1155463.

e. Graphs depict relative outgrowth of SIP-derived organoid structures quantified 3 days after passaging for the indicated genotype, upon treatment with 1 μM A-1155463, at the time of induction. Each dot represents a replicate (minimal n=6 per condition, n=2 independent experiments), error bars indicate s.e.m. **** p<0.0001, ordinary one-way ANOVA.

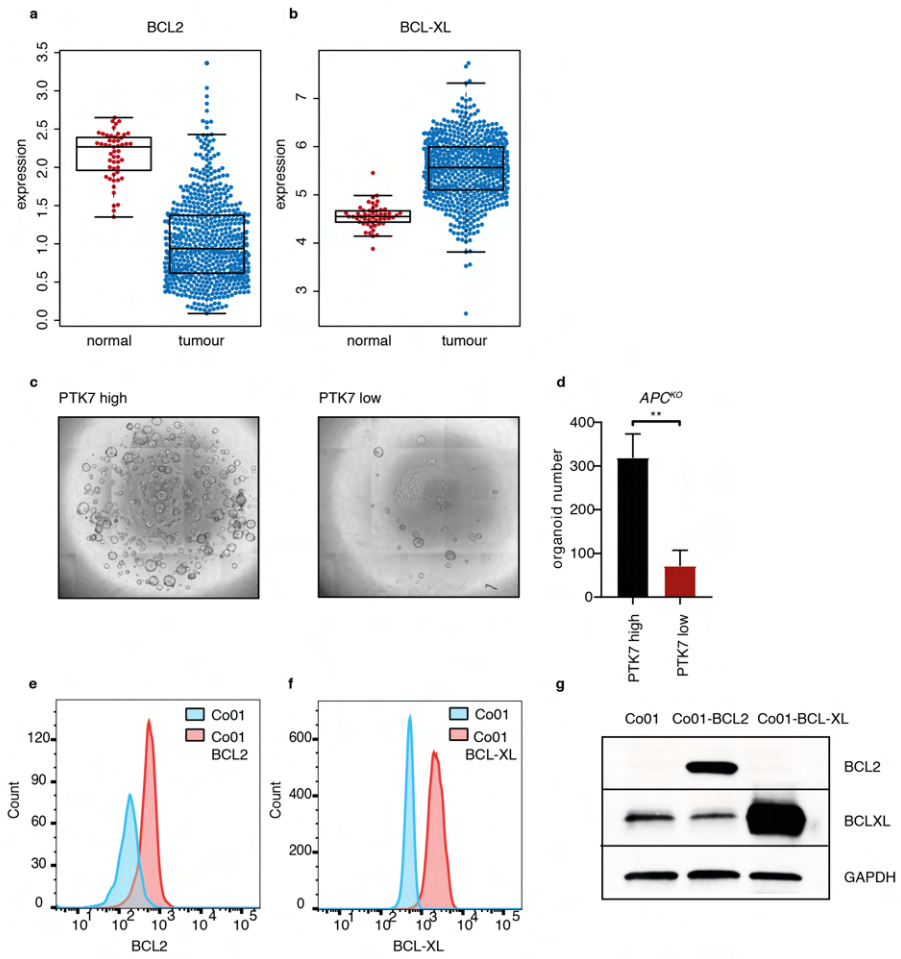

Supplementary Figure 5. BCL-2 expression is decreased upon transformation.
a, b. mRNA expression of *BCL-2* (a) and *BCL-XL* (b) in the TCGA COAD cohort comparing normal and CRC tumor tissues.
c. Representative images of APC^{KO} organoids outgrowth 7 days after sorting for PTK7 high and low fractions. An equal number of cells was plated for both conditions.
d. Quantification of APC^{KO} organoid outgrowth following sorting for PTK7 high and low populations (n=3 independent experiments). **p<0.01, student's t-test.
e, f. Intracellular FACs staining of (e) BCL-2 and (f) BCL-XL in either control or Co01 cells overexpressing the respective proteins.
g. Immunoblot analysis of BCL-2 and BCL-XL protein levels in Co01 control or BCL-2 and BCL-XL overexpressing cells. GAPDH was used as a loading control.

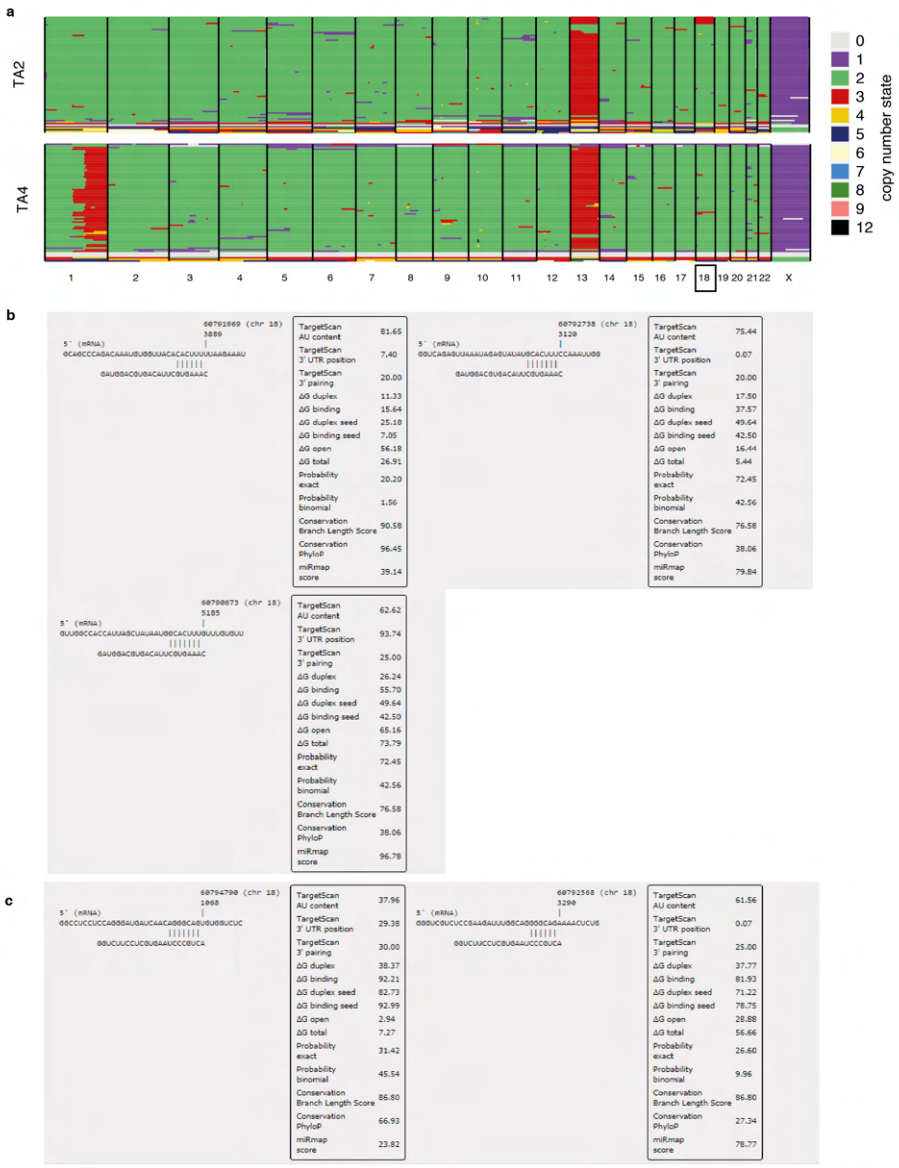

Supplementary Figure 6. MiR-17-5p regulates BCL-2 expression in APC-mutant organoids.

a. single cell karyotype-seq data showing the ploidy in individual cells of TA2 and TA4. Graphs show individual cells (horizontal lines) and colors indicate copy number state for a given chromosome (columns).

b, c. Binding sites of miR-17-5p (b) and miR-18a-3p (c) on the BCL-2 3'UTR as predicted by miRmap.

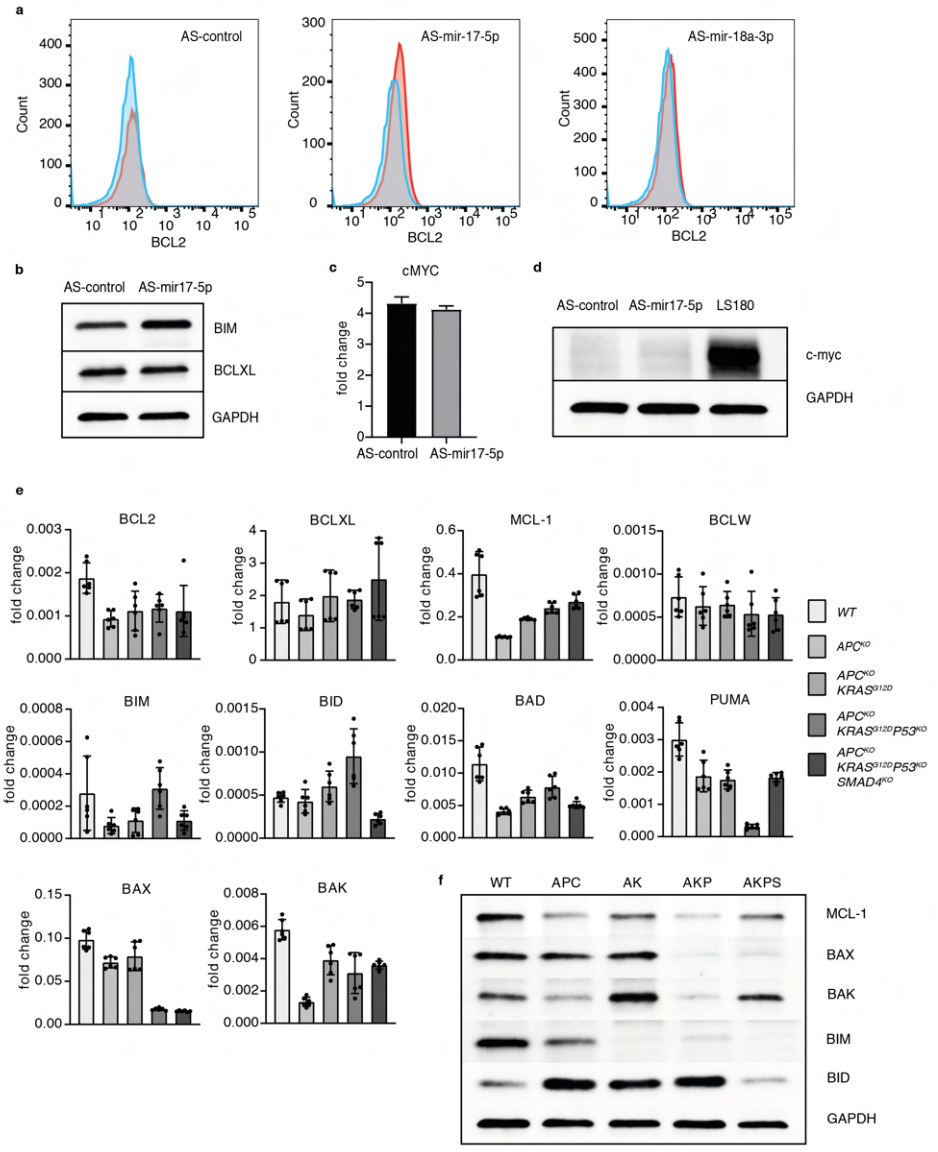

Supplementary Figure 7. MiR-17-5p regulates BCL-2 expression in APC-mutant organoids.

a. BCL-2 Intracellular FACs staining plots of data represented in figure 6h.

b. Immunoblot analysis of BIM and BCL-XL protein levels in control and mir-17-5p anti-sense (AS) transduced *APC*^{KO} organoids. GAPDH was used as a loading control.

c. qRT-PCR analysis of c-Myc expression in *APC*^{KO} organoids transduced with either AS-control or AS- mir-17-5p, normalized to *RPLP0* expression. Data represents mean ± SD.

d. Immunoblot analysis of c-MYC protein levels in AS-control and AS-mir-17-5p transduced *APC*^{KO} organoids. CRC cell line LS180 was used as a positive control. GAPDH was used as a loading control.

e. qRT-PCR analysis of indicated BCL-2 family members in human colon organoids of indicated genotypes, normalized to *RPLP0* expression (n=2 independent experiments). Data represents mean ± SD.

f. Immunoblot analysis of indicated BCL-2 family members in human colon organoids of indicated genotypes. GAPDH was used as a loading control.

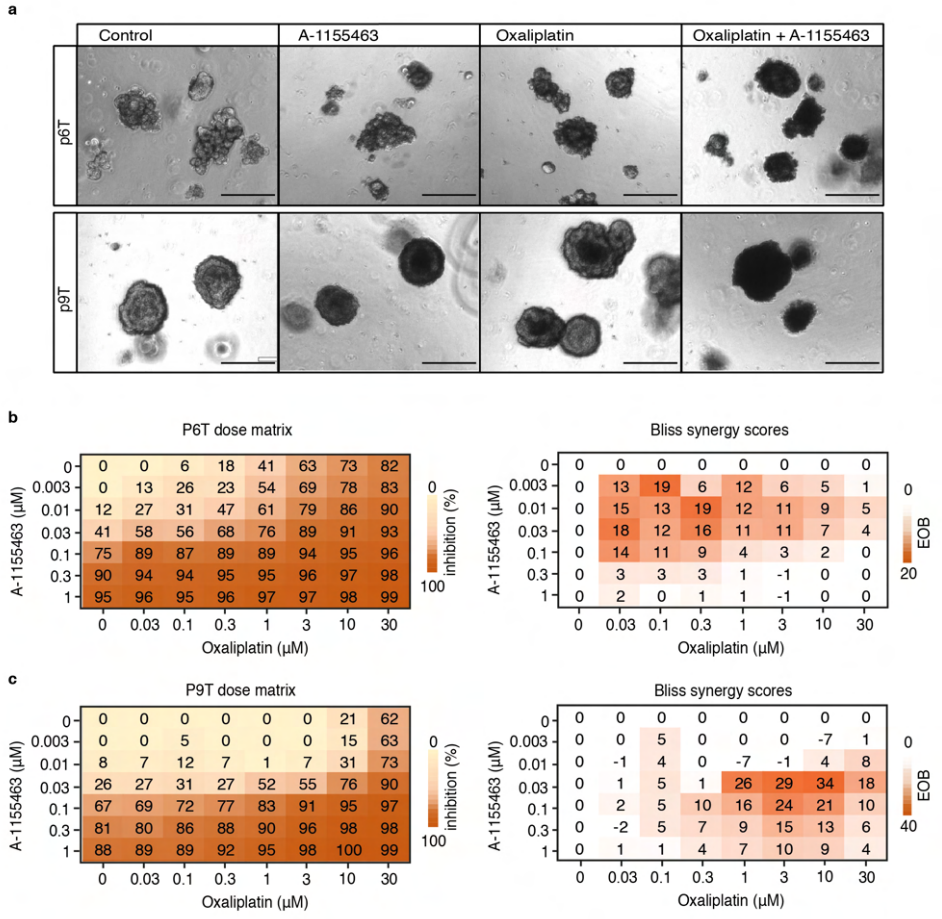

Supplementary Figure 8. BCL-XL inhibition is synergistic with oxaliplatin in tumor-derived organoids.

a. Phase-contrast images of p6T and p9T human CRC organoids treated for 72h with 10μM oxaliplatin alone and in combination with 30nM A-1155463. Scale bars, 250 μm.

b, c. 6 x 7 dose matrices of (b) p6T and (c) p9T human CRC organoids treated with oxaliplatin in combination with A-1155463 for 5 days. % inhibition was calculated from viability data measured by cell titer blue, after normalizing to control. Data represent the average of two independent experiments. Bliss synergy scores were calculated for each dose combination and positive scores indicate synergistic effects.

microRNA	Gene	mirMap Score
hsa-miR-20a-5p	BCL2	96.57
hsa-miR-93-5p	BCL2	96.31
hsa-miR-23a-3p	BCL2	96.06
hsa-miR-17-5p	BCL2	95.60
hsa-miR-663b	BCL2	94.54
hsa-miR-424-3p	BCL2	72.52
hsa-miR-18a-3p	BCL2	66.95
hsa-miR-27a-3p	BCL2	64.36
hsa-miR-24-3p	BCL2	38.72
hsa-miR-501-3p	BCL2	23.71
hsa-miR-21-5p	BCL2	11.50
hsa-miR-25-3p	BCL2	10.43
hsa-miR-92a-3p	BCL2	9.67
hsa-miR-29a-3p	BCL2	9.39
hsa-miR-21-3p	BCL2	7.93
hsa-miR-29b-3p	BCL2	6.55

Supplementary Table 1. List of microRNAs with binding sites on the *BCL-2* 3'UTR that are highly upregulated in colon adenomas and carcinomas. Table indicates mirMAP scores for all the microRNAs that have binding sites in *BCL-2* 3'UTR. miR17-92 family members are in bold.

Primers:		
Gene	**Forward sequence**	**Reverse sequence**
BCL-2	CAGCCAGGAGAAATCAAACAG	GACTGAGTACCTGAACCGGC
BCL-XL	AGCCTTGGATCCAGGAGAAC	AAGAGTGAGCCCAGCAGAAC
MCL-1	AAGCCAATGGGCAGGTCT	TGTCCAGTTTCCGAAGCAT
BCL-W	CTGGCTGACTGGATCCACAG	AGCACTGTCCTCACTGATGC
BIM	TCGATCCTCCAGTGGGTATT	GTCCCAGTTAGCCATTGCAC
BID	CATCCCTCCGGGCCTGGTGA	AGGGTAGGCCTGCAGCAGCT
BAD	CTCCGGAGGATGAGTGACGA	CACCAGGACTGGAAGACTCG
PUMA	AGCAGGGCAGGAAGTAACAA	CCACAAATCTGGCAGGGGA
BAX	TCATGGGCTGGACATTGGAC	GCGTCCCAAAGTAGGAGAGG
BAK	GGCAGGCTGATCCCGTC	CTGCGGAAAACCTCCTCTGT
c-Myc	AGCTGCTTAGACGCTGGATTTT	TTCCTGTTGGTGAAGCTAACGTT
RPLPO	GGCACCATTGAAATCCTGAGT-GATGTG	TTGCGGACACCCTCCAGGAAGC

Supplementary Table 2. List of qPCR primers used in the study.

Chapter 4

BCL-XL inhibition induces an FGFR4 mediated rescue response in colorectal cancer

Prashanthi Ramesh, Simone Di Franco*, Lidia Atencia Taboada*, Le Zhang, Annalisa Nicotra, Giorgio Stassi and Jan Paul Medema.

Accepted for publication in *Cell Reports, 2022.*

*Equal Contribution

Abstract

The heterogeneous therapy response observed in colorectal cancer is in part driven by cancer stem cells (CSCs) that resist chemotherapeutic insults. Anti-apoptotic protein BCL-XL has been shown to play a critical role in CSC chemoresistance, where its inhibition with BH3 mimetics re-sensitizes CSCs to chemotherapy-induced cell death. To unravel the pathways mediating BCL-XL sensitivity in CSCs, we screened a compound library and identified broad inhibitors of receptor tyrosine kinases that synergize with low dose of BCL-XL inhibitor A-1155463. Herein, we find that specific inhibition of FGFR4 mediates sensitization to A-1155463 both *in vitro* and *in vivo*. Mechanistically, we identify a rescue response that is activated upon BCL-XL inhibition and leads to upregulation of MCL-1. FGFR4 inhibition prevents MCL-1 upregulation and thereby sensitizes CSCs to BCL-XL inhibition. Altogether, our findings suggest a rapid and transferable induction of resistance to BCL-XL inhibition in CRC, which can be circumvented by inhibition of FGFR4.

Introduction

Colorectal cancer (CRC) is a leading cause of cancer-related deaths worldwide [1]. Effective treatment strategies have improved 5-year patient survival rates to approximately 90% for early stage disease. However, survival rates drop to as low as 15% at advanced stages, particularly in the case of metastatic disease [2]. Patients with advanced stage CRC are routinely given adjuvant chemotherapy consisting of fluoropyrimidines (capecitabine or 5-fluorouracil) and oxaliplatin or irinotecan, in order to avoid outgrowth of the tumor at distant sites. Such intensive therapeutic regimens appear to be inadequate, as there is convincing evidence for the occurrence of therapy resistance resulting in nearly 30% recurrence at stage 3 disease [3, 4].

Resistance to chemotherapy is in part driven by the intratumoral heterogeneity observed in CRC lesions [5]. CRC tumors are hierarchically organized with cancer stem cells (CSCs) at the apex of this hierarchy. CSCs are a small subset of cells within the tumor population, with the ability to differentiate into multiple progeny and thereby drive tumor growth [6]. Importantly, our previous work suggests that the CSC population displays plasticity, in part regulated by the microenvironment [7]. Moreover, several studies have shown colon CSCs to be particularly resistant to chemotherapeutic insults, thereby enabling tumor repopulation [8-10]. This resistance capacity is also enhanced by the microenvironment and calls for novel treatment opportunities for the eradication of this subpopulation to achieve efficient tumor remission [11].

Chemotherapy-induced stress results in the activation of the mitochondrial apoptosis pathway whereby upregulated pro-apoptotic BH3-only proteins overcome anti-apoptotic BCL-2 proteins and ultimately initiate caspase activity to execute cell death [12]. Resistance to apoptosis by the up-regulation of anti-apoptotic BCL-2 family proteins is frequently observed in several tumor types [13, 14]. Many hematological malignancies rely on BCL-2 for apoptosis evasion and are therefore sensitive to its specific inhibitor,

ABT-199 (Venetoclax) [15]. On the other hand, solid tumors seem to depend more on BCL-XL overexpression as a mechanism of anti-apoptotic adaptation [16]. Several studies have observed upregulation of BCL-XL in CRC lesions and its inhibition with highly specific BH3 mimetics WEHI-539, A-1155463 and A-1331852 effectively target CRC cell lines and xenografts for cell death [8, 17-20]. In this regard, we have previously reported that colon CSCs in particular upregulate BCL-XL and are thereby less primed for mitochondrial cell death in comparison to their differentiated progeny [8]. Therefore, targeting BCL-XL with WEHI-539 impairs CSC clonogenicity and sensitizes them to chemotherapy [8]. More recently, we have shown that BCL-XL plays a critical role in CRC initiation and progression, as targeting BCL-XL with A-1155463 significantly impaired clonogenic potential of adenoma and tumor organoids while sparing normal colon organoids [21]. While this would prove beneficial for CRC therapy, clinical implementation of BCL-XL inhibition is hampered by the observed toxicity to platelets, whose life-span is determined by BCL-XL expression [22]. We therefore designed a screen to elucidate signaling pathways, which when inhibited synergize with the targeting of BCL-XL in CSCs. Such synergistic effects not only provide mechanistic insight into CSC functioning but can also be exploited as a therapeutic target with minimal toxic side-effects.

To elucidate the pathways regulating BCL-XL dependency of colon CSCs, we screened compounds in combination with a low dose of BCL-XL specific inhibitor A-1155463 to identify hits that in combination facilitate cell death, while also circumventing thrombocytopenia. We thus identified a group of receptor tyrosine kinase (RTK) inhibitors that strongly synergize with low dose A-1155463 to target colon CSCs and patient-derived tumor organoids for apoptosis, without inducing toxicity in healthy colon cells and platelets. Gene expression analysis and combinations with selective inhibitors revealed that the efficacy of the identified hits resulted from inhibition of FGFR4 signaling. Importantly, we identified that cells treated with a low dose of A-1155363 activate a rescue response by upregulating MCL-1. Furthermore, we find that BCL-XL inhibition results in FGF2 mediated activation of FGFR4 signaling, which could mediate the observed

MCL-1 upregulation by ERK dependent phosphorylation. Targeting FGFR4 could therefore prevent the activation of this rescue response and facilitate BH3 mimetic-induced cell death in CRC cells. Our findings suggest a rapid induction of resistance to anti-apoptotic protein inhibition, which occurs even in the absence of apoptosis and can be circumvented by concomitant inhibition of the FGFR4 signaling pathway.

Results

Drug screen identifies compounds that synergize with low-dose BCL-XL inhibition

To identify compounds that lower the threshold of A-1155463-induced cell death and thereby facilitate colon CSC apoptosis, we screened a primary CRC spheroid culture Co01 with 1402 unique inhibitors alone and in combination with a low dose of A-1155463 (Fig. 1A). A-1155463 was chosen for BCL-XL inhibition as it was significantly more potent in comparison to previously used WEHI-539 (Supplementary Fig. 1A) [18]. We defined the low dose of A-1155463 as the IC_{10} dose, wherein the drug did not induce significant cell death but was still able to prime CSCs. Based on the titration of A-1155463 on Co01 cells, we set the low dose as 5nM with which we observed an 8% decrease in viability on average, corresponding to the IC_{10} dose (Supplementary Fig. 1B). Furthermore, to ensure that the chosen dose of A-1155463 was non-toxic to platelets, a known side-effect of targeting BCL-XL *in vivo*, we performed a titration on platelets derived from human whole blood samples. Treatment for 2h did not affect platelet viability, while after 6h, only the higher doses resulted in platelet cell death and at 24h, A-1155463 had an IC50 of ~500nM for human platelets, thus confirming that 5nM was a low, non-toxic dose (Supplementary Fig. 1C). As an additional control for the screen, to ensure that the inhibitors specifically overcome BCL-XL-driven resistance, we also screened all compounds on Co01 transduced with a BCL-XL overexpression plasmid. This resistant line had a higher IC_{50} for A-1155463 and inhibitors that also affected this line in combination with A-1155463 were not considered a true hit due to likely

off-target effects or toxic drug-drug interactions (Fig. 1A, Supplementary Fig. 1B).

The compound library included a range of small-molecule inhibitors targeting key signaling pathways, FDA-approved compounds and chemotherapeutics. Prior to the addition of drugs, cells were first allowed to proliferate overnight and subsequently treated for 2 days after which cell viability was analyzed (Fig. 1A; see methods). Viability data was z-score normalized and replicate measurements were highly correlated for both conditions with and without A-1155463, in both spheroid cultures tested (Fig. 1B, C). To further ensure assay reliability, we calculated the median Z factor score across all screening plates and obtained a score of 0.73 (n=128, upper quartile = 0.80, lower quartile =0.66), indicating an experimentally robust assay.

In order to select hits from the screen, we calculated the added effect of each inhibitor in combination with A-1155463 in comparison to its effect alone and normalized the data by z-score (Supplementary Table 1; see methods). Co01 targeting hits were selected with a z-score cut-off of 2 or higher (Fig. 1D). Upon exclusion of compounds that also targeted the BCL-XL overexpressing line, a total of 81 hits were selected based on these parameters. The selected hits were grouped by their common protein targets to identify potential underlying pathways whose inhibition could sensitize colon CSCs for A-1155463-induced apoptosis (Fig. 1E). This analysis revealed that a large percentage of the hit compounds target aurora kinases (15%) (Fig. 1E). Importantly, our earlier work has established that aurora kinases play a role in colon CSC tumorigenicity and chemoresistance [23]. Moreover, the combination of aurora kinase inhibitors with BCL-XL inhibition has been shown to be synergistic in CRC cell lines [24]. We further validated this on Co01 cells and confirmed that aurora kinase inhibitors dramatically impair cell viability in combination with low-dose A-1155463 (Fig. 1F, G). Identification of this previously reported combination confirmed the effectiveness of our screen in detecting relevant targets.

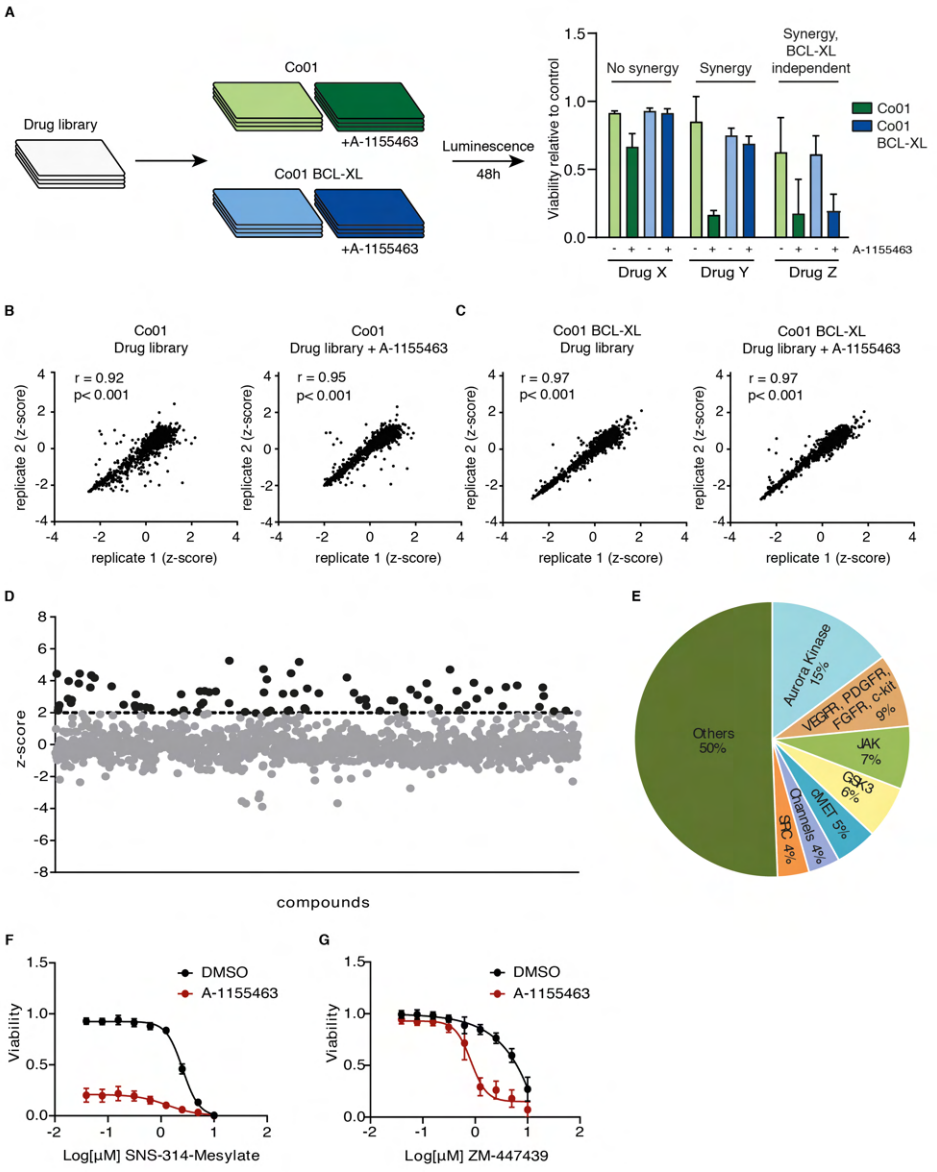

Figure 1. Drug screen identifies compounds that synergize with low-dose BCL-XL inhibition.

A. Schematic overview of the drug screen set-up. Primary spheroid cultures Co01 and Co01 overexpressing BCL-XL were treated with 1402 unique inhibitors either alone or in combination with a low dose of A-1155463 (5nM) and assayed for cell viability 48h later using cell titer blue. Compounds that induced strong cytotoxicity

in combination with A-1155463 on Co01 but not Co01 BCL-XL were selected.
B, C. Scatterplot of z-score normalized viability data of Co01 (B) and Co01 BCL-XL (C) treated with the library alone or in combination with A-1155463 (n = 1402). Plots show the correlation between two technical replicates and data points represents the z-score of each tested compound.
D. Z-score plot of the combination effect with A-1155463 for all inhibitors tested on Co01. Values represent the z-score normalized average of two technical replicates. Hits were selected with a z-score cut-off of 2 or higher (dashed line).
E. Pie chart of the common targets of all hits selected from the screen. The number of inhibitors out of all selected hits that target the respective proteins are indicated in percentages.
F, G. Dose-response curve of Co01 treated with a titration of SNS-314-mesylate (F) or ZM-447439 (G) either alone or in combination with 5nM A-1155463 for 48h. Viability data measured by cell titer blue was blank corrected and normalized to control. Data is represented as mean ± SD (n=3 independent experiments).

Hits from the screen synergize with A-1155463 to induce potent cytotoxicity in colon CSCs and patient-derived tumor organoids

Besides aurora kinase inhibitors, we observed a large fraction of hits targeting a family of RTKs, including VEGFR, PDGFR, FGFR and c-kit, with most inhibitors targeting multiple receptors (Fig. 2A). We validated these inhibitors in a titration on Co01 cells in combination with A-1155463 and found the most consistent and potent efficacy with four of them, namely Ki8751, Axitinib, Nintedanib and Golvatinib (Fig. 2B, Supplementary Fig. 2A-C). Moreover, we analyzed the combinatorial efficacy of these inhibitors with A-1155463 using the Bliss Independence model, where scores above 10 were considered indicative of synergy beyond additive effects. All four inhibitors showed synergy with A-1155463 over a range of concentrations (Fig. 2C). Of the remaining hits in this group, CYC116 not only targets VEGFR but is also a potent inhibitor of Aurora A/B and we therefore concluded that its observed efficacy could also result from aurora kinase inhibition or a combination of the two (Supplementary Fig. 2A). CP-673451 and Crenolanib, both of which are specific inhibitors of PDGFR, showed limited efficacy in a titration with A-1155463 (Supplementary Fig. 2B, C).

Earlier observations indicate that spheroid cultures represent a heterogeneous culture consisting of stem-like and differentiated populations that can be distinguished based on their Wnt-activity, where Wnt-high colon CSCs exhibit enhanced BCL-XL-dependent chemotherapy resistance compared to more differentiated cancer cells [7], [8]. We therefore assessed if the stem cell population in our spheroid culture was effectively sensitized towards A-1155463-induced death by the identified hits. To do this, we took advantage of the Wnt reporter in our Co01 cells (TOP-GFP) and measured cell-death in the Wnt-high population by a FACS-based assay that quantifies levels of activated caspase-3 at the single-cell level. Single treatment with any of the inhibitors did not result in activation of caspase-3, while Axitinib, Ki8751 and Nintedanib significantly induced CSC caspase-3 activity when combined with 5nM A-1155463 (Fig. 2D). Only the combination with Golvatinib did not target CSCs and therefore this drug was excluded from further experiments.

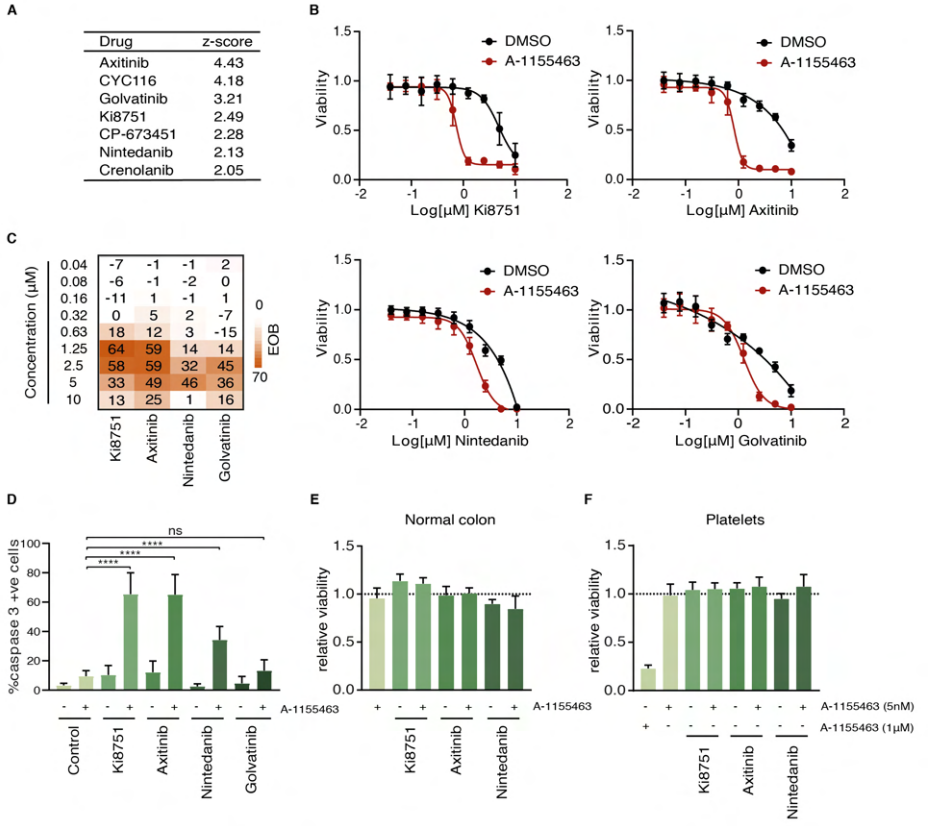

Figure 2. Selected hits induce CSC cell death in combination with A-1155463 while sparing normal colon organoids and platelets.

A. List of hit compounds that target several receptor tyrosine kinases of the VEGFR, PDGFR, FGFR family and c-kit along with their corresponding z-score from the screen.

B. Dose-response curves of Co01 treated with a titration of Ki8751, Axitinib, Nintedanib or Golvatinib, alone and in combination with 5nM A-1155463 for 48h. Viability data measured by cell titer blue was blank corrected and normalized to control. Data is represented as mean ± SD (n=3 independent experiments).

C. Excess over bliss (EOB) synergy scores calculated for the dose-response data in (B).

D. Percentage of activated caspase-3 in the 10% TOP-GFP high Co01 cells after 24h treatment with 1μM Ki8751, Axitinib, Nintedanib or Golvatinib, alone and in combination with 5nM A-1155463. Data is represented as mean ± SD (n=3 independent experiments). ****p value < 0.0001 (two-tailed unpaired Student's t-test).

E. Colon organoids derived from normal tissue were treated with 1μM Ki8751, Axitinib or Nintedanib, alone and in combination with 5nM A-1155463 for 48h, following which viability was measured using cell titer blue. Data is plotted relative to control (dashed line) and represented as mean ± SD (n=3 independent experiments).

F. Viability data of platelets derived from human whole blood treated with 1μM Ki8751, Axitinib or Nintedanib, alone and in combination with 5nM A-1155463 for 24h. Platelets were treated with 1μM A-1155463 as a positive control for platelet toxicity. Data is plotted relative to control (dashed line) and represented as mean ± SD (n=3 independent experiments).

Next, to ensure that the selected combinations were not toxic to healthy colon-derived cells, we treated human normal colon organoids with all three inhibitors alone and in combination with A-1155463 and found that they were not sensitive to any of the inhibitors (Fig. 2E). In addition to this we assessed platelet toxicity of the combinations in human whole blood samples, where A-1155463 was non-toxic in combination with all of the three inhibitors (Fig. 2F).

To ascertain the clinical relevance of these findings, we extended our studies to include four primary patient-derived tumor organoids (p6T, p9T, p16T and p24aT) [25], which we treated in a 5 x 6 matrix titration with the selected inhibitors and A-1155463 (Fig. 3A-D, Supplementary Fig. 3A-C). Synergy was analyzed at each dose combination with the Bliss Independence model and positive scores were observed over a range of concentrations (Fig. 3B, C, D, Supplementary Fig. 3A-C). To assess the overall efficacy of the combinations, we calculated the Bliss synergy scores for the most synergistic 3-by-3 dose window in the dose-response matrices. All inhibitors were synergistic in combination with A-1155463 across the four organoid cultures, except for Ki6751 in p6T and p16T (Fig. 3E). Taken together, we identified and validated three potent inhibitors that synergize with low dose BCL-XL inhibition to induce CRC cell death, including the CSC population, while avoiding toxicity to healthy colon organoids and platelets.

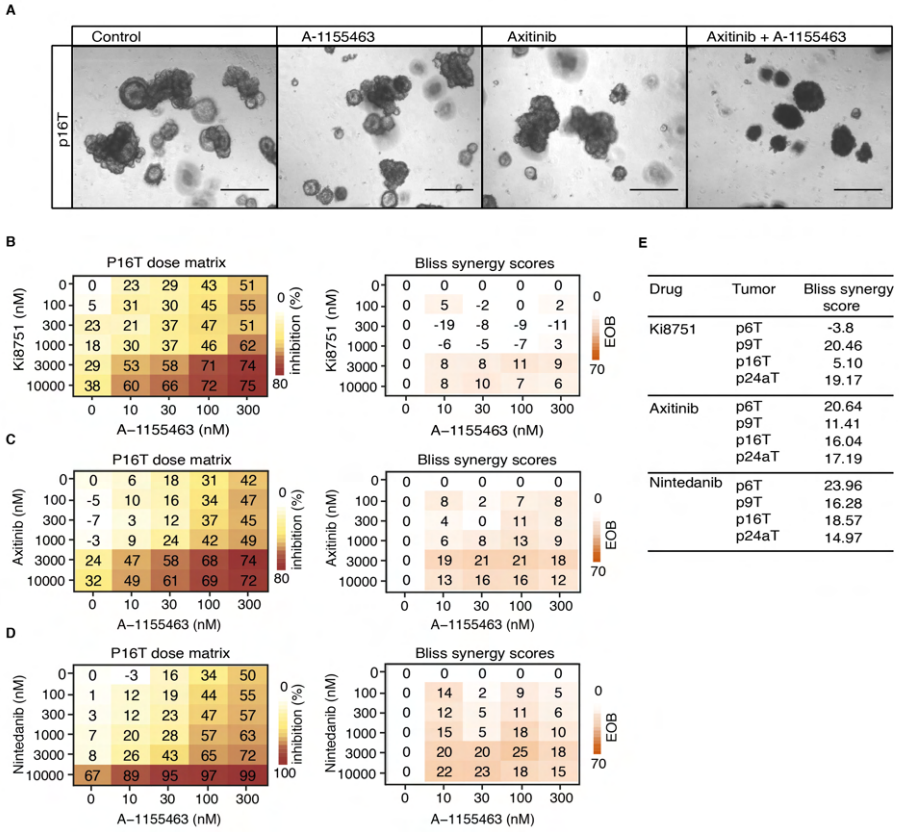

E

Drug	Tumor	Bliss synergy score
Ki8751	p6T	-3.8
	p9T	20.46
	p16T	5.10
	p24aT	19.17
Axitinib	p6T	20.64
	p9T	11.41
	p16T	16.04
	p24aT	17.19
Nintedanib	p6T	23.96
	p9T	16.28
	p16T	18.57
	p24aT	14.97

Figure 3. Ki8751, Axitinib and Nintedanib in combination with A-1155463 induce synergistic cytotoxicity in patient-derived tumor organoids.

A. Phase-contrast images of p16T human CRC organoids treated for 48h with 10μM Axitinib alone and in combination with 30nM A-1155463. Scale bars indicate 250μm.

B-D. 5 x 6 dose matrices of P16T human CRC organoids treated with Ki8751 (B), Axitinib (C) and Nintedanib (D) in combination with A-1155463 for 48h. % inhibition was calculated from viability data measured by cell titer blue, after normalizing to control. Data represent the average of three independent experiments. Bliss synergy scores were calculated for each dose combination.

E. P6T, P9T, P16T and P24aT human CRC organoids were treated in a 5x6 dose response matrix with Ki8751, Axitinib and Nintedanib in combination with A-1155463 for 48h (n=3 independent experiments). The Bliss synergy scores for the most synergistic 3-by-3 dose window in the dose-response matrices are listed in the table for each organoid and drug.

FGFR4 inhibition potentiates A-1155463-mediated CSC cell death

The above validated inhibitors are known to target multiple RTKs and so, to identify the specific protein target responsible for the observed sensitization towards BCL-XL inhibition, we analyzed the mRNA expression profile of Co01 cells and found the highest expressed target to be *FGFR4*, followed by *FGFR3* (Fig. 4A). Expression of FGFR4 in Co01 cells was also confirmed by flow cytometry (Supplementary Fig. 4A). The remaining targets including *VEGFR2 (KDR), PDGFRa/b* and *c-KIT* were all either lowly expressed or not expressed at all (Fig. 4A). In addition, more selective PDGFR, c-KIT or VEGFR inhibitors did not synergize with A-1155463, effectively excluding these receptors as potential targets (Supplementary Fig. 4B and Supplementary Table 1). Analysis of gene-expression data of the patient-derived tumor organoids revealed a similar pattern with *FGFR4* being the highest expressed target, followed by the remaining members of the *FGFR* family, while the other targets were detected at lower levels (Supplementary Fig. 4C).

To assess if FGFR4 inhibition mediates the observed synergy of the validated

hits, we tested two FGFR4-specific inhibitors, BLU9931 and H3B-6527, and found that both significantly potentiated A-1155463-induced cytotoxicity (Supplementary Fig. 4D). In addition, combination of FGFR4 inhibition with low dose A-1155463 did not affect platelet viability *in vitro* (Supplementary Fig. 4E). Furthermore, both inhibitors enhanced A-1155463 mediated apoptosis in the TOP-GFP high CSC population, as measured by caspase-3 activation (Fig. 4B), with a similar effect on the TOP-GFP low differentiated population (Supplementary Fig. 4F). Since other members of the FGFR family are also expressed in these cells, we tested an FGFR1/2/3 inhibitor, AZD4547, in a titration with A-1155463 and found no synergy between the two compounds (Supplementary Fig. 4G). Taken together, our data suggests that FGFR4 is the specific target responsible for the observed synergy of the selected hits with BCL-XL inhibition.

To assess if FGFR4 inhibition could be used as a potential therapeutic regimen to sensitize CRC tumors to BCL-XL inhibition, we treated four patient-derived tumor organoids with a matrix titration of both BLU9931 and H3B-6527 in combination with A-1155463. We observed strong synergy as measured by the Bliss independence model at a range of dose combinations across all four organoid cultures (Fig. 4C, D, E, Supplementary Fig. 5A, B). Furthermore, we performed an *in vivo* experiment where we treated subcutaneously injected Co01 tumors with the inhibitors A-1155463 (1mg/kg) and H3B-6527 (5mg/kg) alone and in combination. At the end of the treatment, we found a significant delay in tumor outgrowth in the combination treatment group compared to the vehicle-treated mice (Fig. 4F). Furthermore, this combination therapy also avoids toxicity that results from BCL-XL targeting. Previous studies have administered A-1155463 *in vivo* at a dose of 5mg/kg, which was found to induce platelet toxicity [18, 26]. We confirmed this in a platelet toxicity assay where a single injection of 5mg/kg and 25mg/kg of A-1155463 resulted in significant platelet loss *in vivo* within 6h (Supplementary Fig. 6A). In our *in vivo* experimental set-up, mice were treated with the lower dose of 1mg/kg, which had no measured impact on platelet counts either when applied alone or in combination with H3B-6527 (Fig. 4G, Supplementary Fig. 6A). Similarly, body weight

measurements remained stable in all conditions throughout the treatment period (Supplementary Fig. 6B), suggesting that the combination therapy did not induce intestinal toxicity. Altogether, our data provides evidence for improving BH3 mimetic efficacy in CRC with combined inhibition of FGFR4 signaling with a reduction in toxicity.

BCL-XL inhibition induces an FGFR4-mediated rescue response

To determine the underlying mechanism by which FGFR4 inhibition sensitizes tumor cells to A-1155463, we first assessed the expression of anti-apoptotic proteins by immunoblotting and found that FGFR4 inhibition with H3B-6527 in Co01 cells significantly lowered the expression of MCL-1 protein levels as quickly as 4h after treatment, while BCL-XL levels remained unchanged (Fig. 5A). Treatment with Ki8751, Axitinib and Nintedanib induced a similar decrease in MCL-1 levels (Supplementary Fig. 7A). More importantly, this analysis revealed an unexpected induction of MCL-1 when cells were treated with 5nM A-1155463 (Fig. 5A). This suggests that low doses of BH3 mimetics trigger a rescue response through upregulation of the anti-apoptotic machinery, while combination with FGFR4 inhibitors prevents this response (Fig. 5A). MCL-1 expression appears to be regulated post-translationally as no increase in *MCL1* mRNA was observed upon A-1155463 treatment (Supplementary Fig. 7B). Intriguingly, a low dose of A-1155463 also induced FGFR4 phosphorylation, suggesting activation of the signaling pathway (Fig. 5B). In addition, we observed a rapid phosphorylation of ERK, but not of AKT, upon treatment with A-1155463, which was also prevented by FGFR4 inhibition (Fig. 5C). To further assess if FGFR4 plays a role in the observed rescue response, we performed an shRNA knockdown (KD) of the gene and found that A-1155463 treatment no longer resulted in MCL-1 upregulation (Fig. 5D, Supplementary Fig. 7C).

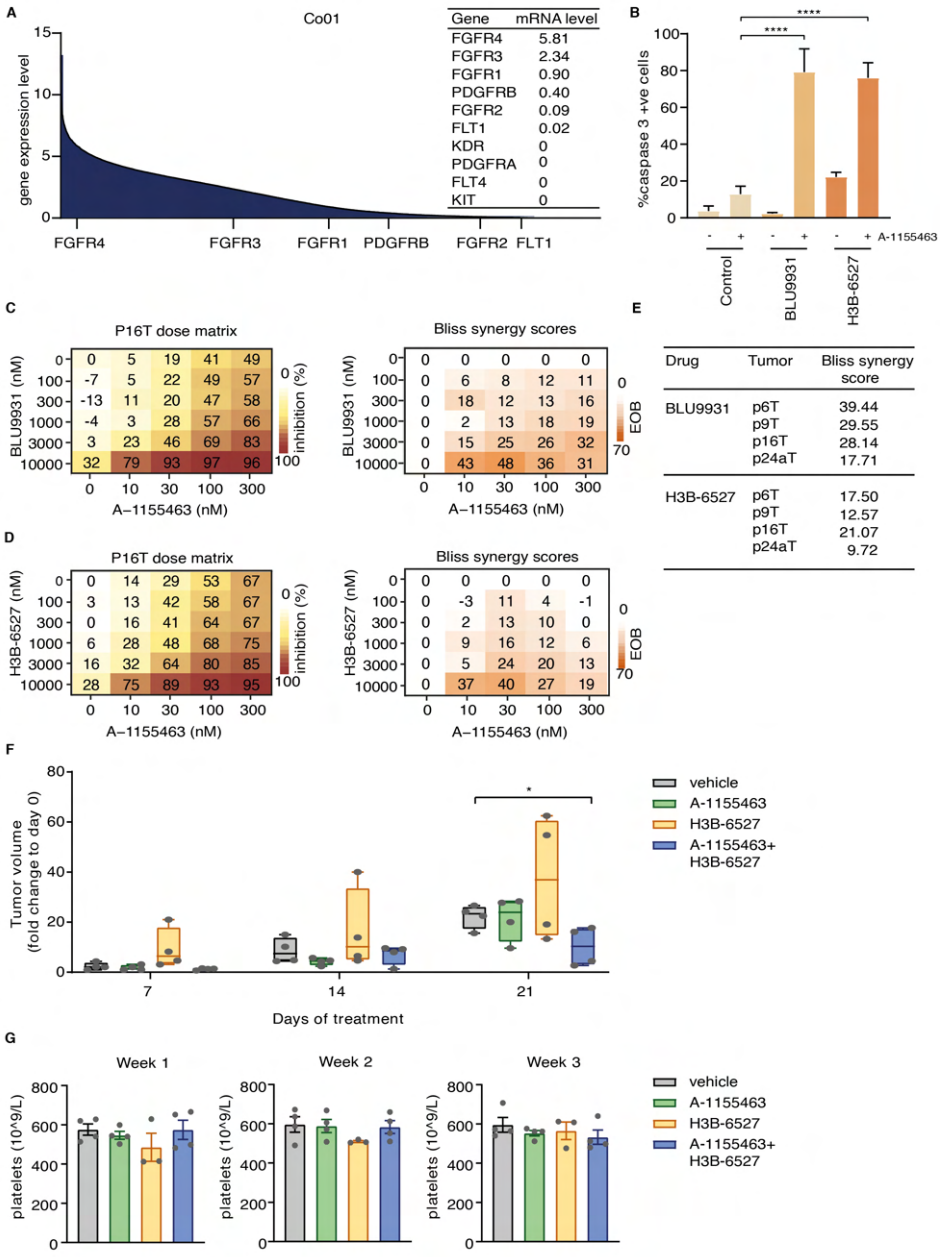

Figure 4. FGFR4 inhibition potentiates A-1155463-mediated CSC cell death.

A. mRNA expression profile of Co01 cells ranked by the Log2 expression level of the genes, ranging from 13 (highest) to 0 (lowest/undetected). The expression of known targets of Ki8751, Axitinib and Nintedanib together are indicated.

B. Percentage of activated caspase-3 in the 10% TOP-GFP high Co01 cells after 24h treatment with 5μM BLU9931 or H3B-6527, alone and in combination with 5nM A-1155463. Data is represented as mean ± SD (n=3 independent experiments). ****p value < 0.0001 (two-tailed unpaired Student's t-test).
C, D. 5 x 6 dose matrices of P16T human CRC organoids treated with BLU9931 (C) and H3B-6527 (D) in combination with A-1155463 for 48h. % inhibition was calculated from viability data measured by cell titer blue, after normalizing to control. Data represent the average of three independent experiments. Bliss synergy scores were calculated for each dose combination.
E. P6T, P9T, P16T and P24aT human CRC organoids were treated in a 5x6 dose response matrix with BLU9931 and H3B-6527 in combination with A-1155463 for 48h (n=3 independent experiments). The Bliss synergy scores for the most synergistic 3-by-3 dose window in the dose-response matrices are listed in the table for each organoid and drug.
F. Box plot of the volume of Co01 subcutaneous tumors on day 7, 14 and 21 compared to day 0. Mice were treated with vehicle, H3B-6527, A-1155463 or a combination (n=4 mice per group). * p <0.05 (two-tailed unpaired Student's t-test).
G. Platelet counts determined from tail vein blood of mice treated with vehicle, H3B-6527, A-1155463 or a combination. Platelets were counted at the end of each week of treatment for three weeks. Data is represented as mean ± SEM.

ERK-mediated phosphorylation of the MCL-1-PEST domain has been reported to limit MCL-1 degradation, our data therefore suggests that the induction of MCL-1 protein upon A-1155463 treatment could be mediated by FGFR4-driven ERK signaling [27] (Fig. 5C). However, it could still be argued that BCL-XL inhibition can induce MCL-1 stabilization through other mechanisms. It has been reported that lowering NOXA binding to MCL-1 can result in increased stability. This could be achieved when BCL-XL binding BH3-only proteins are released due to the treatment with A-1155463. These released proteins could displace NOXA and hence lead to MCL-1 stabilization upon BH3 mimetic treatment [28-30]. To assess if this is involved in upregulation of MCL-1 we made use of HCT-116 cells that are devoid of all pro-apoptotic BH3-only proteins (HCT-116 OctaKO), which are highly resistant to BCL-XL inhibition [31]. Here, with increasing doses

of A-1155463, a clear induction of MCL-1 was still observed, indicating that this rescue response is not dependent on BH3-only proteins (Fig. 5E). However, this does not rule out that displacement of other players such as BAX or BAK from BCL-XL upon A-1155463 treatment contributes to MCL-1 stabilization.

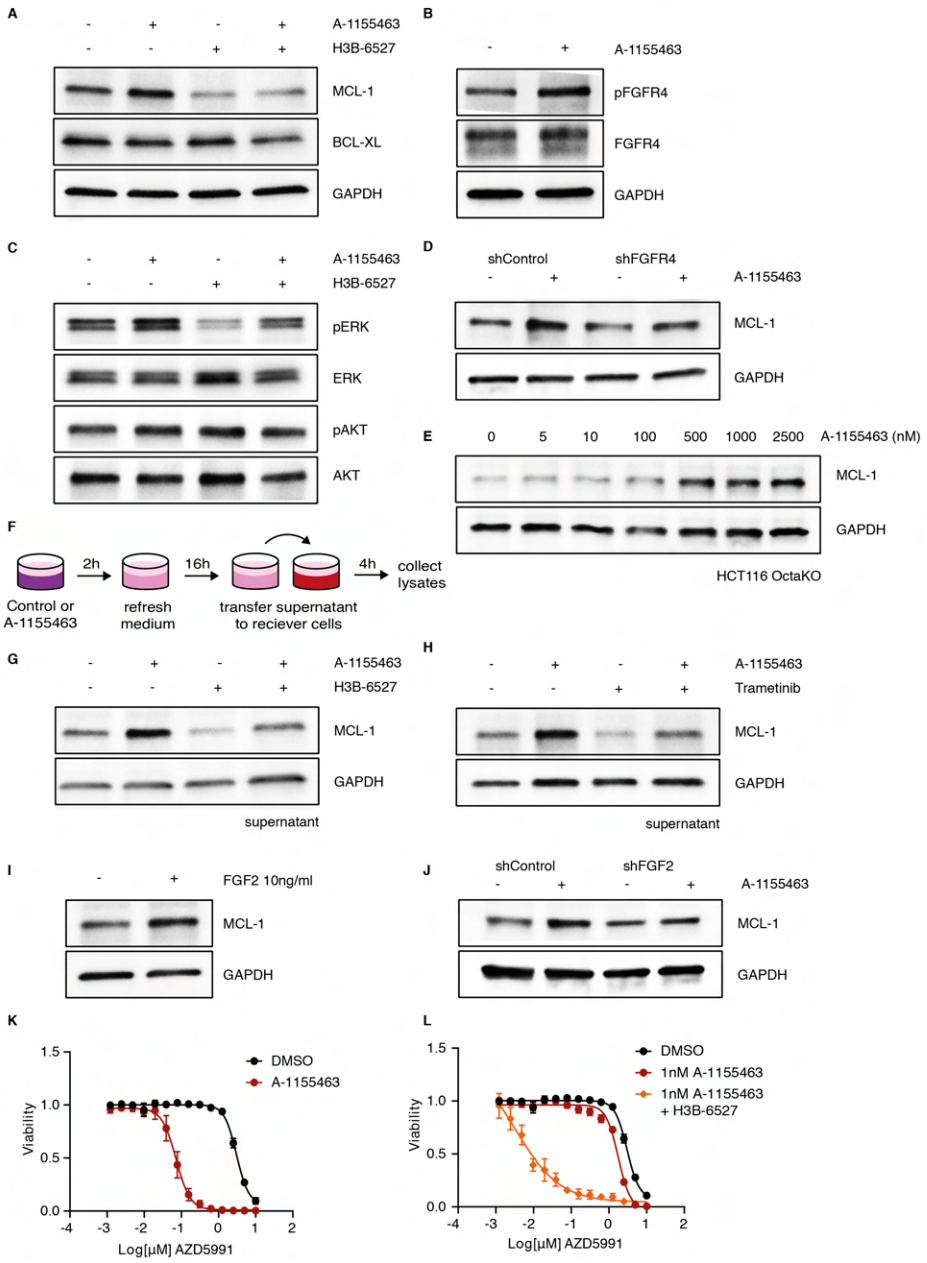

Figure 5. BCL-XL inhibition induces an FGFR4-mediated rescue response.
A. Immunoblot analysis of MCL-1 and BCL-XL levels in Co01 cells treated with 5nM A-1155463, 5μM H3B-6527 or a combination of the two for 4h. GAPDH was used as a loading control. Blots represent one of two independent experiments with similar results.
B. Immunoblot analysis of pFGFR4 an FGFR4 levels in Co01 cells treated with 5nM A-1155463 for 1h, without bFGF in the culture medium. GAPDH was used as a loading control.
C. Immunoblot analysis of pERK, ERK, pAKT and AKT levels in Co01 cells treated with 5nM A-1155463, 5μM H3B-6527 or a combination of the two for 4h. GAPDH was used as a loading control. Blots represent one of two independent experiments with similar results.
D. Immunoblot analysis of MCL-1 levels in Co01 cells with either a control (shControl) or FGFR4 knockdown (shFGFR4) treated with 5nM A-1155463 for 4h. GAPDH was used as a loading control. Blots represent one of two independent experiments with similar results.
E. Immunoblot analysis of MCL-1 levels in HCT116 OctaKO cells, depleted of all BH3 only proteins, treated with indicated doses of A-1155463 for 4h. GAPDH was used as a loading control. Blots represent one of two independent experiments with similar results.
F. Schematic overview of the supernatant transfer experiment. Co01 cells were cultured with or without 5nM A115 for 2h after which medium was refreshed. Supernatants were collected after 16h and transferred to recipient cells for 4h before analysis.
G. Immunoblot analysis of MCL-1 levels in HCT116 cells that received supernatant of control or 5nM A-1155463 conditioned cells as described in (d), in the presence or absence of 5μM H3B-6527 for 4h. GAPDH was used as a loading control. Blots represent one of two independent experiments with similar results.
H. Immunoblot analysis of MCL-1 levels in HCT116 cells that received supernatant of control or 5nM A-1155463 conditioned cells as described in (d), in the presence or absence of 5μM Trametinib for 4h. GAPDH was used as a loading control. Blots represent one of two independent experiments with similar results.
I. Immunoblot analysis of MCL-1 levels in HCT116 cells treated with 10ng/ml FGF2 for 4h. GAPDH was used as a loading control. Blots represent one of two

independent experiments with similar results.
J. Immunoblot analysis of MCL-1 levels in HCT116 cells with either a control (shControl) or FGF2 knockdown (shFGF2) treated with 5nM A-1155463 for 4h. GAPDH was used as a loading control. Blots represent one of two independent experiments with similar results.
K. Dose-response curve of Co01 treated with a titration of MCL-1 inhibitor AZD5991 alone and in combination with 5nM A-1155463 for 48h. Viability data measured by cell titer blue was blank corrected and normalized to control. Data is represented as mean ± SD (n=3).
L. Dose-response curve of Co01 treated with a titration of MCL-1 inhibitor AZD5991 alone and in combination with 1nM A-1155463 and 5μM H3B-6527 for 48h. Viability data measured by cell titer blue was blank corrected and normalized to control. Data is represented as mean ± SD (n=3 independent experiments).

It is important to note though that both the screen and the validation experiments are performed in standard culture medium, which contains FGF2 to facilitate growth of colon CSCs and A-1155463 could thus act by facilitating FGF2-FGFR4 signaling. However, even in the absence of exogenously added FGF2, we still observed FGFR4-dependent induction of MCL-1 upon treatment with A-1155463 (Supplementary Fig. 7D). This suggests that low dose BCL-XL inhibition activates FGFR4 signaling, which then induces MCL-1 upregulation. In agreement, combined treatment with H3B-6527 and A-1155463 also impaired the viability of Co01 cells in the absence of exogenously added FGF2 (Supplementary Fig. 7E). We therefore assessed if cells treated with a low dose of A-1155463 could activate the FGFR4 pathway in a paracrine manner by transferring media from A-1155463 treated cells (Fig. 5F). Supernatant of A-1155463 treated Co01 cells induced the expression of MCL-1 in both HCT116 and SW948 recipient cells (Fig. 5G, Supplementary Fig. 7F). Importantly, this induction of MCL-1 was prevented when H3B-6527 was added to the supernatant to prevent FGFR4 activation (Fig. 5G, Supplementary Fig. 7F). Furthermore, the same effect was observed upon ERK inhibition with Trametinib, confirming a role for this pathway in mediating the rescue response (Fig. 5H, Supplementary Fig. 7G). To address if ligand-driven activation of FGFR4

is responsible for this rescue response, we treated HCT116 cells with FGF2, which resulted in increased MCL-1 protein levels (Fig. 5I). Furthermore, KD of FGF2 blocked the upregulation of MCL-1 upon A-1155463 treatment, suggesting that FGF2 could act as a potential transferable link between BCL-XL inhibition and MCL-1 upregulation (Fig. 5J, Supplementary Fig. 7H).

To further confirm that the observed induction of MCL-1 expression is involved in the resistance of colon CSCs to BCL-XL targeting, we tested the sensitivity of Co01 cells to combined BCL-XL and MCL-1 inhibition. Treatment with MCL-1 inhibitor AZD-5991 is capable of inducing apoptosis in Co01, but only at very high doses. In combination with low-dose A-1155463 a potent (~50 fold) shift in IC50 was observed (Fig. 5K). This confirms a strong synergy between BCL-XL and MCL-1 inhibition similar to earlier reports [32-34], suggesting that decreasing MCL-1 levels by FGFR4 inhibition could act in a similar manner and facilitate A-1155463-induced apoptosis as well. To test this, we hypothesized that lowering MCL-1 expression through FGFR4 inhibition should lower the dose of AZD-5991 needed to completely block MCL-1 and allow low dose A-1155463 to achieve complete cell death. We therefore treated cells with a less effective dose combination of H3B-6527 and A-1155463 to which part of the Co01 cells were still resistant, allowing further analysis of MCL-1 targeting efficiency (Supplementary Fig. 7I, Supplementary Fig. 7E). Upon correcting for the basal apoptosis induced by this combination, we assessed the efficacy of AZD-5991 in inducing apoptosis in the presence of H3B-6527 and A-1155463 and observed a very significant shift in the AZD-5991 concentration needed to kill the cells (Fig. 5L). Altogether, our data points to an FGFR4-dependent rescue response that is activated upon low dose BCL-XL inhibition to induce MCL-1 upregulation (Fig. 6A). Inhibition of this pathway therefore lowers the anti-apoptotic threshold and enhances cell death induced by BCL-XL targeting drugs.

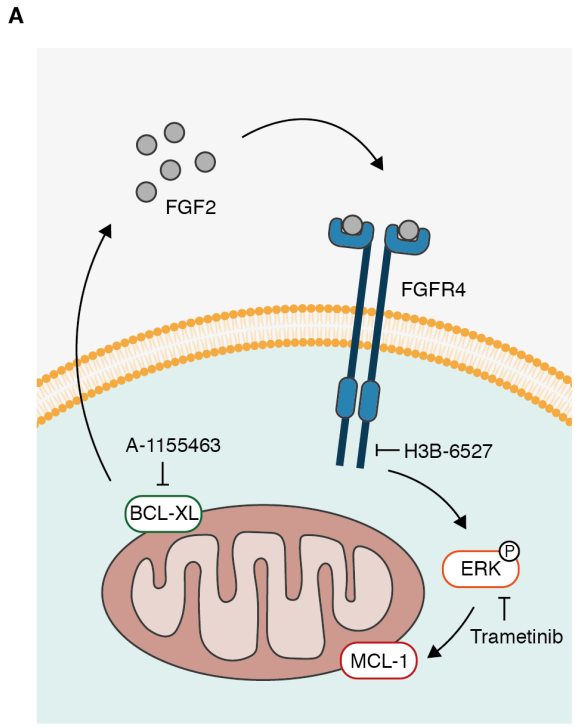

Figure 6. Schematic overview of the rescue response model.
A. Inhibition of BCL-XL by A-1155463 induces a rescue response that activates the FGFR4 signaling pathway by FGF2 release, which ultimately upregulates MCL-1 levels via ERK signaling.

Discussion

Our understanding of stem cell functionality in CRC has advanced remarkably with help from studies that highlight the dynamic nature of this population [35, 36]. Indeed, several intrinsic and extrinsic cues can induce de-differentiation of tumor cells to model more "stem-like" characteristics with associated therapy resistance [11, 37]. Considering the malleability of this population, it is pertinent to identify therapeutic strategies that either target the micro-environmental signals or the cell-intrinsic pathways that govern CSC clonogenicity and resistance [38]. In this regard, we have

previously identified BCL-XL as a key mediator of CRC stem cell therapy resistance, making it a relevant target for eradicating not only CSCs but also differentiated cells with the potential to revert to more stem-like states [8].

Here, we identified and validated FGFR4 as a synergistic target for BCL-XL inhibition in several CRC models. More importantly, our data identifies a rescue response that is induced when cells are treated with A-1155463, which results in MCL-1 upregulation. Importantly, this stimulation is relatively rapid and not due to enhanced transcription, as mRNA levels of MCL-1 were unchanged. Our data would propose regulation of MCL-1 protein stability through ERK-dependent phosphorylation, which is induced by FGFR4 pathway activation upon A-1155463 treatment. However, it cannot be ruled out that the observed increase in MCL-1 levels following BCL-XL inhibition might also arise from FGFR signaling independent effects, such as the displacement of BAX/BAK from BCL-XL to MCL-1, leading to its stabilization by displacement of NOXA or MULE.

The identified FGFR4-mediated rescue pathway could be uniquely exploited to sensitize cancer cells to A-1155463 as shown by the absence of toxicity of the combination therapy in normal intestinal cells and platelets, both *in vitro* and *in vivo*. This likely results from the fact that normal intestinal epithelial cells are resistant to BCL-XL inhibition [21, 39]. Moreover, FGFR4 expression is absent in the intestinal epithelium while it is upregulated in CRC tumors [40-42]. However, in our in vivo model, FGFR4 inhibition on its own leads to variable effects with some tumors showing increased growth upon H3B-6527 treatment. This is in contrast with the *in vitro* effects of H3B-6527 on Co01 cells, where FGFR4 inhibition does induce low levels of apoptosis. This suggests that blocking FGFR4 *in vivo* may have some additional non-tumor cell related effects. Potentially this relates to an effect on stromal cells, which could affect tumor growth indirectly, but the underlying mechanisms need further exploration.

Currently, several clinical trials are ongoing testing selective FGFR4

inhibition mainly in hepatocellular carcinoma, but also including other FGFR4+ advanced solid tumors (*Clinicaltrials.gov*) [43, 44]. Our data suggests that combination with apoptosis inducing drugs would strongly benefit the therapeutic efficacy of FGFR4 inhibition. This observation is not limited to CRC as studies in other solid tumor types report similar synergy between BH3 mimetics and FGFR pathway inhibition [45-47]. In breast cancer cells, A-1155463 was found to significantly potentiate BLU9931-induced cell death in a study examining the role of FGFR4 mediated resistance, indicating broad applicability of this combination strategy in solid tumors [47].

Importantly, our data suggest that treatment with BH3 mimetics alone might not be clinically effective, giving rise to rapid MCL-1 driven resistance. In agreement, treatment with low dose of A-1155463 is ineffective in impairing tumor growth. This is further supported by our recent findings where we used tamoxifen to induce transformation in the mouse colon and treated with A-1155463 either during transformation or after transformation [21]. Interestingly, we found that although BCL-XL inhibition is effective in preventing adenoma formation, once the adenomas are fully formed, A-1155463 treatment on its own no longer deters adenoma growth rate. Therefore, combined inhibition of BCL-XL with FGFR4 or MCL-1 inhibition presents a strategy that could overcome this resistance mechanism.

Recent data indicate that the role of MCL-1 in the intestine is complex [48], where its deletion resulted in aberrant cell death under homeostatic conditions. However, over time MCL-1 deficient crypts presented with increased proliferation and expansion of the stem cell compartment, indicative of a compensatory regenerative mechanism [48]. Proliferation was dependent on Wnt signaling and eventually resulted in adenoma formation, indicating that deletion or targeting of MCL-1 may have detrimental side-effects in the intestine by enhancing compensatory proliferation and carcinogenesis.

Whether this apoptosis-associated proliferation relates to the response we

observe in CRC cells treated with low dose BH3 mimetics is not clear, but is an intriguing possibility. In MCL-1-deficient mice, extensive cell death results in loss of integrity of the epithelial lining and has a significant impact on the epithelial barrier function of the intestine [48]. To resolve this loss, a rapid regeneration is required to avoid a hyper-inflammatory response. A signal emanating from dying cells to alert surroundings cells to start a compensatory proliferative response could be a physiologically relevant response to damage. In this light, it is interesting to note that a similar regenerative response follows upon extensive cell death when the intestine is exposed to irradiation or during inflammatory conditions such as IBD. In the case of irradiation-induced apoptosis, both PUMA and NOXA, two BH3 molecules induced by p53 activation, are reportedly essential [49, 50]. We speculate that in this setting BH3 molecules in dying cells could instruct surrounding cells to become resistant and start dividing to preserve barrier function. Intriguingly, a role for FGF signaling in this regenerative process has been extensively described. For instance, FGF2 is quickly induced upon irradiation and provides a survival benefit for epithelial cells [51]. Rescue induced by FGF family members could therefore be a more general mechanism in the intestinal epithelium that is hijacked by CRC cells. Indeed, our data suggests that deletion of FGF2 blocks the upregulation of MCL-1, in support of this hypothesis. However, this does not exclude that different FGFs can mediate this response, possibly also through different FGF receptors, depending on tissue and disease specific settings. Furthermore, how treatment with BH3 mimetics translates to a signal for FGF release is a mechanism that needs further exploration.

In this study we observe that BCL-XL inhibition relays an FGF2 driven signal that can be transferred with conditioned media, where this signal is activated quite rapidly upon low-dose BH3 mimetic treatment. This suggests that cell death induction is not a pre-requisite for the observed effect. However, whether only cells that are bound for cell death due to increased apoptotic priming release this rescue signal requires further analysis. Nevertheless, we conclude that combining low doses of BCL-XL targeting BH3 mimetics with FGFR4 inhibition provides a non-toxic

therapeutic opportunity to target CRC cells, including the more resistant CSC population. More importantly, this combination circumvents the rapidly induced resistance mechanism observed upon BCL-XL inhibition alone, thus providing a rationale to improve BH3 mimetic efficacy in the treatment of solid tumors.

Materials and methods

Spheroid cultures

The colon cancer spheroid culture Co01 was established and transduced with TCF/LEF reporter TOP-GFP as previously described [7]. Briefly, primary resection from a human colon carcinoma was enzymatically digested with collagenase II (1.5mg/ml, Sigma-Aldrich) for 1h at 37°C. Dissociated tissue was then strained through a 70µm pore, washed and subsequently cultured. Co01 overexpressing BCL-XL was generated by lentiviral transduction with the pHEFTIR-BCL-XL plasmid as previously described [8]. Spheroid cultures were cultured in advanced DMEM/F12 (Thermo Fischer Scientific) supplemented with N2 supplement (Thermo Fischer Scientific), 2mM L-glutamine (Lonza), 0.15% D-glucose (Sigma-Aldrich), 100µM □-mercaptoethanol (Sigma-Aldrich), trace elements B and C (Thermo Fisher Scientific), 5mM HEPES (Thermo Fisher Scientific), 2µg/ml heparin (Sigma-Aldrich), 10µg/ml insulin (Sigma-Aldrich), Epidermal Growth Factor (Peprotech, EGF, 50ng/ml) and basic Fibroblast Growth Factor (Tebu-Bio, FGF, 10ng/ml). Cultures were maintained in ultra-low adherent flasks (Corning) at 37°C and 5% CO2 and tested for mycoplasma on a monthly basis and confirmed to be mycoplasma negative. Co01 cells were transduced with lentiviral shRNA constructs against either control (SHC002, MISSION shRNA, Merck) or FGFR4 (TRCN0000010531, Mission shRNA, Merck). Transduced cells were selected with 2µg/ml puromycin (InvivoGen) for 7 days.

Organoid cultures

Patient-derived CRC tumor organoids were obtained from the Clevers organoid biobank and established as previously described [25]. Normal colon organoids were extracted from a piece of normal mucosa from CRC resection specimens as

previously described, at a distance of at least 10 cm from the cancerous tissue [52]. Organoids were cultured in drops of growth factor-reduced Matrigel (Corning) in pre-warmed 24 well plates. P9T, P16T and P24aT tumor organoids were maintained in Advanced DMEM/F12 supplemented with N2 and B27 supplement (Thermo Fischer Scientific), antimycotic/antibiotic (Thermo Fischer Scientific), gentamicin (Thermo Fischer Scientific), 2mM GlutaMax-1 (Thermo Fischer Scientific), 10mM HEPES, 1mM N-acety-L-cysteine (Sigma-Aldrich), 10nM [Leu15]-gastrin I (Sigma-Aldrich), 10mM nicotinamide (Sigma-Aldrich), 500nM A83-01 (Tocris), 3μM SB202190 (Sigma-Aldrich), 50ng/ml human EGF, 20% RSPO1 conditioned medium, 10% Noggin conditioned medium and 10nM PGE2 (Santa Cruz Biotechnology). The medium of normal colon organoids was further supplemented with 50% Wnt conditioned medium and 10μM ROCK inhibitor (Sigma-Aldrich). P6T was cultured in Advanced DMEM/F12 containing N2 and B27 supplement, gentamycin, 2mM L-glutamine, 0.15% D-glucose, 100μM ß-mercaptoethanol, trace elements B and C, 5mM HEPES, 2 μg/ml heparin, 10μg/ml insulin, 20ng/ml human EGF, and 10μM SB202190. Organoids were maintained at 37°C and 5% CO2 and dissociated every 7-10 days with medium refreshed every 3-4 days. All cultures were confirmed to be mycoplasma negative on a monthly basis.

Cell lines

Adherent colon cancer cell lines HCT116 and SW948 were a kind gift from the Sanger Institute (Cam-bridge, United Kingdom). HCT116 OctaKO cells were kindly provided by the lab of Xu Luo from the University of Nebraska Medical Center [31]. SW948 was maintained in 1:1 DMEM/F12 medium containing 15mM HEPES and 2.5mM L-glutamine (Gibco) supplemented with 8% fetal bovine serum (Serana) and 50 units/mL of penicil-lin/streptomycin (Gibco). HCT116 and HCT116 OctaKO cells were maintained in RPMI 1640 medium supplemented with 25mM HEPES and 2,05mM L-glutamine (Gibco) supplemented with 8% fetal bovine serum, 1% D-glucose solution plus (Sigma-Aldrich), 1mM sodium pyruvate (Gibco) and 50 units/mL of penicillin/streptomycin. Cultures were tested for mycoplasma contaminations on a monthly basis. HCT116 cells were transduced with lentiviral shRNA constructs against either control (SHC002, MISSION shRNA, Merck) or FGF2 (TRCN0000003333, Mission shRNA, Merck). Transduced cells were selected with 1.5 μg/ml puromycin (InvivoGen) for 7 days.

Compounds

The library of 1402 unique inhibitors for high-throughput screening was purchased from Selleck Chemicals (L1100) and includes several small molecule inhibitors, chemotherapeutics and FDA-approved compounds. All compounds were dissolved in DMSO and provided at a concentration of 10mM. A-1155463 (Chemietek) was dissolved in DMSO at 20mM and WEHI-539 (Selleck Chem) was dissolved in DMSO at 10mM. Compounds selected from the screen were purchased from Selleck Chemicals and further validated on several cultures for 48h unless indicated otherwise.

Drug screen workflow

To screen the compounds, Co01 and Co01 BCL-XL were seeded in 96-well flat bottom plates (Corning) at a density of 4000 cells/well. After overnight incubation, cells were treated with the inhibitor library at a final concentration of 1μM, either alone or in combination with 5nM A-1155463. All inhibitors were pre-diluted to a concentration of 10μM in medium and then added to the cells at a further dilution of 1:10 using a dispensing robot. A-1155463 was pre-diluted to a concentration of 50nM in medium before being robotically dispensed into wells at a 1:10 dilution. Cells were treated for 48h following which viability was measured using CellTiter Blue (Promega) as per manufacturer's instructions. Fluorescence readings were measured using the BioTek Synergy HT microplate reader. All drugs were assayed in duplicate on two separate plates and each plate included positive (10μM A-1155463) and negative controls (DMSO only). Drugs that were toxic on their own at 1μM were re-tested at a lower dose of 100nM with and without A-1155463.

Screen data analysis

Viability data from each screening plate was blank corrected and normalized to control wells. To calculate the effect of combining the drug library inhibitors with A-1155463, replicate values of each drug effect were averaged and subtracted by the average effect of the same drug administered with A-1155463 ($Viability_{drug}$ – $Viability_{drug+A\text{-}1155463}$). This combination effect was calculated for all drugs tested. To eliminate compounds that also affect Co01 BCL-XL, we calculated the difference between the combination effect on Co01 and Co01 BCL-XL and excluded the drugs that had a difference below 20%. Co01 combination effect data was z-score

normalized using the formula: z-score = (value – mean of all data)/ SD of all data. Hits were selected with a z-score cut-off of 2 or higher. Assay robustness was measured by the median of the Z-factor scores calculated for each plate using the formula: $Z'=1 - 3(SD_p+SD_n) / |Mean_p - Mean_n|$
where SD is standard deviation, p is positive control, n is negative control. A score between 0.5 and 1 indicative of a robust assay [53].

Viability assays

Spheroid cultures were seeded in 96-well plates at a density of 4000 cells/well and after overnight incubation, treated with indicated inhibitors in a titration using the HP D300 digital dispenser (Hewlett-Packard) for 48h. Viability was assessed using CellTiter-Blue following manufacturer's instructions. Synergy was calculated using the Bliss independence model and scores greater than 10 were considered synergistic.

Tumor organoids were dissociated from Matrigel in cell recovery solution (BD Biosciences) at 4°C for 30 mins. Once Matrigel was fully dissolved, organoid structures were spun down and trypsinized with TrypLE Express (Thermo Fischer Scientific) for 3 mins at 37°C. Following dissociation, single cells were washed, counted and plated in pre-warmed 96-well plates in drops of 6µL Matrigel at a density of 4000 cells/well. After 3-4 days, organoids were treated in a matrix titration using the HP D300 digital dispenser for 48h. Viability was assessed using CellTiter-Blue as per manufacturer's instructions. Synergy was calculated using the Synergy Finder web tool [54] and the Bliss independence model was employed to calculate the Bliss score for the most synergistic 3-by-3 dose window in the dose-response matrices. Bliss scores greater than 10 were considered synergistic.
Normal colon organoids were plated in 48-well plates at approximately 150 - 300 structures/well. After 3-4 days, organoids were treated with inhibitors for 48h following which viability was measured using CellTiter-Blue according to manufacturer's instructions.

Flow cytometry assisted cell sorting (FACS)

For the caspase assay, Co01 expressing TOP-GFP was plated in 12 well plates at a density of 50,000 cells/well and treated with indicated inhibitors for 24h. Following

treatment, cells were dissociated with Trypsin and stained for activated caspase-3 using RED-DEVD-FMK (CaspGLOW Red, BioVision) as per manufacturer's instructions.

For FGFR4 staining, cells were resuspended in 0.1% BSA in PBS and incubated with an FGFR4 antibody coupled to PE (clone 4FR6D3, BioLegend) for 30 min on ice, washed and then measured. Flow cytometry analyses were performed on the FACSCanto II (BD biosciences).

Ex vivo platelet toxicity

Human whole blood was obtained from healthy volunteers in sodium citrate tubes and platelet rich plasma (PRP) was obtained by centrifugation at 180 rcf for 15 min at room temperature. 90µL of PRP was pipetted into each well of a 96-well flat bottom plate and treated with indicated inhibitors for indicated time points at 37°C and 5% CO2. Viability of platelets was then measured using CellTiter-Blue following manufacturer's instructions.

RNA sequencing and data analysis

Total RNA isolation was performed using the Nucleospin RNA isolation kit (Bioke) and duplicate RNA samples of Co01 cells were prepared for RNA sequencing. RNA integrity was assessed using the Agilent 2100 Bioanalyzer (Agilent Technologies). Libraries were prepared using the NEBNext Ultra Directional RNA Library Prep Kit for Illumina as per manufacturer's instructions and DNA sequencing was performed using the Illumina NextSeq 500 (GenomeScan, Leiden). All reads were mapped to the human genome (GRCh38) using HISAT2. Gene counts (Ensembl build 92) were determined using the summarizeOverlaps function of the GenomicAlignments R package and subsequently normalized to FPKM (fragments per kilobase per million mapped fragments) using the DESeq2 R package. For gene-expression analysis of the patient-derived tumor organoids , previously generated data was analysed using the R2 web application, which is freely available at http://r2.amc.nl [25].

Quantitative real-time PCR

Total RNA isolation was performed using the Nucleospin RNA isolation kit

(Bioke) and quantified using the NanoDrop 1000 Spectrophotometer (Thermo Fischer Scientific). Synthesis of cDNA was performed using SuperScript III reverse transcriptase (Thermo Fischer Scientific) with random primers (Thermo Fischer Scientific). 2x SYBR green master mix (Roche) was used to perform qRT-PCR as per manufacturer's instructions and FGFR4 (Forward: GGAGGAGCCAGGTGAGGA, Reverse: CAGGGCTCAAGCTCCACTTC) and FGF2 (Forward: TACAACTTCAAGCAGAAGAG, Reverse: CAGCTCTTAGCAGACATTGG) transcript levels were measured on the Light Cycler 480 (Roche). RPLP0 (Forward: GGCACCATTGAAATCCTGAGTGATGTG, Reverse: TTGCGGACACCCTCCAGGAAGC) was used as housekeeping gene.

Supernatant transfer

Co01 cells were cultured in CSC medium without FGF and treated for 2h with A-1155463, after which medium was refreshed to wash out the drug. Following another 16h incubation, supernatants were collected, spun down and transferred to recipient serum-starved HCT116 or SW948 cells, either with or without H3B-6527 or Trametinib (Selleck Chemicals). After 4h, protein lysates were collected for immunoblot analysis.

Immunobloting

Following treatment for indicated times, cells were lysed using 1x RIPA Lysis and Extraction buffer (Thermo Fischer Scientific) containing Halt protease and phosphatase inhibitor cocktail (1:100, Thermo Fischer Scientific). Protein samples were quantified using the Pierce BCA protein assay kit (Thermo Fischer Scientific) as per manufacturer's instructions. 15 µg protein was loaded per well into 4-15% precast gels (Bio-Rad) and then transferred to PVDF membranes using the Trans-Blot Turbo transfer system (Bio-Rad) according to manufacturer's instructions using the mixed molecular weight transfer settings. Membranes were blocked for 1h in 5% bovine serum albumin (BSA) in Tris-buffered saline and Tween-20 (TBS-T,1x) and stained with primary antibody overnight at 4°C. The following primary antibodies were tested: pFGFR4 (1:1000, PA5-37576, Thermo Fischer) FGFR4 (1:1000, #8562, Cell Signaling), pERK (1:1000, #9101, Cell Signaling), ERK(1:1000, #9107, Cell Signaling), pAKT(1:1000, #4060, Cell Signaling), AKT(1:1000, #9272, Cell Signaling), BCL-XL (1:1000, #2764, Cell Signaling) and MCL-1 (1:1000, #4572,

Cell Signaling), all diluted in 5% BSA in TBS-T. After washing the blots 4 times for 20 mins each with TBS-T, the secondary antibody anti-rabbit-horseradish peroxidase (1:5000, #4050-05, Southern Biotech) or anti-mouse-horseradish peroxidase (1:5000, #1031-05, Southern Biotech) was added for 2h at room temperature. Following another round of 4x 20 min washes, the membranes were developed using the LumiLight western blotting substrate (Sigma-Aldrich) and imaged on the ImageQuanti LAS4000 (GE Healthcare Life Sciences). GAPDH was used as a loading control (1:5000, MAB374, Sigma-Aldrich).

In vivo platelet toxicity experiment

8 week old female NSG mice (Charles River Laboratories) were housed at the University of Palermo in accordance to institutional guidelines of the Italian animal welfare (D.L. n° 26 March 4, 2014) and authorization number 154/2017-PR. Mice (3 per group) were treated intraperitoneally with a single injection of indicated doses of A-1155463. A-1155463 was first dissolved in DMSO (Sigma-Aldrich) at 80mg/ml and injected in a solution of 2.75% DMSO, 30% PEG400 (Sigma-Aldrich), 2% Tween-80 (Sigma-Aldrich) and ddH2O. Platelet counts were evaluated before treatment and at indicated time points by collecting tail vein blood in EDTA microvette tubes (Sarstedt). Blood was diluted 1:100 in 1% ammonium oxalate (Sigma-Aldrich) and incubated for 20min to ensure erythrocyte lysis. 10 µL of diluted blood was pipetted into a hemocytometer and platelets were allowed to settle before manual counting.

In vivo experiment

Six week old male NOD/SCID mice (Charles River Laboratories) were housed at the University of Palermo in accordance to institutional guidelines of the Italian animal welfare (D.L. n° 26 March 4, 2014) and authorization number 154/2017-PR. Subcutaneous injection of colon CSCs was performed in the right flank using 300,000 Co01 cells in 100 µL of 1:1 stem cell medium/Matrigel solution. When tumors reached palpable size (0.03-0.06 cm3), mice were randomized into 4 treatment groups of 4 mice each: Control, A-1155463 (1mg/kg), H3B-6527 (5mg/kg) and A-1155463/H3B-6527 combination. A-1155463 was first dissolved in DMSO (Sigma-Aldrich) at 80mg/ml and injected in a solution of 2.75% DMSO, 30% PEG400 (Sigma-Aldrich), 2% Tween-80 (Sigma-Aldrich) and ddH2O. H3B-

6527 was dissolved in DMSO at 20mg/ml and injected in a solution of 2.75% DMSO, 30% PEG400, 2% Tween-80 and ddH2O. Control mice received a blank injection of 2.75% DMSO, 30% PEG400, 2% Tween-80 and ddH2O. Mice were intraperitoneally treated 3 times a week for 3 consecutive weeks. Tumors were measured twice per week by a digital caliper. Tumor volume was calculated using the formula: (largest diameter x (smallest diameter) 2)/2. Once the endpoints were reached (tumor volume= 2 cm3, or when mice showed signs of suffering), animals were sacrificed accordingly to Directive 2010/63/EU guidelines (D. lgs 26/2016). Platelet counts were evaluated on a weekly basis using the same protocol as described above.

Acknowledgements

This work was supported by Oncode, KWF project 2015-7587 and 10150. Le Zhang was supported by a CSC scholarship. Giorgio Stassi is supported by AIRC 5x1000 #9979, AIRC IG 21445 and PRIN 2017WNKSLR grants. The authors would like to thank the laboratory of Xu Luo at the University of Nebraska Medical Center for kindly providing the HCT116 OctaKO cell line. The authors would also like to thank Ferry de Klein for assistance with the drug dispensing robot.

References

1. Bray, F., et al., Global cancer statistics 2018: GLOBOCAN estimates of incidence and mortality worldwide for 36 cancers in 185 countries. CA Cancer J Clin, 2018. 68(6): p. 394-424.
2. Howlader N, N.A., Krapcho M, Miller D, Brest A, Yu M, Ruhl J, Tatalovich Z, Mariotto A, Lewis DR, Chen HS, Feuer EJ, Cronin KA (eds), SEER Cancer Statistics Review, 1975-2017. National Cancer Institute.Bethesda, MD,https://seer.cancer.gov/csr/1975_2017/, based on November 2019 SEER data submission, posted to the SEER web site, April 2020.
3. Jeffery, M., B.E. Hickey, and P.N. Hider, Follow-up strategies for patients treated for non-metastatic colorectal cancer. Cochrane Database Syst Rev, 2019. 9(9): p. Cd002200.
4. Sargent, D.J., et al., Disease-free survival versus overall survival as a primary end point for adjuvant colon cancer studies: individual patient data from 20,898 patients on 18 randomized trials. J Clin Oncol, 2005. 23(34): p. 8664-70.
5. De Sousa, E.M.F., et al., Cancer heterogeneity--a multifaceted view. EMBO Rep, 2013. 14(8): p. 686-95.
6. Fessler, E., et al., Cancer stem cell dynamics in tumor progression and metastasis: is the microenvironment to blame? Cancer Lett, 2013. 341(1): p. 97-104.

7. Vermeulen, L., et al., Wnt activity defines colon cancer stem cells and is regulated by the microenvironment. Nat Cell Biol, 2010. 12(5): p. 468-76.
8. Colak, S., et al., Decreased mitochondrial priming determines chemoresistance of colon cancer stem cells. Cell Death Differ, 2014. 21(7): p. 1170-7.
9. Todaro, M., et al., Colon cancer stem cells dictate tumor growth and resist cell death by production of interleukin-4. Cell Stem Cell, 2007. 1(4): p. 389-402.
10. Dylla, S.J., et al., Colorectal cancer stem cells are enriched in xenogeneic tumors following chemotherapy. PLoS One, 2008. 3(6): p. e2428.
11. Colak, S. and J.P. Medema, Human colonic fibroblasts regulate stemness and chemotherapy resistance of colon cancer stem cells. Cell Cycle, 2016. 15(12): p. 1531-7.
12. Ramesh, P. and J.P. Medema, BCL-2 family deregulation in colorectal cancer: potential for BH3 mimetics in therapy. Apoptosis, 2020. 25(5-6): p. 305-320.
13. Ni Chonghaile, T., et al., Pretreatment mitochondrial priming correlates with clinical response to cytotoxic chemotherapy. Science, 2011. 334(6059): p. 1129-33.
14. Vo, T.T., et al., Relative mitochondrial priming of myeloblasts and normal HSCs determines chemotherapeutic success in AML. Cell, 2012. 151(2): p. 344-55.
15. Valentin, R., S. Grabow, and M.S. Davids, The rise of apoptosis: targeting apoptosis in hematologic malignancies. Blood, 2018. 132(12): p. 1248-1264.
16. Amundson, S.A., et al., An informatics approach identifying markers of chemosensitivity in human cancer cell lines. Cancer Res, 2000. 60(21): p. 6101-10.
17. Maurer, C.A., et al., Apoptosis inhibiting factor Bcl-xL might be the crucial member of the Bcl-2 gene family in colorectal cancer. Dig Dis Sci, 1998. 43(12): p. 2641-8.
18. Tao, Z.F., et al., Discovery of a Potent and Selective BCL-XL Inhibitor with in Vivo Activity. ACS Med Chem Lett, 2014. 5(10): p. 1088-93.
19. Leverson, J.D., et al., Exploiting selective BCL-2 family inhibitors to dissect cell survival dependencies and define improved strategies for cancer therapy. Sci Transl Med, 2015. 7(279): p. 279ra40.
20. Zhang, H., et al., Genomic analysis and selective small molecule inhibition identifies BCL-X(L) as a critical survival factor in a subset of colorectal cancer. Mol Cancer, 2015. 14: p. 126.
21. Ramesh, P., et al., BCL-XL is crucial for progression through the adenoma-to-carcinoma sequence of colorectal cancer. Cell Death & Differentiation, 2021.
22. Schoenwaelder, S.M., et al., Bcl-xL-inhibitory BH3 mimetics can induce a transient thrombocytopathy that undermines the hemostatic function of platelets. Blood, 2011. 118(6): p. 1663-74.
23. Cammareri, P., et al., Aurora-a is essential for the tumorigenic capacity and chemoresistance of colorectal cancer stem cells. Cancer Res, 2010. 70(11): p. 4655-65.
24. Shah, O.J., et al., Bcl-XL represents a druggable molecular vulnerability during aurora B inhibitor-mediated polyploidization. Proc Natl Acad Sci U S A, 2010. 107(28): p. 12634-9.
25. van de Wetering, M., et al., Prospective derivation of a living organoid biobank of colorectal cancer patients. Cell, 2015. 161(4): p. 933-45.
26. de Jong, Y., et al., Bcl-xl as the most promising Bcl-2 family member in targeted treatment of chondrosarcoma. Oncogenesis, 2018. 7(9): p. 74.
27. Domina, A.M., et al., MCL1 is phosphorylated in the PEST region and stabilized upon

ERK activation in viable cells, and at additional sites with cytotoxic okadaic acid or taxol. Oncogene, 2004. 23(31): p. 5301-15.
28. Leverson, J.D., et al., Potent and selective small-molecule MCL-1 inhibitors demonstrate on-target cancer cell killing activity as single agents and in combination with ABT-263 (navitoclax). Cell Death Dis, 2015. 6(1): p. e1590.
29. Kotschy, A., et al., The MCL1 inhibitor S63845 is tolerable and effective in diverse cancer models. Nature, 2016. 538(7626): p. 477-482.
30. Tron, A.E., et al., Discovery of Mcl-1-specific inhibitor AZD5991 and preclinical activity in multiple myeloma and acute myeloid leukemia. Nat Commun, 2018. 9(1): p. 5341.
31. O'Neill, K.L., et al., Inactivation of prosurvival Bcl-2 proteins activates Bax/Bak through the outer mitochondrial membrane. Genes & development, 2016. 30(8): p. 973-988.
32. Berger, S., et al., Computationally designed high specificity inhibitors delineate the roles of BCL2 family proteins in cancer. Elife, 2016. 5.
33. Greaves, G., et al., BH3-only proteins are dispensable for apoptosis induced by pharmacological inhibition of both MCL-1 and BCL-X(L). Cell Death Differ, 2019. 26(6): p. 1037-1047.
34. Soderquist, R.S., et al., Systematic mapping of BCL-2 gene dependencies in cancer reveals molecular determinants of BH3 mimetic sensitivity. Nat Commun, 2018. 9(1): p. 3513.
35. Shimokawa, M., et al., Visualization and targeting of LGR5(+) human colon cancer stem cells. Nature, 2017. 545(7653): p. 187-192.
36. de Sousa e Melo, F., et al., A distinct role for Lgr5(+) stem cells in primary and metastatic colon cancer. Nature, 2017. 543(7647): p. 676-680.
37. Prasetyanti, P.R. and J.P. Medema, Intra-tumor heterogeneity from a cancer stem cell perspective. Mol Cancer, 2017. 16(1): p. 41.
38. Vermeulen, L., et al., The developing cancer stem-cell model: clinical challenges and opportunities. Lancet Oncol, 2012. 13(2): p. e83-9.
39. van der Heijden, M., et al., Bcl-2 is a critical mediator of intestinal transformation. Nat Commun, 2016. 7: p. 10916.
40. Liu, R., et al., FGFR4 promotes stroma-induced epithelial-to-mesenchymal transition in colorectal cancer. Cancer Res, 2013. 73(19): p. 5926-35.
41. Turkington, R.C., et al., Fibroblast growth factor receptor 4 (FGFR4): a targetable regulator of drug resistance in colorectal cancer. Cell Death Dis, 2014. 5(2): p. e1046.
42. Stark, K.L., J.A. McMahon, and A.P. McMahon, FGFR-4, a new member of the fibroblast growth factor receptor family, expressed in the definitive endoderm and skeletal muscle lineages of the mouse. Development, 1991. 113(2): p. 641-51.
43. Weiss, A., et al., FGF401, A First-In-Class Highly Selective and Potent FGFR4 Inhibitor for the Treatment of FGF19-Driven Hepatocellular Cancer. Mol Cancer Ther, 2019. 18(12): p. 2194-2206.
44. Mercade, T.M., et al., A phase I study of H3B-6527 in hepatocellular carcinoma (HCC) or intrahepatic cholangiocarcinoma (ICC) patients (pts). Journal of Clinical Oncology, 2019. 37(15_suppl): p. 4095-4095.
45. Packer, L.M., et al., Bcl-2 inhibitors enhance FGFR inhibitor-induced mitochondrial-dependent cell death in FGFR2-mutant endometrial cancer. Mol Oncol, 2019. 13(4): p. 738-756.
46. Weeden, C.E., et al., Dual inhibition of BCL-XL and MCL-1 is required to induce tumour

regression in lung squamous cell carcinomas sensitive to FGFR inhibition. Oncogene, 2018. 37(32): p. 4475-4488.
47. Turunen, S.P., et al., FGFR4 phosphorylates MST1 to confer breast cancer cells resistance to MST1/2-dependent apoptosis. Cell Death Differ, 2019. 26(12): p. 2577-2593.
48. Healy, M.E., et al., MCL1 Is Required for Maintenance of Intestinal Homeostasis and Prevention of Carcinogenesis in Mice. Gastroenterology, 2020. 159(1): p. 183-199.
49. Shibue, T., et al., Integral role of Noxa in p53-mediated apoptotic response. Genes Dev, 2003. 17(18): p. 2233-8.
50. Qiu, W., et al., PUMA regulates intestinal progenitor cell radiosensitivity and gastrointestinal syndrome. Cell Stem Cell, 2008. 2(6): p. 576-83.
51. Houchen, C.W., et al., FGF-2 enhances intestinal stem cell survival and its expression is induced after radiation injury. Am J Physiol, 1999. 276(1): p. G249-58.
52. Sato, T., et al., Long-term expansion of epithelial organoids from human colon, adenoma, adenocarcinoma, and Barrett's epithelium. Gastroenterology, 2011. 141(5): p. 1762-72.
53. Zhang, J.H., T.D. Chung, and K.R. Oldenburg, A Simple Statistical Parameter for Use in Evaluation and Validation of High Throughput Screening Assays. J Biomol Screen, 1999. 4(2): p. 67-73.
54. Ianevski, A., et al., SynergyFinder: a web application for analyzing drug combination dose-response matrix data. Bioinformatics, 2017. 33(15): p. 2413-2415.

Supplemental information

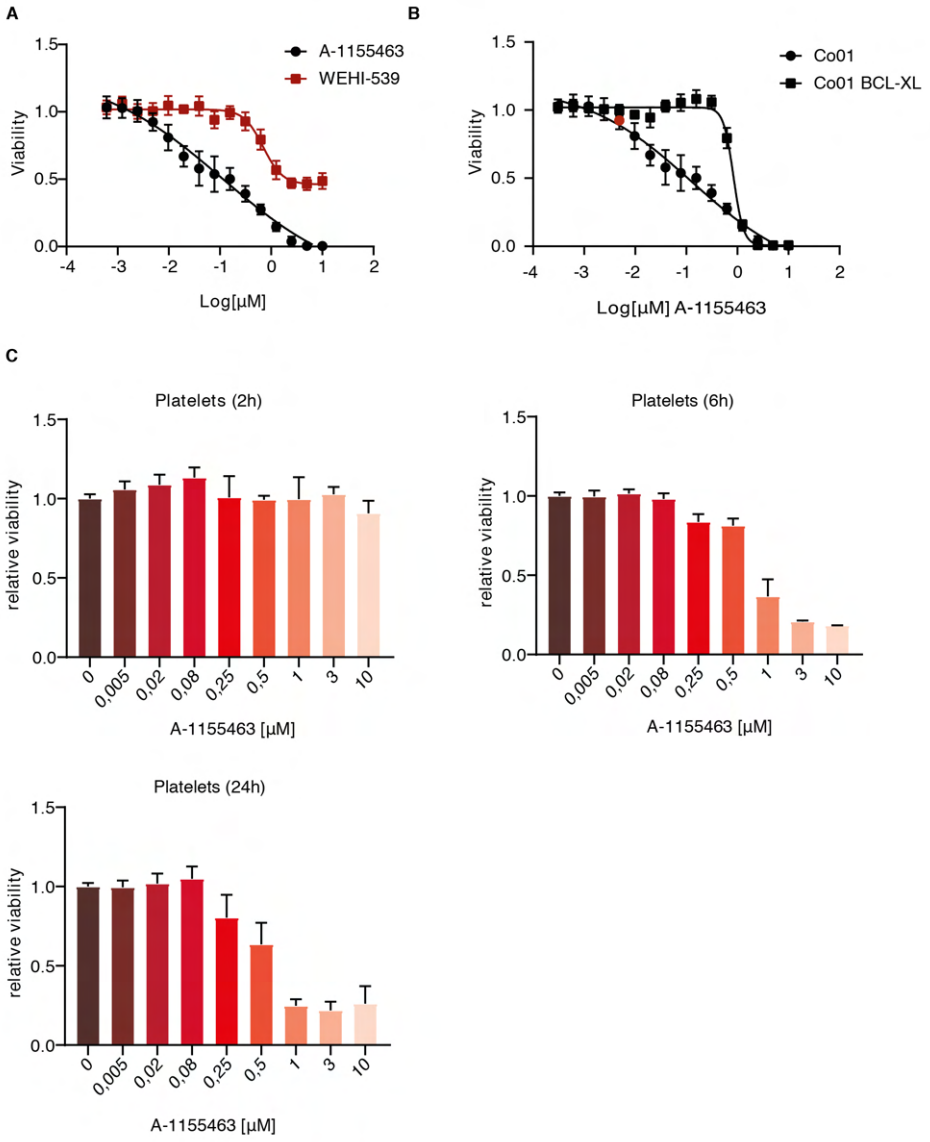

Supplementary Figure 1. Co01 BCL-XL is resistant to A-1155463.

A. Dose-response curve of Co01 cells treated with a titration of WEHI-539 or A-1155463 for 48 h. Viability data measured by cell titer blue was blank corrected and normalized to control. Data is represented as mean ± SD (n=3 independent

experiments).

B. Dose-response curve of Co01 and Co01 BCL-XL treated with a titration of A-1155463 for 48 h. Viability data measured by cell titer blue was blank corrected and normalized to control. Data is represented as mean ± SD (n=3 independent experiments). The 5nM low dose is highlighted in red.

C. Viability data of platelets derived from human whole blood treated with increasing doses of A-1155463 for indicated time points. Data represents mean ± SD (n=3 independent experiments).

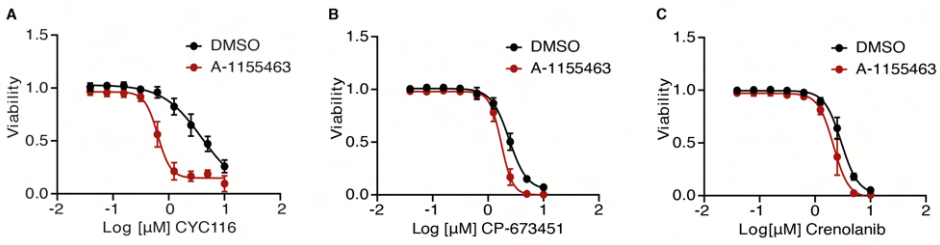

Supplementary Figure 2. Validation of hits selected from the screen.

A-C. Dose-response curve of Co01 treated with a titration of CYC116 (A), CP-673451 (B) and Crenolanib (C) either alone or in combination with 5nM A-1155463 for 48 h. Viability data measured by cell titer blue was blank corrected and normalized to control. Data is represented as mean ± SD (n=3 independent experiments).

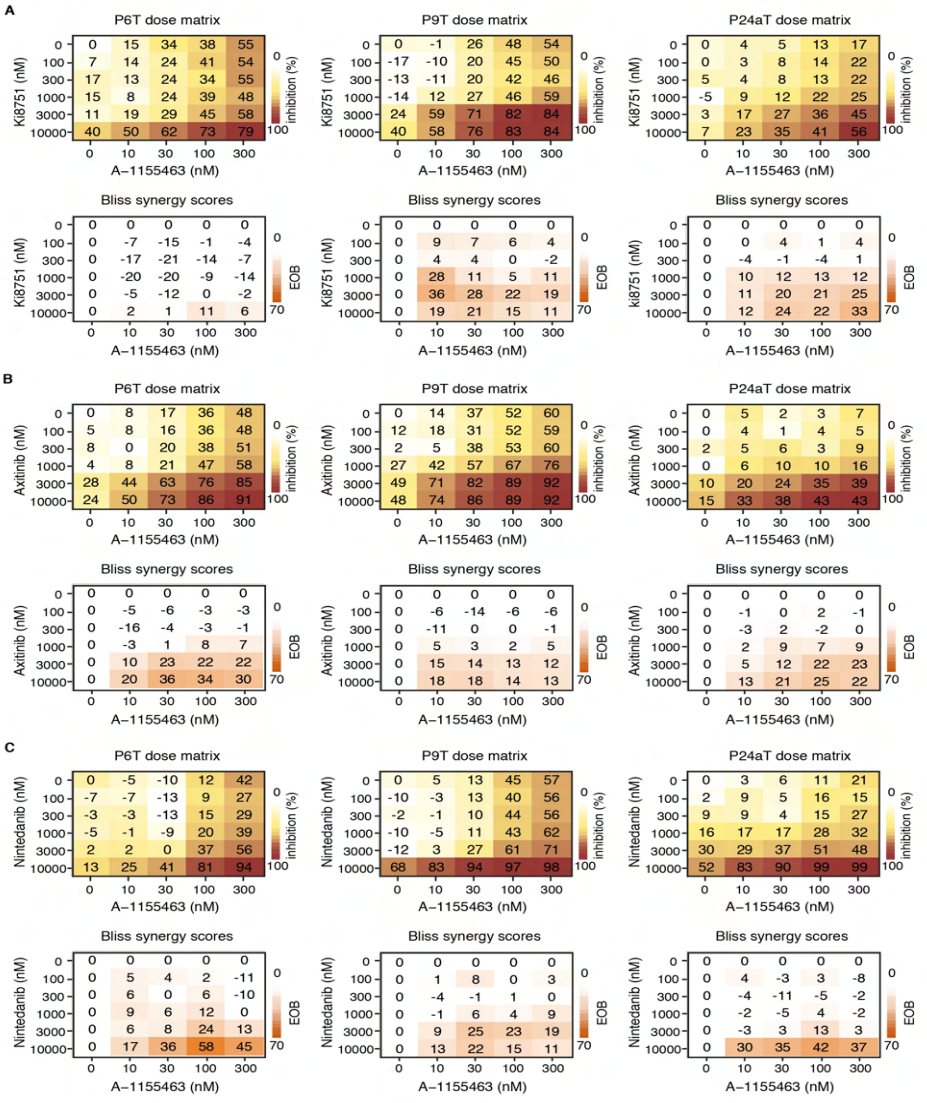

Supplementary Figure 3. Ki8751, Axitinib and Nintedanib in combination with A-1155463 induce synergistic cytotoxicity in primary patient-derived tumor organoids.

A-C. 5 x 6 dose matrices of P6T, P9T and P24aT human CRC organoids treated with Ki8751 (A), Axitinib (B) and Nintedanib (C) in combination with A-1155463 for 48h. % inhibition was calculated from viability data measured by cell titer blue, after normalizing to control. Data represent the average of three independent experiments. Bliss synergy scores were calculated for each dose combination.

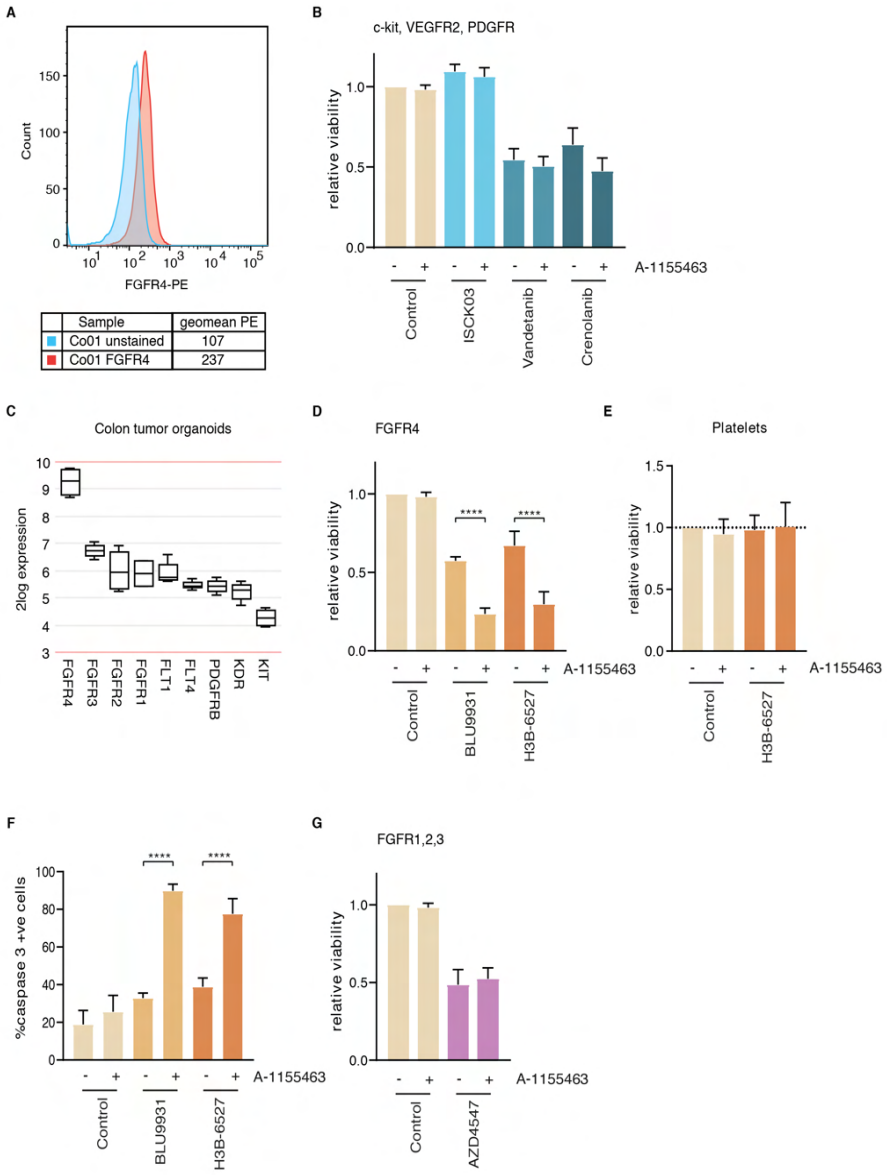

Supplementary Figure 4. FGFR4 inhibition potentiates A-1155463-mediated CSC cell death

A. Histogram of unstained (blue) and FGFR4 (red) stained Co01 cells analyzed by flow cytometry.

B. Viability data of Co01 treated with 2.5μM ISCK03, Vandetanib and Crenolanib either alone or in combination with 5nM A-1155463 for 48 h. Cell titer blue measurements were blank corrected and normalized to control. Data is represented

as mean ± SD (n=3 independent experiments).
C. Box plot of mRNA expression levels of known targets of Ki8751, Axitinib and Nintedanib in the patient-derived tumor organoids p6T, p9T, p16T and p24aT.
D. Viability data of Co01 cells treated with FGFR4 inhibitors BLU9931 and H3B-6527 at 2.5 μM in combination with 5nM A-1155463 for 48h. Cell titer blue measurements were blank corrected and normalized to control. Data is represented as mean ± SD (n=3 independent experiments). ****p value < 0.0001 (two-tailed unpaired Student's t-test).
E. Viability data of platelets derived from human whole blood treated with 5nM of A-1155463 alone and in combination with 5μM H3B-6527 for 24h. Data is plotted relative to control (dashed line) and represented as mean ± SD (n=3 independent experiments).
F. Percentage of activated caspase-3 in the 10% TOP-GFP low Co01 cells after 24h treatment with 5μM BLU9931 and H3B-6527, alone and in combination with 5nM A-1155463. Data is represented as mean ± SD (n=3 independent experiments). ****p value < 0.0001 (two-tailed unpaired Student's t-test).
G. Viability data of Co01 treated with 2.5μM AZD4547 either alone or in combination with 5nM A-1155463 for 48 h. Cell titer blue measurements were blank corrected and normalized to control. Data is represented as mean ± SD (n=3 independent experiments).

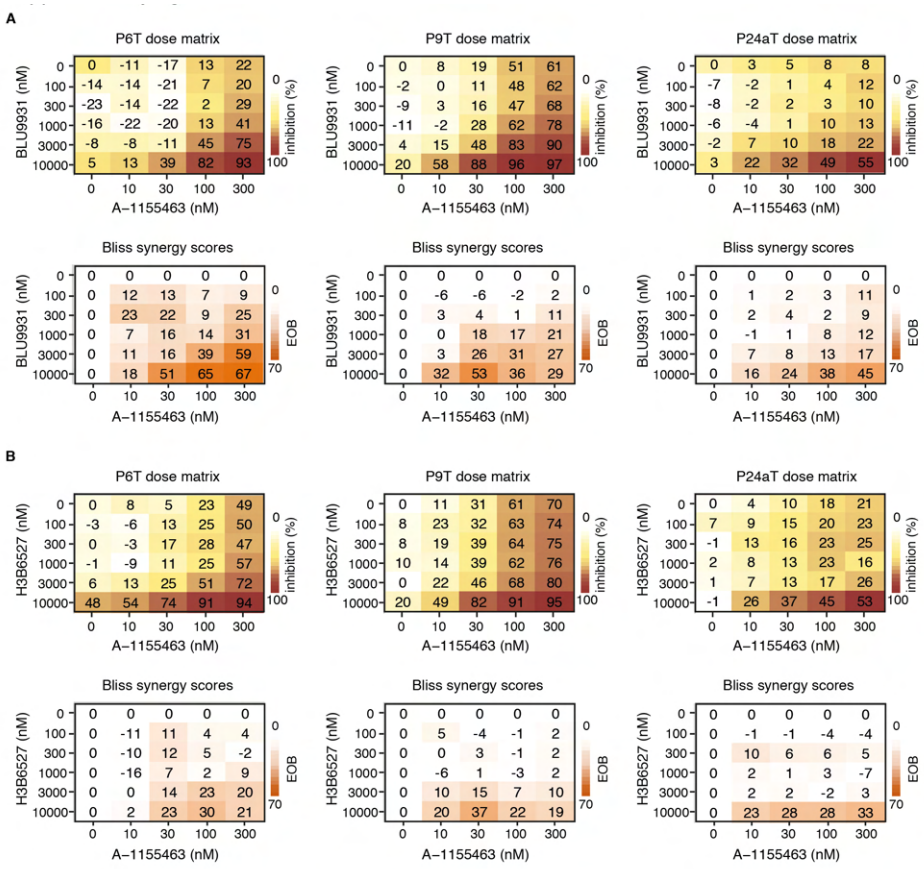

Supplementary Figure 5. FGFR4 specific inhibitors in combination with A-1155463 induce synergistic cytotoxicity in primary patient-derived tumor organoids.

A, B. 5 x 6 dose matrices of P6T, P9T and P24aT human CRC organoids treated with BLU9931 (A) and H3B-6527 (B) in combination with A-1155463 for 48h. % inhibition was calculated from viability data measured by cell titer blue, after normalizing to control. Data represent the average of three independent experiments. Bliss synergy scores were calculated for each dose combination.

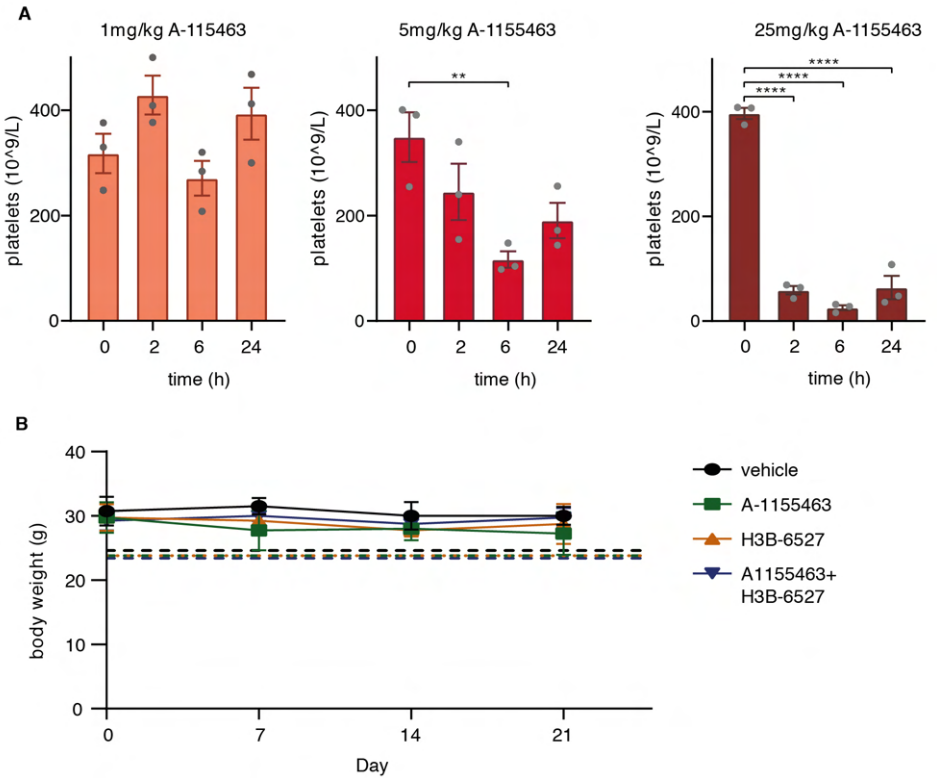

Supplementary Figure 6. FGFR4 specific inhibitors in combination with A-1155463 induce synergistic cytotoxicity in vivo.

A. Platelet counts determined from tail vein blood of mice treated with a single IP injection of A-1155463 at indicated doses, measured at time 0 before treatment and followed up 2, 6 and 24h after. Data is represented as mean ± SEM.**p value <0.01, ****p value < 0.0001 (Ordinary one-way ANOVA).

B. Body weight measurements of mice monitored before treatment at day 0 and at the end of each week of treatment at day 7, 14 and 21. Data represents mean ± SD (n=4 mice per group). Dashed lines indicate tolerable amount of weight loss as 20% below weight at day 0 for each treatment group.

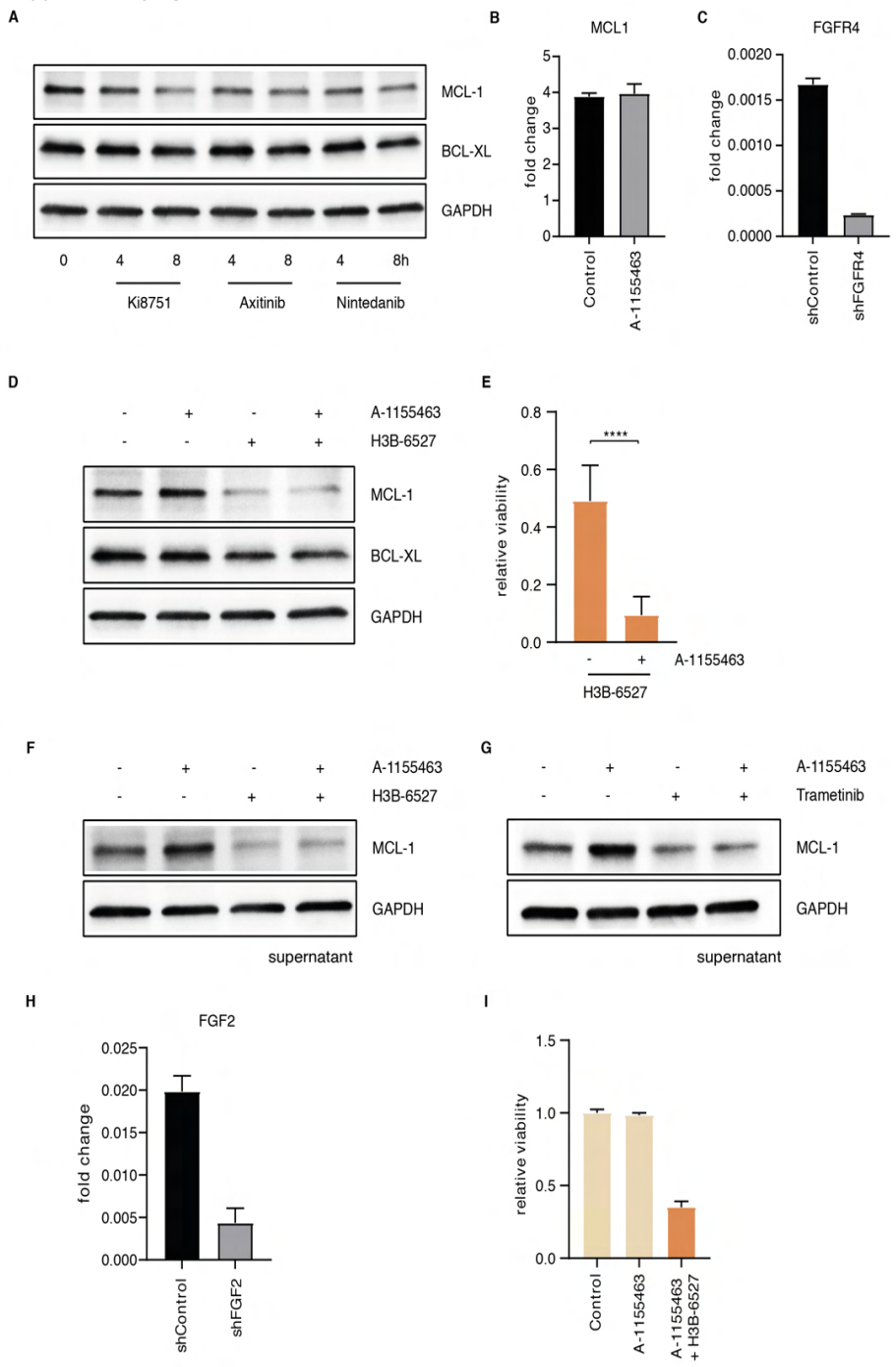
A
MCL-1
BCL-XL
GAPDH
0 4 8 4 8 4 8h
Ki8751
Axitinib
Nintedanib
B
MCL1
fold change
Control
A-1155463
C
FGFR4
fold change
shControl
shFGFR4
D
A-1155463
H3B-6527
MCL-1
BCL-XL
GAPDH
E
relative viability
****
A-1155463
H3B-6527
F
A-1155463
H3B-6527
MCL-1
GAPDH
supernatant
G
A-1155463
Trametinib
MCL-1
GAPDH
supernatant
H
FGF2
fold change
shControl
shFGF2
I
relative viability
Control
A-1155463
A-1155463 + H3B-6527

Supplementary Figure 7. BCL-XL inhibition induces an FGFR4-mediated rescue response.

A. Immunoblot analysis of MCL-1 and BCL-XL levels in Co01 cells treated with Ki8751, Axitinib and Nintedanib at 1μM for several time points. GAPDH was used as a loading control. Blots represent one of two independent experiments with similar results.

B. qRT-PCR analysis of *MCL1* expression levels in Co01 cells treated with 5nM A-1155463 for 24h. Data is represented as mean ± SD (n=3).

C. qRT-PCR analysis of *FGFR4* expression levels in Co01 cells transduced with shControl or shFGFR4 to confirm effective knockdown.

D. Immunoblot analysis of MCL-1 and BCL-XL levels in Co01 cells cultured in medium without bFGF, treated with 5nM A-1155463, 5μM H3B-6527 or a combination of the two for 4h. GAPDH was used as a loading control. Blots represent one of two independent experiments with similar results.

E. Viability data of Co01 cells treated with H3B-6527 at 5μM in combination with 5nM A-1155463 for 48h, without bFGF in the culture medium. Cell titer blue measurements were blank corrected and normalized to control. Data is represented as mean ± SD (n=2 independent experiments). ****p value < 0.0001 (two-tailed unpaired Student's t-test).

F. Immunoblot analysis of MCL-1 levels in SW948 cells that received supernatant of control or 5nM A-1155463 conditioned cells as described in Fig. 5d, in the presence or absence of 5μM H3B-6527 for 4h. GAPDH was used as a loading control. Blots represent one of two independent experiments with similar results.

G. Immunoblot analysis of MCL-1 levels in SW948 cells that received supernatant of control or 5nM A-1155463 conditioned cells as described in Fig. 5d, in the presence or absence of 5μM Trametinib for 4h. GAPDH was used as a loading control.

H. qRT-PCR analysis of *FGF2* expression levels in HCT116 cells transduced with shControl or shFGF2 to confirm effective knockdown.

I. Viability data of Co01 cells treated with 1nM A-1155463 in combination with 5μM H3B-6527 for 48h. Cell titer blue measurements were blank corrected and normalized to control. Data is represented as mean ± SD (n=3).

Supplementary Table 1: Drug screen z-scores for all hit compounds (n= 81, cut off = 2)

Drug	Target	Z-score
Manidipine 2HCl	Calcium Channel	5,258272
IKK-16 (IKK Inhibitor VII)	IKK	5,184138
KX2-391	Src	4,7244
UNC-2025	TAM Receptor	4,696635
BI-D1870	S6 Kinase	4,469111
ZM 447439	Aurora Kinase	4,448515
Axitinib	VEGFR, PDGFR, c-Kit	4,437203
SNS-314 Mesylate	Aurora Kinase	4,343647
Anidulafungin (LY303366)	anti fungal	4,205272
CYC116	Aurora Kinase, VEGFR	4,179572
JTC-801	Opioid Receptor	4,090829
Obatoclax Mesylate (GX15-070)	Bcl-2	3,982645
Ro-3306	CDK	3,874202
MI-2 (MALT1 inhibitor)	MALT1	3,834867
MLN8054	Aurora Kinase	3,828989
AT9283	Bcr-Abl, JAK, Aurora Kinase	3,704231
CHIR-99021 (CT99021)	GSK-3	3,644232
Pacritinib (SB1518)	JAK	3,60392
CHIR-98014	GSK-3	3,58539
Barasertib (AZD1152-HQPA)	Aurora Kinase	3,578242
Evacetrapib (LY2484595)	CETP	3,514391
HTH-01-015	AMPK	3,452692
BIO-acetoxime	GSK-3	3,397805
MI-3 (Menin-MLL Inhibitor)	Histone Methyltransferase	3,372627
MI-2 (Menin-MLL Inhibitor)	Histone Methyltransferase	3,362553
Avasimibe	P450	3,360719
KW-2449	Flt, Bcr-Abl, Aurora Kinase	3,337525
Degrasyn (WP1130)	DUB, Bcr-Abl	3,333488

AZ 960	JAK	3,281221
GSK1838705A	IGF-1, ALK	3,263769
Fingolimod (FTY720) HCl	S1P Receptor, Bcr-Abl, PKC	3,238673
Etravirine (TMC125)	Reverse Transcriptase	3,220174
Golvatinib (E7050)	c-Met, VEGFR	3,2144
Lonafarnib	Ras	3,183913
PHA-680632	Aurora Kinase	3,154507
Amiodarone HCl	Potassium Channel	3,149934
PF-562271 HCl	FAK	3,112049
Tivantinib (ARQ 197)	c-Met	3,045672
Enzastaurin (LY317615)	PKC	2,876338
SU6656	Src	2,874627
LY2090314	GSK-3	2,855153
MK-8745	Aurora Kinase	2,824861
PHA-665752	c-Met	2,803514
Sal003	eIF-2□ phosphatase	2,802311
RG-7112	Mdm2	2,792976
BIO	GSK-3	2,773986
LY2784544	JAK	2,629849
Crizotinib (PF-02341066)	c-Met, ALK	2,606993
Manidipine	Calcium Channel	2,592738
AZD1480	JAK	2,499345
Ki8751	VEGFR, c-Kit, PDGFR, FGFR	2,498458
Bosutinib (SKI-606)	Src	2,472367
YK-4-279	DNA/RNA Synthesis	2,467978
Aurora A Inhibitor I	Aurora Kinase	2,466469
GSK J4 HCl	Histone demethylases	2,428427
Cobimetinib (GDC-0973, RG7420)	MEK	2,410887
JIB-04	Histone demethylases	2,369104
Oligomycin A	ATPase	2,367272
CHIR-124	Chk	2,366081

CCT129202	Aurora Kinase	2,331681
Tipifarnib	Farnesyltransferase, Ras	2,329758
Afatinib (BIBW2992)	EGFR	2,313321
HO-3867	STAT	2,295084
CP-673451	PDGFR	2,285717
Go 6983	PKC	2,280841
Dapivirine (TMC120)	Reverse Transcriptase	2,217095
BMS-265246	CDK	2,159045
TPCA-1	IKK	2,158036
Cerdulatinib (PRT062070, PRT2070)	JAK	2,139671
JNK Inhibitor IX	JNK	2,135353
Nintedanib (BIBF 1120)	VEGFR, PDGFR, FGFR	2,134084
CCT137690	Aurora Kinase	2,132823
CGK 733	ATM/ATR	2,125951
AM251	Cannabinoid Receptor	2,119104
VE-822	ATM/ATR	2,091326
Arecoline	AChR	2,053796
Crenolanib (CP-868596)	PDGFR	2,05266
Bazedoxifene HCl	Estrogen/progestin receptor	2,051512
NMS-873	p97	2,043958
Clemastine Fumarate	Histamine Receptor	2,025866
PH-797804	p38 MAPK	2,006034

Chapter 5

BH3 mimetic sensitivity of colorectal cancer cell lines in correlation with molecular features identifies predictors of response

Le Zhang*, Prashanthi Ramesh*, Maxime Steinmetz and Jan Paul Medema.

Published in *International Journal of Molecular Sciences, 2021.*

* Equal Contribution

Abstract

Colorectal cancer (CRC) is a heterogeneous disease, which in part explains the differential response to chemotherapy observed in the clinic. BH3 mimetics, which target anti-apoptotic BCL-2 family members, have shown potential in the treatment of hematological malignancies and offer promise for the treatment of solid tumors as well. To gain a comprehensive understanding of the response to BH3 mimetics in CRC and the underlying molecular factors predicting sensitivity, we screened a panel of CRC cell lines with four BH3 mimetics targeting distinct anti-apoptotic BCL-2 proteins. Treatment with compounds alone and in combination revealed potent efficacy of combined MCL-1 and BCL-XL inhibition in inducing CRC cell death, irrespective of molecular features. Importantly, expression of the anti-apoptotic protein target of BH3 mimetics on its own did not predict sensitivity. However, the analysis did identify consensus molecular subtype (CMS) specific response patterns, such as higher resistance to single and combined BCL-2 and MCL-1 inhibition in CMS2 cell lines. Furthermore, analysis of mutation status revealed that *KRAS* mutant cell lines were more resistant to MCL-1 inhibition. Conclusively, we find that CRC cell lines presented with distinct responses to BH3 mimetics that can in part be predicted by their CMS profile and *KRAS/BRAF* mutations. Overall, almost all CRC lines share sensitivity in the nanomolar range to combined MCL-1 and BCL-XL targeting suggesting that this would be the preferred approach to target these cancers.

Introduction

Despite significant advances in therapy, colorectal cancer (CRC) is still one of the leading causes of cancer-related deaths worldwide. CRC is characterized by high heterogeneity and unfavorable overall survival in late stage disease [1]. Due to the heterogeneity of the molecular and pathological phenotypes, CRC patients exhibit differential response to adjuvant therapies [2, 3]. Based on the distinct molecular gene expression patterns, a consensus classifier was established to stratify CRC into four consensus molecular subtypes (CMS) to better understand the biological heterogeneity [4]. CMS1 displays high microsatellite instability (MSI), often associated with high immunogenicity. CMS2 is the classical subtype characterized by an epithelial phenotype harboring WNT/MYC activation. CMS3 tumors exhibit metabolic activation and are enriched for KRAS mutations, whereas CMS4 is a poor-prognosis mesenchymal subtype, which is characterized by an increased stromal infiltrate and chemotherapy resistance.

The BCL-2 protein family is a cluster of proteins regulating the intrinsic apoptosis pathway, which can be sub-classified into three subgroups according to their corresponding structure and function. Firstly, BCL-2-associated X protein (BAX), Bcl-2 homologous antagonist/killer (BAK), and Bcl-2-related ovarian killer protein (BOK), the effectors of apoptosis, are able to form pore-like structures on the outer membrane of mitochondria and facilitate the release of cytochrome c to unleash apoptotic cell death [5]. In the absence of an apoptotic signal, these effectors are kept in check by anti-apoptotic BCL-2 family members, including BCL-2, BCL-XL, BCL-W, and MCL-1. Anti-apoptotic BCL-2 proteins translocate to the mitochondrial outer membrane and block the activation of BAX/BAK/BOK [6]. Activation of the apoptotic cascade usually starts with the third group of BCL-2 family members, the BH3 only proteins. Their upregulation or activation and subsequent interaction with pro- and anti-apoptotic BCL-2 family members tips the balance in favor of apoptosis allowing the effectors to act [7]. Tumor cells frequently upregulate anti-apoptotic BCL-2

family members and/or downregulate pro-apoptotic members, conferring resistance to apoptotic signals including those induced by radiotherapy and chemotherapy [8]. In order to sensitize cancer cells to apoptosis, a group of bioactive compounds, so called BH3 mimetics, which functionally mimic intrinsic BH3-only proteins, were developed and show promising efficacy in inducing apoptosis in hematologic malignancies and solid tumors. Corresponding to their selective affinity, BH3 mimetics exhibit distinct specificity in targeting different anti-apoptotic BCL-2 proteins (Table 1). ABT-199 (Venetoclax) is a specific BCL-2 inhibitor and is FDA-approved for treatment of chronic lymphocytic leukemia (CLL) or small lymphocytic lymphoma (SLL). A-1155463 is a specific BCL-XL inhibitor that shows potent efficacy in several solid tumor models [9, 10]. AZD5991, an MCL-1 specific inhibitor, is under investigation in a clinical trial for relapsed or refractory hematological malignancies [11] (ClinicalTrials.gov Identifier: NCT03218683). ABT-263 (Navitoclax), which targets BCL-2, BCL-XL, and BCL-W, is FDA approved as well for combination therapy in hematological malignancies and is being studied in multiple clinical trials for several solid tumors (ClinicalTrials.gov Identifier: NCT02591095; NCT00878449; NCT00891605). Of note, despite their remarkable efficacy in pre-clinical models, only six BH3 mimetics have entered clinical trials, partly due to on-target side-effects on platelets and hematopoietic cells. However, appropriate dosing strategies as well as targeted delivery in antibody-drug conjugate configurations that can overcome these toxicities are under investigation. Additionally, response to BH3 mimetics both in normal and cancer cells is also dependent on tissue origin and distinct molecular properties. Therefore, a better understanding of the anti-apoptotic dependencies in the context of the diverse molecular subtypes of CRC is needed to define the optimal strategy [12, 13].

Herein, we tested four different BH3 mimetics targeting the different anti-apoptotic BCL-2 proteins in 19 CRC lines, which have been classified into four CMSs [14]. Our data show CMS2 lines to be relatively resistant to both BCL-2 or MCL-1 inhibition. In addition, our data reveal a clear relation between the *KRAS/BRAF* mutation status and sensitivity to BH3 mimetics.

Overall, we observe that targeting BCL-XL and MCL-1 simultaneously has a dramatic synergy in CRC cell lines irrespective of CMS. This investigation provides more insight into the relationship between molecular phenotypes of CRCs and their sensitivity to BH3 mimetics.

Table 1. Overview of the targets of the inhibitors and combinations.

Inhibitors and Combinations	BCL-2	BCL-XL	MCL-1	BCL-W
ABT-199	++	-	-	-
A-1155463	-	++	-	-
AZD5991	-	-	++	-
ABT-263	+	+	-	+
ABT-199 + A-1155463	++	++	-	-
ABT-199 + AZD5991	++	-	++	-
A-1155463 + AZD5991	-	++	++	-
ABT-263 + AZD5991	+	+	++	+

Results

CMSs Exhibit Differential Sensitivity to BH3 Mimetics

To assess the sensitivity of CRC to BH3 mimetics, a panel of 19 CRC cell lines were treated with a titration of four BH3 mimetics. The cell lines represent the heterogeneity present in CRC and have previously been classified based on their molecular profile. First, we titrated single BH3 mimetics to determine the individual IC50 values per cell line (Table 1, Figure 1A–D, and Figure S1). Subsequently, a combination of two mimetics were used in an 1:1 ratio to target different combinations of anti-apoptotic BCL-2 family members (Table 1, Figure 1A–D, and Figure S1). Under the combinatory conditions, a concentration of 1 nM indicates 1 nM of mimetic 1 and 1 nM of mimetic 2 added together. Dose-response curves and IC50 values of the combinations were generated and calculated. Inhibitory effects of the combinatorial treatment at each concentration were calculated and plotted as dose-response curves (Figure 1A–D and Figure S1).

Generally, in single treatments, ABT-263 exhibited a relatively higher efficiency in impairing the viability of the majority of CRC lines compared to the other three BH3 mimetics (Figure 1A–I and Figure S2A). This is likely due to the capacity of ABT-263 to target multiple anti-apoptotic family members (BCL-2, BCL-XL, and BCL-W) simultaneously (Table 1). In agreement, when single inhibitors targeting BCL-2 and BCL-XL were combined using the specific mimetics ABT-199 and A-1155463, a similar increase in efficacy was observed. The resultant IC50 values of this combinatorial treatment is strongly correlated to the IC50 values that were determined for the ABT-263 treatment (Figure S2B). Importantly, as the combined inhibition of BCL-2 and BCL-XL with ABT-199/A-1155463 mirrors the efficacy of the BCL-2/BCL-XL/BCL-W inhibitor ABT-263, these data suggest that the role of BCL-W in protecting CRC cell lines is minimal (Figure S2B).

Next, the relation between molecular features and BH3 mimetic sensitivity was analyzed. This revealed that CMS2 cell lines displayed increased resistance to ABT-199 and this was statistically significant when compared to CMS4 lines, while this trend was also observed in comparison to CMS1 and 3 (Figure 1F). Interestingly, CMS2 lines were also more resistant to MCL-1 inhibition by AZD5991, which was significant when compared with CMS3 and CMS4 (Figure 1H), indicating that MCL-1 was more critical in protecting CMS3 and CMS4. No CMS association was observed in A-1155463 and ABT-263 treated cell lines (Figure 1G,I).

The increased efficacy of ABT-263 in comparison to single inhibitors A-1155643 and ABT-199 indicated that CRCs utilize multiple anti-apoptotic family members to prevent the induction of apoptosis. Indeed, the analysis of distinct BH3 mimetic combinations revealed a dramatic synergy between combined BCL-XL and MCL-1 targeting with A-1155463/AZD5991 and/or ABT-263/AZD5991 (Figure 1A–E,J–M and Figure S1). In agreement, the IC50 value was consistently lower for the combination of MCL-1/BCL-XL targeting in relation to targeting of BCL-2/BCL-XL or BCL-2/MCL-1 (Figure 1E,J–L).

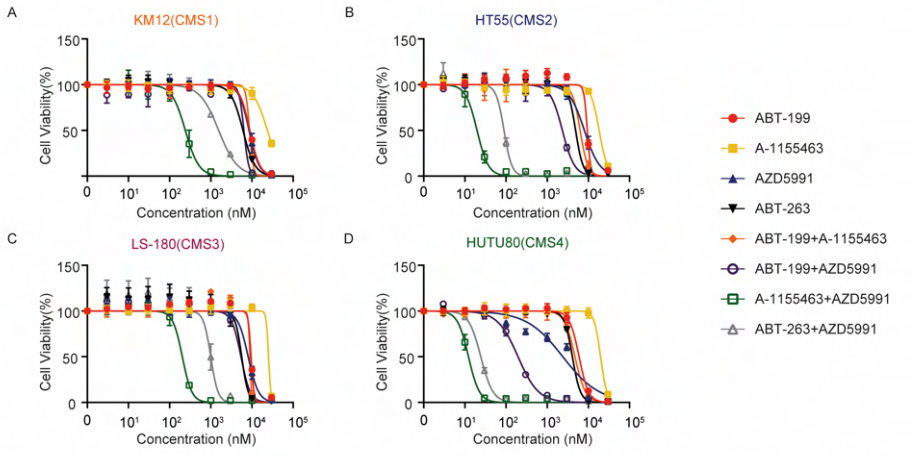

E

	CMS	ABT-199	A-1155463	AZD5991	ABT-263	ABT-199 + A-1155463	ABT-199 + AZD5991	A-1155463 + AZD5991	ABT-263 + AZD5991
HCT-116	1	10,791	1037	11,032	2452	680	8615	108	754
KM12	1	9002	23,792	8662	6058	8746	6384	241	1556
RKO	1	10,016	27,733	6474	4251	9769	1055	197	167
SW48	1	8107	2120	6745	1044	279	517	9	30
HT55	2	9522	18,265	8039	4900	6311	2336	20	89
RCM-1	2	46,051	25,063	29,609	13,440	29,960	35,232	1748	8012
SNU-C1	2	29,142	30,405	25,041	4600	14,356	11,401	1184	346
SW948	2	8287	5210	9863	1789	1688	3015	101	294
LS-1034	2	16,759	755	10,087	2084	544	4477	45	203
T84	2	20,902	26,908	14,220	8283	10,478	4862	108	382
CL-40	3	6117	7808	7116	1623	4068	390	21	39
LS-180	3	9546	25,390	8261	5641	8961	5423	204	1000
LS-513	3	9445	3433	8047	2189	3773	1544	21	60
CaR-1	4	9953	22,218	8372	5021	7823	3404	50	151
COLO-320-HSR	4	10,030	25,271	213	9396	8520	194	139	146
HUTU-80	4	5967	21,823	2403	4092	4730	196	12	24
MDST8	4	7626	778	11,031	820	68	1210	47	72
NCI-H716	4	10,134	12,959	11,497	3722	8519	2075	300	348
OUMS-23	4	7396	10,895	653	3962	3813	127	9	29

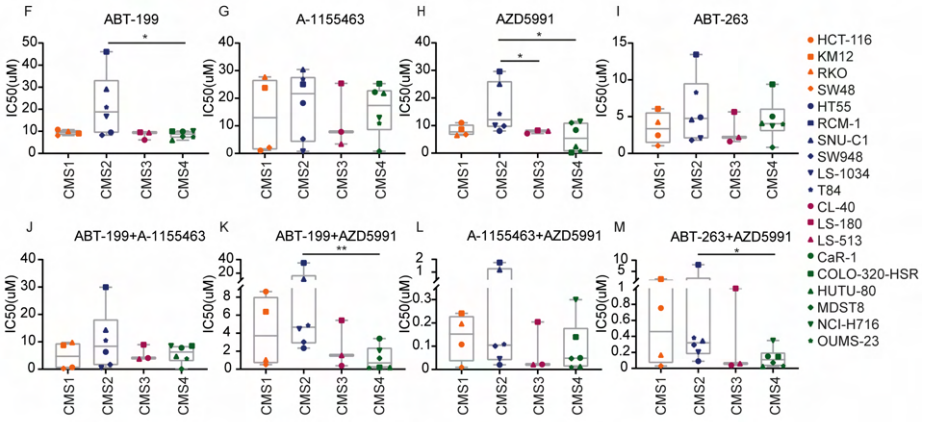

Figure 1. Differential sensitivity to BH3 mimetics in colorectal cancer (CRC) cells. (A–D) Dose-response curves of four BH3 mimetics and four combinations (1:1) in four representative CRC cell lines of each subtype. The Y-axis indicates the relative cell viability normalized to the untreated control. The legend for (A–D) indicates

the symbol for the different mimetic treatments used. (E) IC50 values for BH3 mimetics and combinations tested on all 19 CRC cell lines, in nM; (F–I) IC50 values of four single BH3 mimetics in the CRC cell line panel grouped according to their CMS. *: $p < 0,05$; (J–M) IC50 values of four combinations (1:1) in the CRC cell line panel grouped according to their CMS. **: $p < 0.01$; *: $p < 0,05$, Mann-Whitney test (one-tailed). The legend indicates the symbols assigned for each cell line.

To further verify the synergy and analyze the apoptotic impact exerted by the mimetics, a sub-lethal dose (1 μM) of each BH3 mimetic was administered alone or in combination in four CRC lines representative of each CMS and the percentage of cells with activated caspase-3 was measured by flow cytometry. Importantly, caspase activation was observed with combined inhibition of BCL-XL and MCL-1 (Figure 2A–D) and the level of caspase activity perfectly aligned with the IC50 values that were determined with Cell titer blue (CTB) (Figure 1E).

For instance, ABT-263 + AZD5991 on KM12 was not effective in both CTB and caspase-3 activation, while the same combination effectively killed HT55 in both assays. Moreover, cell death induced by this synergistic combination could be completely blocked by pan-caspase inhibitor Q-VD-OPh suggesting that cell death was caspase dependent and predominantly apoptotic (Figure S2C,D). Additionally, to assess if the cytotoxic effect of different BH3 mimetic combinations is synergistic or not, Bliss synergy scores were calculated for each combination in all CRC lines. This analysis further confirmed that A-1155463/AZD5991 is a highly synergistic combination in CRC (Figure 2E,F). Our data thus indicate that CRC cell lines are strongly dependent on BCL-XL and MCL-1, while the role of BCL-2 is less evident in most lines. Importantly, despite the enhanced efficacy of dual inhibitors, CMS2 lines remained relatively resistant, with especially the lines RCM-1 and SNU-C1 displaying relatively high IC50 values for the most effective combination (A-1155463/AZD5991). CMS2 lines also showed increased resistance to the combined inhibition of BCL-2 and MCL-1 (ABT-199/AZD5991) (Figure 1K), while no CMS association was observed in the combined inhibition of BCL-2 and BCL-XL (ABT-199/A-1155463)

(Figure 1J). Taken together, different CMSs exhibited distinct responses to different BH3 mimetics, with especially the canonical CMS2 lines showing decreased sensitivity to BH3 mimetics.

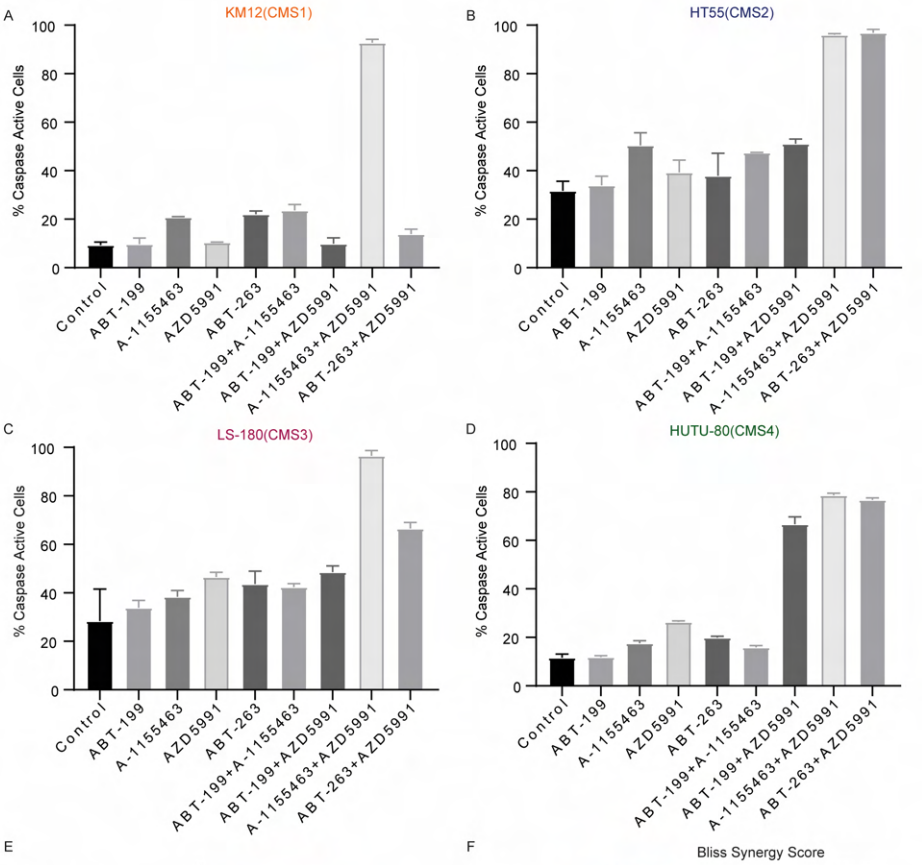

Figure 2. Synergy between different BH3 mimetics in CRC cells. (A–D) Flow cytometry analysis of the activation of caspase-3 induced by different BH3 mimetics and combinations in four representative CRC lines; (E,F) bliss synergy score of the four combinations for all CRC cell lines. Scores below -10 are considered antagonistic, while scores between -10 and 10 are considered additive. Scores above 10 are considered synergistic.

Sensitivity to BH3 Mimetics is not Determined by Expression of the Individual Anti-apoptotic BCL-2 Family Members

In order to reveal the underlying mechanisms determining differential sensitivity to BH3 mimetics in CRC, mRNA and protein expression of *BCL-2*, *BCL-XL*, and *MCL1* were examined in all 19 CRC cell lines in untreated conditions. Generally, *BCL-XL* and *MCL1* mRNA expression was more abundant than *BCL-2*, which was consistent with the drug screening data showing higher dependency on BCL-XL and MCL-1 in CRC cell lines (Figure 3A–G). For *BCL-2* and *BCL-XL*, mRNA expression levels correlated with the corresponding protein level (Figure 3H,I). The mRNA and protein levels of *MCL1* were clearly less well correlated (Figure 3C,J), which is likely due to the extensive post-translational regulation of protein stability described for this family member [15, 16].

On average, there was no clear subtype-related *BCL-2* mRNA and protein expression (Figure 3A,D–G). In contrast, CMS4 cell lines appeared to have lower levels of BCL-XL protein (Figure 3B,D–G). Strikingly, MCL-1 expression was relatively high in the majority of CMS2 lines (Figure 3D–G), which related to their relative resistance to MCL-1 targeting. Combined with a relatively high average expression of BCL-XL, this explains why CMS2 lines were more refractory to (combined) BH3 mimetics. Despite these group-based patterns there was no direct association between target expression and sensitivity to the specific BH3 mimetics (Figure S3A–C). Moreover, even when combining expression patterns of the three anti-apoptotic family members, it did not reveal a clear association between sensitivity and expression (data not shown). Conclusively, CRC cell lines show distinct anti-apoptotic BCL-2 proteins expression and depend on

multiple anti-apoptotic BCL-2 proteins, which is not correlated to sensitivity to BH3 mimetics.

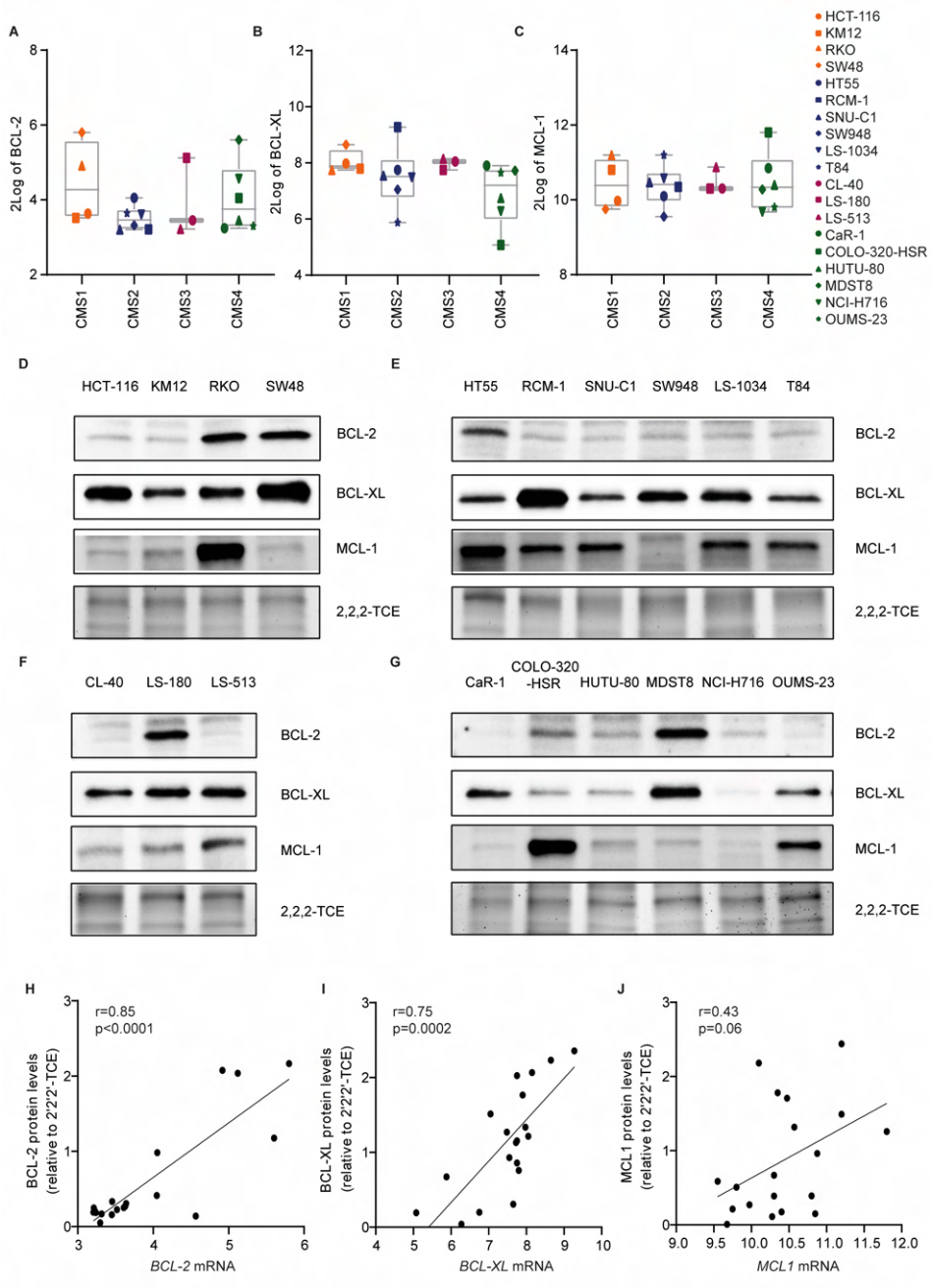

Figure 3. The mRNA and protein expression of BCL-2 family members in CRC cell lines. (A–C) 2Log expression of *BCL-2* (A), *BCL-XL* (B), and *MCL1* (C) mRNA in the CRC cell line panel grouped according to their CMS subtype. The legend indicates the symbols assigned for each cell line. (D–G) Western blot analysis for BCL-2, BCL-XL, and MCL-1 expression in CMS1 (D), CMS2 (E), CMS3 (F), and CMS4 (G) cell lines. 2,2,2-Trichloroethanol (2,2,2-TCE) signal (excerpt taken around 40 kDa region) indicates the amount of protein loaded per cell line. (H–J) Correlation between RNA (as in panel A–C) and protein (as in panel D–G) levels of BCL-2 (H), BCL-XL (I), and MCL-1 (J) in the cell line panel. N = 19. Pearson's correlation (two-tailed p-value).

Sensitivity to BH3 Mimetics Correlates with the KRAS/BRAF Mutation Status

Next to the association patterns between CMS and sensitivity, the relation between individual oncogenic mutations and sensitivity was analyzed. Previous findings have highlighted an important role for p53 signaling in the regulation of apoptosis, but also of the RAS/RAF/MAPK pathway in regulating sensitivity to mitochondrial dependent apoptosis. As these pathways are frequently mutated in CRC, we analyzed the association between BH3 mimetic response and specific molecular features.

To this end, we grouped CRC cell lines based on their molecular features including microsatellite instability (MSI vs. MSS, Figure 4A and Figure S4A), CpG island methylator phenotype (CIMP-high vs. CIMP-low, Figure 4B and Figure S4B), and five most common gene mutations in CRC (APC, KRAS, BRAF, TP53, PIK3CA mutant vs. wild type, Figure 4C–G and Figure 4C–G). This analysis revealed no significant correlation between the sensitivity and MSI or CIMP status of the cell lines (Figure 4A,B and Figure S4A,B). Similarly, APC and PIK3CA mutations did not show a significant correlation with sensitivity (Figure 4C,G and Figure S4C,G). Surprisingly, despite its clear role in apoptosis signaling, no relation between the p53 mutation status and sensitivity was found (Figure 4F and Figure S4F). In contrast, KRAS-mutant CRC cells exhibited significantly less sensitivity to MCL-1 inhibition or BCL-2/MCL-1 co-inhibition (Figure 4D and Figure S4D). Surprisingly,

this relative resistance was not observed for the BRAF mutation, which is downstream of KRAS in the signaling pathway. If anything, the reverse was observed and indeed a significant higher sensitivity was evident for BCL-2 inhibition (Figure 4E), as well as several combinatory treatments (Figure S4E).

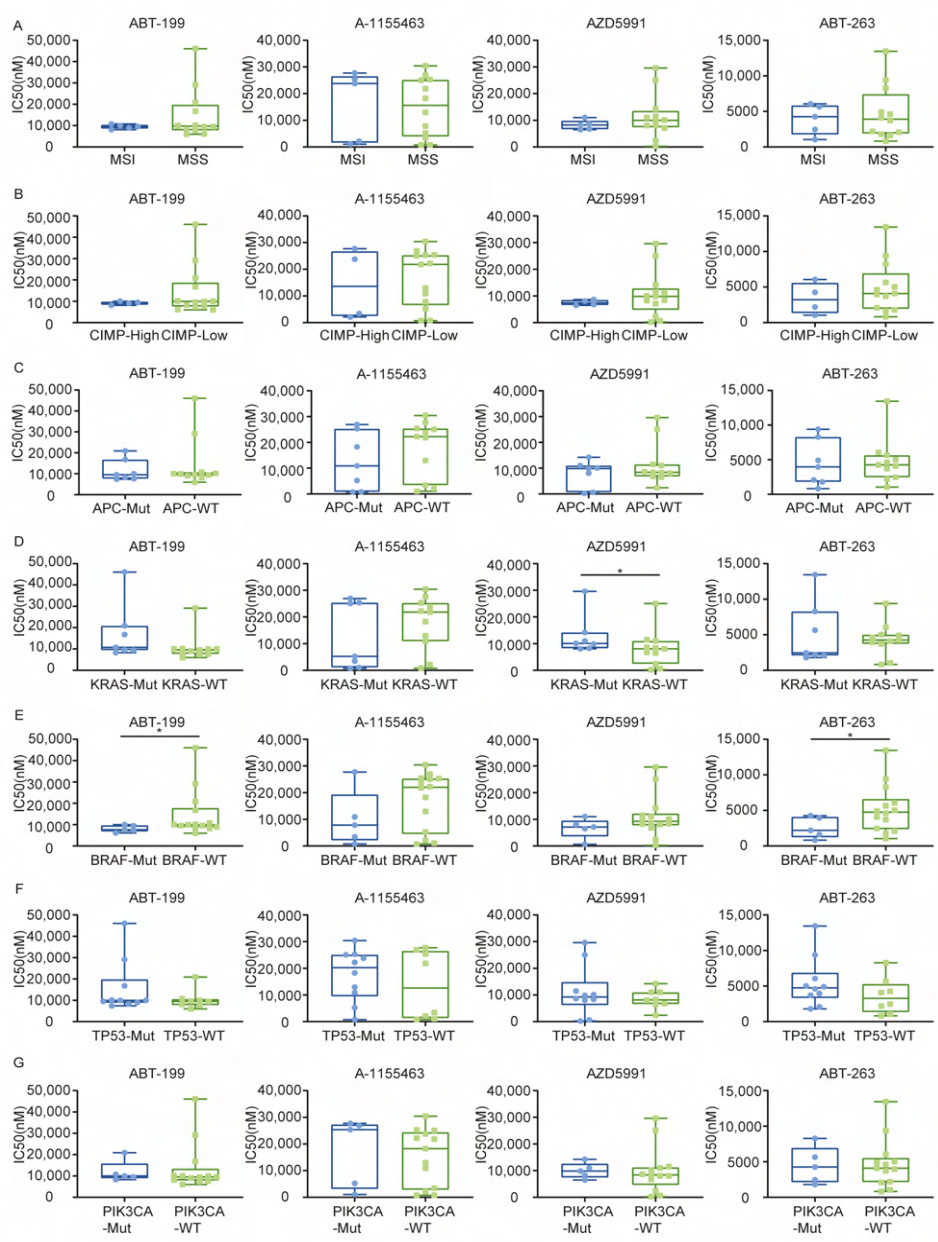

Figure 4. Correlation analysis of IC50 values of four BH3 mimetics and molecular phenotypes in CRCs. (A) Microsatellite instability MSI, MSI microsatellite instable; MSS: Microsatellite stable; (B) CpG island methylator phenotype CIMP, CIMP-high: High CpG island methylation; CIMP-low: Low CpG island methylation; (C–G) Mutation: Mut: Mutant; WT: Wild type; *: $p < 0,05$; Mann-Whitney test (one-tailed).

Discussion

Evasion of apoptosis is a hallmark of cancer, contributing to tumor cell survival and therapy resistance. Tumor cells often upregulate several anti-apoptotic BCL-2 family proteins as a survival mechanism and in CRC, we and others have previously shown that BCL-XL plays a crucial role, particularly also in the stem cell compartment [17, 18]. However, we have recently shown that CRC tumors are highly heterogeneous and can be unbiasedly classified into four distinct subtypes, each with unique features and therapy response [4, 14]. In this study, by examining anti-apoptotic dependencies in the context of these subtypes and other defining molecular features of CRC, we provide an in-depth overview of not only the therapeutic vulnerabilities but also the predictors of response to BH3 mimetics.

When testing individual BH3 mimetics, we find that the inhibition of multiple BCL-2 family members by ABT-263 shows higher efficiency in CRC compared to BCL-2, BCL-XL or MCL-1 inhibition alone. Therefore, we also tested all four BH3 mimetics in combination and found that especially BCL-XL and MCL-1 inhibition is highly synergistic in all 19 CRC cell lines. Unsurprisingly, as competent inhibitors of anti-apoptotic proteins that are capable of inducing mitochondrial outer membrane permeabilization (MOMP), a combination of BH3 mimetics is sufficient to activate caspase-3 and their efficacy is dampened by the pan-caspase inhibitor Q-VD-OPh, which suggests that caspase-dependent apoptotic cell death is the predominant pathway induced upon the BH3 mimetic treatment. However, as reported by Tait et al. [19], cells can still die upon MOMP even in the absence of caspase activity via a so-called caspase independent cell death

(CICD). Although this was not observed in the time-frame tested here, we cannot exclude that after a longer exposure time, BH3 mimetics treated cells may still succumb to the mitochondrial insult and hence undergo CICD after MOMP. Additionally, this does not rule out that other types of cell death that can also be blocked by Q-VD-Oph, such as pyroptosis, might be involved. In general, CRC cells express higher levels of *BCL-XL* and *MCL1*, while *BCL-2* mRNA levels are lower, suggesting that they are more dependent on the former two for apoptosis resistance. In line with our observation, Luo et al. have also shown that the co-inhibition of BCL-XL and MCL-1 using A-1331852 and S64845 showed higher cytotoxicity than the co-inhibition of BCL-XL/BCL-2 or MCL-1/BCL-2 [20]. Moreover, this potent combination has been shown to induce apoptosis in HCT-116 even in the absence of all BH3-only proteins, in a BAX-dependent manner [21]. A similar synergy between BCL-XL and MCL-1 inhibition has also been observed in other types of solid tumor such as cervical cancer [22] and melanoma [23]. Taken together, our data suggest that BCL-XL and MCL-1 could contribute complementarily to maintaining cancer cell survival and co-inhibition, therefore dramatically enhances cytotoxicity.

We have previously shown that CRC cell lines vary in their response to chemotherapy in vitro and in vivo, with CMS4 tumors showing increased resistance [14]. In this study, we also observe a differential response to the BH3 mimetic treatment depending on the subtype. With a single inhibitor treatment, we find that CMS2 cell lines are particularly resistant to BCL-2 and MCL-1 inhibition. This resistance is also observed in the combination therapy setting as CMS2 lines have higher IC50 values for most combinations of BH3 mimetics. This is a rather surprising observation in light of the observed sensitivity of CMS2 lines to chemotherapy. We did observe that CMS2 cell lines express higher levels of BCL-XL and MCL-1 in general, which might contribute to the observed resistance to BH3 mimetics. Importantly, all CMS4 lines tested harbor wild type *KRAS*, while the majority of CMS2 (4/6) cell lines have a *KRAS* mutation, which could explain the higher resistance to MCL-1 inhibition as suggested by the correlation analysis. Nevertheless, regardless of this basal resistance

to MCL-1 inhibition, the combined inhibition of MCL-1 and BCL-XL also induces potent cell death in this subtype, as well.

The underlying reason for the observed difference between BH3 mimetic sensitivity of CMS4 lines in comparison to the reported resistance towards chemotherapy remains to be established. This is especially important to understand when related to the higher sensitivity of CMS2 tumors towards chemotherapy, while they present with lower sensitivity towards BH3 mimetics. This suggests that anti-apoptotic protein reliance on its own does not completely explain the difference in chemotherapy response between these subtypes. Obviously, chemotherapy sensitivity is defined by multiple aspects and does not only involve cell cycle speed, which is reportedly lower for CMS2 lines [14], but also involves the presence of downstream pathways and BH3 proteins signaling towards the mitochondria. Moreover, chemotherapy efficacy is also strongly dependent on drug efflux pumps, which are differentially expressed between the cell lines (results not shown). Therefore, direct relations between chemotherapy and BH3 sensitivity are difficult to draw. Nevertheless, our data do allow us to conclude that BH3 mimetics may provide a better option for mesenchymal CMS4 tumors as compared to chemotherapy, showing relatively effective cell death induction especially for the combination of BCL-XL and MCL-1 targeting mimetics.

To further address if the differential sensitivity to BH3 mimetics could be defined by the corresponding target expression, BCL-2, BCL-XL, and MCL-1 protein levels were defined, which revealed that the sensitivity is neither determined by the relative expression of the corresponding targets of BH3 mimetics nor the overall expression of all three anti-apoptotic BCL-2 members. Consistently, Smith et al. also indicated that the co-expression of related anti-apoptotic BCL-2 family proteins may limit the activity of ABT-199 in diffuse large B cell lymphoma despite having a high BCL-2 expression [24]. On the other hand, Touzeau et al. have shown that sensitivity to BH3 mimetics in multiple myeloma could be related to BH3 profiling suggesting that the BH3 only protein expression is also involved

in defining sensitivity to BH3 mimetics [25]. BCL-XL sensitivity has been shown to closely relate to MCL-1 activity, in particular predicted by NOXA levels, which specifically inhibits MCL-1 [26, 27]. Furthermore, a recent study has used a computational model reflecting the dynamic regulation of this pathway in order to identify high-risk CRC patients [28]. Considering that apoptosis is tightly regulated by a balance of interactions between BCL-2 family members, it is likely that an overarching understanding of this balance in a context-specific manner is necessary to determine the BH3 mimetic response. Alternatively, a simple screen such as performed here or performed by BH3 profiling [29], will provide such an overarching snapshot of the sensitivity of cancers to different mimetics.

In addition to CMS and BH3 mimetic target expression, we also assessed if the mutation status influences the BH3 mimetic response. This analysis revealed that CRC cell lines harboring KRAS mutations are less responsive to MCL-1 inhibition than the wild type lines, indicating that KRAS activation might be involved in resistance to apoptosis mediated by MCL-1. It has been reported by Okamoto et al. that CRC tumors with mutant KRAS are able to upregulate BCL-XL via the ERK pathway, which confers resistance to the proteasome inhibitor, Carfilzomib [30]. However, it is unexpected that BRAF-mutant lines have higher sensitivity to BCL-2 inhibition. It has been shown that BRAF mutation in melanoma could increase MCL-1 expression, suggesting that activating BRAF mutations would confer resistance to apoptosis [31]. Furthermore, it is surprising that TP53 mutations show no correlation with the efficacy of BH3 mimetics, considering the crucial role that TP53 plays in apoptosis regulation [32]. Therefore, a further investigation is required to gain a comprehensive understanding of the exact implications of these oncogenic mutations in determining susceptibility to BH3 mimetics.

Altogether, we show that CRC cell lines display differential response to BH3 mimetics, which in part relates to CMS and KRAS or BRAF mutation status. Our findings provide an in-depth overview of BCL-2 family expression and sensitivity in the context of several molecular features, which can guide

future investigations to optimize the application of BH3 mimetics in CRC. Furthermore, our results emphasize the potent efficacy of combined MCL1 and BCL-XL inhibition for CRC therapy, regardless of pre-existing molecular features.

Materials and Methods

Cell Lines and Profiling

Nineteen colorectal cancer cell lines were kindly provided by Sanger Institute (Cambridge, UK) and authenticated by STR profiling. Cell lines RKO, SW48, HT55, SW948, T84, CL-40, LS-180, CaR-1, HUTU-80, and OUMS-23 were maintained in Dulbecco's modified Eagle's medium/F-12 medium with L-glutamine, 15 mM HEPES (Gibco, Paisley, Scotland) supplemented with 8% fetal bovine serum (Serana, Pessin, Germany) and 50 units/mL of penicillin and streptomycin. HCT-116, KM12, RCM-1, SNU-C1, LS-1034, LS-513, COLO-320-HSR, MDST8, and NCI-H716 were maintained in RPMI 1640 with L-glutamine, 25 mM HEPES (Gibco, Paisley, Scotland) supplemented with 8% fetal bovine serum, 50 units/mL of penicillin and streptomycin, 1% D-glucose solution plus (Sigma-Aldrich, Saint Louis, MO, US), and 100 μM sodium pyruvate (Gibco, Paisley, Scotland). All cells were cultured in a humidified atmosphere at 37 °C 5% CO2.

All 19 CRC lines were classified into four CMSs by our previous work based on the consensus molecular pattern described in [14]. The gene mutation status, microsatellite instability (MSI), and CpG island methylator phenotype (CIMP) of all these 19 lines were also determined as shown in [14].

Compounds

ABT-199, ABT-263, and Q-VD-OPh were purchased from Selleckchem, Houston, TX, US. A-1155463 and AZD5991 were purchased from Chemietek, Indianapolis, IN, US. All compounds were dissolved in dimethyl sulfoxide (DMSO) at a 10 mM stock concentration.

Cell Viability Assay

To assess the sensitivity to four BH3 mimetics, CRC cells were plated into 96-well

plates and treated with two BH3 mimetics in a matrix dilution at a time. After 48 h of treatment, the CellTiter-Blue® cell viability assay (Promega, Madison, WI, US) was used to determine the cell viability by measuring mitochondrial respiration according to the manufacturer's instruction. The relative viability was calculated by normalizing to the untreated control. Dose-response curves and IC50 values were generated and calculated on GraphPad Prism 8.0 (GSL Biotech LLC, Biomatters, Chicago, IL, US) with log(inhibitor) vs. normalized response—variable slope.

Flow Cytometry and CaspaTag Staining

Fifty thousand cells were plated and treated with different BH3 mimetics. After 48 h, cells were trypsinized and harvested. CaspaTag caspase-3/7 in situ assay kit, Sulforhodamine (Merck, Sigma-Aldrich, US) or propidium iodide (Sigma-Aldrich, Saint Louis, MO, US) were used to label cells to detect activated caspase-3 or compromised cytoplasmic membrane, respectively. The percentage of positive cells were measured by flow cytometry on the CytoFLEX (Beckman Coulter Life Sciences, Brea, CA, US).

Bliss Synergy Scoring

According to [33], the Bliss Synergy score was automatically calculated by Synergyfinder [34]. To interpret the results, scores below -10 were considered antagonistic. Scores between -10 and 10 were considered additive and scores above 10 were considered synergistic.

The mRNA Expression Analysis

The RNA expression analysis of the CRC cell lines was performed as described in [14]. Briefly, microarrays expression profiles were obtained using the GeneTitantm MC system from Affymetrix according to the standard protocols of the Cologne Center for Genomics (CCG), University of Cologne, Germany. The dataset is publicly available in the gene expression omnibus (GEO) repository under the accession number GSE100478. Data were normalized using the robust multi-array average (rma) method as implemented in the affy R package (version 1.52.0). Probes were annotated with the hgu133plus2.db R data package (version 3.2.3).

Western Blotting

For the Western blot analysis of BCL-2 family members, cells were lysed using the 1x RIPA lysis and extraction buffer (Thermo Fischer Scientific, Waltham, MA, US) containing Halt protease and phosphatase inhibitor cocktail (1:100, Thermo Fischer Scientific, Waltham, MA, US). Protein samples were quantified using the Pierce BCA protein assay kit (Thermo Fischer Scientific, Waltham, MA, US) as per the manufacturer's instructions. In addition, 20 µg of protein was loaded per well into 4–15% precast gels (Bio-Rad, Hercules, CA, US) and then transferred to PVDF membranes using the Trans-Blot Turbo transfer system (Bio-Rad, Hercules, CA, US) according to the manufacturer's instructions using the mixed molecular weight transfer settings. Membranes were blocked for 1 h in 5% bovine serum albumin (BSA) in Tris-buffered saline and Tween-20 (TBS-T,1x) and stained with a primary antibody overnight at 4 °C. The following primary antibodies were tested: BCL-2 (1:1000 #15071, Cell Signaling, Danvers, MA. US), BCL-XL (1:1000, #2764, Cell Signaling, Danvers, MA. US), and MCL-1 (1:1000, #4572, Cell Signaling, Danvers, MA. US), all diluted in 5% BSA in TBS-T. After washing the blots four times for 20 min each with TBS-T, the secondary antibody anti-rabbit-horseradish peroxidase (1:5000, #4050-05, Southern Biotech, Birmingham, AL, US) or anti-mouse-horseradish peroxidase (1:5000, #1031-05, Southern Biotech, Birmingham, AL, US) was added for 2 h at room temperature. Following another round of 4× 20 min washes, the membranes were developed using the LumiLight Western blotting substrate (Sigma-Aldrich, Saint Louis, MO, US) and imaged on the ImageQuant LAS4000 (GE Healthcare Life Sciences, Chicago, IL, US). Before proceeding with blotting for protein expression, the polyacrylamide gel was incubated for 5 min in an electrophoresis buffer containing 1% 2,2,2-Trichloroethanol (2,2,2-TCE, cat. #T54801, Sigma-Aldrich) to allow for tryptophan visualization and thereby a comparison of the amount of protein loaded between the cell lines [35]. The gels were imaged using the UV sample tray of a ChemiDoc imaging system (Bio-Rad, Hercules, CA, US). Western blot images were quantified using ImageJ, wherein a region of interest (ROI) was defined and used for each lane to select the band of interest. The mean grey value of the ROI was measured for each band as well as the background region of each lane. Each protein band expression was blank corrected and normalized to the 2'2'2'-TCE loading control levels.

Correlation Analysis and Statistics

To analyze the correlation between the drug sensitivity and the phenotype of CRC cell lines, IC50 values were plotted and grouped based on their CMSs or mutation status. The significant difference between groups were tested by the one-tailed Mann-Whitney test. A $P < 0.05$ was considered statistically significant. The correlation between IC50 values and target expression were analyzed by Spearman's rank correlation.

Funding: This research was funded by Oncode Institute and Dutch cancer society grants 10150, UvA2015-7587.

Data Availability Statement: Microarrays expression profiles were obtained using the GeneTitantm MC system from Affymetrix according to the standard protocols of the Cologne Center for Genomics (CCG), University of Cologne, Germany. The dataset is publically available in the Gene Expression Omnibus (GEO) repository under the accession number GSE100478.

References

1. Dekker, E.; Tanis, P.J.; Vleugels, J.L.A.; Kasi, P.M.; Wallace, M.B. Colorectal cancer. Lancet 2019, 394, 1467–1480, doi:10.1016/s0140-6736(19)32319-0.
2. Dienstmann, R.; Vermeulen, L.; Guinney, J.; Kopetz, S.; Tejpar, S.; Tabernero, J. Consensus molecular subtypes and the evolution of precision medicine in colorectal cancer. Nat. Rev. Cancer 2017, 17, 79–92, doi:10.1038/nrc.2016.126.
3. De Roock, W.; De Vriendt, V.; Normanno, N.; Ciardiello, F.; Tejpar, S. KRAS, BRAF, PIK3CA, and PTEN mutations: Implications for targeted therapies in metastatic colorectal cancer. Lancet Oncol. 2011, 12, 594–603, doi:10.1016/s1470-2045(10)70209-6.
4. Guinney, J.; Dienstmann, R.; Wang, X.; de Reyniès, A.; Schlicker, A.; Soneson, C.; Marisa, L.; Roepman, P.; Nyamundanda, G.; Angelino, P.; et al. The consensus molecular subtypes of colorectal cancer. Nat. Med. 2015, 21, 1350–1356, doi:10.1038/nm.3967.
5. Tait, S.W.; Green, D.R. Mitochondria and cell death: Outer membrane permeabilization and beyond. Nat. Rev. Mol. Cell Biol. 2010, 11, 621–632, doi:10.1038/nrm2952.
6. Czabotar, P.E.; Lessene, G.; Strasser, A.; Adams, J.M. Control of apoptosis by the BCL-2 protein family: Implications for physiology and therapy. Nat. Rev. Mol. Cell Biol. 2014, 15, 49–63, doi:10.1038/nrm3722.
7. Huang, D.C.; Strasser, A. BH3-Only proteins-essential initiators of apoptotic cell death. Cell 2000, 103, 839–842, doi:10.1016/s0092-8674(00)00187-2.
8. Maji, S.; Panda, S.; Samal, S.K.; Shriwas, O.; Rath, R.; Pellecchia, M.; Emdad, L.; Das, S.K.; Fisher, P.B.; Dash, R. Bcl-2 Antiapoptotic Family Proteins and Chemoresistance in Cancer. Adv. Cancer Res. 2018, 137, 37–75, doi:10.1016/bs.acr.2017.11.001.

9. Tao, Z.F.; Hasvold, L.; Wang, L.; Wang, X.; Petros, A.M.; Park, C.H.; Boghaert, E.R.; Catron, N.D.; Chen, J.; Colman, P.M.; et al. Discovery of a Potent and Selective BCL-XL Inhibitor with in Vivo Activity. ACS Med. Chem. Lett. 2014, 5, 1088–1093, doi:10.1021/ml5001867.
10. de Jong, Y.; Monderer, D.; Brandinelli, E.; Monchanin, M.; van den Akker, B.E.; van Oosterwijk, J.G.; Blay, J.Y.; Dutour, A.; Bovée, J. Bcl-xl as the most promising Bcl-2 family member in targeted treatment of chondrosarcoma. Oncogenesis 2018, 7, 74, doi:10.1038/s41389-018-0084-0.
11. Tron, A.E.; Belmonte, M.A.; Adam, A.; Aquila, B.M.; Boise, L.H.; Chiarparin, E.; Cidado, J.; Embrey, K.J.; Gangl, E.; Gibbons, F.D.; et al. Discovery of Mcl-1-specific inhibitor AZD5991 and preclinical activity in multiple myeloma and acute myeloid leukemia. Nat. Commun. 2018, 9, 5341, doi:10.1038/s41467-018-07551-w.
12. Merino, D.; Kelly, G.L.; Lessene, G.; Wei, A.H.; Roberts, A.W.; Strasser, A. BH3-Mimetic Drugs: Blazing the Trail for New Cancer Medicines. Cancer Cell 2018, 34, 879–891, doi:10.1016/j.ccell.2018.11.004.
13. Ashkenazi, A.; Fairbrother, W.J.; Leverson, J.D.; Souers, A.J. From basic apoptosis discoveries to advanced selective BCL-2 family inhibitors. Nat. Rev. Drug Discov. 2017, 16, 273–284, doi:10.1038/nrd.2016.253.
14. Linnekamp, J.F.; Hooff, S.R.V.; Prasetyanti, P.R.; Kandimalla, R.; Buikhuisen, J.Y.; Fessler, E.; Ramesh, P.; Lee, K.; Bochove, G.G.W.; de Jong, J.H.; et al. Consensus molecular subtypes of colorectal cancer are recapitulated in in vitro and in vivo models. Cell Death Differ. 2018, 25, 616–633, doi:10.1038/s41418-017-0011-5.
15. Zhong, Q.; Gao, W.; Du, F.; Wang, X. Mule/ARF-BP1, a BH3-only E3 ubiquitin ligase, catalyzes the polyubiquitination of Mcl-1 and regulates apoptosis. Cell 2005, 121, 1085–1095, doi:10.1016/j.cell.2005.06.009.
16. Mojsa, B.; Lassot, I.; Desagher, S. Mcl-1 ubiquitination: Unique regulation of an essential survival protein. Cells 2014, 3, 418–437, doi:10.3390/cells3020418.
17. Colak, S.; Zimberlin, C.D.; Fessler, E.; Hogdal, L.; Prasetyanti, P.R.; Grandela, C.M.; Letai, A.; Medema, J.P. Decreased mitochondrial priming determines chemoresistance of colon cancer stem cells. Cell Death Differ. 2014, 21, 1170–1177, doi:10.1038/cdd.2014.37.
18. Ishikawa, K.; Kawano, Y.; Arihara, Y.; Kubo, T.; Takada, K.; Murase, K.; Miyanishi, K.; Kobune, M.; Kato, J. BH3 profiling discriminates the anti-apoptotic status of 5-fluorouracil-resistant colon cancer cells. Oncol. Rep. 2019, 42, 2416–2425, doi:10.3892/or.2019.7373.
19. Tait, S.W.; Ichim, G.; Green, D.R. Die another way--non-apoptotic mechanisms of cell death. J. Cell Sci. 2014, 127, 2135–2144, doi:10.1242/jcs.093575.
20. Luo, M.J.; Palmieri, M.; Riffkin, C.D.; Sakthianandeswaren, A.; Djajawi, T.M.; Hirokawa, Y.; Shuttleworth, V.; Segal, D.H.; White, C.A.; Nhu, D.; et al. Defining the susceptibility of colorectal cancers to BH3-mimetic compounds. Cell Death Dis. 2020, 11, 735, doi:10.1038/s41419-020-02815-0.
21. Greaves, G.; Milani, M.; Butterworth, M.; Carter, R.J.; Byrne, D.P.; Eyers, P.A.; Luo, X.; Cohen, G.M.; Varadarajan, S. BH3-only proteins are dispensable for apoptosis induced by pharmacological inhibition of both MCL-1 and BCL-X(L). Cell Death Differ. 2019, 26, 1037–1047, doi:10.1038/s41418-018-0183-7.
22. Abdul Rahman, S.F.; Muniandy, K.; Soo, Y.K.; Tiew, E.Y.H.; Tan, K.X.; Bates, T.E.;

Mohana-Kumaran, N. Co-inhibition of BCL-XL and MCL-1 with selective BCL-2 family inhibitors enhances cytotoxicity of cervical cancer cell lines. Biochem. Biophys. Rep. 2020, 22, 100756, doi:10.1016/j.bbrep.2020.100756.

23. Lee, E.F.; Harris, T.J.; Tran, S.; Evangelista, M.; Arulananda, S.; John, T.; Ramnac, C.; Hobbs, C.; Zhu, H.; Gunasingh, G.; et al. BCL-XL and MCL-1 are the key BCL-2 family proteins in melanoma cell survival. Cell Death Dis. 2019, 10, 342, doi:10.1038/s41419-019-1568-3.
24. Smith, V.M.; Dietz, A.; Henz, K.; Bruecher, D.; Jackson, R.; Kowald, L.; van Wijk, S.J.L.; Jayne, S.; Macip, S.; Fulda, S.; et al. Specific interactions of BCL-2 family proteins mediate sensitivity to BH3-mimetics in diffuse large B-cell lymphoma. Haematologica 2020, 105, 2150–2163, doi:10.3324/haematol.2019.220525.
25. Touzeau, C.; Ryan, J.; Guerriero, J.; Moreau, P.; Chonghaile, T.N.; Le Gouill, S.; Richardson, P.; Anderson, K.; Amiot, M.; Letai, A. BH3 profiling identifies heterogeneous dependency on Bcl-2 family members in multiple myeloma and predicts sensitivity to BH3 mimetics. Leukemia 2016, 30, 761–764, doi:10.1038/leu.2015.184.
26. Soderquist, R.S.; Crawford, L.; Liu, E.; Lu, M.; Agarwal, A.; Anderson, G.R.; Lin, K.H.; Winter, P.S.; Cakir, M.; Wood, K.C. Systematic mapping of BCL-2 gene dependencies in cancer reveals molecular determinants of BH3 mimetic sensitivity. Nat. Commun. 2018, 9, 3513, doi:10.1038/s41467-018-05815-z.
27. Okumura, K.; Huang, S.; Sinicrope, F.A. Induction of Noxa sensitizes human colorectal cancer cells expressing Mcl-1 to the small-molecule Bcl-2/Bcl-xL inhibitor, ABT-737. Clin. Cancer Res. 2008, 14, 8132–8142, doi:10.1158/1078-0432.Ccr-08-1665.
28. Lindner, A.U.; Salvucci, M.; Morgan, C.; Monsefi, N.; Resler, A.J.; Cremona, M.; Curry, S.; Toomey, S.; O'Byrne, R.; Bacon, O.; et al. BCL-2 system analysis identifies high-risk colorectal cancer patients. Gut 2017, 66, 2141–2148, doi:10.1136/gutjnl-2016-312287.
29. Deng, J.; Carlson, N.; Takeyama, K.; Dal Cin, P.; Shipp, M.; Letai, A. BH3 profiling identifies three distinct classes of apoptotic blocks to predict response to ABT-737 and conventional chemotherapeutic agents. Cancer Cell 2007, 12, 171–185, doi:10.1016/j.ccr.2007.07.001.
30. Okamoto, K.; Zaanan, A.; Kawakami, H.; Huang, S.; Sinicrope, F.A. Reversal of Mutant KRAS-Mediated Apoptosis Resistance by Concurrent Noxa/Bik Induction and Bcl-2/Bcl-xL Antagonism in Colon Cancer Cells. Mol. Cancer Res. 2015, 13, 659–669, doi:10.1158/1541-7786.Mcr-14-0476.
31. McKee, C.S.; Hill, D.S.; Redfern, C.P.; Armstrong, J.L.; Lovat, P.E. Oncogenic BRAF signalling increases Mcl-1 expression in cutaneous metastatic melanoma. Exp. Dermatol. 2013, 22, 767–769, doi:10.1111/exd.12254.
32. Gottlieb, T.M.; Oren, M. p53 and apoptosis. Semin. Cancer Biol. 1998, 8, 359–368, doi:10.1006/scbi.1998.0098.
33. Bliss, C. The toxicity of poisons applied jointly. Ann. Appl. Biol. 1939, 26, 585-615.
34. Ianevski, A.; Giri, A.K.; Aittokallio, T. SynergyFinder 2.0: Visual analytics of multi-drug combination synergies. Nucleic Acids Res. 2020, 48, W488–W493, doi:10.1093/nar/gkaa216.
35. Ladner, C.L.; Yang, J.; Turner, R.J.; Edwards, R.A. Visible fluorescent detection of proteins in polyacrylamide gels without staining. Anal. Biochem. 2004, 326, 13–20, doi:10.1016/j.ab.2003.10.047.

Supplementary Information

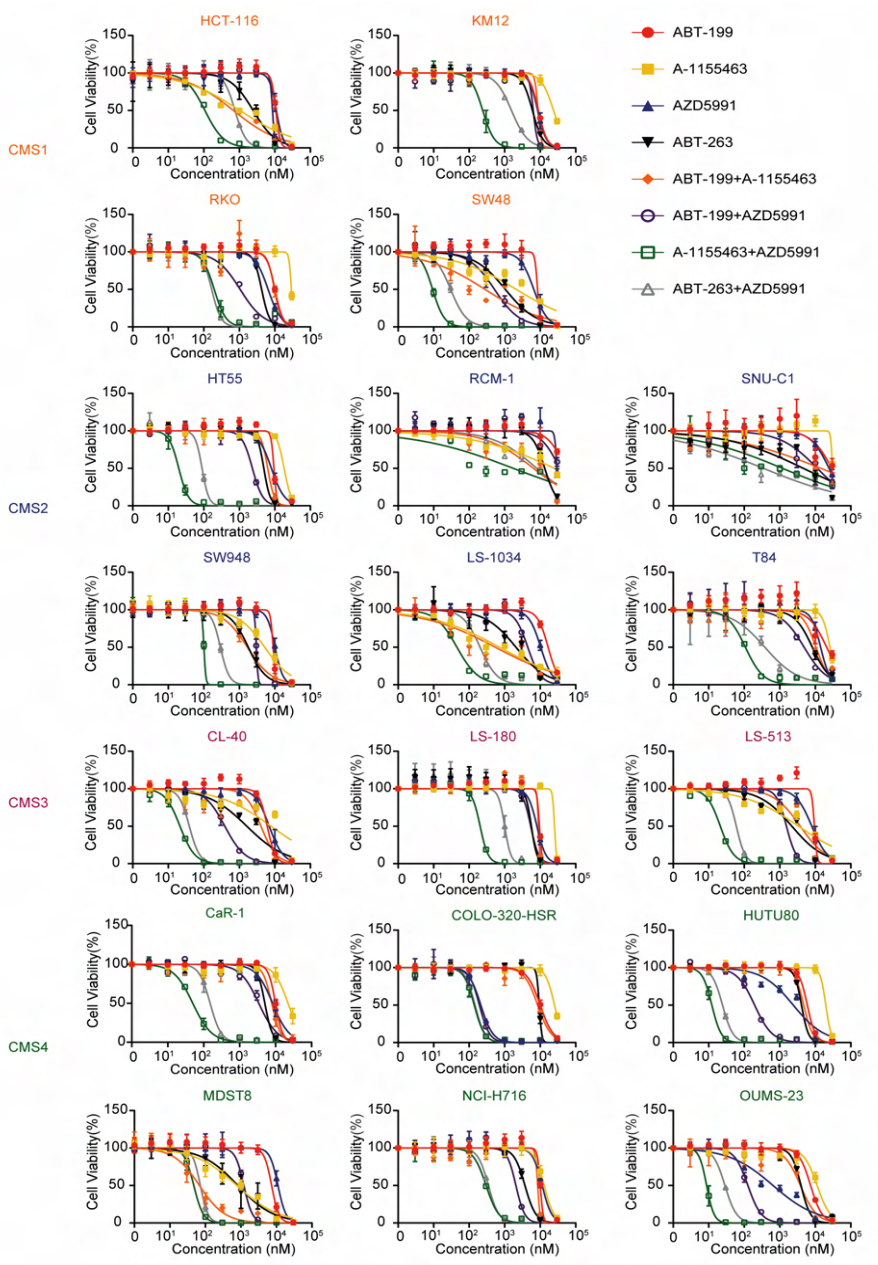

Supplementary Figure S1. Doses-Response curves of four BH3 mimetics and four combinations (1:1) in all CRC cell lines. Y axis indicates the relative cell viability normalized to untreated control.

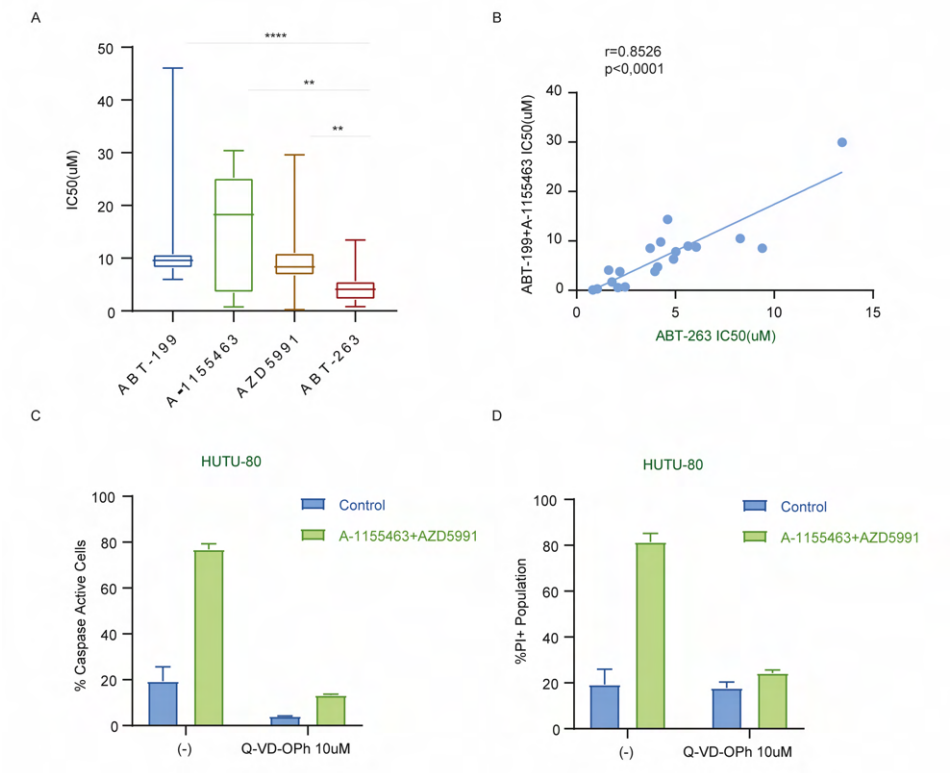

Supplementary Figure S2. (A)IC50 range of four BH3 mimetics in single treatment, ****:p<0,0001, **:0,005<p<0,01; (B) Correlation analysis between sensitivity to ABT-263 and combined ABT-199 and A-1155463 in the CRC cell line panel. Spearman's rank correlation was performed. Mann-Whitney test (two-tailed) was performed. (C) Flow cytometry of activation of caspase 3 induced by A-1155463+AZD5991 with or without 10uM Q-VD-OPh in HUTU-80; (D) Flow cytometry of PI incorporation induced by A-1155463+AZD5991 with or without 10uM Q-VD-OPh in HUTU-80.

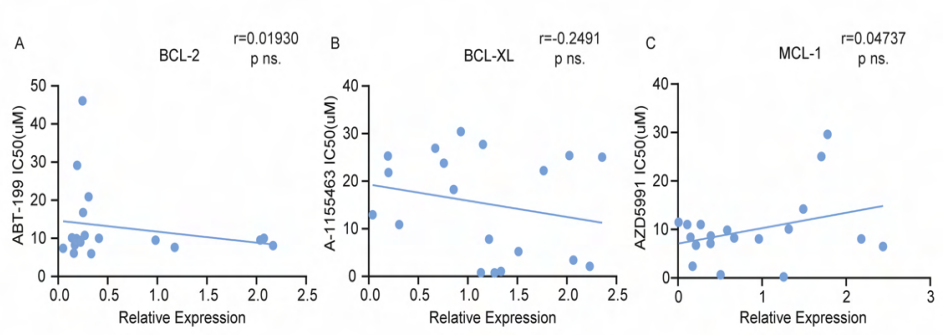

Supplementary Figure S3. Correlation between target expression and sensitivity. (A-C) Correlation between IC50 of ABT-199(A), A-1155463(B) and AZD5991(C) to relative expression of BCL-2(A), BCL-XL(B) and MCL-1(C). Relative expression is normalized to 2,2,2-TCE signal as described. Spearman's rank correlation was performed.

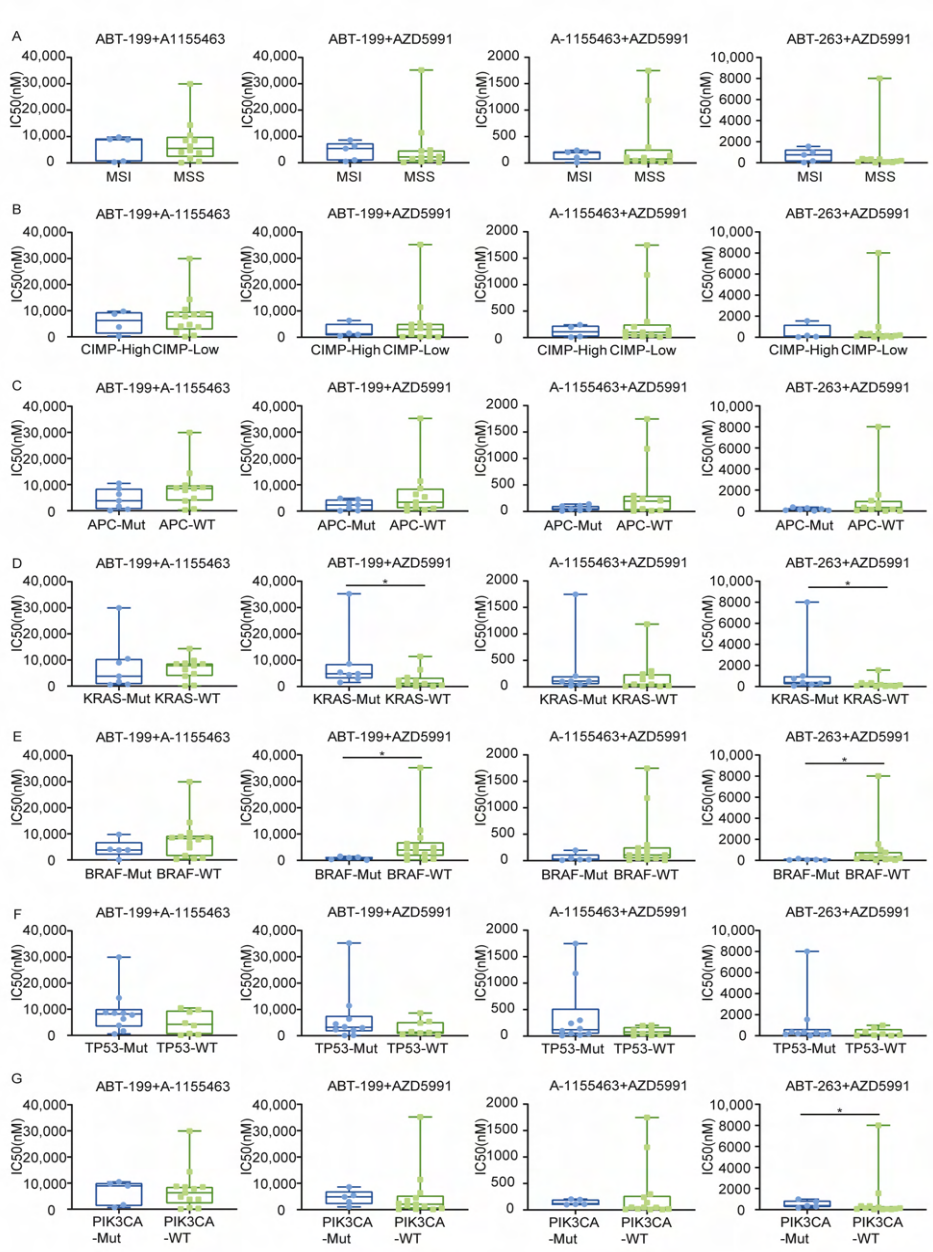

Supplementary Figure S4. Correlation analysis of IC50s of four combination (1:1) and molecular phenotypes in CRCs. (A) Microsatellite instability MSI, MSI microsatellite instable; MSS: microsatellite stable; (B) CpG Island Methylator Phenotype CIMP, CIMP-High: high CpG island Methylation; CIMP-Low: low CpG island Methylation; (C-G) Mutation: Mut: mutated; WT: wild type; *: p<0,05. Mann-Whitney (one-tailed) test was performed.

Chapter 6

Discussion

The gut is an essential point of contact with the outside environment, carrying out the important function of digestion, nutrient absorption and excretion of waste. It is therefore no surprise that this organ is highly dynamic and complex, with a rapid turnover rate and several cellular components playing a role in its tightly regulated function. The entire epithelial lining of the intestine renews itself in approximately every 4-5 days [1]. This remarkable turnover is facilitated by intestinal stem cells (ISCs) at the bottom of the crypt, with the potential to self-renew and give rise to progenitor cells that differentiate to maintain the entire epithelial lining. The interactions of these intestinal epithelial cells (IECs) with microenvironmental cues from immune cells, gut microbiota and stromal cells ultimately govern healthy intestinal function.

The rapid turnover in the colon helps prevent accumulation of damaged and potentially transformed epithelial cells, particularly considering the heightened exposure of IECs to environmental chemicals. Two essential cellular processes facilitate this turnover: proliferation and apoptosis. Cell growth at the bottom of the crypt and cell death at the top are regulated in a tight balance to ensure intestinal homeostasis, forming a conveyer belt for the epithelial cell life-cycle [2]. Tipping the balance of this controlled see-saw of life and death in favor of either leads to altered intestinal integrity. While altered proliferation and excessive cell death manifests in intestinal diseases such as inflammatory bowel disease (IBD), uncontrolled proliferation in combination with the evasion of apoptosis is a crucial step in colorectal cancer (CRC) initiation [3].

The BCL-2 family plays an integral role in apoptosis regulation and is frequently altered in CRC tumor cells to aid cell death evasion (**Chapter 1**) [4]. In this thesis, we dove in-depth into the function of three key anti-apoptotic members of this family, namely BCL-2, BCL-XL and MCL-1, in the context of CRC development, progression and therapy response. We believe that understanding the mechanisms by which cell death deregulation contributes to CRC carcinogenesis can provide insights to improve therapeutic management of the disease. Here we integrate the

findings of this thesis in light of current literature and highlight potential avenues for future research in this field.

Apoptosis in colorectal cancer progression

Our understanding of the complex molecular mechanisms underpinning cancer biology has been greatly facilitated by increasingly advanced model systems that recapitulate the multidimensional processes occurring in the human body. While 2D cell lines have been an integral asset in the field of molecular biology, they generally do not reflect the heterogeneous nature of tumors nor the complex tissue architecture. 3D culture systems such as spheroids and organoids derived from the mouse intestine and primary patient material address these pitfalls, as they can recapitulate different cell types found *in vivo* as well as their spatial organization and interactions [5, 6]. In **Chapter 2**, we established organoids from mouse intestinal crypts using specific culture conditions [7]. Mouse intestinal organoids present several advantages, requiring relatively limited culture reagents and reflecting specific genetic backgrounds derived from selective breeding, thereby serving as a relevant model for cancer formation in vitro. However, differences are observed in CRC tumorigenesis in the mouse and human intestine, the most striking of which being that mouse tumors mostly arise in the small intestine while human tumors are largely localized to the colon [8]. Human organoids however are more challenging to establish and maintain indefinitely, requiring a number of growth factors and inhibitors for extended propagation [6]. In **Chapter 3**, we used both mouse and human organoids in order to evaluate anti-apoptotic dependencies in CRC progression, thereby excluding any species differences in BH3 mimetic sensitivity.

Different pathways for CRC development have been described, of which the classical adenoma to carcinoma sequence is most frequently detected in patients. The dominant driver mutations of this pathway include inactivation of *APC*, activation of *KRAS* and inactivation of tumor suppressors *P53* and *SMAD4* [9]. The regulation of several members of the BCL-2 family interweaves with these progressing mutations and ultimately determines

the apoptotic threshold of these disease states. To gain insights into the varying apoptotic sensitivities through CRC progression, we made use of human organoids with CRISPR/Cas9 engineered mutations in the four common driver mutations [10]. Using techniques developed in **Chapter 2**, we dissected the role of anti-apoptotic proteins BCL-2, BCL-XL and MCL-1 in the context of increasing CRC mutation loads.

BCL-2 has previously been shown to play a critical role in intestinal tumorigenesis, where stem cell specific *Bcl2* deletion resulted in reduced adenoma outgrowth upon transformation in the mouse intestine [11] . Elevated NF-kB activity in ISCs drives transformation by upregulating its target BCL-2, thus potentially alleviating cellular stress associated with Apc mutations [11]. However, in **Chapter 3** we find that stem cell specific BCL-2 expression is decreased following transformation, while NF-kB activity is known to continue regulating tumor progression in CRC [12]. Indeed, most studies have shown that BCL-2 expression is decreased in CRC tumor lesions compared to normal and adenoma samples [13-15]. Earlier studies assessing BCL-2 expression changes from normal to adenoma stage based on immunohistochemistry were inconclusive, potentially due to technical difficulties of accurately accessing expression levels specifically in the cancer stem cell population (**Chapter 1**). In **Chapter 3**, we conclusively establish BCL-2 expression level changes in CRC progression at the RNA and protein level, particularly also in the stem cell compartment. Apc loss driven transformation results in a decrease in stem cell BCL-2 levels, which is reflected in expression datasets of normal colon and adenoma samples. We find that this rapid reduction in BCL-2 expression is a consequence of Wnt pathway driven upregulation of miR-17-5p, which targets BCL-2 for degradation[16]. MiR-17 is part of the oncogenic miR17-92 family (oncomir-1) and is known to be progressively upregulated in CRC from adenoma to carcinoma stages [17]. Intriguingly, miR17HG (the host gene for miR-17-92 cluster) is a transcriptional target of the NF-kB heterodimer RELA and moreover, reciprocally upregulates RELA expression levels by sponging its negative regulator miR-375 [17]. Thus, miR17HG promotes CRC tumorigenesis and metastasis by forming a positive feedback loop

with the NF-kB signaling pathway [17]. Upregulation of oncogenic miR17HG contributes to tumor progression and concomitantly results in degradation of BCL-2 [18]. This could explain why despite high NF-kB activity in CRC progression, expression of its target BCL-2 is still decreased. We propose that this counterintuitive loss of an anti-apoptotic protein in the context of tumorigenesis is very likely an inadvertent consequence of miR17-5p upregulation, whose oncogenic potential far outweighs that of BCL-2. In agreement, decrease in BCL-2 levels does not affect tumor progression as BCL-XL takes over the role of anti-apoptotic gatekeeper.

A reciprocal increase in BCL-XL expression is observed in CRC progression as BCL-2 levels progressively decrease (**Chapter 3**) [15]. Increase in BCL-XL levels in CRC has previously been shown to result from a gain in chromosome 13, which is where the gene is located [19]. Chromosome 20 gain is an early event in CRC progression and indeed, this is confirmed by sc-karyoseq of our tubular adenomas where 3 out of 4 samples present with this alteration [20]. CRC driver mutations such as *KRAS, P53* and *SMAD4* do not significantly alter BCL-XL expression levels in human organoids. However, these mutations do affect sensitivity to BCL-XL inhibition, as increasing mutation loads result in reduced sensitivity to the BCL-XL specific BH3 mimetic A-1155463. We find that this is most likely a result of shifts in the apoptotic threshold caused by *P53* loss, a known regulator of pro-apoptotic molecules BAX, PUMA and NOXA [21]. A decrease in these pro-apoptotic proteins would generate a situation where more BCL-XL is available to sequester the BH3-mimetics effectively elevating the threshold for cell death induction. Nevertheless, we show that BCL-XL is crucial for progression through the adenoma-to-carcinoma stage as its inhibition impairs clonogenicity of adenoma and tumor-derived organoids, while sparing healthy colon organoids. On the other hand, BCL-2 inhibition with ABT-199 affects only transforming organoids and becomes dispensable thereafter, in line with the decrease in its expression following loss of *APC*. Shifts in anti-apoptotic reliance during cancer progression have previously been reported in lymphomas where BCL-XL is crucial for lymphoma development while BCL-2 is dispensable [22, 23]. In a p53 deficient model

of thymic lymphoma, BCL-XL becomes dispensable while MCL-1 plays a crucial role in apoptosis resistance [24].

In a recent study, Healy et al. have established an important role for MCL-1 in the normal colon [25]. While loss of both BCL-2 and BCL-XL is dispensable for colon homeostasis, IEC specific MCL-1 deletion in the mouse intestine induces aberrant apoptosis and completely disrupts colonic integrity [25]. This would suggest a strong sensitivity to MCL-1 inhibition in normal organoids, however, we observe that both mouse and human-derived healthy colon organoids are insensitive to MCL-1 targeting with BH3 mimetic AZD-5991 (**Chapter 3**). This suggests a disparity in the effect of deletion versus inhibition of MCL-1 in the colon. This could perhaps be due to the fact that short-term pharmacological MCL-1 inhibition might not be equivalent to irreversible knockout of the gene. It could also be that MCL-1 has additional roles that are relevant for maintaining colon homeostasis, which are not linked to its anti-apoptotic function and may only be evident upon genetic loss [26]. Interestingly, recent studies have highlighted an important role for MCL-1 in cell cycle entry and progression, which is not affected by BH3 mimetic inhibition [27, 28]. Indeed, MCL-1 binding with PCNA, an essential regulator of replication during S phase, does not require BH3-like interactions [27]. Furthermore, compared to BCL-2 and BCL-XL, MCL-1 is known to be heavily post-transcriptionally regulated through its unique amino terminus [29]. Such studies highlight that rather than being redundant regulators of apoptosis, controlled expression and post-transcriptional regulation of these proteins modulates their activity, localization, stability and interactions to ultimately determine their function across multiple contexts.

In the context of transformation, the role of MCL-1 is particularly interesting and unexpected, as Healy et al. identified a tumor suppressive function for the protein [25]. IEC specific deletion of MCL-1 ($Mcl1^{\Delta IEC}$) results in aberrant IEC apoptosis, which then drives ISCs towards a Wnt-dependent hyperproliferative state that results in spontaneous tumor formation. Tumors arising in $Mcl1^{\Delta IEC}$ mice are remarkably similar to human CRCs characterized

by active Wnt signaling. In support of this, they find that organoids derived from Mcl-1 deficient crypts can only be established with the added deletion of Apc and that $Apc^{\Delta IE}CMcl1^{\Delta IEC}$ derived organoids grow faster than $Apc^{\Delta IEC}$ organoids. This strongly suggests that MCL-1 has a direct role in regulating ISC proliferation in the presence of constitutive Wnt signaling. In Chapter 3, we find that the anti-apoptotic contribution of MCL-1 during transformation is minimal as its inhibition with AZD-5991 does not affect organoid clonogenicity in any way. Considering the observations of Healy et al, inhibition of MCL-1 should support tumor formation rather than deter it. However, we do not observe any increase in organoid outgrowth following MCL-1 inhibition during concomitant *Apc* loss. This discrepancy could be due to the above discussed differences between inhibition and deletion of the protein, suggesting a unique tumor suppressive role for MCL-1 in regulating ISC proliferation that is separate from its anti-apoptotic functions. Interestingly, we find that protein levels of MCL-1 are decreased in APC^{KO} human organoids in comparison to their wildtype counterpart, suggesting an active Wnt-driven MCL-1 repression mechanism that could ultimately support tumorigenesis. How transformation results in MCL-1 downregulation is unclear and warrants further exploration, particularly considering the implications for early stages of cancer development. Interestingly, miR-17-5p has binding sites on the MCL-1 3'UTR and has been shown to directly target the protein for degradation in macrophages [30]. Whether or not this is also the case in colon adenomas would require further experimentation and could have interesting implications.

Transformation driven by *APC* loss does not alter BCL-XL expression levels but results in decreased levels of both BCL-2 and MCL-1. Thus, it would seem that it is the loss of two important gatekeepers of apoptosis, coupled with chromosome 20 gain, that drives the strong dependence on BCL-XL observed in colon adenomas and carcinomas. This increased dependency puts cancer cells in a precarious position where they require this anti-apoptotic block to hold for their survival, thereby providing a therapeutic window of opportunity. Importantly, normal colon cells are insensitive to BCL-XL inhibition while transformation induces a strong dependence on the

protein. Understanding the regulation and role of anti-apoptotic proteins in the context of CRC transformation and progression thus provides an informed basis for employing therapeutic strategies that target the BCL-2 family regulated apoptotic pathway.

Targeting apoptosis for colorectal cancer therapy

The ISC population is critical for preserving intestinal homeostasis and is considered to be the initiating cell type for CRC [31]. Mutations that give ISCs a competitive advantage, such as the loss of *APC*, results in an increased likelihood of clonal fixation and driving malignant transformation [32, 33]. In the case of an *APC* mutation, it would be expected that all CRC cells arising from an *APC* deficient clone should present with similar levels of Wnt activity. However, a heterogeneous distribution of Wnt activity is observed in CRC spheroids with Wnt activity reflecting the clonogenic potential of CRC cells [34, 35]. Wnt-high cells present with a cancer stem cell (CSC) phenotype, with increased clonogenicity and expression of stem cell markers in comparison to their Wnt-low counterparts, in the same culture conditions [34]. Importantly, a difference in chemosensitivity is observed between these two populations, with Wnt-high CSCs being more resistance to most conventional chemotherapies given to CRC patients [36]. CSC chemoresistance arises from a decreased apoptotic threshold, where high BCL-XL activity is mainly responsible for therapy refractoriness and inhibition with WEHI-539 induces chemosensitivity [36].

In **Chapter 3**, we show that this anti-apoptotic dependence on BCL-XL is already established during transformation and persists throughout CRC progression. While CRC derived CSCs are completely insensitive to BCL-2 inhibition with ABT-199, we find that transforming stem cells do depend on BCL-2 for adenoma outgrowth [11, 36]. This would suggest that inhibition of both BCL-2 and BCL-XL could prove effective as a chemo-preventative for FAP patients, who are highly susceptible to *Apc*-driven CRC development. Indeed, van der Heijden et al. have shown that treatment of *Lgr5.Apc*$^{fl/fl}$ mice with ABT-199 during transformation (intraperitoneal tamoxifen injection) severely diminished adenoma outgrowth [11]. Surprisingly, in

our *Villin*Cre^{ER}*Apc*$^{fl/fl}$ mouse model, where transformation was induced with a single bolus of tamoxifen injected specifically in the colon, ABT-199 treatment during transformation did not affect adenoma outgrowth. *In vitro*, we do not observe a difference in ABT-199 sensitivity between mouse small intestine (SI) and colon derived organoids, so this does not explain the remarkably different outcomes between these two *in vivo* experiments. As treatment dosing and timing were similar, the most likely explanation for this difference could be drug pharmacokinetics. ABT-199, which is orally bioavailable, most likely reaches high concentrations in the SI, where it is absorbed and then, due to the first pass effect, no longer reaches the colon in effective amounts. This emphasizes the importance of assessing drug efficacy in colon-specific pre-clinical models before translation to clinical studies for CRC. Moreover, this finding also highlights the potential of inhibitors that might be considered irrelevant in most clinical settings due to their low oral bioavailability, but could prove particularly useful in CRC treatment.

In the same intracolonic *in vivo* experiment, we found that BCL-XL inhibition with the less orally bioavailable A-1155463 proved extremely effective in impairing adenoma outgrowth when administered during transformation. However, it would be more important to assess if the inhibitor is also effective in impairing the growth of established adenomas, when given as a treatment after tamoxifen induction. Intriguingly, in this setting, A-1155463 treatment no longer deterred the growth of colonic adenomas. The first pass effect can be ruled out considering the potent efficacy of A-1155463 when administered along with tamoxifen-induced transformation. More likely, this suggests a potential resistance mechanism that is evident in the transformed epithelium that deters efficacy of BCL-XL inhibition in this setting.

Our findings in **Chapter 4** could provide a potential explanation for this observation. Here, in an attempt to find synergistic combinations with low-dose BCL-XL inhibition that could circumvent platelet toxicity, we identified a rescue response that is induced upon BCL-XL inhibition in

the form of MCL-1 upregulation. Increase in anti-apoptotic BCL-2 family proteins is frequently observed as a mechanism of apoptotic resistance [37]. Importantly, apoptosis induction is not a prerequisite for the observed increase in MCL-1 protein levels, as it is observed with very low doses of A-1155463 and also in cells devoid of all pro-apoptotic BH3-only proteins (HCT116 OctaKO). The rapid induction of this resistance mechanism suggests that BCL-XL targeting on its own might not be effective in CRC, as evidenced by our *in vivo* therapeutic experiment in chapter 3. Combination strategies that keep this response in check would therefore be more effective for clinical application. We find that inhibition of FGFR4 prevents this rescue response and is therefore highly synergistic with A-1155463 treatment in patient-derived tumor organoids and *in vivo*, while sparing platelets. Along with FGFR4 activation, A-1155463 treatment also mediates a rapid phosphorylation of ERK, a known downstream effector of FGFR signaling. MCL-1-PEST domain phosphorylation by ERK is known to limit MCL-1 degradation and therefore could be a mechanism by which FGFR4 signaling induces MCL-1 protein levels [38]. In line with this, inhibition of ERK with Trametinib also prevents MCL-1 upregulation upon A-1155463 treatment.

BCL-XL inhibition combined with direct MCL-1 inhibition is also highly synergistic, as further evidenced by our findings in **Chapter 5** where the combination is highly effective in inducing apoptosis across a panel of 18 CRC cell lines, irrespective of their CMS subtype [39]. Our findings are confirmed by another recent study that screened BH3 mimetics on CRC cell lines, where again the combination of BCL-XL and MCL-1 inhibition proved most potent [40]. The synergy of this combination might not be limited to CRC, as reports suggest potent efficacy in melanoma, lung and cervical cancer [41-43]. Interestingly, BCL-XL targeting is far more potent in combination with direct MCL-1 inhibition than with FGFR4 inhibition, which in principle should also result in MCL-1 downregulation. This might be because MCL-1 de-stabilization resulting from FGFR4 inhibition might not be as potent as direct blocking of MCL-1's BH3 groove, which could prove far more effective in inducing apoptosis. Moreover, while the MCL-

1 inhibitor inhibits all expressed protein, FGFR4 inhibition only prevents induction of additional MCL-1, leaving the basal levels unmodified. However, considering the important role of MCL-1 in colon homeostasis and as a potential tumor suppressor, the effects of its inhibition warrants thorough exploration in relevant pre-clinical models to rule out the potential of inducing detrimental side-effects.

In addition to FGFR4, the drug screen also identified several other novel hits that synergized with BCL-XL inhibition (**Chapter 4**). The most potent hit was Manidipine, a calcium channel blocker that is clinically approved as an anti-hypertensive agent [44]. No cancer specific applications of manidipine have been reported so far, however ongoing work in our lab suggests strong efficacy of this compound in combination with A-1155463 in targeting CRC spheroid and organoid cultures for cell death, particularly also the stem cell compartment. Preliminary data indicates that the mechanism behind this synergy has little to do with the calcium channel regulation, but rather involves a completely novel effect on the lipid composition profile of targeted cells. Specifically, manidipine treatment alters sphingolipid metabolism, which ultimately impairs mitochondrial oxidative phosphorylation and thereby sensitizes to BCL-XL inhibition. Another highly synergistic target identified in the screen was GSK3, a protein with multifaceted roles in cancer. Inhibition of GSK3 has been shown to induce and inhibit apoptosis in a context-dependent manner, therefore understanding the exact mechanism behind this synergy would be important [45]. Intriguingly, GSK3 inhibition also results in potent Wnt pathway activation, which would lead to an enrichment of the CSC population. The observed synergy likely results from non-Wnt related effects of GSK3 inhibition, particularly considering a recent report that identified Wnt inhibition to be highly synergistic with BCL-XL targeting in KRAS-mutant CRC [46]. Interestingly, Wnt inhibition was shown to result in transcriptional repression of MCL-1 expression, which ultimately contributed to the observed synergy with BCL-XL inhibition [46].

All three TKIs targeting the VEGFR, PDGFR, FGFR and c-kit family identified

as hits from the drug screen in **Chapter 4** downregulate MCL-1 protein levels, suggesting that this could be a common mechanism for synergy with BCL-XL inhibition. Whether the synergy observed with other screen hits, such as aurora kinase, also results from blocking MCL-1 activity would be interesting to evaluate, as it would suggest that overriding BH3 mimetic treatment induced MCL-1 dependence is a crucial determinant for effective cancer cell death induction. A role for MCL-1 in therapy resistance is well documented, in response to treatment with BH3 mimetics targeting BCL-2/BCL-XL [47, 48], oncogene targeted therapies [49, 50] and chemotherapy [51, 52]. In a recent study, Montero et al have elegantly demonstrated a crucial role for MCL-1 in resistance to targeted therapies across a panel of 21 cancer cell lines driven by oncogenes such as BRAF, EGFR, MET and HER2 [49]. Here, siRNA mediated suppression of MCL-1 enhanced the efficacy of their cognate targeted therapies more so than any other BCL-2 family member, irrespective of tumor lineage, driver oncogene or targeted therapy. Mechanistically this MCL-1 dependence is mediated differently, as therapy-driven priming of MCL-1 was induced by destabilization of NOXA mRNA, the endogenous inhibitor of MCL-1 [49]. This frees up MCL-1 to bind and inhibit pro-apoptotic BIM, which can be overcome with MCL-1 specific inhibitor S63845 that shows potent synergy with targeted therapies. Altogether, such studies highlight the importance of mapping lineage specific BCL-2 family dependencies to select the appropriate BH3 mimetic to employ alongside targeted therapies to improve their efficacy. Furthermore, such an understanding provides valuable approaches to identify and target vulnerabilities in tumors cells that resist primary therapeutic interventions.

In **Chapter 5**, we performed a comprehensive analysis of anti-apoptotic protein expression and sensitivities in relation to molecular features in a subtyped panel of CRC cell lines [39, 53]. Importantly, we found that expression levels of individual anti-apoptotic proteins did not correlate with sensitivity to inhibitors targeting them. Considering that apoptosis is regulated by a balanced interaction between several players, it is likely that sensitivity to specific BH3-mimetics is determined by the expression, activity

and interactions of other pro-apoptotic factors as well, such as BH3-only proteins and BAX/BAK [54-56]. However, in contrast to our findings, a study mapping BH3 mimetic dependencies in cancer cells identified that BCL-2 expression level correlates with sensitivity to ABT-199, while EMT status predicts dependence on BCL-XL and MCL-1 co-inhibition [57]. Interestingly, we did not observe significant difference in sensitivity to this combination between CMS2 and CMS4 cell lines, where the latter presents with a high EMT signature [58]. When analyzing subtype specific dependencies, we found that CMS2 lines were more resistant to BCL-2 and MCL-1 targeting inhibitors. This is likely due to differences in *KRAS* mutation status, as all CMS4 lines tested were wild-type for *KRAS* while the majority of CMS2 lines were mutant (4/6). Indeed, *KRAS* mutant organoids have been shown to be particularly unresponsive to MCL-1 targeting inhibitors alone but were highly sensitized to MCL-1 inhibition in combination with Mek inhibitors [56]. Furthermore, *KRAS* mutations are associated with higher expression of BCL-XL [59], which is indeed observed in our CMS2 lines. This could contribute to increased resistance to MCL-1 targeting, as suggested by Soderquist et al [57]. CMS4 tumors have been shown to be more resistant to chemotherapy in comparison to CMS2 tumors, yet we find that the latter presents with a higher apoptotic threshold in general [53]. This apparent incongruity requires further exploration but could indicate that sensitivity of CRC lines to chemotherapy might not necessarily be predicted by mitochondrial priming levels alone. Nonetheless, we find that BCL-XL inhibition synergizes with Oxaliplatin treatment in primary patient-derived FAP and CRC tumor organoids representing the classical CMS2 subtype (**Chapter 3**). Whether serrated adenomas and CMS4 tumor organoids can be similarly sensitized to chemotherapy in combination with BH3 mimetics remains to be assessed and would provide a relevant therapeutic strategy to target these chemoresistant tumors.

While CSCs play an important role in CRC tumor growth and chemoresistance, evidence suggests that stemness itself is a dynamic property that can be installed by microenvironmental signals [60, 61]. Myofibroblast-derived factors can restore CSC phenotype in differentiated cells and induce

chemoresistance, by upregulation of BCL-XL [34, 62]. Recent studies have highlighted an important role for tumor stroma in CRC growth dynamics with clonal CRC cells mostly residing on the outer edge of the tumor, where stromal interaction dictates CSC functionality [61]. Furthermore, high stromal infiltration is associated with poor patient outcomes [63]. CMS4 tumors contain a high abundance of tumor-associated fibroblasts and also present with increased chemoresistance, suggesting a pivotal role for the tumor microenvironment in CRC therapy resistance. Effective CRC therapies therefore need to tackle both tumor-specific vulnerabilities and microenvironmental signals that can fuel tumor re-growth and resistance. In chapter 4, we identified one such signal that induces rapid resistance to BH3 mimetics, which arises not from the microenvironment but rather, from dying tumor cells themselves.

Conversations with the dead: Apoptotic signaling

"If a cell dies in the forest of a body, does it make a sound?"

This is one of the riddles posed by Doug Green in his recent perspective of topics that could guide the next decade of cell death research [64]. Scientists are discovering that a dead cell indeed has an afterlife, with the larger organism paying close attention to the loss of individual cells and their parting message. Apoptosis results in the release of various factors, which in addition to affecting the immune system, profoundly influence the direct neighborhood of dying cells to activate cellular processes such as migration, proliferation, survival and differentiation [65]. A recent study identified several metabolites enriched in the supernatant of apoptotic cells, which varied depending on the cell type and mode of inducing apoptosis [66]. Conserved metabolites secreted by different cell types included ATP, GMP, Creatine, and AMP, which were interestingly also shown to be secreted by HCT116 cells treated with BH3 mimetic ABT-737 in a validation experiment [66]. These metabolites were shown to induce an anti-inflammatory response in phagocytes, which could be harnessed to reduce disease severity in mouse models of inflammatory arthritis [66]. In addition to immunomodulatory and anti-inflammatory effects, apoptotic secretion of growth promoting factors such as VEGF and HGF has been

documented [67-69]. Production of growth factors by apoptotic cells ensures cell replacement through "compensatory" proliferation, which has been demonstrated in flies and mammals [70, 71].

The homeostatic properties of apoptosis, essential for tissue repair and regeneration following damage, have been shown to be hijacked by cancer cells as a mechanism for malignant disease development and progression [70, 72]. Evidence that irradiated tumor cells can promote tumorigenesis has long been shown [73]. Several factors secreted by apoptotic cells upon cytotoxic therapy, including signaling molecules, cytosolic contents and extracellular vesicles (EVs), are implicated in modulating the tumor microenvironment to promote proliferation, metastasis and chemoresistance [reviewed in [72]]. The eicosanoid, PGE2, is secreted in a caspase-3 dependent manner by dying tumor cells and promotes tumor repopulation following irradiation and chemoresistance [74, 75]. Inosine is also shown to be released by dying tumor cells and promote neighboring cell proliferation via adenosine receptors [76]. EVs released from Cisplatin treated ovarian cancer cells can induce invasiveness and chemoresistance in bystander cells [77]. The paradoxical efforts of anti-tumor therapy aimed at inducing cell death that then results in such compensatory tumor promoting signaling highlights the importance of continued research in this field to effectively prevent or curb such responses.

In **Chapter 4**, we identified a transferable signal that is released into the supernatant by cells treated with low-dose BH3 mimetics and rapidly induces resistance in untreated receiver CRC cells. We identified FGF2 as the secreted growth factor that drives this response, most likely through the activation of FGFR4-ERK signaling which leads to stabilization of MCL-1. FGF2 has been implicated in tissue regeneration response, where is it secreted upon irradiation and provides survival benefit for epithelial cells [78, 79]. This indeed suggests that a physiological tissue repair response is taken advantage of by cancer cells for survival. Importantly, our findings are supported by a parallel study performed by Bock et al, who also reveal a similar FGF2-driven BH3 mimetic resistance mechanism [80].

Using HeLa tBID2A cells that stably express tBID together with BCL-2, they show that treatment with BH3 mimetics targeting BCL-2 (ABT-199) strongly and rapidly induces both BCL-2 and MCL-1 expression, which therefore results in resistance to re-treatment with BCL-2 and MCL-1 targeting mimetics. Interestingly, in their model, FGFR1 and 3 were the key receptors transmitting the FGF2 mediated resistance signal, while FGFR2 and 4 were dispensable. This would suggest that FGF receptors could act interchangeably in relaying this signal, particularly considering that FGF2 is known to bind effectively to all four receptors [81]. Indeed in CRC, where FGFR4 is often overexpressed [82], it might simply be the most abundant receptor present for FGF2 binding, thus suggesting a context-specific receptor dependence for this resistance mechanism.

We find that knockdown of FGF2 blocks the induction of MCL-1 following BH3 mimetic treatment (Chapter 4). It is likely that other FGFs, or even other growth factors, could induce this resistance mechanism in different tissue or treatment-dependent contexts. How inhibition of BCL-XL translates to the release of FGF2 remains to be established, particularly considering that the release occurs irrespective of apoptosis induction and in the absence of BH3-only proteins. This suggests that priming of CRC cells, even with low-doses of BH3 mimetics, sends a stress signal that translates to FGF2 release. Secretion of FGF2 occurs in an unconventional manner by its direct translocation across the plasma membrane, where three key actors interact with FGF2: ATP1A1, Tec kinase and the membrane lipid phosphatidylinositol-4,5-bisphosphate [PI(4,5)P2] [83]. Whether blocking this process, with for example Tec kinase inhibitors/knockdown, could also impair the rescue response and sensitize to BCL-XL inhibition remains to be explored. Ongoing work using an FGF2 reporter based system in a kinase CRISPR screen will likely provide insights into the signaling pathways mediating this release.

The transient nature of the FGF2-driven response supports the concept of plasticity in tumor cell resistance. This could lead to the persistence of cells that no longer depend on the drug-targeted pathway and give

rise to resistant tumors [84]. Treatment discontinuation, however, could restore sensitivity by abolishing the transient signal. Intermittent treatment strategies that could indeed avoid prolonged activation of resistance pathways might be an effective means of counteracting this response. However, our findings stress the importance of identifying and targeting such therapy induced pro-tumorigenic responses to ensure effective eradication of resistant cancer cells. Altogether, targeting apoptosis in CRC remains a relevant and potent therapeutic strategy but requires thorough understanding of its implications for residual cells in vivo. Given the preliminary mechanistic insights regarding the oncogenic consequences of apoptosis, future investigation in this area holds much promise for advancing the effective implementation of BH3 mimetics in clinical CRC management.

References

1. van der Flier, L.G. and H. Clevers, Stem cells, self-renewal, and differentiation in the intestinal epithelium. Annu Rev Physiol, 2009. 71: p. 241-60.
2. Clevers, H., The intestinal crypt, a prototype stem cell compartment. Cell, 2013. 154(2): p. 274-84.
3. Ramachandran, A., M. Madesh, and K.A. Balasubramanian, Apoptosis in the intestinal epithelium: its relevance in normal and pathophysiological conditions. J Gastroenterol Hepatol, 2000. 15(2): p. 109-20.
4. Ramesh, P. and J.P. Medema, BCL-2 family deregulation in colorectal cancer: potential for BH3 mimetics in therapy. Apoptosis, 2020. 25(5-6): p. 305-320.
5. Sato, T., et al., Single Lgr5 stem cells build crypt-villus structures in vitro without a mesenchymal niche. Nature, 2009. 459(7244): p. 262-5.
6. Sato, T., et al., Long-term expansion of epithelial organoids from human colon, adenoma, adenocarcinoma, and Barrett's epithelium. Gastroenterology, 2011. 141(5): p. 1762-72.
7. Ramesh, P., et al., Isolation, Propagation, and Clonogenicity of Intestinal Stem Cells. Methods Mol Biol, 2019. 2002: p. 61-73.
8. Jackstadt, R. and O.J. Sansom, Mouse models of intestinal cancer. J Pathol, 2016. 238(2): p. 141-51.
9. Fearon, E.R. and B. Vogelstein, A genetic model for colorectal tumorigenesis. Cell, 1990. 61(5): p. 759-67.
10. Drost, J., et al., Sequential cancer mutations in cultured human intestinal stem cells. Nature, 2015. 521(7550): p. 43-7.
11. van der Heijden, M., et al., Bcl-2 is a critical mediator of intestinal transformation. Nat

Commun, 2016. 7: p. 10916.
12. Ramesh, P., et al., BCL-XL is crucial for progression through the adenoma-to-carcinoma sequence of colorectal cancer. Cell Death & Differentiation, 2021.
13. Flohil, C.C., P.A. Janssen, and F.T. Bosman, Expression of Bcl-2 protein in hyperplastic polyps, adenomas, and carcinomas of the colon. J Pathol, 1996. 178(4): p. 393-7.
14. Kaklamanis, L., et al., Early expression of bcl-2 protein in the adenoma-carcinoma sequence of colorectal neoplasia. J Pathol, 1996. 179(1): p. 10-4.
15. Krajewska, M., et al., Elevated expression of Bcl-X and reduced Bak in primary colorectal adenocarcinomas. Cancer Res, 1996. 56(10): p. 2422-7.
16. Li, Y., et al., Adenomatous polyposis coli (APC) regulates miR17-92 cluster through ?-catenin pathway in colorectal cancer. Oncogene, 2016. 35(35): p. 4558-4568.
17. Xu, J., et al., Long Noncoding RNA MIR17HG Promotes Colorectal Cancer Progression via miR-17-5p. Cancer Res, 2019. 79(19): p. 4882-4895.
18. Scherr, M., et al., Differential expression of miR-17~92 identifies BCL2 as a therapeutic target in BCR-ABL-positive B-lineage acute lymphoblastic leukemia. Leukemia, 2014. 28(3): p. 554-65.
19. Sillars-Hardebol, A.H., et al., BCL2L1 has a functional role in colorectal cancer and its protein expression is associated with chromosome 20q gain. J Pathol, 2012. 226(3): p. 442-50.
20. Tabach, Y., et al., Amplification of the 20q chromosomal arm occurs early in tumorigenic transformation and may initiate cancer. PLoS One, 2011. 6(1): p. e14632.
21. Aubrey, B.J., et al., How does p53 induce apoptosis and how does this relate to p53-mediated tumour suppression? Cell Death Differ, 2018. 25(1): p. 104-113.
22. Kelly, P.N., et al., Endogenous Bcl-xL is essential for Myc-driven lymphomagenesis in mice. Blood, 2011. 118(24): p. 6380-6.
23. Kelly, P.N., et al., Endogenous bcl-2 is not required for the development of Emu-myc-induced B-cell lymphoma. Blood, 2007. 109(11): p. 4907-13.
24. Grabow, S., et al., MCL-1 but not BCL-XL is critical for the development and sustained expansion of thymic lymphoma in p53-deficient mice. Blood, 2014. 124(26): p. 3939-46.
25. Healy, M.E., et al., MCL1 Is Required for Maintenance of Intestinal Homeostasis and Prevention of Carcinogenesis in Mice. Gastroenterology, 2020. 159(1): p. 183-199.
26. Widden, H. and W.J. Placzek, The multiple mechanisms of MCL1 in the regulation of cell fate. Commun Biol, 2021. 4(1): p. 1029.
27. Fujise, K., et al., Regulation of apoptosis and cell cycle progression by MCL1. Differential role of proliferating cell nuclear antigen. J Biol Chem, 2000. 275(50): p. 39458-65.
28. Streletskaia, A.Y., et al., Upregulation of Mcl-1S Causes Cell-Cycle Perturbations and DNA Damage Accumulation. Front Cell Dev Biol, 2020. 8: p. 543066.
29. Germain, M. and V. Duronio, The N terminus of the anti-apoptotic BCL-2 homologue MCL-1 regulates its localization and function. J Biol Chem, 2007. 282(44): p. 32233-42.
30. Kumar, R., et al., MicroRNA 17-5p regulates autophagy in Mycobacterium tuberculosis-infected macrophages by targeting Mcl-1 and STAT3. Cell Microbiol, 2016. 18(5): p. 679-91.
31. Barker, N., et al., Crypt stem cells as the cells-of-origin of intestinal cancer. Nature, 2009. 457(7229): p. 608-11.
32. Vermeulen, L., et al., Defining stem cell dynamics in models of intestinal tumor initiation.

Science, 2013. 342(6161): p. 995-8.
33. van Neerven, S.M., et al., Apc-mutant cells act as supercompetitors in intestinal tumour initiation. Nature, 2021. 594(7863): p. 436-441.
34. Vermeulen, L., et al., Wnt activity defines colon cancer stem cells and is regulated by the microenvironment. Nat Cell Biol, 2010. 12(5): p. 468-76.
35. Fodde, R. and T. Brabletz, Wnt/beta-catenin signaling in cancer stemness and malignant behavior. Curr Opin Cell Biol, 2007. 19(2): p. 150-8.
36. Colak, S., et al., Decreased mitochondrial priming determines chemoresistance of colon cancer stem cells. Cell Death Differ, 2014. 21(7): p. 1170-7.
37. Campbell, K.J. and S.W.G. Tait, Targeting BCL-2 regulated apoptosis in cancer. Open Biol, 2018. 8(5).
38. Domina, A.M., et al., MCL1 is phosphorylated in the PEST region and stabilized upon ERK activation in viable cells, and at additional sites with cytotoxic okadaic acid or taxol. Oncogene, 2004. 23(31): p. 5301-15.
39. Zhang, L., et al., BH3 Mimetic Sensitivity of Colorectal Cancer Cell Lines in Correlation with Molecular Features Identifies Predictors of Response. International Journal of Molecular Sciences, 2021. 22(8): p. 3811.
40. Luo, M.J., et al., Defining the susceptibility of colorectal cancers to BH3-mimetic compounds. Cell Death Dis, 2020. 11(9): p. 735.
41. Abdul Rahman, S.F., et al., Co-inhibition of BCL-XL and MCL-1 with selective BCL-2 family inhibitors enhances cytotoxicity of cervical cancer cell lines. Biochem Biophys Rep, 2020. 22: p. 100756.
42. Lee, E.F., et al., BCL-XL and MCL-1 are the key BCL-2 family proteins in melanoma cell survival. Cell Death Dis, 2019. 10(5): p. 342.
43. Tada, M., et al., MCL1 inhibition enhances the therapeutic effect of MEK inhibitors in KRAS-mutant lung adenocarcinoma cells. Lung Cancer, 2019. 133: p. 88-95.
44. McKeage, K. and L.J. Scott, Manidipine: a review of its use in the management of hypertension. Drugs, 2004. 64(17): p. 1923-40.
45. Chiara, F. and A. Rasola, GSK-3 and mitochondria in cancer cells. Front Oncol, 2013. 3: p. 16.
46. Jung, H.R., et al., CRISPR screens identify a novel combination treatment targeting BCL-X(L) and WNT signaling for KRAS/BRAF-mutated colorectal cancers. Oncogene, 2021. 40(18): p. 3287-3302.
47. Yecies, D., et al., Acquired resistance to ABT-737 in lymphoma cells that up-regulate MCL-1 and BFL-1. Blood, 2010. 115(16): p. 3304-13.
48. Coloff, J.L., et al., Akt-dependent glucose metabolism promotes Mcl-1 synthesis to maintain cell survival and resistance to Bcl-2 inhibition. Cancer Res, 2011. 71(15): p. 5204-13.
49. Montero, J., et al., Destabilization of NOXA mRNA as a common resistance mechanism to targeted therapies. Nat Commun, 2019. 10(1): p. 5157.
50. Tong, J., et al., Mcl-1 Degradation Is Required for Targeted Therapeutics to Eradicate Colon Cancer Cells. Cancer Res, 2017. 77(9): p. 2512-2521.
51. Akagi, H., et al., Suppression of myeloid cell leukemia-1 (Mcl-1) enhances chemotherapy-associated apoptosis in gastric cancer cells. Gastric Cancer, 2013. 16(1): p. 100-10.
52. Lee, K.M., et al., MYC and MCL1 Cooperatively Promote Chemotherapy-Resistant Breast Cancer Stem Cells via Regulation of Mitochondrial Oxidative Phosphorylation.

Cell Metab, 2017. 26(4): p. 633-647.e7.
53. Linnekamp, J.F., et al., Consensus molecular subtypes of colorectal cancer are recapitulated in in vitro and in vivo models. Cell Death Differ, 2018. 25(3): p. 616-633.
54. Smith, V.M., et al., Specific interactions of BCL-2 family proteins mediate sensitivity to BH3-mimetics in diffuse large B-cell lymphoma. Haematologica, 2020. 105(8): p. 2150-2163.
55. Touzeau, C., et al., BH3 profiling identifies heterogeneous dependency on Bcl-2 family members in multiple myeloma and predicts sensitivity to BH3 mimetics. Leukemia, 2016. 30(3): p. 761-4.
56. Nangia, V., et al., Exploiting MCL1 Dependency with Combination MEK + MCL1 Inhibitors Leads to Induction of Apoptosis and Tumor Regression in KRAS-Mutant Non-Small Cell Lung Cancer. Cancer Discov, 2018. 8(12): p. 1598-1613.
57. Soderquist, R.S., et al., Systematic mapping of BCL-2 gene dependencies in cancer reveals molecular determinants of BH3 mimetic sensitivity. Nat Commun, 2018. 9(1): p. 3513.
58. Guinney, J., et al., The consensus molecular subtypes of colorectal cancer. Nat Med, 2015. 21(11): p. 1350-6.
59. Zaanan, A., et al., The Mutant KRAS Gene Up-regulates BCL-XL Protein via STAT3 to Confer Apoptosis Resistance That Is Reversed by BIM Protein Induction and BCL-XL Antagonism. J Biol Chem, 2015. 290(39): p. 23838-49.
60. Todaro, M., et al., Colon cancer stem cells dictate tumor growth and resist cell death by production of interleukin-4. Cell Stem Cell, 2007. 1(4): p. 389-402.
61. Lenos, K.J., et al., Stem cell functionality is microenvironmentally defined during tumour expansion and therapy response in colon cancer. Nat Cell Biol, 2018. 20(10): p. 1193-1202.
62. Colak, S. and J.P. Medema, Human colonic fibroblasts regulate stemness and chemotherapy resistance of colon cancer stem cells. Cell Cycle, 2016. 15(12): p. 1531-7.
63. Calon, A., et al., Stromal gene expression defines poor-prognosis subtypes in colorectal cancer. Nat Genet, 2015. 47(4): p. 320-9.
64. Green, D.R., The Coming Decade of Cell Death Research: Five Riddles. Cell, 2019. 177(5): p. 1094-1107.
65. Gregory, C.D. and J.D. Pound, Cell death in the neighbourhood: direct microenvironmental effects of apoptosis in normal and neoplastic tissues. J Pathol, 2011. 223(2): p. 177-94.
66. Medina, C.B., et al., Metabolites released from apoptotic cells act as tissue messengers. Nature, 2020. 580(7801): p. 130-135.
67. Morimoto, K., et al., Alveolar macrophages that phagocytose apoptotic neutrophils produce hepatocyte growth factor during bacterial pneumonia in mice. Am J Respir Cell Mol Biol, 2001. 24(5): p. 608-15.
68. Golpon, H.A., et al., Life after corpse engulfment: phagocytosis of apoptotic cells leads to VEGF secretion and cell growth. Faseb j, 2004. 18(14): p. 1716-8.
69. Hristov, M., et al., Apoptotic bodies from endothelial cells enhance the number and initiate the differentiation of human endothelial progenitor cells in vitro. Blood, 2004. 104(9): p. 2761-6.
70. Fogarty, C.E. and A. Bergmann, Killers creating new life: caspases drive apoptosis-

induced proliferation in tissue repair and disease. Cell Death Differ, 2017. 24(8): p. 1390-1400.
71. Pérez-Garijo, A., E. Shlevkov, and G. Morata, The role of Dpp and Wg in compensatory proliferation and in the formation of hyperplastic overgrowths caused by apoptotic cells in the Drosophila wing disc. Development, 2009. 136(7): p. 1169-77.
72. Jiang, M.J., et al., Dark Side of Cytotoxic Therapy: Chemoradiation-Induced Cell Death and Tumor Repopulation. Trends Cancer, 2020. 6(5): p. 419-431.
73. Revesz, L., Effect of tumour cells killed by x-rays upon the growth of admixed viable cells. Nature, 1956. 178(4547): p. 1391-2.
74. Huang, Q., et al., Caspase 3-mediated stimulation of tumor cell repopulation during cancer radiotherapy. Nat Med, 2011. 17(7): p. 860-6.
75. Kurtova, A.V., et al., Blocking PGE2-induced tumour repopulation abrogates bladder cancer chemoresistance. Nature, 2015. 517(7533): p. 209-13.
76. Chen, J., et al., Inosine Released from Dying or Dead Cells Stimulates Cell Proliferation via Adenosine Receptors. Front Immunol, 2017. 8: p. 504.
77. Samuel, P., et al., Cisplatin induces the release of extracellular vesicles from ovarian cancer cells that can induce invasiveness and drug resistance in bystander cells. Philos Trans R Soc Lond B Biol Sci, 2018. 373(1737).
78. Houchen, C.W., et al., FGF-2 enhances intestinal stem cell survival and its expression is induced after radiation injury. Am J Physiol, 1999. 276(1): p. G249-58.
79. Nunes, Q.M., et al., Fibroblast growth factors as tissue repair and regeneration therapeutics. PeerJ, 2016. 4: p. e1535.
80. Bock, F.J., et al., Apoptosis-induced FGF signalling promotes non-cell autonomous resistance to cell death. bioRxiv, 2020: p. 2020.07.12.199430.
81. Ornitz, D.M. and N. Itoh, The Fibroblast Growth Factor signaling pathway. Wiley Interdiscip Rev Dev Biol, 2015. 4(3): p. 215-66.
82. Turkington, R.C., et al., Fibroblast growth factor receptor 4 (FGFR4): a targetable regulator of drug resistance in colorectal cancer. Cell Death Dis, 2014. 5(2): p. e1046.
83. Steringer, J.P. and W. Nickel, The molecular mechanism underlying unconventional secretion of Fibroblast Growth Factor 2 from tumour cells. Biol Cell, 2017. 109(11): p. 375-380.
84. Boumahdi, S. and F.J. de Sauvage, The great escape: tumour cell plasticity in resistance to targeted therapy. Nat Rev Drug Discov, 2020. 19(1): p. 39-56.

Addendum

Summary

Colorectal cancer (CRC) is the second leading cause of cancer related deaths with more than 1.9 million new cases diagnosed and nearly 1 million deaths reported in 2020. Survival rate at early localized stages of the disease is nearly 90%, however mortality can be largely attributed to metastasis of the disease to distant organs, particularly to the liver, upon which the 5-year survival rate drops to 14%. CRC treatment primarily involves surgical resection to remove the primary tumor. Depending on the stage of disease, adjuvant chemotherapy, potentially in combination with targeted therapy, is administered to provide improved therapeutic benefit. Chemotherapy is known to induce several detrimental side-effects due to non-specific targeting of healthy cells. Moreover, resistance to chemotherapy is frequently observed and contributes to disease relapse. The main goal of novel cancer therapeutics is to effectively and specifically induce tumor cell death, while on the other hand, cancer cells continuously evolve mechanisms to evade apoptosis.

In **Chapter 1**, we provide an in-depth overview of the intrinsic pathway of apoptosis and its key players, the BCL-2 family of proteins, whose interactions dictate the decision between life and death. This tightly regulated pathway is frequently deregulated to favor tumor cell survival, particularly also in CRC. Several members of the BCL-2 family play a critical role in regulating apoptosis in the normal colon and more so, in facilitating survival during intestinal transformation, progression and chemoresistance. Understanding the mechanisms behind the deregulation of this family in different stages of CRC could support the effective application of targeted inhibitors of this pathway for CRC therapy.

In **Chapter 2**, we develop some of the key model systems and assays used to assess anti-apoptotic dependencies in organoid models. We describe a detailed methodology for the isolation and propagation of crypts from the mouse intestine, both from the small intestine and colon. 3D culture in Matrigel requires adjustment of usual 2D culture protocols and assays for

assessing stem cell sensitivities. In this regard, we outline protocols that allow measurement of treatment-induced changes in clonogenicity and stem cell specific cell death, with a microscopic counting based protocol. Furthermore, we describe a immunohistochemistry protocol for paraffin embedding of organoids, which can facilitate analysis of treatment efficacy and changes in cellular states or compositions.

We exploit these models and techniques developed to dissect the role of anti-apoptotic proteins BCL-2, BCL-XL and MCL-1 in the context of increasing CRC mutation loads in **Chapter 3**. Based on previous work, we hypothesized that a shift in anti-apoptotic protein reliance occurs in intestinal stem cells (ISCs) as CRC progresses from normal to adenoma to carcinoma. Using both mouse and human derived organoid models of CRC progression, we targeted anti-apoptotic proteins with specific BH3 mimetics to reveal that BCL-2 is essential only during ISC transformation while MCL-1 inhibition on its own does not affect stem cell survival at any stage of the disease. We identified that the limited window of BCL-2 reliance is a result of its downregulation by miR-17-5p, a microRNA that is upregulated upon APC-mutation driven transformation. Importantly, we identified a critical and indispensable role for BCL-XL in CRC transformation and throughout progression. BCL-XL inhibition effectively impairs adenoma outgrowth in vivo and enhances chemotherapy efficacy in patient –derived tumor organoids. In line with this dependency, we show that high BCL-XL expression is associated with worse outcomes for chemotherapy-treated patients.

These findings indicate that targeting BCL-XL with specific BH3 mimetics would be highly effective for CRC treatment. However, their clinical use is limited due to thrombocytopenia, as BCL-XL is known to regulate platelet lifespan. In order to circumvent this toxicity and identify molecular mechanisms that enhance sensitivity to BH3 mimetics, we screened a broad range of inhibitors in combination with low-dose BCL-XL inhibition in **Chapter 4**. Herein, we find that FGFR4 inhibition strongly synergizes with BCL-XL targeting both in patient-derived tumor organoids and an in

vivo CRC model. Mechanistically, we identified a novel rescue response that is rapidly activated upon low-dose BH3 mimetic treatment, which ultimately results in FGFR4 meditated MCL-1 upregulation. Blocking this pathway, or directly inhibiting MCL-1, effectively synergizes with BCL-XL inhibition. Importantly, we find that this rescue response is transferable, as supernatant from BH3 mimetic treated cells results in MCL-1 upregulation when transferred to untreated cells. We identified FGF2 as the secreted ligand that communicates the danger signal upon apoptotic priming and initiates the rescue response by activating FGFR4. Blocking this response represents a relevant therapeutic strategy for ensuring BH3 mimetic efficacy in CRC.

In **Chapter 5**, we screened a panel of CRC cell lines with known molecular features and subtypes, to assess their sensitivity to BH3 mimetics targeting BCL-2, BCL-XL and MCL-1. Treatment with inhibitors alone and in combination revealed potent efficacy of MCL-1 and BCL-XL co-inhibition across all cell lines, regardless of subtype. Moreover, we find that expression levels of anti-apoptotic proteins do not predict sensitivity to their respective inhibitors. Analysis of correlation between molecular features and anti-apoptotic sensitivity identified KRAS mutant lines to be more resistant to MCL-1 inhibition. Subtype analysis identified an intriguing resistance of CMS2 lines to BCL-2 and MCL-1 targeting mimetics. Overall, our findings in this chapter provide an in-depth overview of BCL-2 family expression and dependencies in the context of several CRC molecular features and highlight the therapeutic efficacy of BCL-XL and MCL-1 inhibition.

In **Chapter 6**, we integrate the findings of this thesis in light of relevant publications and identify avenues for future research to unravel the consequences of targeting apoptosis in vivo and thereby enable the rational use of BH3 mimetics in CRC management.

Nederlandse Samenvatting

Colorectaal carcinoom oftewel darmkanker is de tweede belangrijkste oorzaak van kanker gerelateerde sterfgevallen met meer dan 1,9 miljoen nieuwe gevallen en ruim 1 miljoen doden in 2020. Het overlevingspercentage in vroege stadia van de ziekte is bijna 90%, maar de mortaliteit kan grotendeels worden toegeschreven aan metastase van de ziekte naar andere organen, met name naar de lever, waarna de 5-jaarsoverleving daalt naar 14%. Darmkankerbehandeling omvat voornamelijk chirurgische resectie om de primaire tumor te verwijderen. Afhankelijk van het stadium van de ziekte wordt adjuvante chemotherapie, mogelijk in combinatie met targeted therapie, toegediend om een groter therapeutisch voordeel te bieden. Van chemotherapie is bekend dat het verschillende nadelige bijwerkingen veroorzaakt als gevolg van het niet-specifiek aanvallen van gezonde cellen. Bovendien wordt vaak resistentie tegen chemotherapie waargenomen die bijdraagt aan terugval van de ziekte. Het belangrijkste doel van nieuwe kankertherapieën is het effectief en specifiek doden van tumorcellen, terwijl aan de andere kant kankercellen voortdurend mechanismen ontwikkelen om apoptose te omzeilen.

In **Hoofdstuk 1** geven we een gedetailleerd overzicht van de intrinsieke signalering van apoptose en de belangrijkste spelers, de BCL-2 familie van eiwitten, waarvan de onderlinge interacties de beslissing tussen leven en dood bepalen. Deze strak gereguleerde signalering wordt vaak ontwricht om de overleving van tumorcellen te bevorderen, met name in darmkanker. Verschillende leden van de BCL-2-familie spelen een cruciale rol bij het reguleren van apoptose in de normale dikke darm en meer nog bij het bevorderen van overleving tijdens het ontstaan van darmkanker en de progressie van de ziekte. Een beter begrip van de mechanismen die ten grondslag liggen aan de ontwrichting van de organisatie van deze familie in verschillende stadia van darmkanker zou de effectieve toepassing van gerichte remmers van deze eiwitten voor darmkankertherapie kunnen ondersteunen.

In **Hoofdstuk 2** beschrijven we de ontwikkeling van enkele van de belangrijkste modelsystemen en experimentele testen die worden gebruikt om anti-apoptotische afhankelijkheden in organoïde modellen te beoordelen. We beschrijven een gedetailleerde methode voor de isolatie en vermeerdering van crypten uit de darm van de muis, zowel uit de dunne darm als de dikke darm. 3D-kweek in Matrigel vereist aanpassing van de gebruikelijke 2D-kweekprotocollen en -assays voor het beoordelen van stamcelgevoeligheden. Hiervoor schetsen we protocollen die het mogelijk maken om door de behandeling geïnduceerde veranderingen in stamcel-specifieke celdood te meten met een protocol dat op telling middels microscopie gebaseerd isl. Verder beschrijven we een protocol voor immunohistochemie op organoïden in paraffine, wat de analyse van de werkzaamheid van de behandeling en veranderingen in cellulaire toestanden of samenstelling kan vergemakkelijken.

We gebruiken deze modellen en technieken die zijn ontwikkeld om de rol van de anti-apoptotische eiwitten BCL-2, BCL-XL en MCL-1 te bestuderen. Dit gebeurt in de context van darmkanker organoïden die steeds meer oncogene mutaties bevatten (**Hoofdstuk 3**). Op basis van eerder werk veronderstelden we dat een verschuiving in anti-apoptotische afhankelijkheid optreedt in darmstamcellen (ISC's) als darmkanker zich ontwikkelt van normaal naar adenoom naar carcinoom. Met behulp van organoïde modellen van darmkanker, afkomstig uit zowel muizen als patiënten, hebben we ons gericht op anti-apoptotische eiwitten met specifieke BH3-mimetica. Deze BH3-mimetica blokkeren selectief de functie van de anti-apoptotische BCL-2 familieleden. Met behulp van die mimetica hebben we onthuld dat BCL-2 alleen essentieel is tijdens de eerste stap in de vorming van kanker, terwijl MCL-1-remming de overleving van stamcellen niet beïnvloedt in welk stadium van de ziekte dan ook. We hebben vastgesteld dat het verlies van BCL-2-afhankelijkheid na de eerste stap een gevolg is van een regulatie door miR-17-5p, een microRNA dat wordt aangeschakeld nadat de eerste transformatie heeft plaatsgevonden na de mutatie in APC.. Door deze uitschakeling van BCL-2 ontstaat er een cruciale en onmisbare rol voor BCL-XL in darmkanker. BCL-XL-remming is

daarom een effectieve manier om de uitgroei van adenomen in muizen te verhinderen. Tevens verbetert het de werkzaamheid van chemotherapie bij van patiënten afkomstige tumororganoïden. In overeenstemming met deze afhankelijkheid laten we zien dat hoge BCL-XL-expressie in darmtumoren van patiënten geassocieerd is met slechtere resultaten van de chemotherapie in behandelde patiënten.

Deze bevindingen geven aan dat het blokkeren van de activiteit van BCL-XL met specifieke medicijnen (BH3-mimetica) zeer effectief zou kunnen zijn voor de behandeling van darmkanker. Het klinische gebruik van deze medicijnen wordt echter beperkt vanwege de bijwerkingen op bloedplaatjes (trombocytopenie), aangezien bekend is dat BCL-XL ook de levensduur van bloedplaatjes bepaalt. Om deze toxiciteit te omzeilen en moleculaire mechanismen te identificeren die de gevoeligheid voor BH3-mimetica verhogen, hebben we in **Hoofdstuk 4** een breed scala aan remmers gescreend in combinatie met een lage dosis BCL-XL-remming. Hier vonden we dat FGFR4-remming sterke synergie vertoont met de remming van BCL-XL zowel in van de patiënt afgeleide tumor-organoïden als in een in vivo darmkanker-model. Verdere studies leverden inzichten in een verassend resistentiemechanisme dat snel na de toevoeging van de BH3-mimetica wordt aangezet .. Deze behandeling resulteert uiteindelijk in een stimulatie van de FGFR4 receptor en de verhoging van het MCL-1 eiwit, dat net als BCL-XL beschermend werkt. Het blokkeren van dit proces dat leidt tot resistentie, of het direct remmen van MCL-1, werkt effectief samen met BCL-XL-remming. Opmerkelijk is dat we constateerden dat deze ontsnapping van celdood overdraagbaar is, aangezien het medium van met BH3-mimetica behandelde cellen een factor bevat die andere (onbehandelde) cellen kan aanzetten tot het maken van meer MCL-1. Deze overdraagbare factoor bleek FGF2 te zijn die effectief aan FGFR4 kan binden en die dus een alarmsignaal afgeeft direct nadat de cellen BH3-mimetica behandeling krijgen. Dit alarmsignaal kan leiden tot verhoogde resistentie via FGFR4 activatie . Het blokkeren van deze respons zou, samen met BH3-mimetica, een interessante therapeutische strategie kunnen zijn in darmkanker.

In **Hoofdstuk 5** hebben we darmkanker-cellijnen met bekende moleculaire kenmerken en subtypes gescreend op hun gevoeligheid voor BH3-mimetica gericht tegen BCL-2, BCL-XL en MCL-1. Behandeling met remmers alleen en in combinatie leverde duidelijke inzichten en bevestigde dat de combinatie van MCL-1 en BCL-XL remming voor alle cellijnen, ongeacht het subtype, de beste combinatietherapie was. Bovendien constaterden we dat expressieniveaus van anti-apoptotische eiwitten de gevoeligheid voor hun respectievelijke remmers niet voorspellen. Analyse van de correlatie tussen moleculaire kenmerken en anti-apoptotische gevoeligheid gaf aan dat KRAS-mutante darmkankerlijnen resistenter zijn tegen MCL-1-remming dan lijnen die geen mutatie in het KRAS oncogen hebben. Subtype-analyse identificeerde een intrigerende resistentie van CMS2-lijnen tegen BCL-2- en MCL-1-targeting-mimetica. Samengenomen bieden onze bevindingen in dit hoofdstuk een gedetailleerd overzicht van de expressie en afhankelijkheden van de BCL-2-familie in de context van verschillende moleculaire kenmerken van darmkanker en benadrukken ze de therapeutische werkzaamheid van BCL-XL- en MCL-1-remming.

In **Hoofdstuk 6** integreren we de bevindingen van dit proefschrift in het licht van relevante publicaties en identificeren we mogelijkheden voor toekomstig onderzoek om de gevolgen van het aangrijpen op apoptose in vivo te ontrafelen en daardoor het rationele gebruik van BH3-mimetica in darmkanker-management mogelijk te maken.

PhD Portfolio

PhD period: October 2015 – July 2021
Name PhD supervisor: Prof. Dr. Jan Paul Medema
Name PhD co-supervisor: Prof. Dr. Louis Vermeulen

PhD Training	Year	ECTS
Courses		
Entrepreneurship in health and life sciences	2020	1.5
Cellular Imaging: Pixel to Publication	2019	0.8
Cellular Imaging: Basic microscopy	2017	1.6
Computing in R	2016	0.4
R2 Genomics Analysis and Visualization Platform	2016	0.1
Practical Biostatistics	2016	1.4
Seminars		
Department Seminars (CEMM)	2015-2019	4
AMC Oncology Seminars (OASIS)	2015-2019	4
Cancer Center Amsterdam Seminars (CCA)	2017-2021	4
Conferences		
Annual Scientific Meetings (CGC and Oncode)	2015-2020	4
Oncology Graduate School (OOA) PhD retreat	2017	1
EWCD (poster and presentation)	2016, 2018	2
A Matter of Life or Death: EACR (presentation)	2015, 2017	2
Cancer Center Amsterdam retreat (presentation)	2017-2020	4
Supervision		
Bachelor student Life Sciences – Research Internship, Hogeschool InHolland	2021	1
Master Student Biomedical Sciences – Research Internship, University of Amsterdam	2019	2
Master Student Biomedical Sciences – Literature Review, University of Amsterdam	2018	0.5
Master Student Biomedical Sciences – Research Internship, University of Amsterdam	2017	2

List of publications

J. F. Linnekamp, S. R. V. Hooff, P. R. Prasetyanti, R. Kandimalla, J. Y. Buikhuisen, E. Fessler, **P. Ramesh**, K. Lee, G. G. W. Bochove, J. H. de Jong, K. Cameron, R. V. Leersum, H. M. Rodermond, M. Franitza, P. Nürnberg, L. R. Mangiapane, X. Wang, H. Clevers, L. Vermeulen, G. Stassi and J. P. Medema. "Consensus molecular subtypes of colorectal cancer are recapitulated in in vitro and in vivo models." *Cell Death & Differentiation* (2018).

D. Fiore, **P. Ramesh**, M. C. Proto, C. Piscopo, S. Franceschelli, S. Anzelmo, J. P. Medema, M. Bifulco and P. Gazzerro. "Rimonabant kills colon cancer stem cells without inducing toxicity in normal colon organoids." *Frontiers in pharmacology* (2018).

P. Ramesh, A. B. Kirov, D. J. Huels and J. P. Medema. "Isolation, Propagation, and Clonogenicity of Intestinal Stem Cells." *Methods in Molecular Biology* (2019).

P. Ramesh and J. P. Medema. "BCL-2 family deregulation in colorectal cancer: potential for BH3 mimetics in therapy." *Apoptosis* (2020).

N. Serna, P. Álamo*, **P. Ramesh***, D. Vinokurova, L. Sánchez-García, U. Unzueta, A. Gallardo, M. V. Céspedes, E. Vázquez and A. Villaverde. "Nanostructured toxins for the selective destruction of drug-resistant human CXCR4+ colorectal cancer stem cells." *Journal of Controlled Release* (2020).

W. L. Smit, C. N. Spaan, R. J. de Boer, **P. Ramesh**, T. M. Garcia, B. J. Meijer, J. L. M. Vermeulen, M. Lezzerini, A. W. MacInnes and J. Koster. "Driver mutations of the adenoma-carcinoma sequence govern the intestinal epithelial global translational capacity." *Proceedings of the National Academy of Sciences* (2020).

L. Zhang*, **P. Ramesh***, M. Steinmetz and J. P. Medema. "BH3 Mimetic Sensitivity of Colorectal Cancer Cell Lines in Correlation with Molecular Features Identifies Predictors of Response." *International Journal of Molecular Sciences* (2021).

S. M. van Neerven, N. E. de Groot, L. E. Nijman, B. P. Scicluna, M. S. van Driel, M. C. Lecca, D. O. Warmerdam, V. Kakkar, L. F. Moreno, F. A. Vieira Braga, D. R. Sanches, **P. Ramesh**, S. Ten Hoorn, A. S. Aelvoet, M. F. van Boxel, L. Koens, P. M. Krawczyk, J. Koster, E. Dekker, J. P. Medema, D. J. Winton, M. F. Bijlsma, E. Morrissey, N. Léveillé and L. Vermeulen. "Apc-mutant cells act as supercompetitors in intestinal tumour initiation." *Nature* (2021).

P. Ramesh, T. R. M. Lannagan, R. Jackstadt, L. Atencia Taboada, N. Lansu, P. Wirapati, S. R. van Hooff, D. Dekker, J. Pritchard, A. B. Kirov, S. M. van Neerven, S. Tejpar, G. J. P. L. Kops, O. J. Sansom and J. P. Medema. "BCL-XL is crucial for progression through the adenoma-to-carcinoma sequence of colorectal cancer." *Cell Death & Differentiation* (2021).

* Shared authorship

Acknowledgements

I am wrapping up a six year-long roller coaster ride, full of many exciting and unexpected turns, with a big content smile as it reaches its end. This is largely thanks to the wonderful people who were part of this journey and gave me the courage to step into the wagon and blast off (and not jump off at any point!) I could not have done this without you.

My biggest thanks to you, **Jan Paul,** for believing in me and giving me the opportunity to be a part of your team. I have learnt so much from your infectious optimism, quick-thinking and creative ideas. Many a time when I felt stuck and out of options, our discussions gave me renewed drive to try new things. Thank you for being an inspiring and caring mentor, for giving me the freedom to grow and nudging me in the right directions.

My sincere thanks to **Louis**, thank you for being my co-promoter and for sharing your thoughtful and unique ideas, your passion for science is truly inspiring!

I would like to thank my **committee members**, Eric Eldering, Evelien Dekker, Marcel Spaargaren, Giorgio Stassi and Lianne Koens for evaluating this thesis and making the time for participating in the defense.

I was lucky to perform an integral part of my thesis work with great collaborators. **Giorgio**, a big thank you to you and your lab for so generously hosting me in Palermo and giving me the opportunity to work with you. **Simone**, thank you for your endless support, not only with the cute mice! Your sense of humour made Palermo brighter, and I will always remember your funny complaints as we climbed up to the cave church :) **Annalisa** and **Maria-Teresa**, thank you for your warmth and kindness, I enjoyed sharing laughs and eating the amazing Sicilian snacks and pastries with you all. **Owen, Rene** and **Tammy**, I cannot thank you enough for all your efforts for the mouse experiments in Glasgow, especially during the peak of corona times. I am forever grateful to you all. My thanks also to **Wouter** for sharing

organoids and nice coffee breaks, it was a pleasure to collaborate with you.

I started this journey as a nervous newbie with many inspiring OG LEXORians to show me the way. **Cheryl**, you have a heart of gold, thank you for sharing your amazing expertise with me in my early days and even thereafter. **Serena**, I felt so welcome thanks to your warmth and friendship, thank you for the many laughs and happy hugs! **Evelyn**, I am so grateful for your kindness and the advice you shared with me, and I really enjoyed our metro ride conversations very much! **Janneke**, thank you for sharing your enthusiasm and keeping the lab spirits up! **Sander**, thank you for your bioinformatics genius and all the fun stories, I always looked forward to early morning chats with you. **Anne**, you are an inspirational power woman, thank you for the lovely chats whenever we crossed paths. **Maartje**, thank you for your genuine kindness and answering my endless questions about Bcl-2. **Robin, Dita, Arlene** – thank you for the many laughs and good times, especially during the Florence trip! **Joyce**, from then to now, we have come a long way and I am happy to have shared these years working, ranting and laughing with you - you are such a fun, interesting and joyful person, I wish you the best always! **Eva**, western blot goddess, thank you for showing me how to get perfect blots with your infectious brightness! **Donatella** and **Naroa**, I am happy you chose to do your PhD visits in our lab, it was a pleasure working with you! My thanks also to **Ana, Salvatore, Raju** and **Luigi** for the helping hand and friendly encounters.

Kate, thank you for the many funny stories, silly dancing and good times in and out of the lab! **Joan**, you are such a sweetheart, thank you for going out of your way to help, always. **Saskia**, I enjoyed our many lovely conversations and seeing your beautiful knit-work. **Veerle**, you are such a dedicated and strong person, I admire your work ethic. **Lauri**, it was a pleasure to work with you, even though for a short time. **Maria**, your smile always brightened my day. **Danielle**, thank you for all the funny stories! **Cynthia, Gregor, Hella** and **Hans**, thank you for all your support in the lab. **Lisanne** and **Nina**, thank you for always helping when I came by looking for missing things :)

Patricia and **Valerie**, two cute peas in a pod, you girls are the sweetest and it has been a pleasure watching you grow into awesome scientists! Thank you for all the fun memories along with **Rana** and **Laura**, especially all the animated chats in cell culture :) **Etienne**, thank you for being the most amazing vogue partner anyone could ask for! **David**, your approach to science is so inspiring, thank you for bringing your positivity to LEXOR! **Sanne** (vN), I have not met anyone as eager to help as you, thank you for all your kindness in and out of the lab, I have learnt a lot from you! **Arezo**, I don't know how to thank you for always helping me when I came to you with the most annoying last-minute requests. You are so selflessly kind and generous, thank you for all the fun memories :) **Simone**! You always make me laugh, I miss our corridor chats and your silly jokes, and being greeted by "hey cutie". Keep inspiring us with your amazing sporty adventures, along with **Roxanne** and **Leonie**! **Mei**, thank you for being such a sweet roomie and teaching me how to make Di San Xian, so tasty :) **Alex**, thank you for sharing your hearty laugh with the lab and **Selami**, thank you for sharing your amazing dance moves! **Tom** (vdE), thank you for your kindness and helping me draw blood from innocent passers-by in the lab :) **Lidia**, a big thank you for all your unwavering help in the last phase of my PhD, I wish you and **Ciro** good luck for the journey ahead.

My thanks to **MoniQue, Heleen** and **Bianca**, for all the administrative support throughout my PhD. **Monique**, thank you for all the help with the orders everytime I came running to you with another emergency missing reagent :) **Maarten, Arnold** and **Hanneke**, thank you for your valuable inputs during meetings. To my students, **Jessica** and **Jalisa**, thank you for your dedication to learning and doing such a great job in the lab. **Aafke**, talking to you always made me smile, thank you for your genuineness. **Amber, Paul, Tim, Sophie** and **Nicolas** - thank you for the lovely smiles and conversations whenever we crossed paths! **Mark, Sanne, Leandro, Kristiaan, Tom, Oscar, Milou, Adriaan, Daniel, Shulin, Dajia, Marloes** – thank you for the good memories and making LEXOR so gezellig!

Larry, thank you for all the good times in the years working with you. I admire your calm attitude and strength, and love for Mani :) **Sanne** (tH), your energy shines so bright and I enjoyed sharing the office with you, thank you for the many happy meals in and out of the lab :) **Nesrin**, your laugh makes me smile even if I don't know what the joke is, thank you for the many wonderful memories we have shared – some too funny to write down here, someone might spill their coffee reading :) **Cansu**, thank you for your friendship since the start of the PhD, it has been such a pleasure to share this journey with you and I cherish all our joint experiences! **Clara**, you are so inspiring with your endless energy and enthusiasm for life, it has been an honor to learn from you! **Francesco**, I am so happy to have met you, your genuine kindness and nerdiness made us instant friends for life :) **Ronja**, your friendship means so much to me! You are such a pure soul, full of kindness and love. Thank you for being you. **Dasha**, dudie, I thank all the stars for bringing you into my life, for it is so much better with you in it. Thank you for being your inspiring awesome self, the wonderful laughs, dancing, long talks, fun trips and for just always being there no matter what.

To my paranymphs, **Paris** and **Vaishali**, having some brownies next to me on this journey made it so much sweeter. You have been a constant source of strength, honesty and happiness in my life. Paris, thank you for being your mad self, so full of love and so giving, I never know how to thank you for the endless extravagant surprises and gifts you have given me, biggest of all being your and Enzo's awesometastic friendship (and game-nights!). V, you are one badass woman I look up to always, the way you handle everything - home, work, friendships, life (and workouts!)– is so inspiring. You are both so dear to me and quite often our tea breaks were the best part of my day!

To my dear friends and family outside the lab bubble, I cannot thank you enough for keeping me sane throughout the years. **Dana**, words cannot describe my feelings of gratitude towards you. I love talking science and life with you and your friendship means the world to me! **Kulsoom**, you

quickly entered my life with your radiant smile and zest for life and I am so lucky to have you as a dear friend. To my friends who are far but so close in my heart - **Judith, Chiaki, Marieke, Sherry** and **Maria**, thank you for making me feel your love no matter the distance. **Miska**, ľúbim ťa chica, I am in awe of your passion and dedication to everything you believe in! **Mithra, Raman, Karan** and **Akhi**, thank you for all the ridiculous fun we've had and for trusting my word because "I am a scientist" :) To the OG Special Crew, **Minh, Flo, Vince** and **Isabel**, you are my constants and I am so thankful that we have our decade-long bond, taking us through countless dinners, parties and special experiences...may we stay like this for many decades to come :)

A big thank you to my extended family in India who care for me and make me feel at home always, especially **Chitta, Chitti, Varsha** and **Megha**. To my family in the Netherlands, **Shoba, Ashish** and **Ayush**, thank you for always welcoming me with open arms and a big smile, I cherish our many lovely dinners, games and long walks in the woods.

Amma and **Appa**, everything I am is because of you. I cannot thank you enough for the amazing life you have given me through your hard work and sacrifices, and somehow you made sure I didn't turn out to be a complete brat despite spoiling me endlessly with your love (and concern for my food intake). This book is dedicated to you, thank you for everything.

Janani, my dear Jannu, you are the best little sis I could ever dream of having (15-year-old me would have puked before saying that). I am so proud of you and admire your creativity, strength and resilience – you never cease to amaze me and I am so incredibly thankful for you!

Akshay, my love, thank you for asking me to hang out with you all those years ago :) Thank you for making me laugh when nothing is funny, for making me believe in myself the way you believe in me, for dancing with me through this beautiful mess. To many more wonderful adventures together, with you everything is awesome :)

About the author

Prashanthi Ramesh was born on 27th April 1992 in Kumbakonam, India. During her early childhood, her family moved from Bengaluru to Delhi and finally to Mumbai, where she lived for 11 years and completed most of her primary and secondary education. In 2008, they moved to Eindhoven, the Netherlands, where she completed the International Baccalaureate (IB) program at the International Secondary School of Eindhoven (ISSE). With vague and changing ideas of her future, she started a BSc in Liberal Arts and Sciences at University College Utrecht (UCU), when she chanced upon a course in cell and molecular biology and found her passion. After completion of her undergraduate studies in 2013, she continued her postgraduate education with an MSc in Oncology at the Vrije Universiteit in Amsterdam. She performed her thesis in the laboratory of Dr. Michiel Pegtel at the Cancer Center Amsterdam, where she studied pH sensitive reporters for exosome release. For her second thesis, she studied the role of microRNA in endothelial cell function under the supervision of Prof. Dr. Anna Randi at the National Heart and Lung Institute of Imperial College London, UK. Soon after, the beautiful city of Amsterdam was calling her back and in October 2015, she began her PhD under the supervision of Prof. Dr. Jan Paul Medema at the Amsterdam UMC. During her doctoral work, she explored the role of cell death regulating proteins in colorectal cancer, which is presented in this thesis.

A